

Review

Dynamics of a Quantum Phase Transition and Relaxation to a Steady State

Jacek Dziarmaga^{a*}

^a *Instytut Fizyki im. Mariana Smoluchowskiego and Mark Kac Complex Systems Research Centre, Uniwersytet Jagielloński, ul. Reymonta 4, PL-30-059 Kraków, Poland*

(May 26, 2010)

We review recent theoretical work on two closely related issues: excitation of an isolated quantum condensed matter system driven adiabatically across a continuous quantum phase transition or a gapless phase, and apparent relaxation of an excited system after a sudden quench of a parameter in its Hamiltonian. Accordingly the review is divided into two parts. The first part revolves around a quantum version of the Kibble-Zurek mechanism including also phenomena that go beyond this simple paradigm. What they have in common is that excitation of a gapless many-body system scales with a power of the driving rate. The second part attempts a systematic presentation of recent results and conjectures on apparent relaxation of a pure state of an isolated quantum many-body system after its excitation by a sudden quench. This research is motivated in part by recent experimental developments in the physics of ultracold atoms with potential applications in the adiabatic quantum state preparation and quantum computation.

Keywords: quantum phase transition; thermalisation; Landau-Zener model; adiabatic theorem;

* Email: dziarmaga@th.if.uj.edu.pl

Contents

1. Introduction
2. Dynamics of a quantum phase transition
 - 2.1. Introduction
 - 2.2. Kibble-Zurek mechanism (KZM) in a classical phase transition
 - 2.3. KZM in a quantum phase transition
 - 2.4. KZM: adiabatic transition in a finite system
 - 2.5. KZM in a non-linear quench
 - 2.6. KZM: from a critical point into a gapped phase
 - 2.7. KZM in space
 - 2.8. KZM and dynamics of an inhomogeneous phase transition
 - 2.9. The Landau-Zener (LZ) model
 - 2.10. The LZ model in the adiabatic-impulse approximation
 - 2.11. KZM as a set of independent Landau-Zener transitions
 - 2.12. KZM from adiabatic perturbation theory
 - 2.13. Quantum Ising chain: transition across an isolated critical point
 - 2.13.1 Landau-Zener argument
 - 2.13.2 Transition in a finite chain
 - 2.13.3 Exact solution of the time-dependent Bogoliubov-de Gennes equations
 - 2.13.4 Entropy of a block of spins in the final state
 - 2.13.5 Impurity of the final state
 - 2.13.6 Correlation functions in the final state
 - 2.13.7 Fidelity between the final state and the final ground state
 - 2.13.8 Geometric phase of the final state
 - 2.13.9 Generalised entanglement in the final state
 - 2.13.10 Linear quench to $t \rightarrow \infty$: quantum dephasing after KZM
 - 2.13.11 Transition in space
 - 2.13.12 Inhomogeneous transition
 - 2.14. Quench across a multicritical point of the XY chain
 - 2.15. Kitaev model in 2D: quench across a gapless phase
 - 2.16. The random Ising chain: logarithmic dependence of excitation density on transition rate
 - 2.17. Topological insulators: anomalous excitation of edge modes
 - 2.18. The Lipkin-Meshkov-Glick model: KZM and infinite coordination number
 - 2.19. The Bose-Hubbard model: transition between gapped Mott insulator and gapless superfluid
 - 2.19.1 Slow transition from Mott insulator to superfluid
 - 2.19.2 Fast transition from Mott insulator to superfluid at small density
 - 2.19.3 Fast transition from Mott insulator to superfluid at large density
 - 2.19.4 Fast transition from superfluid to Mott insulator at large density
 - 2.20. Loading a 1D Bose gas into an optical lattice: transition into the gapped phase of the sine-Gordon model
 - 2.21. Spin-1 Bose-Einstein condensate: transition from the paramagnetic to the ferromagnetic phase
 - 2.22. Adiabatic sweep across a gapless regime
 - 2.23. Many-particle Landau-Zener problem: adiabatic passage across a Feshbach resonance
3. Apparent relaxation of an isolated quantum system after a sudden quench
 - 3.1. Introduction
 - 3.2. Quasiparticle light cone effect in dephasing after a sudden quench
 - 3.3. Generalised Gibbs ensemble (GGE) for a quadratic Hamiltonian
 - 3.4. Local relaxation to GGE with a quadratic Hamiltonian
 - 3.5. GGE and the transverse Ising chain
 - 3.6. GGE and the Luttinger model
 - 3.7. GGE and hard core bosons
 - 3.8. GGE and the Bose-Hubbard model
 - 3.9. GGE and a system solvable by Bethe ansatz
 - 3.10. Eigenstate thermalisation hypothesis (ETH)
 - 3.11. Dynamics of relaxation to a steady state
 - 3.12. Summary
3. Conclusion

1. Introduction

Experiments with ultracold atoms provide unprecedented opportunities to emulate precisely tailored model Hamiltonians at temperatures close to zero [1]. These model quantum systems are not only well isolated from their environment, but also their parameters can be changed in time in a prescribed way [2–9]. Consequently, the emerging field of non-equilibrium quantum systems driven out of their initial ground state by a time-dependent Hamiltonian is no longer of purely academic interest. Quite to the contrary, it becomes essential for such practical applications as adiabatic quantum state preparation for quantum simulation [1, 9–13] and, in particular, adiabatic quantum computation [14]. In this article we review recent theoretical work on two closely related issues: excitation of a condensed matter system driven across a continuous quantum phase transition or a gapless phase, and apparent relaxation of an excited system towards thermal equilibrium or a non-thermal steady state.

The former issue had been intensively studied both theoretically and experimentally in different systems at finite temperature including cosmological phase transitions, liquid crystals, superfluid helium, convection cells, superconductors, and Bose-Einstein condensation, where the excitation is described by the Kibble-Zurek mechanism (KZM). In this review we collected recent evidence that, although in many situations many details are different than in the finite temperature KZM, its key ingredients – which are crossovers between adiabatic and non-adiabatic stages of time evolution – remain the same in the zero temperature quantum limit. Consequently, the excitation of a system in general scales with a power of a transition rate. We also include examples where the KZM paradigm is not so predictive, like when driving the system across a gapless bosonic phase, even though the excitation is still a power of the driving rate, and an example of a disordered system where it is the KZM that predicts a logarithmic dependence on the rate instead of the usual power law. Finally, we mention an example where the evolution is essentially non-adiabatic, i.e., the excitation density diverges with increasing system size.

Once a system got excited the latter issue becomes important: does an excited state of an isolated quantum system relax to any steady state? A quick “global” answer is “no”, because unitary evolution cannot evolve an initial pure state into a mixed state. However, this does not exclude some sort of apparent *local* relaxation, where expectation values of local observables relax to become the same as in a global mixed state. With this distinction in mind, we can further ask what is the nature of the global steady state? In this article we briefly review recent work on integrable and non-integrable quantum systems. General arguments together with exactly solvable examples suggest that non-interacting quadratic bosonic or fermionic Hamiltonians appear to relax *locally* to a non-thermal generalised Gibbs ensemble (GGE). The ensemble is strongly constrained by integrals of motion which in this case are the numbers of Bogoliubov quasiparticles. In case of non-integrable systems the evidence is less conclusive. When an excited state of a many-body system after a sudden quench has a narrow energy distribution then, according to the conjectured “eigenstate thermalisation hypothesis” (ETH), for simple few-body observables the state appears to relax to a microcanonical ensemble. This thermalisation mechanism is qualitatively different than the ergodicity required of classical non-integrable systems.

Even though in practice the two issues cannot be always sharply “disentangled”, because the relaxation begins already during the excitation of a system, this review is divided into two corresponding major parts in Sections 2 and 3.

2. Dynamics of a quantum phase transition

2.1. Introduction

A quantum phase transition is a fundamental change in the ground state of a quantum system when one of parameters in its Hamiltonian is driven across a critical point [15]. A continuous (or second order) quantum phase transition can often be characterised by an energy gap between the ground state and the first excited state or, more generally, a relevant energy scale which vanishes at the critical point in the thermodynamic limit of infinite system size. Consequently, no matter how slowly the parameter is driven the quantum state of the system cannot follow adiabatically the instantaneous ground state near the critical point. It is the aim of this part to quantify the level of this inevitable excitation in different systems.

This research is motivated in part by adiabatic quantum computation [14], where one would like to prepare a system in a simple ground state of an initial Hamiltonian H_i , and then drive the system adiabatically to a final Hamiltonian H_f , whose ground state is a solution to a non-trivial computational problem. Unfortunately, since H_i and H_f are qualitatively different, they are generally separated by a critical point, where the driving cannot be adiabatic in the limit of infinite system size. Consequently, there is an upper limit to the size of the system (or number of qubits) which can cross the critical point adiabatically at a given transition rate and, consequently, the minimal necessary time of “adiabatic computation” increases with the number of qubits. The same problem can arise in the context of quantum simulators [12, 16], where the key idea is to emulate a model condensed matter Hamiltonian with, say, ultracold atoms in an optical lattice potential [1, 8, 13], ions in an ion trap [9, 10] or NMR molecules [11]. In this context, one usually prepares the system in the uncorrelated ground state of a simple initial Hamiltonian H_i , like e.g. a Bose-Einstein condensate, and then drives it into a correlated state by a slow change of a parameter in the Hamiltonian [2, 6, 8, 9, 11].

A quantum phase transition across an isolated quantum critical point between two gapped phases turns out to be well described by a quantum version of the Kibble-Zurek mechanism (KZM). The essence of the mechanism is an adiabatic-impulse-adiabatic approximation, where evolution of a system driven slowly across a phase transition is assumed adiabatic in the gapped phases sufficiently far from criticality, and impulse in a close neighbourhood of the gapless critical point, where the state of the system does not change in this approximation. Consequently, the state after the transition can be argued to have a finite correlation length $\hat{\xi} \sim \tau_Q^{\frac{\nu}{1+\nu z}}$, where τ_Q is a characteristic time of the adiabatic transition between the two phases and ν, z are the critical exponents. This universal scale of length determines density of excitations and other physical quantities. For example, the density of excitations or excitation energy above the ground state scales as an inverse power of the transition time τ_Q .

However, the world of quantum critical phenomena is rich: phase diagrams have gapless lines and gapless phases, and a system driven across a gapless line or phase also gets excited. It turns out that in many of such non-standard situations the adiabatic-impulse-adiabatic approximation still applies and is able to predict the correct scaling of the density of excitations (or density of excitation energy) with the transition time, but there are also systems where this approximation is not practical or not predictive enough. These include some bosonic systems, which are non-adiabatic in the thermodynamic limit, i.e., their density of excitations diverges with increasing system size. Nevertheless, the adiabatic-impulse-adiabatic approximation is the leading motif of Section 2.

Section 2 is organised as follows. In Section 2.2 we briefly review KZM in the historical context of finite temperature classical phase transitions, and then in Section 2.3 we generalise KZM to a zero temperature quantum phase transition between two gapped phases. Once KZM is reformulated in this most “canonical” set-up its key ingredient, which is the adiabatic-impulse-adiabatic approximation, can be bend and twisted in many different ways as required by actual application. Some general examples are described in Sections 2.4, 2.6, 2.7, 2.8, and 2.5. In Section 2.4 we drive a finite system across the critical value of the parameter in its Hamiltonian and estimate how slow the driving rate has to be for the transition to be adiabatic. In Section 2.6 we drive an infinite system into a gapped phase starting exactly at a critical point. In Section 2.7 a quantum phase transition takes place not in time but in space, i.e., the parameter in the Hamiltonian driving the transition is time-independent but inhomogeneous in space, so that different parts of the system are in different phases. In Section 2.8 the phase transition is driven in an inhomogeneous way such that some parts of the system cross the critical point earlier than the other. The inhomogeneous transition turns out to be a way to suppress excitations at the critical point. Another way to minimise excitations is a transition with a non-linear time-dependence of the driving parameter considered in Section 2.5.

After this incomplete review of non-standard generalisations, we return to the basics and in Sections 2.9, 2.10, 2.11 investigate relations between KZM and the Landau-Zener (LZ) model of level anti-crossing [17]. We begin in Section 2.9 by a review of the standard LZ model together with more exotic transitions that begin or end at the anti-crossing centre. In Section 2.10 we apply the adiabatic-impulse-adiabatic approximation, which is central to KZM, to obtain approximate solutions of the LZ model in some limits of parameters. Finally, in Section 2.3 we consider a general quadratic fermionic Hamiltonian which can be mapped to sets of independent LZ transitions. This class of integrable models provides exact solutions supporting KZM or its generalisations. In the following Section 2.12 we rederive KZM within the time-dependent perturbation theory. This perturbative treatment reproduces approximately the exact results in the integrable models, but it does not seem limited to the quadratic Hamiltonians. Section 2.12 completes the general part of Section 2, and the following Sections describe applications of the general ideas to a number of specific integrable and non-integrable models.

The list of examples is opened in Section 2.13 by one of the cornerstones of the theory of quantum phase transitions – the integrable quantum Ising chain in transverse magnetic field. It has a quantum phase transition between two gapped phases: paramagnetic and ferromagnetic. Since the model can be mapped via the Jordan-Wigner transformation [18] to a quadratic fermionic Hamiltonian, virtually all the general ideas mentioned above are illustrated in the subsections of Section 2.13. This is why the quantum Ising chain takes relatively large portion of this article.

Once the review of the Ising chain is completed, in Sections 2.14 and 2.15 we review another two quadratic fermionic systems: the XY spin chain and the 2D Kitaev model. They provide exactly solvable examples where KZM requires careful generalisation to obtain correct scaling of the density of excitations with the transition rate. The next example in Section 2.16 is the random quantum Ising chain, where the density of excitations turns out to be a logarithmic function of the transition rate. There is no usual KZ power-law scaling in this model, but the logarithmic dependence can still be obtained from the adiabatic-impulse-adiabatic approximation like in KZM. This example is followed by topological insulators in Section 2.17, where the edge zero modes that must exist in a topological insulator

have a different scaling of the excitation probability than in the bulk of the same insulator. In Section 2.18 the quantum KZM is extended to the Lipkin-Meshkov-Glick model with infinite coordination number, and in Section 2.19 to the non-integrable Bose-Hubbard model.

The last model is important because it is another cornerstone of the theory of quantum phase transitions and it was realised experimentally in Refs. [2, 13, 19]. The 1D version of the model has the Berezinski-Kosterlitz-Thouless transition between the gapped Mott insulator and gapless superfluid. Since the model is non-integrable, we review different approximate results for transitions between the two phases. Another closely related model is considered in Section 2.20, where a quasi-1D gas of bosonic atoms is loaded into an optical lattice potential. The gas is a gapless (critical) Luttinger liquid for which a weak optical lattice potential is a relevant perturbation leading to an effective sine-Gordon model with a finite gap in its excitation spectrum. This is an example of a transition starting at a critical point and going into a gapped phase introduced in Section 2.6. In Section 2.21 we review mean-field treatment of the transition from a paramagnetic to a ferromagnetic phase in a spin-1 Bose-Einstein condensate.

Finally, in Section 2.22 we consider adiabatic sweep across a gapless phase in a quadratic model of harmonic oscillators, and in Section 2.23 a semiclassical treatment of a many-body Landau-Zener model. The 1D gapless harmonic model turns out to be non-adiabatic in a sense that its density of excitations increases with the system size. The many-body LZ model is in turn an example, where the density of LZ anti-crossings is so large that they cannot be treated as independent transitions, so the whole problem has to be and can be treated by semiclassical methods. A summary of Section 2 is made in Section 2.24.

2.2. *KZM in a classical phase transition*

Phase transition is a fundamental change in the state of a system when one of its parameters passes through the critical point. In a second order phase transition, the fundamental change is continuous and the critical point is characterised by divergent correlation length and relaxation time. This critical slowing down implies that no matter how slowly a system is driven across the transition, its evolution cannot be adiabatic close to the critical point. As a result, ordering of the state after a transition from a disordered symmetric phase to an ordered broken symmetry phase is not perfect: the state is a mosaic of ordered domains whose finite size ξ depends on the rate of the transition. This scenario was first described in the cosmological context by Kibble [20] who appealed to relativistic causality to set the size of the domains. The dynamical mechanism relevant for second order phase transitions was proposed by Zurek [21] and it is briefly as follows.

A dimensionless distance from the critical point at a finite temperature T_c can be defined as

$$\epsilon = \frac{T - T_c}{T_c} . \quad (1)$$

In the initial symmetric phase above T_c there are finite thermal fluctuations of the order parameter with diverging correlation length

$$\xi \sim |\epsilon|^{-\nu} . \quad (2)$$

and relaxation time

$$\tau \sim \xi^z \quad (3)$$

describing reaction time of the system to external perturbations. This divergent relaxation time becomes infinitely slow at the critical point.

The system can be driven below T_c either directly by cooling, or by increasing T_c above a constant T by varying another parameter such as pressure [22, 23]. In any case, there is a time-dependent $\epsilon(t)$ running continuously from an initial $\epsilon_i > 0$ to a final $\epsilon_f < 0$. Near the critical point it can be linearised as

$$\epsilon(t) \approx -\frac{t}{\tau_Q}, \quad (4)$$

where the coefficient τ_Q can be identified as a “quench time”. This linearised form implies a relative transition rate $|\epsilon^{-1} \frac{d\epsilon}{dt}| = t^{-1}$ which diverges near the critical point. The evolution of the system with a time-dependent $\epsilon(t)$ can be divided into three stages, see Fig. 1. Initially the transition rate is slower than the relaxation time τ and the system adiabatically follows the instantaneous state of thermal equilibrium for current $\epsilon(t)$. This adiabatic stage lasts until

$$\hat{\epsilon} \sim \tau_Q^{-\frac{1}{1+\nu z}} \quad (5)$$

when the transition rate t^{-1} equals the instantaneous relaxation rate τ^{-1} of the system and long wavelength fluctuations begin to go out of equilibrium. After $\hat{\epsilon}$ reactions of the system are too sluggish to follow the varying $\epsilon(t)$ and, in a first impulse approximation, the state does not change until $-\hat{\epsilon}$ when the reactions of the system become faster than the transition rate again. In this way the system arrives at $-\hat{\epsilon}$, which is already in the symmetry broken phase, still remaining in the state of thermal equilibrium at the $+\hat{\epsilon}$ in the symmetric phase, where there are small thermal fluctuations of the order parameter with a finite correlation length

$$\hat{\xi} \sim \hat{\epsilon}^{-\nu} \sim \tau_Q^{\frac{\nu}{1+\nu z}}. \quad (6)$$

These small fluctuations are the initial state for the last adiabatic stage of the evolution after $-\hat{\epsilon}$.

Around $-\hat{\epsilon}$ the system “realises” at last that zero order parameter is no longer its state of equilibrium. The proper equilibrium state has a finite order parameter whose eventual variations in space can be characterised by a finite healing length $|-\hat{\epsilon}|^{\nu z}$, which is incidentally the same as the correlation length $\hat{\xi}$ (but see Ref. [24]). Near $-\hat{\epsilon}$ the small fluctuations of the order parameter with wave lengths longer than the healing length $\hat{\xi}$ blow up quasi-exponentially in time until magnitude of the order parameter becomes comparable to its finite equilibrium value. At this point the order parameter becomes a mosaic of ordered domains whose average size is set by $\hat{\xi}$. The orientation of the order parameter is approximately constant in each domain, but uncorrelated between different domains.

In the finite temperature context the focus was on topological defects. When a vacuum manifold of the order parameter has a non-trivial homotopy group, then there are stable topological defects. Their density after a transition is set by the size $\hat{\xi}$ of the correlated domains [20]. For example, the density of point-like monopoles in 3D is $\simeq \hat{\xi}^{-3}$, and vortices in 2D is $\simeq \hat{\xi}^{-2}$. Topologically stable defects are a robust and relatively easy to detect imprint of the non-equilibrium phase transition.

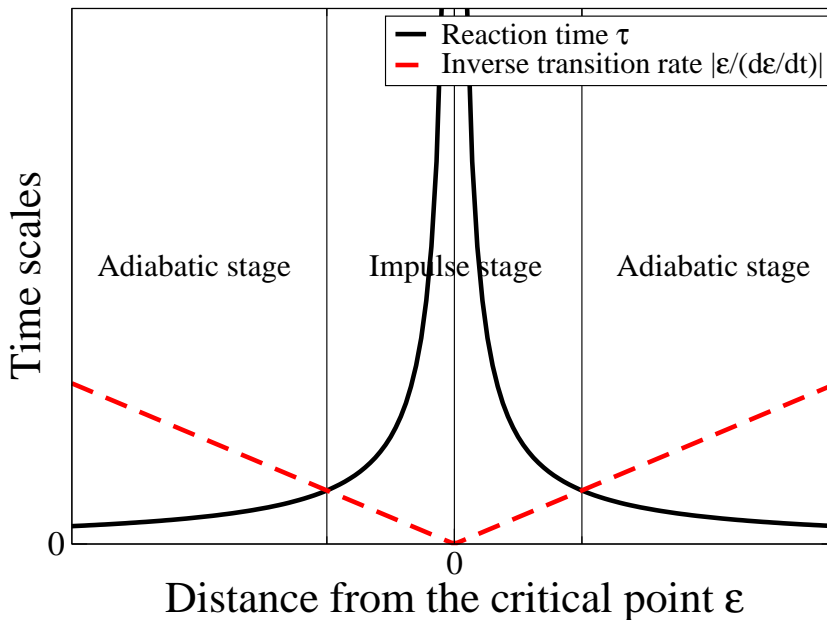


Figure 1. The reaction time τ and the inverse transition rate $|\epsilon/\dot{\epsilon}|$ as a function of dimensionless distance ϵ from the critical point. The reaction time equals the inverse transition rate at $+\hat{\epsilon}$ and $-\hat{\epsilon}$. These two points mark crossovers between the impulse and adiabatic stages of time evolution.

However, most of them are not permanent because, for instance, pairs of vortices with opposite winding number attract each other and annihilate. This equilibration process, known as phase ordering kinetics [25], leads to gradual coarse-graining of the order parameter on increasing scale of length. What eventually remains is a net winding number of the initial mosaic. This is why in the finite temperature experiments one has to prevent defects from phase ordering by, e.g., stabilizing them in a rotating cryostat [26], or trapping them in a superconducting ring [27].

KZM for classical phase transitions was confirmed by numerical simulations of the time-dependent Ginzburg-Landau model [28] and successfully tested by experiments in a wide range of condensed matter systems including liquid crystals [29], superfluid ^3He [26], both high- T_c [30] and low- T_c [27] superconductors, non-equilibrium convection systems [31], and Bose-Einstein condensation driven by evaporative cooling [32]. With the exception of superfluid ^4He - where the early detection of defect formation [22] was subsequently attributed to vorticity introduced by stirring [23], and the situation remains unclear - experimental results are consistent with KZM, but more quantitative experimental tests are needed to verify e.g. the KZ scaling of defect density with transition rate.

KZM is a universal theory of the dynamics of continuous symmetry-breaking phase transitions whose applications range from the low temperature Bose-Einstein condensation to the ultra high temperature transitions in the grand unified theories of high energy physics. However, the zero temperature quantum limit remained unexplored until recently and quantum phase transitions are in many respects qualitatively different from transitions at finite temperature. Most importantly time evolution is unitary, so there is no damping, and there are no thermal fluctuations to initialise the symmetry breaking.

In the next Section, following Ref. [36], we rederive KZM at zero temperature where the scalings turn out to be formally the same but the underlying physics is different.

2.3. KZM in a quantum phase transition

Near an isolated quantum critical point between two gapped phases both the reaction time τ and the correlation (or healing) length ξ diverge as

$$\tau \sim |\epsilon|^{-\nu z} , \quad (7)$$

$$\xi \sim |\epsilon|^{-\nu} , \quad (8)$$

where ϵ is a dimensionless parameter which measures distance from the critical point. For instance, when the transition is driven by varying a parameter g in the Hamiltonian across a critical point at a finite g_c , then

$$\epsilon = \frac{g - g_c}{g_c} . \quad (9)$$

The reaction time determines how fast the system can react to external perturbations and the healing length sets the scale on which the order parameter heals in space, i.e., returns to its ground state value. In a quantum phase transition the reaction time is set by an inverse of a gap Δ between the ground state and the first relevant excited state

$$\tau \simeq \Delta^{-1} , \quad (10)$$

because this is the shortest time scale on which the ground state can adjust adiabatically to a varying ϵ . Near the critical point the gap vanishes as

$$\Delta \sim |\epsilon|^{\nu z} \quad (11)$$

implying that the evolution across the critical point cannot be adiabatic.

We consider a second order quantum phase transition that is crossed at a finite rate set by the quench timescale τ_Q :

$$\epsilon(t) = -\frac{t}{\tau_Q} . \quad (12)$$

In general, $\epsilon(t)$ does not need to be a linear function of t , but here we assume the generic case when $\epsilon(t)$ can be *linearised* near the critical point as

$$\epsilon(t) = \frac{d\epsilon}{dt}(0) t + \mathcal{O}(t^2) . \quad (13)$$

The quench time in Eq. (12) can be identified as $\tau_Q = |\frac{d\epsilon}{dt}(0)|^{-1}$. A more general, but not quite generic, non-linear quench which cannot be linearised near $\epsilon = 0$ is considered in Section 2.5.

Initially, at $t \rightarrow -\infty$, the system is prepared in the ground state. As long as the reaction time in Eq. (7) is fast enough or, equivalently, the gap in Eq. (11) is large enough, the state of the system follows its adiabatic ground state. The adiabaticity fails near an instant $t = -\hat{t}$ when the transition rate $|\dot{\epsilon}/\epsilon| = 1/|t|$ equals the gap $\Delta \sim |\epsilon|^{\nu z} = |t/\tau_Q|^{\nu z}$ or

$$\hat{t} \sim \tau_Q^{\frac{\nu z}{1+\nu z}} , \quad (14)$$

From this time on long wavelength modes cease to be adiabatic. In a first approximation, after $-\hat{t}$ the evolution becomes impulse, i.e., the state effectively freezes out between $-\hat{t}$ and $+\hat{t}$ when the reaction time τ is too slow for the system to follow the evolving parameter $\epsilon(t)$. The adiabatic evolution of the state restarts again at $+\hat{t}$ when the gap becomes less than the transition rate, see Fig. 1.

Near the freeze-out time $-\hat{t}$, corresponding to

$$\hat{\epsilon} \sim \tau_Q^{-\frac{1}{1+\nu z}}, \quad (15)$$

the state is still in the instantaneous ground state with correlation length

$$\hat{\xi} \sim \hat{\epsilon}^{-\nu} \sim \tau_Q^{\frac{\nu}{1+\nu z}}. \quad (16)$$

In the adiabatic-impulse-adiabatic approximation, this state does not change between $-\hat{t}$ and \hat{t} . When the adiabatic evolution restarts near \hat{t} , corresponding to $-\hat{\epsilon}$, the ground state frozen at $\hat{\epsilon}$ becomes an initial excited state for the last adiabatic stage of the evolution.

In this approximation, the impulse stage of the linear quench in Eq. (12) is equivalent to a sudden quench from $\hat{\epsilon}$ to $-\hat{\epsilon}$, where the initial ground state at $\hat{\epsilon}$ becomes an initial excited state for the following adiabatic evolution after $-\hat{\epsilon}$.

Note that when the quench time τ_Q is large, then $\hat{\epsilon}$ in Eq. (15) is small and the linearisation in Eq. (13) is self-consistent because all the non-trivial KZM physics happens in the narrow interval between $\hat{\epsilon}$ and $-\hat{\epsilon}$ which is very close to the critical point.

In the adiabatic-impulse-adiabatic approximation the state after the transition at $-\hat{\epsilon}$ is equal to the ground state of the system at $+\hat{\epsilon}$. In the adiabatic limit of large τ_Q this ground state is very close to the critical point so, by the usual scaling hypothesis of the renormalisation group theory, expectation value of an operator O in this state is proportional to a power of the diverging correlation length $\hat{\xi}$ in the ground state at $\hat{\epsilon}$. Moreover, since $\hat{\xi}$ itself scales with the transition time, see Eq. (16), the expectation value $\langle O \rangle$ also scales with a power of the transition time τ_Q . For example, if the phase after the transition admits quasiparticle excitations, then their density scales like

$$n_{\text{ex}} \simeq \hat{\xi}^{-d} \sim \tau_Q^{-\frac{d\nu}{1+\nu z}}, \quad (17)$$

where d is the number of space dimensions. The same scale $\hat{\xi}$ determines a range of correlations and other physical quantities.

In the same way as $\hat{\xi}$ is the universal scale of length, the freeze-out time \hat{t} in Eq. (14) is the universal scale of time. For instance, the density of excitations during the transition depends on time as

$$n_{\text{ex}}(t) \simeq \tau_Q^{-\frac{d\nu}{1+\nu z}} F(t/\hat{t}), \quad (18)$$

where F is a non-universal scaling function. Examples can be found in Refs. [33–35] and in Section 2.19.

KZM predicts a correlation length $\hat{\xi}$ and a characteristic timescale \hat{t} . These are the basic quantities from which one can derive many other physical observables simply by dimensional analysis. This conjecture is confirmed by a series of examples, notably the Ising model, where quantities such as density of excitations, excitation

energy, correlation functions (often equivalent by a Fourier transform to the momentum distribution that is usually measured in the time of flight experiments), residual magnetization, entropy of entanglement, generalized entanglement, Berry phase, penetration depth in a transition in space, or threshold velocity in an inhomogeneous transition are all constructed out of $\hat{\xi}$ and/or \hat{t} . These are the basic building blocks from which one can construct other physical quantities.

In this Section we presented KZM in its most “canonical” form. However, the following Sections provide examples how the adiabatic-impulse-adiabatic approximation, which is the essence of KZM, can be bend and twisted in many different ways as required by actual application.

2.4. *KZM: adiabatic transition in a finite system*

The discussion in the previous Section assumes an infinite system where the correlation length (16) can diverge to infinity as the transition time becomes infinitely slow. However, in a large but finite system of linear size L the divergence must be terminated when $\hat{\xi} \simeq L$, or equivalently

$$\tau_Q \sim L^{\frac{1+\nu z}{\nu}}. \quad (19)$$

For slower transitions the scaling (16) breaks down and the transition becomes adiabatic. This adiabatic regime is a consequence of a non-zero gap Δ_c at the critical point of a finite system. When the transition is slow enough, then the finite gap suppresses any excitation exponentially. This effect was discussed in Ref. [36] and it is illustrated by an exact solution in the quantum Ising chain, see Section 2.13.2 and Refs. [37, 38]. A similar crossover to an adiabatic regime, which can be characterized by a steeper scaling of n_{ex} with τ_Q instead of an exponential decay, was discussed in Ref. [39] in case of a “half-quench” considered in Section 2.6 below.

2.5. *KZM in a non-linear quench*

The adiabatic-impulse-adiabatic approximation of Section 2.3 can be also applied to the non-linear quench considered in Refs. [40, 41], where

$$\epsilon(t) \approx -\text{sign}(t) \left| \frac{t}{\tau_Q} \right|^r \quad (20)$$

near the critical point $\epsilon = 0$. This function cannot be linearised as in Eq. (13) but, nevertheless, essentially the same argument can be applied here as in the linear case.

Indeed, the transition rate $|\dot{\epsilon}/\epsilon| = r/|t|$ equals the gap $\Delta \sim |\epsilon|^{\nu z}$ at $\hat{\epsilon} \sim (r/\tau_Q)^{r/(1+r\nu z)}$ corresponding to the KZ correlation length and density of excitations

$$\hat{\xi} \sim \tau_Q^{\frac{r\nu}{1+r\nu z}}, \quad n_{\text{ex}} \simeq \hat{\xi}^{-d} \sim \tau_Q^{-\frac{r\nu d}{1+r\nu z}} \quad (21)$$

respectively. These equations reduce to the corresponding Eqs. (16,17) for the linear quench (12) where $r = 1$.

Equation (21) shows that the linear quench is not the best choice if we want to minimize n_{ex} for a given transition time τ_Q , but it is better to take a non-linear exponent $r \gg 1/\nu z$ such that $n_{\text{ex}} \sim \tau_Q^{-d/z}$. This density is less than the density

after the linear quench by a factor

$$\frac{n_{\text{ex}}(r \gg 1/\nu z)}{n_{\text{ex}}(r = 1)} \sim \tau_Q^{-\frac{d}{1+\nu z}} \quad (22)$$

which tends to zero for large τ_Q .

The non-linear quench with a sufficiently large $r \gg 1/\nu z$ is a good choice if we want to improve adiabaticity of the transition. However, the non-linear quench requires better experimental control over a system than the linear quench. Not only $\epsilon(t)$ has to be made non-linear, but it has to be non-linear precisely at the critical point. If not, i.e., when the critical point is misplaced by $\delta\epsilon$,

$$\epsilon(t) = \delta\epsilon - \text{sign}(t) \left| \frac{t}{\tau_Q} \right|^r, \quad (23)$$

then the quench (23) can be linearised as in Eq. (13) and the linearisation is self-consistent for large enough τ_Q when $\hat{\epsilon}$ in Eq. (15) is much less than $\delta\epsilon$. However, as we will see in the next Section and especially in Section 2.20 this technical problem does not arise in some “half-quenches” that are robust enough to begin precisely at a critical point and go into a gapped phase.

2.6. *KZM: from a critical point into a gapped phase*

In the previous Sections we considered adiabatic passage across an isolated quantum critical point separating two gapped phases, where KZM was essentially the adiabatic-impulse-adiabatic approximation. Here we consider a transition from a critical point into a gapped phase and argue that it can be described by an impulse-adiabatic approximation.

As above, the distance from the critical point is measured by the dimensionless parameter

$$\epsilon(t) = \left(\frac{t}{\tau_Q} \right)^r \geq 0, \quad (24)$$

which is in general a non-linear function of time running from 0 to ∞ .

The initial ground state at the critical $\epsilon = 0$ has infinite correlation length while the ground state at a finite $\epsilon > 0$ has a finite correlation length $\xi \sim \epsilon^{-\nu}$. On one hand, in first approximation the two ground states look different on length scales longer than ξ , but they appear the same on distances less than the correlation length. On the other hand, the critical ground state is a non-stationary excited state with a finite density of excitations with respect to the Hamiltonian at the finite $\epsilon > 0$. This excited state and the ground state at $\epsilon > 0$ appear different when we look on a scale much longer than the average distance between the excitations, but they appear the same when we focus on a shorter scale. Consequently, we can identify the density of excitations as $n_{\text{ex}} \simeq \xi^{-1}$.

The evolution with the non-linear ramp (24) is initially non-adiabatic. It becomes adiabatic near \hat{t} when the quench rate $|\dot{\epsilon}/\epsilon| = r/|\hat{t}|$ equals the gap $\Delta \sim \epsilon^{z\nu}$, or equivalently at

$$\hat{\epsilon} \equiv \epsilon(\hat{t}) \sim \tau_Q^{-\frac{r}{1+r\nu z}}. \quad (25)$$

In the crudest impulse-adiabatic approximation, the initial critical ground state

at $\epsilon = 0$ remains the state of the system until $\hat{\epsilon}$ when the evolution becomes adiabatic. Since there is a finite correlation length $\hat{\xi} \sim \hat{\epsilon}^{-\nu}$ in the ground state of the Hamiltonian at $\hat{\epsilon}$, the density of excitations is

$$n_{\text{ex}} \simeq \hat{\xi}^{-d} \sim \tau_Q^{-\frac{d\nu}{1+\nu z}}. \quad (26)$$

It does not change in the following adiabatic evolution after $\hat{\epsilon}$. The density (26) was obtained for the first time in Refs. [39, 42] within the adiabatic perturbation theory reviewed in Section 2.12.

The scaling exponent in Eq. (26) is the same as in the corresponding Eq. (17) for a full passage across a critical point, but there is in general a difference in numerical pre-factors omitted at the excuse of using “ \sim ”. We can expect the n_{ex} in Eq. (26) to be less than that in Eq. (17) because in the “half-quench” starting from the critical point the impulse stage is shorter than in the full passage across this point.

However, a quench from a critical point into a gapped phase is not always a mere half-quench, as illustrated in Section 2.20 by the process of loading a one-dimensional Bose gas (critical Luttinger liquid) into an optical lattice potential. An infinitesimally weak potential induces an energy gap proportional to the potential strength. This is a realistic experiment, see Ref. [8], where a transition into a gapped phase begins exactly at a critical point.

We will make one more comment on the half-quench after Eq. (49) below where we discuss “one-half” of the Landau-Zener transition. In the next Section we describe a more unusual application of KZM to a phase transition that takes place in space rather than happens in time.

2.7. KZM in space

References [44–48] considered a symmetry breaking “phase transition in space” where, instead of being time-dependent, a local parameter $\epsilon(\vec{r})$ is a time-independent function of spatial coordinates \vec{r} . This is a generic scenario in ultracold atom gases confined in magnetic/optical traps, where the trapping potential results in an inhomogeneous density of atoms $\rho(\vec{r})$ and, in general, the critical point g_c depends on the local atomic density. Thus even a perfectly uniform parameter g translates into an inhomogeneous

$$\epsilon(\vec{r}) = \frac{g - g_c[\rho(\vec{r})]}{g_c[\rho(\vec{r})]}, \quad (27)$$

with the critical point on the surface where $\epsilon(\vec{r}) = 0$. The part of the atomic cloud where $\epsilon(\vec{r}) > 0$ is in a different phase than the part where $\epsilon(\vec{r}) < 0$. The phase transition between the two phases coexisting in a trap takes place near the critical surface $\epsilon(\vec{r}) = 0$. A classic example of such a phase coexistence is shown in Fig. 2. Another plausible experimental scenario can be found in Section 2.21 and Fig. 34.

In order to apply KZM in this situation, we proceed in a similar way as in Eq. (13) and linearise

$$\epsilon(x) \approx \alpha (x - x_c), \quad (28)$$

near the critical point at x_c where $\epsilon(x_c) = 0$. Here the gradient α of $\epsilon(\vec{r})$ is along the x -axis. The system is in the broken symmetry phase where $x < x_c$ and in the symmetric phase where $x > x_c$. In the first “local density approximation” (LDA),

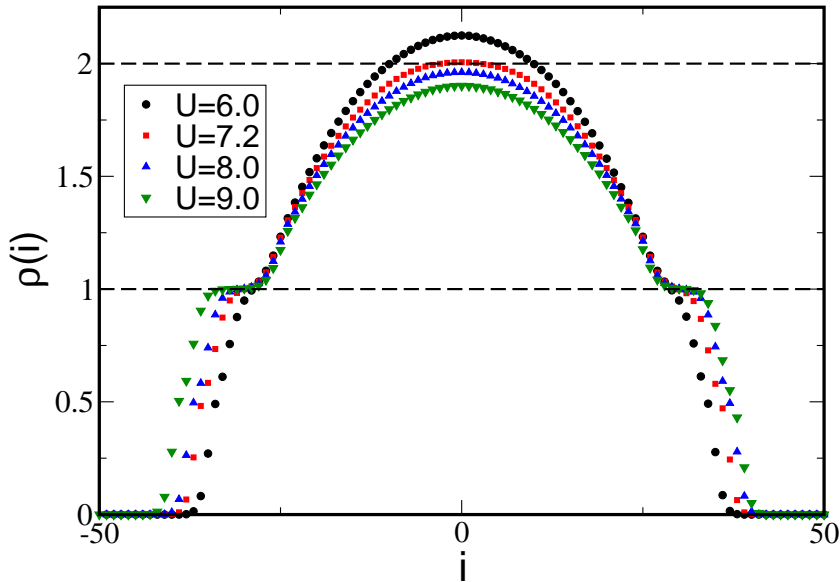


Figure 2. Density profiles in the ground state of the one-dimensional Bose-Hubbard model (229) at different repulsion strengths U [43]. The model describes bosonic atoms in an optical lattice potential subject to additional harmonic trap confinement, compare Fig. 22 for a typical experimental set up. Here $\rho(i)$ is average number of atoms at site i . The dashed lines are to draw attention to density plateaux at the integer value of $\rho = 1$ manifesting areas occupied by incompressible Mott insulator phases. These Mott phases coexist with superfluid phases at non-integer ρ . There are no sharp boundaries between the “integer” Mott and “non-integer” superfluid phases. The phase boundaries are rounded off on a finite length scale $\hat{\xi}$. This scale is long enough to round off plateaux expected at $\rho = 2$. (Figure from Ref.[43]b)

we would expect that the order parameter behaves as if the system were locally uniform, i.e., it is non-zero only for $x < x_c$ and tends to zero as $(x_c - x)^\beta$ when $x \rightarrow x_c^-$ with the critical exponent β , see Fig. 3 .

However, the LDA is not consistent with the divergence of the healing length $\xi \sim |\epsilon|^{-\nu}$ near the critical point. The diverging ξ is the shortest scale of length on which the order parameter can adjust to (or heal with) the varying $\epsilon(x)$. Consequently, when approaching x_c from the broken symmetry side, the local approximation $(x_c - x)^\beta$ must break down when the local correlation length $\xi \sim [\alpha(x_c - x)]^{-\nu}$ equals the distance $(x_c - x)$ remaining to the critical point. Solving this equality with respect to ξ we obtain

$$\hat{\xi} \sim \alpha^{-\frac{\nu}{1+\nu}} . \quad (29)$$

From the point $(x - x_c) \simeq -\hat{\xi}$ the “evolution” of the order parameter in x becomes “impulse”, i.e, the order parameter does not change until $(x - x_c) \simeq +\hat{\xi}$ in the symmetric phase, where it begins to catch up with the local $\epsilon(x) > 0$ and decays to zero on the length scale of $\hat{\xi}$. Thus the “adiabatic-impulse-adiabatic” approximation in space, or the “KZM in space”, predicts that the non-zero order parameter penetrates into the symmetric phase to the depth of $\hat{\xi}$ in Eq. (29). As compared to the non-analytic LDA prediction $(x_c - x)^\beta$, in KZM the order parameter is effectively “rounded off” on the length scale of $\hat{\xi}$, see Fig. 3.

We expect that other physical quantities, which are normally singular or discontinuous at the critical point, are also “rounded off” on the scale of $\hat{\xi}$. In particular, the energy gap that in a homogeneous system vanishes like $\Delta \sim \xi^{-z}$ when ξ di-

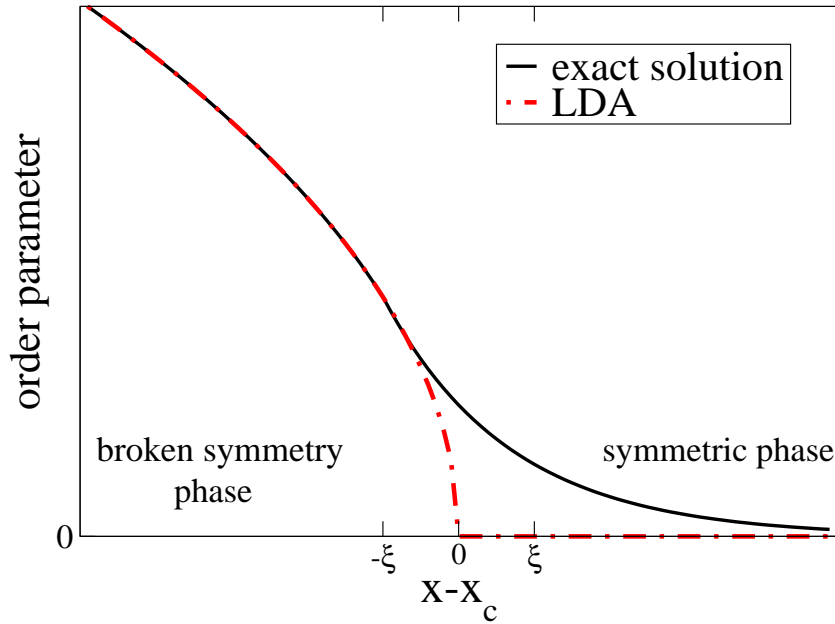


Figure 3. Phase transition in space from a broken symmetry phase to a symmetric phase. Order parameter is shown as a function of position $x - x_c$ with respect to a critical point x_c where $\epsilon(x_c) = 0$. In the local density approximation (LDA) the order parameter is zero in the symmetric phase and follows $(x_c - x)^\beta$ with the critical exponent β in the symmetry broken phase. It is non-analytic at the critical point x_c . In contrast, the exact order parameter in the ground state of the system is rounded off on the length scale $\hat{\xi}$ in Eq. (29). A non-zero order parameter penetrates into the symmetric phase to a depth $\simeq \hat{\xi}$.

verges near the critical point, here should remain finite and scale as ¹

$$\hat{\Delta} \sim \hat{\xi}^{-z} \sim \alpha^{\frac{z\nu}{1+\nu}}. \quad (30)$$

This finite gap sharply contrasts with the LDA, where one might expect gapless quasiparticle excitations localized near the critical point at x_c .

Two examples supporting KZM in space are described in Sections 2.13.11 and 2.21 below. Encouraged by these examples, in the next Section we consider an inhomogeneous phase transition that, in a sense, takes place in both space and time.

2.8. KZM and dynamics of an inhomogeneous phase transition

As pointed out already in the finite temperature context [49, 50], in a realistic experiment it is difficult to make ϵ exactly homogeneous throughout a system. For instance, in the classic superfluid ^3He experiments [26] a phase transition was forced by neutron irradiation of helium 3. Heat released in each fusion event, $n + ^3\text{He} \rightarrow ^4\text{He}$, created a bubble of normal fluid above the superfluid critical temperature T_c . Thanks to quasiparticle diffusion, the bubble was expanding and cooling with a local temperature $T(t, r) = \exp(-r^2/2Dt)/(2\pi Dt)^{3/2}$, where r is a distance from the centre of the bubble and D is a diffusion constant. Since this $T(t, r)$ is hottest in the centre, the transition back to the superfluid phase, driven

¹A non-linear generalization of Eq. (28), $\epsilon(x) = \text{sign}(x - x_c)|\alpha(x - x_c)|^r$, results in a critical point rounded off on a length scale $\hat{\xi} \sim \alpha^{-\nu r/(1+\nu r)}$ and a finite energy gap scaling as $\hat{\Delta} \sim \alpha^{z\nu r/(1+\nu r)}$.

by an inhomogeneous parameter

$$\epsilon(t, r) = \frac{T(t, r) - T_c}{T_c}, \quad (31)$$

proceeded from the outer to the central part of the bubble with a critical front $r_c(t)$, where $\epsilon(t, r_c) = 0$, shrinking with a finite velocity $v = dr_c/dt < 0$.

A similar scenario is likely in the ultracold atom gases in magnetic/optical traps. The trapping potential results in an inhomogeneous density of atoms $\rho(\vec{r})$ and, in general, a critical point g_c depends on atomic density ρ . Thus even a transition driven by a perfectly uniform $g(t)$ is effectively inhomogeneous,

$$\epsilon(t, \vec{r}) = \frac{g(t) - g_c[\rho(\vec{r})]}{g_c[\rho(\vec{r})]}, \quad (32)$$

with the surface of critical front, where $\epsilon(t, \vec{r}) = 0$, moving with a finite velocity.

According to KZM, in a homogeneous symmetry breaking transition, a state after the transition is a mosaic of finite ordered domains of average size $\hat{\xi}$. Within each finite domain the orientation of the order parameter is constant, but uncorrelated to orientations in other domains. In contrast, in an inhomogeneous symmetry breaking transition [49] the parts of the system that cross the critical point earlier may be able to communicate their choice of orientation of the order parameter to the parts that cross the transition later and bias them to make the same choice. Consequently, the final state may be correlated at a range longer than $\hat{\xi}$, or even end up being a ground state with long range order. In other words, the final density of excited quasiparticles may be lower than the KZ estimate in Eq. (17) or even zero.

From the point of view of testing KZM, this inhomogeneous scenario, when relevant, may sound like a negative result because an imperfect inhomogeneous transition suppresses system excitation by KZM. However, from the point of view of adiabatic quantum computation or adiabatic quantum state preparation, it is the KZM itself that is a negative result: no matter how slow the homogeneous transition is, there is a finite density of excitations (17) in the final state which decays only as a power of the transition time τ_Q . From this perspective, the inhomogeneous transition may be the way to suppress KZ excitations and prepare the desired final ground state adiabatically.

In order to estimate if and when the inhomogeneity is actually relevant, we linearise the parameter $\epsilon(t, x)$ in both t and x near the critical front where $\epsilon(t, x) = 0$, as

$$\epsilon(t, x) \approx \alpha (x - vt), \quad (33)$$

in a similar way as in Eq. (12). Here α is an inhomogeneity of the quench and v is velocity of the critical front. When observed locally at a fixed x , the inhomogeneous transition in Eq. (33) looks like the homogeneous quench in Eq. (12) with

$$\tau_Q = \frac{1}{\alpha v}. \quad (34)$$

The part of the system where $x < vt$, or equivalently $\epsilon(t, x) < 0$, is already in the broken symmetry phase. The orientation of the order parameter chosen in this part

can be communicated across the critical point not faster than a threshold velocity

$$\hat{v} \simeq \frac{\hat{\xi}}{\hat{t}}. \quad (35)$$

When $v \gg \hat{v}$ the communication is too slow for the inhomogeneity to be relevant, but when $v \ll \hat{v}$ we can expect the final state to be less excited than predicted by KZM.

Given the relation (34), the condition (35) can be rewritten either as

$$\hat{v} \sim \tau_Q^{-\frac{(z-1)\nu}{z\nu+1}}, \quad (36)$$

$$\hat{v} \sim \alpha^{\frac{\nu(z-1)}{1+\nu}}, \quad (37)$$

or as a relation between the slope and the threshold transition time,

$$\hat{\tau}_Q \sim \alpha^{-\frac{z\nu+1}{1+\nu}}. \quad (38)$$

The last relation means that, for a given inhomogeneity α , the transition is effectively homogeneous when $\tau_Q \ll \hat{\tau}_Q$, but the inhomogeneity becomes relevant when the transition is slow enough and $\tau_Q \gg \hat{\tau}_Q$. In the homogeneous limit of $\alpha \rightarrow 0$ the threshold transition time $\hat{\tau}_Q \rightarrow \infty$.

An example of inhomogeneous transition is solved in detail in Section 2.13.12 and in Refs. [44, 45, 48, 51, 52]. In the next Section we return to the basics and review the Landau-Zener model.

2.9. The Landau-Zener (LZ) model

In this Section we briefly review the Landau-Zener (LZ) model [17] because in a number of integrable models KZM can be derived exactly by mapping a model to a set of independent LZ anti-crossings, see Section 2.11 and the Sections that follow. After this brief review in Section 2.10 we will attempt to invert the relation between the LZ model and KZM and estimate LZ excitation probabilities in the adiabatic-impulse-adiabatic approximation essential for KZM [53, 54].

In dimensionless variables, the LZ model is defined by a two-level time-dependent Hamiltonian

$$H = \frac{1}{2} \begin{pmatrix} \epsilon(t) & 1 \\ 1 & -\epsilon(t) \end{pmatrix} \quad (39)$$

where

$$\epsilon(t) = \frac{t}{\tau_Q} \quad (40)$$

and τ_Q is a transition time. The Hamiltonian passes through an anti-crossing at $\epsilon = 0$. At any fixed ϵ , it has two instantaneous eigenstates: the ground state $|\downarrow(\epsilon)\rangle$ and the excited state $|\uparrow(\epsilon)\rangle$. In the time-independent basis $|1\rangle, |2\rangle$ of the Hamiltonian (39), the instantaneous eigenstates are

$$|\uparrow(\epsilon)\rangle = |1\rangle \cos \frac{\theta}{2} + |2\rangle \sin \frac{\theta}{2}, \quad |\downarrow(\epsilon)\rangle = -|1\rangle \sin \frac{\theta}{2} + |2\rangle \cos \frac{\theta}{2}, \quad (41)$$

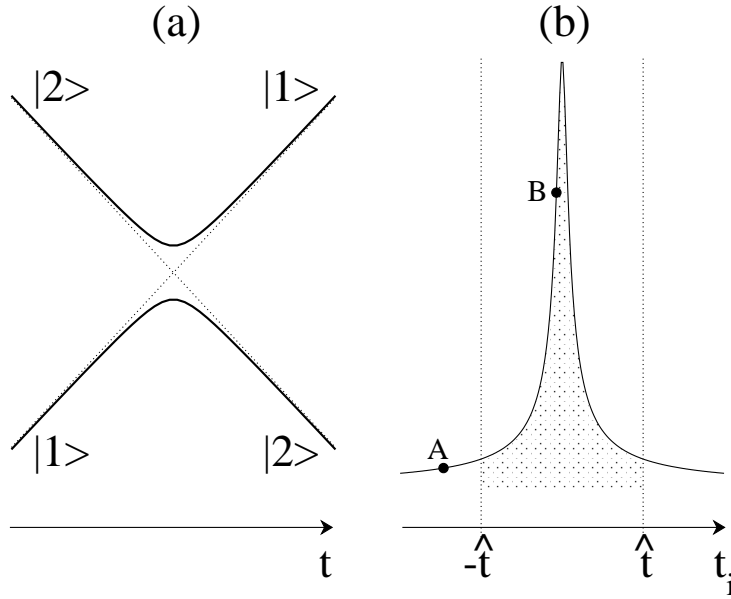


Figure 4. In panel A, the instantaneous energy spectrum of the two-level system in Eq. (39) parametrised by the time t . In panel B, the adiabatic ($t < -\hat{t}$ or $t > \hat{t}$) and impulse regimes ($-\hat{t} < t < \hat{t}$) in the two-level system dynamics. Note the similarity of panel B to Figure 1. (Figure from Ref. [54])

where $\cos \theta = \epsilon/\sqrt{1 + \epsilon^2}$ and $\sin \theta = 1/\sqrt{1 + \epsilon^2}$. Their eigenenergies are $\Delta/2$ and $-\Delta/2$ respectively, where

$$\Delta = \sqrt{1 + \epsilon^2} \quad (42)$$

is an instantaneous energy gap. It is minimal at the anti-crossing centre at $\epsilon = 0$. A good example of the Landau-Zener two level system is the Feshbach resonance in Figure 5, see also Section 2.23.

In the LZ problem the system is prepared in the ground state at an initial time t_i and we want to know the probability P that it is excited at a final time t_f . A general solution to this problem was obtained in Ref. [17] and then analysed in Refs. [54, 56]:

$$|\psi(t)\rangle = \left[|1\rangle \left(2i\partial_t + \frac{t}{\tau_Q} \right) + |2\rangle \right] \left[a D_{-1-i\tau_Q/4}(iz) + b D_{-1-i\tau_Q/4}(-iz) \right] \quad (43)$$

where $z = \frac{t}{\sqrt{\tau_Q}} e^{-i\pi/4}$, $D_m(s)$ is a Weber function [57], and a, b are constants to be determined by initial conditions.

The excitation probability P can be obtained in a closed form in a number of special cases:

- (i) In the textbook case of $t_i \rightarrow -\infty$ and $t_f \rightarrow \infty$ we obtain the exponential LZ formula

$$P = e^{-\pi\tau_Q/2} . \quad (44)$$

- (ii) When the evolution begins at $t_i = 0$ in the ground state at the anti-crossing

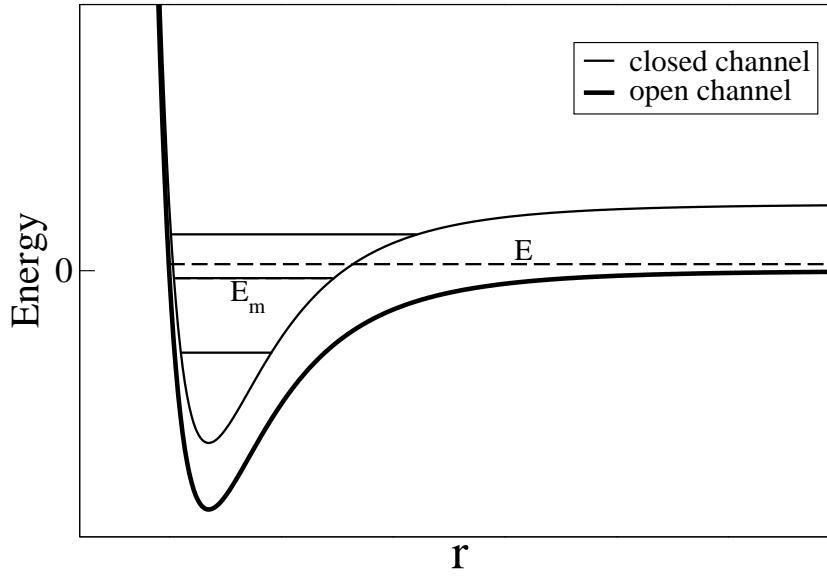


Figure 5. The plot shows a scattering potential for two atoms as a function of their separation r . The scattering potential depends on internal states of the colliding atoms. For a small scattering energy E the atoms can be either in an open (thick solid line) or closed (thin solid line) channel. When one of the bound states in the closed channel with energy E_m is close to the scattering energy $E \approx 0$, then we have the Feshbach resonance [55]. An external magnetic field coupled to magnetic moments of the colliding atoms can shift the energy in the closed channel moving the energy E_m either up or down with respect to the open channel. The field can be used to tune the scattering atoms close to the Feshbach resonance [55]. In Section 2.23 we consider scattering of two fermions, corresponding to fermionic annihilation operators c_\uparrow and c_\downarrow , near resonance with a bound molecular state E_m , corresponding to a bosonic annihilation operator b . A coupling between the two fermions and the molecular state is described by a Landau-Zener Hamiltonian $H = -\frac{1}{2}\epsilon b^\dagger b + \frac{1}{4}\epsilon (c_\uparrow^\dagger c_\uparrow + c_\downarrow^\dagger c_\downarrow) + \frac{1}{2}(b^\dagger c_\downarrow c_\uparrow + c_\uparrow^\dagger c_\downarrow^\dagger b)$. Here ϵ is a distance from the resonance proportional to a difference between the actual and resonant values of the magnetic field. The state with two fermions corresponds to the state |1) and the state with a molecule to the state |2) in Eq. (39). In a scattering of two fermions far from the resonance a weakly occupied molecular state can be eliminated and in a second order perturbative expansion one obtains an effective Hamiltonian for fermions $H_{\text{eff}} = \frac{1}{\epsilon} (c_\uparrow^\dagger c_\uparrow c_\downarrow^\dagger c_\downarrow)$. Depending on the sign of ϵ this is additional repulsion or attraction, so the magnetic field can be used to change the strength and even sign of the interaction between the fermions. This effective interaction strength diverges at $\epsilon = 0$, but this is where the occupation of the molecular state is large so it cannot be eliminated and has to be included explicitly in the calculations.

centre and runs to $t_f \rightarrow \infty$, then according to Refs. [54, 56]

$$P = 1 - \frac{2 \sinh\left(\frac{\pi\tau_Q}{4}\right)}{\pi\tau_Q} e^{-\pi\tau_Q/8} \left| \Gamma\left(1 + \frac{i\tau_Q}{8}\right) + e^{i\pi/4} \sqrt{\frac{\tau_Q}{8}} \Gamma\left(\frac{1}{2} + \frac{i\tau_Q}{8}\right) \right|^2$$

$$\approx \frac{1}{4} \tau_Q^{-2}, \quad (45)$$

where $\Gamma(x)$ is the gamma function [57] and the last approximate form is the asymptote when $\tau_Q \gg 1$. Note that, unlike in the full LZ transition (i), here the probability does not decay exponentially with τ_Q , but only as τ_Q^{-2} .

- (iii) When the evolution runs from $t_i \rightarrow -\infty$ to $t_f = 0$, then the excitation probability P is the same as in case (ii), see Ref. [54, 56].
- (iv) When the LZ problem is not symmetric with respect to the anti-crossing and

$$\epsilon(t) = \begin{cases} \frac{t}{\tau_Q}, & \text{when } t < 0 \\ \frac{t}{\tau_Q \delta}, & \text{when } t \geq 0 \end{cases} \quad (46)$$

with $\delta \neq 1$, then the excitation probability after a passage from $t_i \rightarrow -\infty$

to $t_f \rightarrow +\infty$ is [54, 56]

$$P = 1 - \frac{1}{2} \sinh\left(\frac{\pi\tau_Q\delta}{4}\right) e^{-\frac{\pi(1+\delta)\tau_Q}{8}} \left| \frac{\Gamma\left(\frac{1}{2} + \frac{i\tau_Q\delta}{8}\right)}{\Gamma\left(\frac{1}{2} + \frac{i\tau_Q}{8}\right)} + \sqrt{\frac{1}{\delta}} \frac{\Gamma\left(1 + \frac{i\tau_Q\delta}{8}\right)}{\Gamma\left(1 + \frac{i\tau_Q}{8}\right)} \right|^2$$

$$\approx \frac{1}{4} \left(\frac{1-\delta}{\delta}\right)^2 \tau_Q^{-2}, \quad (47)$$

where the last asymptote is accurate when $\tau_Q \gg 1$. Note that when $\delta \rightarrow \infty$ the second half of the transition becomes adiabatic, the excitation probability does not change in this adiabatic part of the evolution, and the final P becomes the same as in case (iii) where the transition ends at $t_f = 0$.

In the adiabatic limit of $\tau_Q \gg 1$, the excitation probability P is exponentially small in the standard LZ model (i), but in the non-symmetric cases (ii,iii,iv) there is much slower power-law decay $P \sim \tau_Q^{-2}$. In these cases an instantaneous rate of the transition $d\epsilon/dt$ is a discontinuous function of time. For instance, in case (ii)

$$\frac{d\epsilon}{dt} = \begin{cases} 0, & \text{when } t < 0, \\ \frac{1}{\tau_Q}, & \text{when } t \geq 0. \end{cases} \quad (48)$$

The discontinuity at $t = 0$ translates into a fat high frequency tail in the Fourier transform of $\epsilon(t)$ which helps to excite the system despite its finite energy gap. More generally, as discussed in Refs. [17, 39], any non-analytic behaviour of $\epsilon(t)$ results in a power law decay of the excitation probability. A discontinuity in the r -th derivative of $\epsilon(t)$ leads to ¹

$$P \sim \tau_Q^{-2r} \quad (49)$$

for large enough τ_Q .

Case (ii) above is similar to the half-quench in Section 2.6. This connection will become more transparent in Section 2.11, where KZM will be represented as a series of independent LZ transitions. The non-linear parameter $\epsilon(t)$ in Eq. (20) has a discontinuous r -th time derivative at $t = 0$. Since on a microscopic level KZM excitations originate from LZ transitions, then one might expect their density to decay as $n_{\text{ex}} \sim \tau_Q^{-2r}$ for large enough τ_Q . However, in the thermodynamic limit the density of excitations n_{ex} is dominated by contributions from low frequency modes, with wavelength longer than $\hat{\xi}$, whose excitation probabilities are close to 1 and for whom the asymptotic tail in Eq. (49) does not apply.

These comments complete our brief review of the LZ model. In Section 2.11 below the LZ model is applied to derive KZM in a class of exactly solvable models, but in

¹Indeed, in the basis of instantaneous eigenstates (41) the state is $|\psi(t)\rangle = \alpha|\uparrow(\epsilon)\rangle e^{-\frac{1}{2}i \int_{-\infty}^t dt' \Delta[\epsilon(t')]} + \beta|\downarrow(\epsilon)\rangle e^{+\frac{1}{2}i \int_{-\infty}^t dt' \Delta[\epsilon(t')]/2}$. In the adiabatic limit we have $|\alpha| \ll 1, \beta \approx 1$ and, to leading order in the small α , we obtain a perturbative excitation probability

$$P = |\alpha|^2 \approx \left| \int_{-\infty}^{\infty} dt \frac{d\epsilon}{dt} \langle \uparrow | \frac{d}{d\epsilon} | \downarrow \rangle e^{i \int_{-\infty}^t dt' \Delta(t')} \right|^2.$$

The discontinuity in Eq. (48) yields $P \simeq \tau_Q^{-2}$ for $\tau_Q \gg 1$. A more general non-linear

$$\epsilon(t) = \begin{cases} 0, & \text{when } t < 0 \\ (t/\tau_Q)^r, & \text{when } t \geq 0 \end{cases}$$

has a discontinuous r -th derivative at $t = 0$ and we obtain $P \simeq \tau_Q^{-2r}$ for large τ_Q .

the next Section we will attempt to rederive and reinterpret cases (i-iv) using the adiabatic-impulse-adiabatic approximation essential for KZM, see Refs. [53, 54].

2.10. The Landau-Zener model in the adiabatic-impulse approximation

A unitary evolution with the time-dependent Hamiltonian (39) is adiabatic when $t \rightarrow \mp\infty$ and the gap in Eq. (42) is large enough, but it may be not adiabatic near the anti-crossing centre at $t = 0$ where the gap is minimal. In the adiabatic-impulse-adiabatic approximation, the evolution is adiabatic before $-\hat{t}$ and after $+\hat{t}$, but it is impulse between $-\hat{t}$ and $+\hat{t}$, see panel (b) in Figure 4. The crossover time \hat{t} between the adiabatic and impulse stages is the time when the transition rate measured by $|\dot{\epsilon}/\epsilon| = 1/|t|$ equals the instantaneous energy gap in Eq. (42):

$$\sqrt{1 + \left(\frac{\hat{t}}{\tau_Q}\right)^2} = \frac{\alpha}{|\hat{t}|}, \quad (50)$$

where $\alpha \simeq 1$ is an adjustable parameter, compare Fig. 4. The solution is

$$\hat{\epsilon} = \frac{\hat{t}}{\tau_Q} = \frac{1}{\sqrt{2}} \sqrt{\sqrt{1 + \frac{4}{(\alpha\tau_Q)^2}} - 1}. \quad (51)$$

With this estimate at hand, we can reiterate the cases (i-iv) listed in Section 2.9:

- (i) The evolution (39) starts from the instantaneous ground state at $t_i \ll -\hat{t}$ and ends at $t_f \gg \hat{t}$. In the adiabatic stage before $-\hat{t}$ the state follows the instantaneous ground state. Then in the impulse stage between $-\hat{t}$ and $+\hat{t}$ the state does not change and remains equal to the instantaneous ground state $|\downarrow(-\hat{\epsilon})\rangle$ at $-\hat{t}$. Thus in the adiabatic-impulse-adiabatic approximation, the excitation probability at \hat{t} is

$$P_{\text{AI}} = |\langle\uparrow(\hat{\epsilon})|\downarrow(-\hat{\epsilon})\rangle|^2 = \frac{\hat{\epsilon}^2}{1 + \hat{\epsilon}^2} \quad (52)$$

and it does not change in the following adiabatic evolution after \hat{t} . Its expansion up to second power of τ_Q ,

$$P_{\text{AI}} = 1 - \alpha\tau_Q + \frac{(\alpha\tau_Q)^2}{2} + \mathcal{O}(\tau_Q^3), \quad (53)$$

matches the corresponding expansion of the exact exponent in Eq. (44) when we set $\alpha = \pi/2 \simeq 1$.

- (ii) The evolution (39) begins at $t_i = 0$ in the instantaneous ground state $|\downarrow(0)\rangle$ and ends at $t_f \gg \hat{t}$. Since this state does not change in the initial impulse stage of the evolution until \hat{t} , the excitation probability at \hat{t} is

$$P_{\text{AI}} = |\langle\uparrow(\hat{\epsilon})|\downarrow(0)\rangle|^2 = \frac{1}{2} \left(1 - \frac{1}{\sqrt{1 + \hat{\epsilon}^2}}\right), \quad (54)$$

and it does not change in the following adiabatic evolution after \hat{t} . Its

expansion in powers of τ_Q is

$$P_{\text{AI}} = \frac{1}{2} - \frac{1}{2}\sqrt{\alpha\tau_Q} + \frac{1}{8}(\alpha\tau_Q)^{3/2} + \mathcal{O}(\tau_Q^{5/2}), \quad (55)$$

while the corresponding expansion of the exact solution (45) is

$$P = \frac{1}{2} - \frac{\sqrt{\pi\tau_Q}}{4} + \frac{\pi^{3/2}}{64} \left(2 - \frac{4 \ln 2}{\pi} \right) \tau_Q^{3/2} + \mathcal{O}(\tau_Q^{5/2}). \quad (56)$$

Given that $2 - 4 \ln 2 / \pi = 1.1 \approx 1$, the two expansions are in good agreement when we choose $\alpha = \pi/4 \simeq 1$.

- (iii) The evolution (39) begins at $t_i \ll -\hat{t}$ and ends at $t_f = 0$. It is adiabatic before $-\hat{t}$ and impulse from $-\hat{t}$ to 0. In the impulse stage the state remains the instantaneous ground state $|\downarrow(-\hat{\epsilon})\rangle$ at $-\hat{t}$. Similarly as for the exact solution, the final excitation probability $P_{\text{AI}} = |\langle \uparrow(0) | \downarrow(-\hat{\epsilon}) \rangle|^2$ is the same as in case (ii).
- (iv) The evolution (39) begins in the ground state at $t_i \ll -\hat{t}$ and ends at $t_f \gg \hat{t}_\delta$. The transition is not symmetric: when $t > 0$ the transition time is $\tau_Q \delta$ instead of τ_Q for $t < 0$. Consequently, the crossover from the adiabatic to impulse stage takes place near $-\hat{t}$ as before, but the second crossover from the impulse to adiabatic stage is at \hat{t}_δ given by Eq. (51), but with τ_Q replaced by $\tau_Q \delta$. Similarly as in case (i), the excitation probability is

$$\begin{aligned} P_{\text{AI}} &= |\langle \uparrow(\hat{\epsilon}_\delta) | \downarrow(-\hat{\epsilon}) \rangle|^2 \\ &= 1 - \frac{1}{4} (1 + \sqrt{\delta})^2 \alpha \tau_Q + \frac{1}{16} (1 + \delta)(1 + \sqrt{\delta})^2 (\alpha \tau_Q)^2 + \mathcal{O}(\tau_Q^3), \end{aligned} \quad (57)$$

while the corresponding expansion of the exact solution (47) is

$$P = 1 - \frac{\pi}{8} (1 + \sqrt{\delta})^2 \tau_Q + \frac{\pi^2}{64} (1 + \delta)(1 + \sqrt{\delta})^2 \tau_Q^2 + \mathcal{O}(\tau_Q^3). \quad (58)$$

The two expansions match when we set $\alpha = \pi/2 \simeq 1$.

In all cases, after fitting only one adjustable parameter $\alpha \simeq 1$, we obtain accurate leading and next-to-leading order terms of the expansion in powers of τ_Q , so the adiabatic-impulse-adiabatic approximation is accurate when $\tau_Q \ll 1$ and the excitation probability P is substantial. Since the KZM excitation density n_{ex} in Eq. (17) is dominated by contributions from long wavelength modes, whose excitation probability is close to 1, the adiabatic-impulse-adiabatic approximation can accurately predict n_{ex} . The approximation is not accurate for long wavelength modes, but their contribution to the total n_{ex} is negligible.

In view of the above conclusion, it is not quite surprising that in the next Section the LZ model provides exact solutions which are consistent with KZM.

2.11. KZM as a set of independent Landau-Zener transitions

The KZM argument in Section 2.3 was confirmed by exact solutions in a number of integrable models, see e.g. Ref. [35, 37, 38, 58, 59] and the following Sections. There is, however, an assumption in Section 2.3 that the transition passes through an isolated quantum critical point between two gapped phases. As demonstrated by exact solutions in a number of integrable models, KZM does require careful

generalisation for a transition across a multicritical point [60, 61], along a gapless line [62], or across a gapless phase [63]. The generalisation was obtained in integrable spin models, such as the XY spin chain or the two-dimensional Kitaev model [64], all of which can be mapped to non-interacting fermions by a Jordan-Wigner transformation [18]. A transition in a translationally invariant system of non-interacting fermions can be mapped to a set of independent LZ anti-crossings. The general LZ argument summarized in this Section was gradually developed in Refs. [35, 37, 53, 58–63, 65–68].

We assume a general local Hamiltonian quadratic in fermionic creation/annihilation operators and translationally invariant on a d -dimensional lattice. Its quasimomentum representation is

$$H = \frac{1}{2} \sum_{\vec{k}} \begin{pmatrix} c_{\vec{k}}^\dagger & c_{-\vec{k}} \end{pmatrix} H_{\vec{k}} \begin{pmatrix} c_{\vec{k}} \\ c_{-\vec{k}}^\dagger \end{pmatrix}, \quad (59)$$

where \vec{k} is a quasimomentum running over the first Brillouin zone, $c_{\vec{k}}$ is fermionic annihilation operator, and $H_{\vec{k}}$ is a 2×2 Hermitian matrix. The Hamiltonian can be diagonalized by a Bogoliubov transformation

$$c_{\vec{k}} = u_{\vec{k}} \gamma_{\vec{k}} + v_{-\vec{k}}^* \gamma_{-\vec{k}}^\dagger, \quad (60)$$

where $\gamma_{\vec{k}}$ annihilates a fermionic Bogoliubov quasiparticle, and $(u_{\vec{k}}, v_{\vec{k}})$ is an eigenmode of stationary Bogoliubov-de Gennes equations

$$\omega_{\vec{k}} \begin{pmatrix} u_{\vec{k}} \\ v_{\vec{k}} \end{pmatrix} = H_{\vec{k}} \begin{pmatrix} u_{\vec{k}} \\ v_{\vec{k}} \end{pmatrix} \quad (61)$$

with positive eigenfrequency $\omega_{\vec{k}}$. The diagonalized Hamiltonian is $H = \sum_{\vec{k}} \omega_{\vec{k}} \left(\gamma_{\vec{k}}^\dagger \gamma_{\vec{k}} - \frac{1}{2} \right)$. Its ground state is a Bogoliubov vacuum $|0\rangle$ annihilated by all $\gamma_{\vec{k}}$. This ground state is an initial state for a dynamical quantum phase transition.

A time-dependent problem can be solved in the Heisenberg picture, where the state remains the initial Bogoliubov vacuum $|0\rangle$, but the operators $c_{\vec{k}}$ evolve in time. Their evolution can be conveniently described by time-dependent modes $(u_{\vec{k}}, v_{\vec{k}})$ in Eq. (60). Indeed, given that $\gamma_{\vec{k}}$ remains time-independent in the Heisenberg picture, a Heisenberg equation $i \frac{d}{dt} c_{\vec{k}} = [c_{\vec{k}}, H(t)]$ is equivalent to time-dependent Bogoliubov-de Gennes equations

$$i \frac{d}{dt} \begin{pmatrix} u_{\vec{k}} \\ v_{\vec{k}} \end{pmatrix} = H_{\vec{k}}(t) \begin{pmatrix} u_{\vec{k}} \\ v_{\vec{k}} \end{pmatrix}. \quad (62)$$

Thus the problem was separated into a set of independent two-level systems enumerated by \vec{k} .

For each \vec{k} , an initial state $[u_{\vec{k}}(-\infty), v_{\vec{k}}(-\infty)]$ is the positive- $\omega_{\vec{k}}$ eigenmode of Eq. (61) with the initial $H_{\vec{k}}(-\infty)$. This positive eigenmode represents the initial vacuum ground state for the quasiparticle $\gamma_{\vec{k}}$. What we want to know is a probability $p_{\vec{k}}$ that after the dynamical transition a quasiparticle $\gamma_{\vec{k}}$ of the final Hamiltonian $H(\infty)$ is excited. Since this excited state is represented by the negative eigenmode of Eq. (61) with eigenfrequency $-\omega_{\vec{k}}$, then $p_{\vec{k}}$ is equal to the probability that the solution of Eq. (62) ends in the negative eigenmode of the final $H_{\vec{k}}(\infty)$ or, simply, the initially excited two-level system becomes deexcited. This is essentially the

same question as in the Landau-Zener (LZ) model in Section 2.9 so in order to answer this question we map Eq. (62) to the LZ model in Eq. (39).

Near a quantum phase transition driven by a parameter ϵ the two-level Hamiltonian can be linearised, or is linear, in the small ϵ :

$$H_{\vec{k}}(t) = \epsilon(t) \sigma(\vec{k}) + \sigma'(\vec{k}). \quad (63)$$

Here $\sigma(\vec{k}) = \sum_i a_i(\vec{k}) \sigma^i$, σ^i with $i = x, y, z$ are Pauli matrices, $\sigma'(\vec{k}) = \sum_i a'_i(\vec{k}) \sigma^i$, a_i and a'_i are model-dependent functions, and $\epsilon(t) = t/\tau_Q$ is the dimensionless parameter in Eq. (12) quenched from $t \rightarrow -\infty$ to $t \rightarrow +\infty$. Notice that in this general Hamiltonian we ignored a c -number term proportional to the 2×2 identity matrix because it would contribute to the global phase only, but see Ref. [69]. The instantaneous eigenvalues of the Hamiltonian $H_{\vec{k}}$ are $\pm\omega_{\vec{k}}$, where

$$\omega_{\vec{k}} = \sqrt{(\epsilon \vec{a} + \vec{a}')^2}. \quad (64)$$

The question is what is the probability for the initially excited state $+\omega_{\vec{k}}$ to become deexcited to the ground state $-\omega_{\vec{k}}$?

To answer this question, we map the general Eqs. (62,63) to the LZ model (39). The main obstacle is that, unlike in the LZ model, the “spin matrices” σ and σ' in the Hamiltonian (63) are not necessarily pointing in orthogonal directions. This minor problem can be easily fixed by orthonormalisation¹. The orthonormalised Hamiltonian is

$$H_{\vec{k}}(t) = \left[a(\vec{k}) \epsilon(t) + b(\vec{k}) \right] \hat{\sigma}(\vec{k}) + \Delta(\vec{k}) \hat{\sigma}_{\perp}(\vec{k}) \quad (65)$$

with instantaneous quasiparticle spectrum

$$\omega_{\vec{k}} = \sqrt{\left[\epsilon a(\vec{k}) + b(\vec{k}) \right]^2 + \Delta^2(\vec{k})}. \quad (66)$$

We can eliminate $b(\vec{k})$ by shifting the time variable in $\epsilon(t) = t/\tau_Q$ to $t' = t + \tau_Q b(\vec{k})/a(\vec{k})$:

$$H_{\vec{k}}(t') = \frac{t'}{\tau_Q} a(\vec{k}) \hat{\sigma}(\vec{k}) + \Delta(\vec{k}) \hat{\sigma}_{\perp}(\vec{k}). \quad (67)$$

Up to an unimportant rotation of “spin” quantization axes, this is the Landau-Zener Hamiltonian (39) and we can use the LZ formula for the (de)excitation probability

$$p_{\vec{k}} = \exp\left(-\frac{\pi \tau_Q \Delta^2(\vec{k})}{a(\vec{k})}\right). \quad (68)$$

¹Indeed, we rewrite the matrix $\sigma(\vec{k}) = a(\vec{k})\hat{\sigma}(\vec{k})$, where $a = \sqrt{\vec{a}^2}$ is the length of vector \vec{a} , and $\hat{\sigma}(\vec{k}) = \sum_i \hat{a}_i(\vec{k})\sigma^i$ is a normalized Pauli spin matrix pointing along the unit vector $\hat{a}(\vec{k}) = \vec{a}(\vec{k})/a(\vec{k})$. Next, we decompose $\sigma'(\vec{k}) = b(\vec{k})\hat{\sigma}(\vec{k}) + \Delta(\vec{k})\hat{\sigma}_{\perp}(\vec{k})$, where $b(\vec{k}) = \hat{a}(\vec{k}) \cdot \vec{a}'(\vec{k})$ is the component of vector $\vec{a}'(\vec{k})$ along the unit vector $\hat{a}(\vec{k})$, $\vec{a}_{\perp}(\vec{k}) = \vec{a}'(\vec{k}) - b(\vec{k})\hat{a}(\vec{k})$ is the component of $\vec{a}'(\vec{k})$ orthogonal to $\hat{a}(\vec{k})$, $\Delta(\vec{k}) = \sqrt{\vec{a}_{\perp}(\vec{k})^2}$ is the length of the orthogonal component, and $\hat{\sigma}_{\perp} = \sum_i \frac{a'_{\perp i}(\vec{k})}{\Delta(\vec{k})} \sigma^i$ is a normalized Pauli spin matrix pointing perpendicular to $\hat{\sigma}(\vec{k})$.

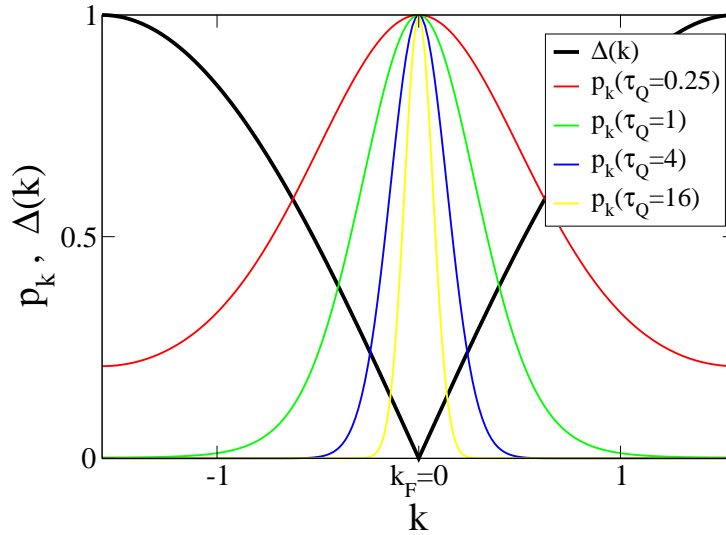


Figure 6. The minimal gap function $\Delta(k) = |2\sin(k)|$ and excitation probability $p_k = \exp\left(-\frac{\pi\tau_Q\Delta^2(k)}{2}\right)$ for different quench times τ_Q in the one-dimensional transverse field quantum Ising chain in Section 2.13. The gap function is zero at the Fermi point $k_F = 0$. With increasing τ_Q the excitation probability becomes a Gaussian $p_k \approx \exp(-2\pi\tau_Q k^2)$ localised around the Fermi point. Its integral $n_{\text{ex}} = \int \frac{dk}{2\pi} p_k = \frac{1}{2\sqrt{2\pi}} \tau_Q^{-1/2}$ is the density of excited quasiparticles.

Consequently, the density of quasiparticles is an average of $p_{\vec{k}}$ over the first Brillouin zone

$$n_{\text{ex}} = \frac{1}{N} \sum_{\vec{k}} p_{\vec{k}} \approx \int \frac{d^d k}{(2\pi)^d} p_{\vec{k}}, \quad (69)$$

where N is a number of lattice sites and the integral becomes accurate in the thermodynamic limit $N \rightarrow \infty$.

In order to evaluate the integral in Eq. (69), we note that in the LZ Hamiltonian (67) the minimal instantaneous gap at $t' = 0$ is twice $\Delta(\vec{k})$. It vanishes on a ‘‘Fermi manifold’’ (point/line/surface) in quasimomentum space where

$$\Delta(\vec{k}) = 0. \quad (70)$$

Consequently, Eq. (68) implies that $p_{\vec{k}} = 1$ only on the Fermi manifold and, in the adiabatic limit $\tau_Q \rightarrow \infty$, the integrand $p_{\vec{k}}$ in Eq. (69) remains non-negligible only very close to the Fermi manifold, see the examples in Figures 6 and 7. In this limit the integral (69) can be easily done in a few special cases:

- (i) When the quench runs through an isolated critical point between two gapped phases, as in Section 2.3, then there is an isolated Fermi point \vec{k}_F where $\Delta(\vec{k}_F) = 0$. When the Fermi point is isotropic in \vec{k} -space, then the gap vanishes like

$$\Delta^2(\vec{k}) \sim |\vec{k} - \vec{k}_F|^{z_\Delta} \quad (71)$$

near \vec{k}_F , and the integral in Eq. (69) yields

$$n_{\text{ex}} \sim \tau_Q^{-d/z_\Delta}, \quad (72)$$

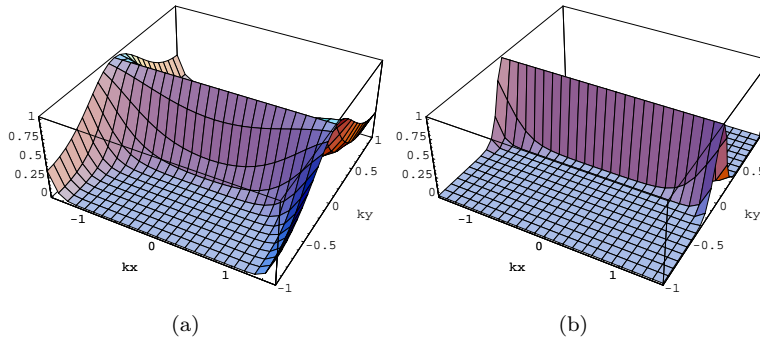


Figure 7. In the two-dimensional Kitaev model on a honeycomb lattice in Section 2.15 the minimal gap function is $\Delta(\vec{k}) = 2[J_1 \sin(\vec{k}\vec{M}_1) - J_2 \sin(\vec{k}\vec{M}_2)]$, where $\vec{M}_1 = \frac{\sqrt{3}}{2}\hat{i} + \frac{3}{2}\hat{j}$ and $\vec{M}_2 = \frac{\sqrt{3}}{2}\hat{i} - \frac{3}{2}\hat{j}$ are spanning vectors of triangular reciprocal lattice. Here we assume $J_x = J_y = 1$ so that the Fermi line is $k_y = 0$. The 3D plots show excitation probabilities $p_{\vec{k}}$ for $\tau_Q = 1$ (left panel) and $\tau_Q = 16$ (right panel). With increasing τ_Q the excitation probability localizes on the Fermi line.

when τ_Q is large enough for $p_{\vec{k}}$ to be localised close enough to \vec{k}_F . Examples of case (i) are the transverse field quantum Ising chain in Section 2.13 and the quench across a multicritical point of the transverse field XY chain in Section 2.14.

- (ii) More generally, when an isolated Fermi point in d dimensions is not isotropic and has different critical exponents in different directions, then the density of excitations scales as

$$n_{\text{ex}} \sim \tau_Q^{-\left(\frac{m\nu}{1+\nu z} + \frac{(d-m)\nu_{\perp}}{1+\nu_{\perp} z_{\perp}}\right)} \quad (73)$$

for large enough τ_Q . Here the exponents z, ν and z_{\perp}, ν_{\perp} apply in respectively m and $(d-m)$ directions. This is the case of the semi-Dirac points in optical lattices considered in Ref. [67].

- (iii) When the Fermi manifold is an m -dimensional surface and the minimal gap depends on the distance from the Fermi surface as $\Delta^2(\vec{k}) \sim |\vec{k} - \vec{k}_F|^{z_{\Delta}}$, where \vec{k}_F is the point on the Fermi surface closest to \vec{k} , then the integration in Eq. (69) yields

$$n_{\text{ex}} \sim \tau_Q^{-(d-m)/z_{\Delta}} \quad (74)$$

when τ_Q is large enough. An interesting example is the 2D Kitaev model in Section 2.15 and Ref. [63], see Figure 7.

- (iv) When, as in case (iii), the Fermi manifold is an m -dimensional surface with $\Delta^2(\vec{k}) \sim |\vec{k} - \vec{k}_F|^{z_{\Delta}}$ near a generic point \vec{k}_F on the surface, but there is an isolated “dominant” Fermi point \vec{k}_F^D where $\Delta^2(\vec{k}) \sim |\vec{k} - \vec{k}_F^D|^{z_{\Delta}^D}$ with $z_{\Delta}^D < z_{\Delta}$, then the integral in Eq. (69) is dominated by a neighbourhood of the dominant Fermi point and

$$n_{\text{ex}} \sim \tau_Q^{-d/z_{\Delta}^D} \quad (75)$$

when τ_Q is large enough. An example can be found in Ref. [35].

Case (i) is the problem treated in Section 2.3 by the standard KZM, while cases (ii-iv) are generalisations that go beyond that simple argument. However, even in

case (i) we obtain the density of excitations (72) with an exponent d/z_Δ which in principle can be different than the exponent $d\nu/(1+\nu z)$ in the KZM equation (2.3), unless

$$z_\Delta \stackrel{?}{=} \frac{1+\nu z}{\nu} . \quad (76)$$

Here z_Δ on the left hand side characterizes the minimal gap function $\Delta(\vec{k})$ while the critical exponents z, ν on the right hand side characterize the critical point.

To see if the relation (76) holds, we return to the Hamiltonian (65) with the quasiparticle spectrum (66). Without loss of generality, we can assume that $b(\vec{k}_F) = 0$ at the Fermi point ¹ and its asymptote near \vec{k}_F is

$$b^2(\vec{k}) \sim |\vec{k} - \vec{k}_F|^{z_b} . \quad (77)$$

On one hand, the critical exponents z and ν are defined by the asymptotes near the Fermi point: $\omega_{\vec{k}} \sim |\vec{k} - \vec{k}_F|^z$ at $\epsilon = 0$ and $\omega_{\vec{k}_F} \sim |\epsilon|^{\nu z}$ for small ϵ , see Ref. [15]. On the other hand, the actual asymptotes of the spectrum (66) are $\omega_{\vec{k}} \sim |\vec{k} - \vec{k}_F|^{\frac{1}{2}\min(z_b, z_\Delta)}$ at $\epsilon = 0$ and $\omega_{\vec{k}_F} \sim |\epsilon|^1$ for small ϵ . Comparing the definitions with the actual asymptotes we obtain $z = \frac{1}{2}\min(z_b, z_\Delta)$ and $\nu z = 1$. The equality (76) holds if

$$z_\Delta \leq z_b \quad (78)$$

or, equivalently, near the Fermi point the function $b^2(\vec{k})$ is negligible as compared to $\Delta^2(\vec{k})$. The inequality is the condition for the KZM argument in Section 2.3 to give the same scaling as the exact solution in case (i).

This condition may be not quite surprising because when we neglect $b^2(\vec{k})$, then for each \vec{k} the instantaneous gap in Eq. (66) is minimised at the critical point $\epsilon = 0$. Since the critical point is the anti-crossing center for each \vec{k} , the dynamical excitation of each two-level system takes place near the critical point, so the excitation probabilities $p_{\vec{k}}$ must be determined by the critical exponents that characterize the quasiparticle spectrum near this critical point. Given the accumulated evidence, the condition (78) seems to be satisfied by most quenches across an isolated quantum critical point, but it is not fulfilled by quenches across a multicritical point considered in Refs. [60, 61] and Section 2.14.

For instance, in the quench considered in Section 2.14 one finds $z_\Delta = 6, z_b = 4$ and $z = 1/\nu = 2$, the inequality (78) is not satisfied, and the exact scaling $n_{\text{ex}} \sim \tau_Q^{-1/6}$ in Eq. (72) is different than the $n_{\text{ex}} \sim \tau_Q^{-1/4}$ predicted by Eq. (17). In this example $b^2(\vec{k})$ is not negligible, so it shifts the anti-crossings away from the critical point, and the excitation probabilities $p_{\vec{k}}$ are dominated by non-critical energy modes away from $\epsilon = 0$. The shifts, and the anomalous exponent 1/6, originate in the fact that the dynamical excitation process takes place asymmetrically with respect to the multicritical point. As a consequence, dynamical scaling may require introducing new non-static exponents ²

¹This can be always achieved by a \vec{k} -independent shift $\epsilon' = \epsilon + b(\vec{k}_F)/a(\vec{k}_F)$.

²Indeed, the effective Hamiltonian (67) has instantaneous spectrum $\omega'_{\vec{k}} = \sqrt{(\epsilon')^2 + \Delta^2}$, where $\epsilon' = t'/\tau_Q$. From this spectrum we formally obtain effective exponents $z' = z_\Delta/2$ and $\nu' z' = 1$. With these effective exponents z' and ν' in place of the ‘‘canonical’’ z and ν , the KZM Eq. (17) gives the exact scaling in Eq. (72).

In this Section we obtained exact scalings by mapping a class of integrable fermionic systems to the LZ model. In the next Section we rederive the KZM scaling in Eq.(17) from the adiabatic perturbation theory. This approximate derivation does not seem limited to integrable models.

2.12. KZM from adiabatic perturbation theory

An alternative derivation of the KZ scaling in Eq. (17) was presented in Refs. [39, 70]. In the integrable models equivalent to non-interacting fermions considered in the previous Section, this derivation is a perturbative approximation to the exact LZ argument, but its validity does not seem limited to integrable models. The argument is as follows.

Let the set of functions $\phi_p(\epsilon)$ represent an eigenbasis of a Hamiltonian $H(\epsilon)$ depending on a parameter ϵ . A wave function of the system can be expanded in the eigenbasis

$$\psi = \sum_p a_p(r) \phi_p(\epsilon) . \quad (79)$$

We assume the linear $\epsilon(t) = t/\tau_Q$ in Eq. (12) with a large $\tau_Q \rightarrow \infty$. The Schrödinger equation is equivalent to

$$i \frac{da_p}{dt} + \frac{i}{\tau_Q} \sum_q a_q \langle p | \frac{d}{d\epsilon} | q \rangle = \omega_p a_p , \quad (80)$$

where $\omega_p(\epsilon)$ is the eigenenergy of the Hamiltonian $H(\epsilon)$ corresponding to the eigenstate $\phi_p(\epsilon)$ (or $|p\rangle$). After a unitary transformation eliminating the dynamical phase

$$a_p(t) = \tilde{a}_p(t) e^{-i \int^t dt' \omega_p[\epsilon(t')]} = \tilde{a}_p(\epsilon) e^{-i \tau_Q \int^\epsilon d\epsilon' \omega_p(\epsilon')} , \quad (81)$$

the Schrödinger equation becomes

$$\frac{d\tilde{a}_p}{d\epsilon} = - \sum_q \tilde{a}_q(\epsilon) \langle p | \frac{d}{d\epsilon} | q \rangle e^{i \tau_Q \int^\epsilon d\epsilon' [\omega_p(\epsilon') - \omega_q(\epsilon')]} . \quad (82)$$

Since the system were initially prepared in the ground state $|0\rangle$, then in the adiabatic limit the single term $q = 0$ dominates the sum and the excitation probability is given by

$$P_{\text{ex}} \approx \sum_{p \neq 0} \left| \int_{-\infty}^{\infty} d\epsilon \langle p | \frac{d}{d\epsilon} | 0 \rangle e^{i \tau_Q \int^\epsilon d\epsilon' [\omega_p(\epsilon') - \omega_0(\epsilon')]} \right|^2 . \quad (83)$$

The derivative of the ground state $\frac{d}{d\epsilon}|0\rangle$ is finite at a continuous phase transition.

We assume a uniform d -dimensional system with a single (relevant) branch of excitations which can be labelled by (quasi-)momentum \vec{k} . The branch has a dispersion relation with a gap $\Delta(\epsilon)$. The gap is non-zero everywhere except the critical point at $\epsilon = 0$, where it vanishes like $\Delta \sim |\epsilon|^{\nu_z}$ and the excitation $\vec{k} = 0$ is gapless. Conservation of momentum implies that only pairs of excitations with opposite momenta $(\vec{k}, -\vec{k})$ can be excited by the time-dependent ϵ . In this framework, Eq.

(83) gives the following density of excitations

$$n_{\text{ex}} \approx \int \frac{d^d k}{(2\pi)^d} p_{\vec{k}} , \quad (84)$$

$$p_{\vec{k}} \approx \left| \int_{-\infty}^{\infty} d\epsilon \langle \vec{k}, -\vec{k} | \frac{d}{d\epsilon} |0\rangle e^{i\tau_Q \int_{-\infty}^{\epsilon} d\epsilon' [\omega_{\vec{k}}(\epsilon') - \omega_0(\epsilon')]} \right|^2 , \quad (85)$$

Here $|\vec{k}, -\vec{k}\rangle$ is an excited state with one pair of excitations of opposite momenta $\pm\vec{k}$.

A general scaling argument implies that

$$\omega_{\vec{k}}(\epsilon) - \omega_0(\epsilon) = \Delta F(\Delta/k^z) = |\epsilon|^{z\nu} \tilde{F}(|\epsilon|^{z\nu}/k^z) , \quad (86)$$

where $k = |\vec{k}|$ and F (or \tilde{F}) is a non-universal function with a universal tail $F(x) \sim 1/x$ for large x . Substituting Eq. (86) to Eq. (85) we obtain

$$p_{\vec{k}} \approx \left| \int_{-\infty}^{\infty} dx \langle \vec{k}, -\vec{k} | \frac{d}{dx} |0\rangle e^{i(\tau_Q k^{\frac{1+z\nu}{\nu}}) \int_{-\infty}^x dx' |x'|^{z\nu} \tilde{F}(|x'|^{z\nu})} \right|^2 , \quad (87)$$

where $x = k^{-1/\nu}\epsilon$ and $x' = k^{-1/\nu}\epsilon'$. Another scaling argument

$$\langle \vec{k}, -\vec{k} | \frac{\partial}{\partial \Delta} |0\rangle = \frac{1}{k^z} G(\Delta/k^z) \rightarrow \langle \vec{k}, -\vec{k} | \frac{\partial}{\partial \epsilon} |0\rangle = \text{sign}(\epsilon) \frac{|\epsilon|^{z\nu-1}}{k^z} \tilde{G}(|\epsilon|^{z\nu}/k^z) \quad (88)$$

transforms Eq. (87) into

$$p_{\vec{k}} \approx \left| \int_{-\infty}^{\infty} dx \text{sign}(x) |x|^{z\nu-1} \tilde{G}(|x|^{z\nu}) e^{i(\tau_Q k^{\frac{1+z\nu}{\nu}}) \int_{-\infty}^x dx' |x'|^{z\nu} \tilde{F}(|x'|^{z\nu})} \right|^2 , \quad (89)$$

which depends on k only through the dimensionless combination $\tau_Q k^{\frac{1+z\nu}{\nu}}$. This means that there is a characteristic wave vector

$$\hat{k} \simeq \tau_Q^{-\frac{\nu}{1+z\nu}} , \quad (90)$$

corresponding to the KZ wavelength $\hat{\xi} \simeq \hat{k}^{-1}$ in Eq. (16). The \hat{k} marks a crossover between a regime of large $k \gg \hat{k}$, where the adiabatic approximation is self-consistent and Eq. (89) accurately predicts small p_k , and a regime of small $k \ll \hat{k}$ where we do not expect Eq. (89) to be accurate. It is expected to be an overestimate for fermionic excitations and an underestimate for bosons.

Since \hat{k} is the only momentum scale in Eq. (84), then for dimensional reasons the integration yields

$$n_{\text{ex}} \simeq \hat{k}^d \simeq \hat{\xi}^{-d} \sim \tau_Q^{-\frac{d\nu}{1+z\nu}} \quad (91)$$

up to possible logarithmic corrections [70]. This is again the KZ equation (17).

This Section completes our general discussion of KZM. The following Sections provide specific examples in a number of model systems.

2.13. Quantum Ising chain: transition across an isolated critical point

Much of our understanding of quantum phase transitions is based on the prototypical integrable quantum Ising chain [15]

$$H = - \sum_{n=1}^N (g \sigma_n^z + \sigma_n^x \sigma_{n+1}^x) \quad (92)$$

with periodic boundary conditions $\sigma_{N+1} = \sigma_1$. In the thermodynamic limit $N \rightarrow \infty$ the model has two critical points at $g_c = \pm 1$ between a ferromagnetic phase when $|g| < 1$ and two paramagnetic phases when $|g| > 1$. Their critical exponents are $z = \nu = 1$. Today the quantum Ising chain is not only an exactly solvable toy model, but it is also becoming a subject of quantum simulation in experiments: the NMR simulation in Ref. [11] and the ion trap experiment in Ref. [9], see Figs. 8 and 9 respectively.

Here, like in Refs. [36–38, 58], we consider a linear ramp

$$g(t) = - \frac{t}{\tau_Q} \quad (93)$$

with t running from $-\infty$ to 0 across the critical point at $g_c = 1$. The quench begins at $g \rightarrow \infty$ in the ground state $|\uparrow\uparrow\uparrow \dots \uparrow\rangle$ with all spins polarized along the z -axis. At the final $g = 0$ there are two degenerate ferromagnetic ground states with all spins pointing either left or right along the x -axis: $|\rightarrow\rightarrow\rightarrow \dots \rightarrow\rangle$ or $|\leftarrow\leftarrow\leftarrow \dots \leftarrow\rangle$. In an adiabatic classical transition from the paramagnetic to ferromagnetic phase, the system would choose one of the two ferromagnetic states. In the analogous quantum case, any superposition of these two states is also a ‘legal’ ground state providing it is consistent with other quantum numbers conserved by the transition from the initial paramagnetic state.

However, when $N \rightarrow \infty$, then energy gap at $g = 1$ tends to zero (quantum version of the critical slowing down) and it is impossible to pass the critical point at a finite speed without exciting the system. As a result, the system ends in a quantum superposition of states like

$$|\dots \rightarrow\leftarrow\leftarrow\leftarrow\leftarrow\leftarrow\rightarrow\rightarrow\rightarrow\rightarrow\rightarrow\rightarrow\leftarrow\leftarrow\leftarrow\leftarrow\rightarrow\rightarrow\rightarrow\rightarrow\rightarrow\leftarrow \dots\rangle \quad (94)$$

with finite domains of spins pointing left or right and separated by kinks where the polarisation of spins changes its orientation. Average size of the domains or, equivalently, average density of kinks depends on the transition rate. When the transition is slow, then the domain size is large, but when it is very fast, then orientation of individual spins can become random, uncorrelated with their nearest neighbours.

When we define a dimensionless parameter

$$\epsilon = \frac{g - g_c}{g_c} = g - 1, \quad (95)$$

then according to KZM in Section 2.3 the evolution is adiabatic before $\hat{\epsilon} \simeq \sqrt{\tau_Q}$ and after $-\hat{\epsilon}$, and impulse near the critical point. The correlation length in the adiabatic ground state at $\hat{\epsilon}$ is proportional to

$$\hat{\xi} = \tau_Q^{1/2}. \quad (96)$$

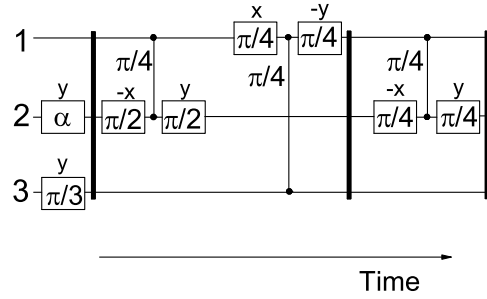


Figure 8. NMR gate sequence to prepare an effective pure state $|\rightarrow\rightarrow\rightarrow\rangle$ in the quantum Ising chain (92) by spatial averaging from thermal equilibrium state. (Figure from Ref. [11])

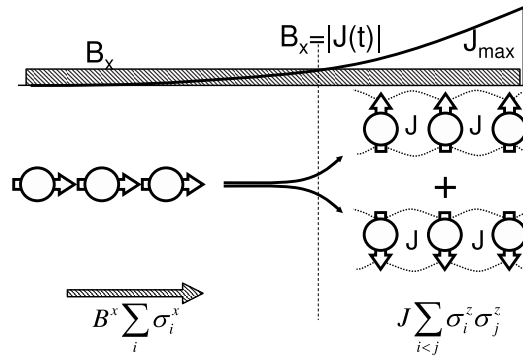


Figure 9. Schematic picture of the ion trap experiment in Ref. [9]. By adiabatically increasing effective spin-spin interaction an initial paramagnetic state is driven into a superposition of two ferromagnetic states with opposite magnetisation. (Figure from Ref. [9])

This ground state is (approximately) the initial state for the last adiabatic stage of the evolution after $-\hat{e}$. This argument shows that when passing across the critical point, the state of the system gets imprinted with a finite KZ correlation length proportional to $\hat{\xi}$. In particular, this coherence length determines average density of kinks after the transition as

$$n_{\text{ex}} \simeq \hat{\xi}^{-1} = \tau_Q^{-1/2}. \quad (97)$$

This is an order of magnitude estimate with a pre-factor $\simeq 1$.

In the following we derive an exact solution [37, 38, 58] not only to confirm the scaling exponent in Eq. (97) and provide an unknown numerical pre-factor, but also to see how much the state after the transition resembles the adiabatic

ground state at $\hat{\epsilon}$. In the adiabatic limit $\tau_Q \rightarrow \infty$ this near-critical ground state has a divergent correlation length $\hat{\xi}$ which, by the standard scaling hypothesis of the renormalisation group, determines all physical observables according to their scaling dimensions.

2.13.1. Landau-Zener argument

Here we assume that N is even for convenience. After the non-local Jordan-Wigner transformation [18],

$$\sigma_n^x = \left(c_n^\dagger + c_n \right) \prod_{m < n} (1 - 2c_m^\dagger c_m), \quad (98)$$

$$\sigma_n^y = i \left(c_n^\dagger - c_n \right) \prod_{m < n} (1 - 2c_m^\dagger c_m), \quad (99)$$

$$\sigma_n^z = 1 - 2c_n^\dagger c_n, \quad (100)$$

introducing fermionic operators c_n which satisfy $\{c_m, c_n^\dagger\} = \delta_{mn}$ and $\{c_m, c_n\} = \{c_m^\dagger, c_n^\dagger\} = 0$ the Hamiltonian (92) becomes [71]

$$H = P^+ H^+ P^+ + P^- H^- P^-. \quad (101)$$

Above

$$P^\pm = \frac{1}{2} [1 \pm P] \quad (102)$$

are projectors on subspaces with even (+) and odd (-) parity

$$P = \prod_{n=1}^N \sigma_n^z = \prod_{n=1}^N (1 - 2c_n^\dagger c_n) \quad (103)$$

and

$$H^\pm = \sum_{n=1}^N \left(2g c_n^\dagger c_n - c_n^\dagger c_{n+1} - c_{n+1}^\dagger c_n - c_{n+1} c_n - c_n^\dagger c_{n+1}^\dagger - g \right) \quad (104)$$

are corresponding reduced Hamiltonians. The c_n 's in H^- satisfy periodic boundary condition $c_{N+1} = c_1$, but the c_n 's in H^+ obey $c_{N+1} = -c_1$ - what we call "antiperiodic" boundary conditions.

The parity P of the number of c -quasiparticles is a good quantum number and the ground state has even parity for any $g \neq 0$. Assuming that a quench begins in the ground state, we can confine to the subspace of even parity. H^+ is diagonalised by a Fourier transform followed by a Bogoliubov transformation [71]. The Fourier transform consistent with the antiperiodic boundary condition is

$$c_n = \frac{e^{-i\pi/4}}{\sqrt{N}} \sum_k c_k e^{ikn}, \quad (105)$$

where the pseudomomentum k takes “half-integer” values

$$k = \pm \frac{1}{2} \frac{2\pi}{N}, \dots, \pm \frac{N-1}{2} \frac{2\pi}{N}. \quad (106)$$

The Hamiltonian (104) becomes

$$H^+ = \sum_k \left\{ 2[g - \cos k] c_k^\dagger c_k + \sin k \left[c_k^\dagger c_{-k}^\dagger + c_{-k} c_k \right] - g \right\}. \quad (107)$$

Diagonalisation of H^+ is completed by a Bogoliubov transformation

$$c_k = u_k \gamma_k + v_{-k}^* \gamma_{-k}^\dagger, \quad (108)$$

provided that Bogoliubov modes (u_k, v_k) are eigenstates of the stationary Bogoliubov-de Gennes equations

$$\omega \begin{pmatrix} u_k \\ v_k \end{pmatrix} = \begin{bmatrix} 2(g - \cos k) & 2 \sin k \\ 2 \sin k & -2(g - \cos k) \end{bmatrix} \begin{pmatrix} u_k \\ v_k \end{pmatrix}. \quad (109)$$

There are two eigenstates for each k with energies $\omega = \pm \omega_k$, where

$$\omega_k = 2\sqrt{(g - \cos k)^2 + \sin^2 k}. \quad (110)$$

The positive energy eigenstate

$$(u_k, v_k) = \left(\cos \frac{\theta_k}{2}, \sin \frac{\theta_k}{2} \right), \quad (111)$$

where $\tan \theta_k = \sin k / (g - \cos k)$, defines the quasiparticle operator

$$\gamma_k = u_k^* c_k + v_{-k}^* c_{-k}^\dagger, \quad (112)$$

and the negative energy eigenstate $(u_k^-, v_k^-) = (-v_k, u_k)$ defines $\gamma_k^- = (u_k^-)^* c_k + (v_{-k}^-)^* c_{-k}^\dagger = -\gamma_{-k}^\dagger$. After the Bogoliubov transformation, the Hamiltonian $H^+ = \frac{1}{2} \sum_k \omega_k \left(\gamma_k^\dagger \gamma_k - \gamma_k^- \gamma_k^- \right)$ is equivalent to

$$H^+ = \sum_k \omega_k \left(\gamma_k^\dagger \gamma_k - \frac{1}{2} \right). \quad (113)$$

This is a simple-looking sum of quasiparticles with half-integer pseudomenta. However, thanks to the projection $P^+ H^+ P^+$ in Eq. (101) only states with even numbers of quasiparticles belong to the spectrum of H .

In the linear quench (93), the system is initially in its ground state at large initial value of $g \gg 1$, but as g is ramped down to zero, the system gets excited from its instantaneous ground state and, in general, its final state at $t = 0$ has finite number of kinks. Comparing the Ising Hamiltonian (92) at $g = 0$ with the Bogoliubov Hamiltonian (113) at $g = 0$ we obtain a simple expression for the

operator of the number of kinks

$$\mathcal{N} \equiv \frac{1}{2} \sum_{n=1}^N (1 - \sigma_n^z \sigma_{n+1}^z) = \sum_k \gamma_k^\dagger \gamma_k. \quad (114)$$

The number of kinks is equal to the number of quasiparticles excited at $g = 0$. The excitation probability

$$p_k = \langle \gamma_k^\dagger \gamma_k \rangle \quad (115)$$

in the final state at $g = 0$ can be found with the time-dependent Bogoliubov method.

The initial ground state at $g \rightarrow \infty$ is a Bogoliubov vacuum $|0\rangle$ annihilated by all quasiparticle operators γ_k determined in Eq. (112) by the positive- ω eigenmodes $(u_k, v_k) \approx (1, 0)$ of Eq. (109). As $g(t)$ is ramped down, the quantum state gets excited from the instantaneous ground state. We work in the Heisenberg picture where the state remains the initial Bogoliubov vacuum and the operators γ_k do not depend on time, but the operators c_k are time-dependent

$$c_k = u_k(t) \gamma_k + v_{-k}^*(t) \gamma_{-k}^\dagger, \quad (116)$$

with the initial condition $[u_k(-\infty), v_k(-\infty)] = (1, 0)$. They satisfy Heisenberg equations $i \frac{d}{dt} c_k = [c_k, H^+]$ equivalent to a time-dependent version of the Bogoliubov-de Gennes equations (109):

$$i \frac{d}{dt} \begin{pmatrix} u_k \\ v_k \end{pmatrix} = \begin{bmatrix} 2[g(t) - \cos k] & 2 \sin k \\ 2 \sin k & -2[g(t) - \cos k] \end{bmatrix} \begin{pmatrix} u_k \\ v_k \end{pmatrix}. \quad (117)$$

These equations are an example of the general equations (62).

Comparing equations (62,65) and (117) with $g(t) = 1 + \epsilon(t)$, we can identify $a(k) = 2$, $b(k) = 2(\cos k - 1)$,

$$\Delta(k) = 2 \sin k, \quad (118)$$

$\hat{\sigma}(k) = -\sigma^x$, and $\hat{\sigma}_\perp(k) = \sigma^z$. There are two Fermi points $k_F = 0, \pi$ where $\Delta(k_F) = 0$ which correspond to the critical points $g_c = 1, -1$ respectively. Modes near $k_F = \pi$ do not get excited in our quench from $g \rightarrow \infty$ through $g_c = 1$ to $g = 0$, so we can focus on $k_F = 0$ only. Expansion in $k - k_F$ like in Eqs. (71,77) yields $z_\Delta = 2$ and $z_b = 4$ and the LZ argument in Section 2.11 case (i) yields

$$n_{\text{ex}} \simeq \tau_Q^{-1/z_\Delta} = \tau_Q^{-1/2} \quad (119)$$

for $\tau_Q \gg 1$. This is the same as the KZ prediction (97) because the condition $z_\Delta \leq z_b$ in Eq. (78) is satisfied.

What is more, with the minimal gap function $\Delta \approx 2|k|$ near $k_F = 0$ we have

$$p_k \approx e^{-2\pi\tau_Q k^2}, \quad (120)$$

localised near $k = 0$ when $\tau_Q \gg 1$, see Figure 6, and the integral in Eq. (69) yields

the density of excitations

$$n_{\text{ex}} = \frac{1}{2\sqrt{2\pi}} \tau_Q^{-1/2}. \quad (121)$$

The numerical pre-factor is $\frac{1}{2\sqrt{2\pi}} = 0.113$. For comparison, in Ref. [70] the perturbative Eqs. (84,85) were used to estimate the same density of defects as $n_{\text{ex}} \approx 0.124 \tau_Q^{-1/2}$. The scaling is the same as in the exact solution (121) but, as a result of the perturbative approximation in Eq. (85), the numerical pre-factor is overestimated as expected for fermionic quasiparticles, see Section 2.12.

2.13.2. Adiabatic transition in a finite chain

No matter how long τ_Q is, a quench across a critical point in an infinite system is not adiabatic because the energy gap at the critical point is zero. However, in a finite system the gap is finite and we can expect the quench to become adiabatic for a sufficiently long τ_Q , see Section 2.4. For instance, in the periodic Ising chain the (relevant) energy gap at $g_c = 1$ for excitation of the lowest two energy quasiparticles with $k = \pm\pi/N$ is $\omega_{+\pi/N} + \omega_{-\pi/N} = 4\pi/N$ and decays like $1/N$. Since p_k is a probability to excite a pair of quasiparticles $(+k, -k)$ and different pairs evolve independently, a probability for the state to follow the adiabatic ground state without any quasiparticles is a product

$$P_{\text{GS}} = \prod_{k>0} (1 - p_k) \quad (122)$$

over the positive ‘‘half-integer’’ $k = (m + 1/2)2\pi/N$ in Eq. (106). Well on the adiabatic side $p_{\pi/N} \approx \exp(-2\pi^3 \frac{\tau_Q}{N^2}) \ll 1$ is exponentially small and $p_{(1+2m)\pi/N} \approx (p_{\pi/N})^{(1+2m)^2} \ll p_{\pi/N}$ for $m > 0$, so we can safely approximate

$$P_{\text{GS}} = 1 - p_{\pi/N} + \mathcal{O}(p_{\pi/N}^9) \approx 1 - \exp\left(-2\pi^3 \frac{\tau_Q}{N^2}\right). \quad (123)$$

This $P_{\text{GS}} \approx 1$ and the quench in a finite chain is adiabatic when

$$\tau_Q \gg \frac{N^2}{2\pi^3}, \quad (124)$$

i.e., when even the lowest energy pair of quasiparticles with $k = \pm\pi/N$ is not likely to get excited. Reading this inequality from right to left, the size N of a defect-free chain grows like $\tau_Q^{1/2}$. This is consistent with Eqs. (96) and (121).

2.13.3. Exact solution of the time-dependent Bogoliubov-de Gennes equations

If we want to go beyond the simple result for n_{ex} in Eq. (121), then we need an exact solution of Eq. (117). When $k > 0$ a new time variable

$$\tau = 4\tau_Q \sin k \left(\frac{t}{\tau_Q} + \cos k \right) \quad (125)$$

brings Eqs. (117) to the canonical LZ form (39)

$$i \frac{d}{d\tau} \begin{pmatrix} u_k \\ v_k \end{pmatrix} = \frac{1}{2} \begin{bmatrix} -R_k \tau & 1 \\ 1 & R_k \tau \end{bmatrix} \begin{pmatrix} u_k \\ v_k \end{pmatrix}, \quad (126)$$

with a transition rate $R_k = 1/4\tau_Q \sin^2 k$. A general solution of the Landau-Zener equations (126), see Section 2.9, is

$$\begin{aligned} v_k(\tau) &= aD_{-s-1}(-iz) + bD_{-s-1}(iz) , \\ u_k(\tau) &= \left(\tau R_k - 2i \frac{\partial}{\partial \tau} \right) v_k(\tau) , \end{aligned} \quad (127)$$

with arbitrary complex parameters a, b . Here $D_m(x)$ is a Weber function, $s = \frac{1}{4iR_k}$, and $z = \sqrt{R_k}\tau e^{i\pi/4}$. The parameters a, b are fixed by the initial conditions $u_k(-\infty) = 1$ and $v_k(-\infty) = 0$. Using the asymptotes of the Weber functions when $\tau \rightarrow -\infty$, we obtain

$$a = 0 , \quad |b|^2 = \frac{e^{-\pi/8R_k}}{4R_k} . \quad (128)$$

At the end of the quench at $t = 0$ when $\tau = 2\tau_Q \sin(2k)$, the argument of the Weber function is $iz = \sqrt{R_k}\tau e^{i\pi/4} = 2\sqrt{\tau_Q}e^{i\pi/4} \cos(k)\text{sign}(k)$. When $\tau_Q \gg 1$ the modulus of this argument is large for most k , except near $k = \pm\frac{\pi}{2}$, and we can again use asymptotes of Weber functions to obtain products

$$\begin{aligned} |u_k|^2 &= \frac{1 - \cos k}{2} + e^{-2\pi\tau_Q k^2} , \\ |v_k|^2 &= 1 - |u_k|^2 , \\ u_k v_k^* &= \frac{1}{2} \sin k + \text{sign}(k) e^{-\pi\tau_Q k^2} \sqrt{1 - e^{-2\pi\tau_Q k^2}} e^{i\varphi_k} , \\ \varphi_k &= \frac{\pi}{4} + 2\tau_Q - (2 - \ln 4)\tau_Q k^2 + k^2\tau_Q \ln \tau_Q - \arg [\Gamma(1 + i\tau_Q k^2)] . \end{aligned} \quad (129)$$

These products depend on k and τ_Q through two dimensionless combinations: $\tau_Q k^2$, which implies the usual KZ correlation length $\hat{\xi} = \sqrt{\tau_Q}$, and $k^2\tau_Q \ln \tau_Q$ which implies a second scale of length $\sqrt{\tau_Q \ln \tau_Q}$. The final quantum state at $g = 0$ cannot be characterised by a unique scale of length. Physically, this reflects a combination of two processes: KZM that sets up the initial post-transition state of the system at $-\hat{\xi}$, and the subsequent adiabatic evolution with quantum dephasing.

2.13.4. Entropy of a block of spins after a quench

The Von Neumann entropy of a block of L spins,

$$S(L) = - \text{Tr} \rho_L \log_2 \rho_L , \quad (130)$$

measures entanglement between the block and the rest of the chain. Above ρ_L is reduced density matrix of the subsystem of L spins. In recent years this entropy was studied extensively in ground states of quantum critical systems [72–79]. At a quantum critical point, the entropy diverges like $\log L$ for large L with a pre-factor determined by the central charge of an effective conformal field theory [72, 76, 80]. In the quantum Ising model at the critical $g_c = 1$

$$S^{\text{GS}}(L) \simeq \frac{1}{6} \log_2 L \quad (131)$$

for large L . Slightly away from the critical point, the entropy saturates at a finite asymptotic value [76]

$$S_\infty^{\text{GS}} \simeq \frac{1}{6} \log_2 \xi \quad (132)$$

when the block size L exceeds the finite correlation length ξ in the ground state of the system.

In a dynamical quantum phase transition the quantum state of the system develops a finite correlation length $\hat{\xi} = \sqrt{\tau_Q}$. If this dynamical correlation length were the only relevant scale of length, then one could expect the entropy of entanglement after a dynamical transition to be given by Eq. (132) with ξ simply replaced by $\hat{\xi}$. However, as we could see in Eq. (129), there are two scales of length, and – strictly speaking – there is no reason to expect that either of them alone is relevant in general. This is why we cannot rely on scaling arguments and the entropy has to be calculated “from scratch”.

We proceed in a similar way as in Ref. [72, 73, 75, 77, 79] and define a correlator matrix for the block of L spins

$$\Pi = \begin{pmatrix} \alpha & \beta^\dagger \\ \beta & 1 - \alpha \end{pmatrix}, \quad (133)$$

where α and β are $L \times L$ matrices of quadratic correlators

$$\begin{aligned} \alpha_{m,n} \equiv \langle c_m c_n^\dagger \rangle &= \frac{1}{2\pi} \int_{-\pi}^{\pi} dk |u_k|^2 e^{ik(m-n)} \stackrel{\tau_Q \gg 1}{\approx} \\ &\frac{1}{2} \delta_{0,|m-n|} - \frac{1}{4} \delta_{1,|m-n|} + \frac{e^{-\frac{(m-n)^2}{8\pi \hat{\xi}^2}}}{2\sqrt{2\pi} \hat{\xi}}. \end{aligned} \quad (134)$$

and

$$\begin{aligned} \beta_{m,n} \equiv \langle c_m c_n \rangle &= \frac{1}{2\pi i} \int_{-\pi}^{\pi} dk u_k v_k^* e^{ik(m-n)} \stackrel{\ln \tau_Q \gg 1}{\approx} \\ \text{sign}(m-n) &\left[\frac{1}{4} \delta_{1,|m-n|} - \frac{e^{2i\tau_Q - \frac{i|m-n|^2}{4 \hat{\xi} l} - \frac{\pi|m-n|^2}{4 l^2}}}{2\sqrt{\pi \hat{\xi} l}} \sqrt{1 - e^{-\frac{\pi|m-n|^2}{4 l^2}}} \right] \end{aligned} \quad (136)$$

where we used Eqs. (129). Here $\hat{\xi} = \sqrt{\tau_Q}$ is the KZ correlation length and

$$l = \sqrt{\tau_Q} \ln \tau_Q \quad (137)$$

is a dephasing length¹. When the linear quench is extended to $g \rightarrow -\infty$, as in Section 2.13.10, the dephasing length continues to grow like $l(t) = 4t$.

¹Indeed, for large τ_Q , the non-ground-state part of $\beta_{m,n}$, i.e the second term in the square bracket in Eq. (136), is negligible on distances $|m-n| \ll l$ as a result of dephasing the integral over k in Eq. (135). Its integrand has the phase φ_k in Eq. (129) whose fast rotation with k is driven mainly by the term $k^2 \tau_Q \ln \tau_Q$. This term introduces a length scale $l_0 = \sqrt{\tau_Q \ln \tau_Q}$ and, if it were the only length scale, the integral would be negligible or “dephased” for $|m-n| \ll l_0$. However, Eq. (129) depends on k also through the combination $\tau_Q k^2$ introducing $\hat{\xi}$ as the second scale. Due to conspiracy between the two scales, the integral is actually dephased on distances up to the net dephasing length $l = l_0^2 / \hat{\xi}$ in Eq. (137)

We note that α and β are Toeplitz matrices with constant diagonals. The expectation values $\langle \dots \rangle$ are taken in the Bogoliubov vacuum state. Since this state is Gaussian, all higher order correlators can be expressed by the matrices α and β - they provide complete characterization of the quantum state after the dynamical transition. Since the matrices depend on both scales $\hat{\xi}$ and l , both scales are necessary to characterize the Gaussian state.

As noted in Ref. [72, 73, 75, 77, 79], the block entropy can be calculated as

$$S(L, \tau_Q) = - \text{Tr } \rho \log_2 \rho = - \text{Tr } \Pi \log_2 \Pi . \quad (138)$$

In this calculation we use Eq. (128) and Eqs. (134,135). The calculation involves numerical evaluation of the integrals in Eqs. (134,135) and numerical diagonalisation of the matrix Π . Results are shown in Panel A of Fig.10. The entropy grows with the block size L and saturates at a finite value $S_\infty(\tau_Q)$ for large enough L . In Panel B, the asymptotic entropy is fitted with the (linear) function $S_\infty(\tau_Q) = A + B \ln \tau_Q$. On one hand, KZM suggests a simple replacement of the ground state correlation length ξ in Eq. (132) by the dynamical KZ length $\hat{\xi} = \sqrt{\tau_Q}$ implying the asymptotic value

$$S_\infty(\tau_Q) \simeq \frac{1}{6} \log_2 \hat{\xi} \simeq \frac{\ln 2}{12} \ln \tau_Q = 0.120 \ln \tau_Q . \quad (139)$$

On the other hand, the best fit gives $B = 0.128 \pm 0.004$ and $A = 1.80 \pm 0.05$. The best B is in reasonably good agreement with the expected value of 0.120.

In Panels C and D of the same figure, the entropy $S(L, \tau_Q)$ is rescaled by its asymptotic value $S_\infty(\tau_Q) \approx A + B \ln \tau_Q$. After this transformation we can better focus on how the entropy depends on the block size L . A simple hypothesis would be that the entropy depends on $\hat{\xi}$ and saturates when $L \gg \hat{\xi}$. To check if this is true, in Panel C the block size L is rescaled by $\hat{\xi} = \sqrt{\tau_Q}$ and this rescaling brings the plots close to overlap, although they do not overlap as well as one might have hoped. By contrast, as shown in Panel D, rescaling the block size L by the dephasing length l makes the multiple plots collapse. Thus we can conclude that the entropy saturates at

$$S_\infty(\tau_Q) \simeq \frac{1}{6} \log_2 \hat{\xi} \text{ when } L \gg l \quad (140)$$

i.e. the entropy of a large block of spins is determined by the KZ dynamical correlation length $\hat{\xi} = \sqrt{\tau_Q}$, but the entropy saturates when the block size is greater than the dephasing length $l = \sqrt{\tau_Q} \ln \tau_Q$. A similar conclusion was also obtained in the numerical simulations in Ref. [81], where the non-integrable case with non-zero longitudinal magnetic field was considered as well.

According to KZM the correlation length $\hat{\xi}$ is determined in the impulse stage when the system is crossing the critical point, while the second scale l builds up by dephasing the excited state in the following adiabatic stage. This scenario is confirmed by the block entropy at the moment when the system is crossing the critical point at $g_c = 1$, see Figure 11. The entropy saturates at

$$S_\infty(\tau_Q) \simeq \frac{1}{6} \log_2 \hat{\xi} \text{ when } L \gg \hat{\xi} . \quad (141)$$

Near the critical point, when the scale l set up by dephasing just begins to build up, $\hat{\xi}$ is still the only relevant scale of length. The result (141) confirms the KZM replacement rule $\xi \rightarrow \hat{\xi}$ in Eq. (132). As predicted by the adiabatic-impulse-adiabatic

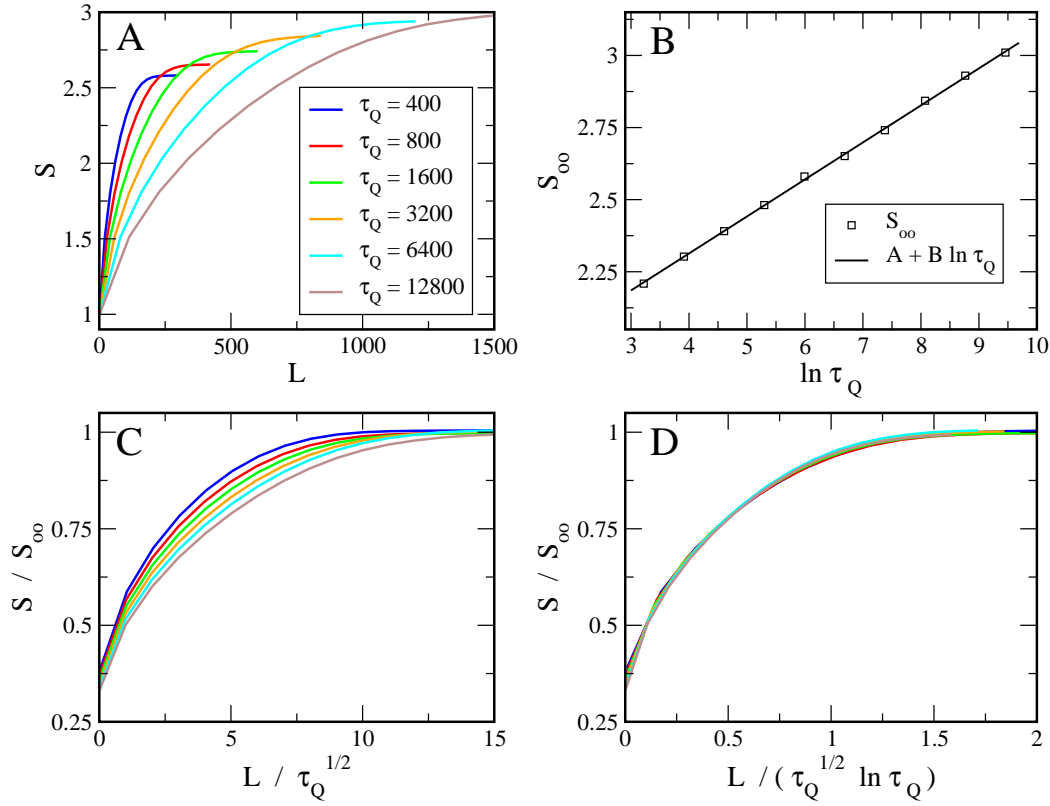


Figure 10. Panel A shows entropy of a block of L spins after the dynamical phase transition as a function of the block size L . The multiple plots correspond to different values of the quench time τ_Q . For all τ_Q , the entropy grows with the block size L and saturates at a finite value $S_\infty(\tau_Q)$ for large enough L . In Panel B, this asymptotic value of entropy is fitted with the function $S_\infty(\tau_Q) = A + B \ln \tau_Q$. The best fit has $B = 0.128 \pm 0.004$ and $A = 1.80 \pm 0.05$. This B is in reasonably good agreement with the expected value of $B = \frac{\ln 2}{12} = 0.120$. In Panels C and D, entropy $S(L, \tau_Q)$ is rescaled by the best fit to its asymptotic value $S_\infty(\tau_Q) = A + B \ln \tau_Q$. With this rescaling one can focus on how the entropy depends on the block size L . In Panel C, the block size is rescaled by $\hat{\xi} = \sqrt{\tau_Q}$ but the rescaled plots do not overlap. However, as shown in Panel D, rescaling the block size L by the second scale $l = \sqrt{\tau_Q} \ln \tau_Q$ makes the six plots collapse. (Figure from Ref. [38])

approximation in Section 2.3, the entropy is the same as if the state were the ground state at \hat{e} .

2.13.5. Impurity of a block of spins after a quench

Since a fully analytic calculation of entropy does not seem possible, it is worthwhile to calculate another more easily tractable entanglement-related quantity. For example, an ‘‘impurity’’ of the correlator matrix Π in Eq. (133)

$$I(\Pi) = \text{Tr} \Pi (1 - \Pi) \quad (142)$$

is zero only when the L spins are in a pure state i.e. when all eigenvalues of Π are either 0 or 1. It is maximal when all the eigenvalues are $\frac{1}{2}$, or when the state is most entangled. Thanks to its simple quadratic form, the impurity can be calculated relatively easily.

Simple calculation using the block structure of Π in Eq. (133) and the Toeplitz property of the block matrices α and β leads to

$$I(L) = 2 \left(L\alpha_0 - \sum_{j=1-L}^{j=L-1} (L - |j|)(\alpha_j^2 + |\beta_j|^2) \right), \quad (143)$$

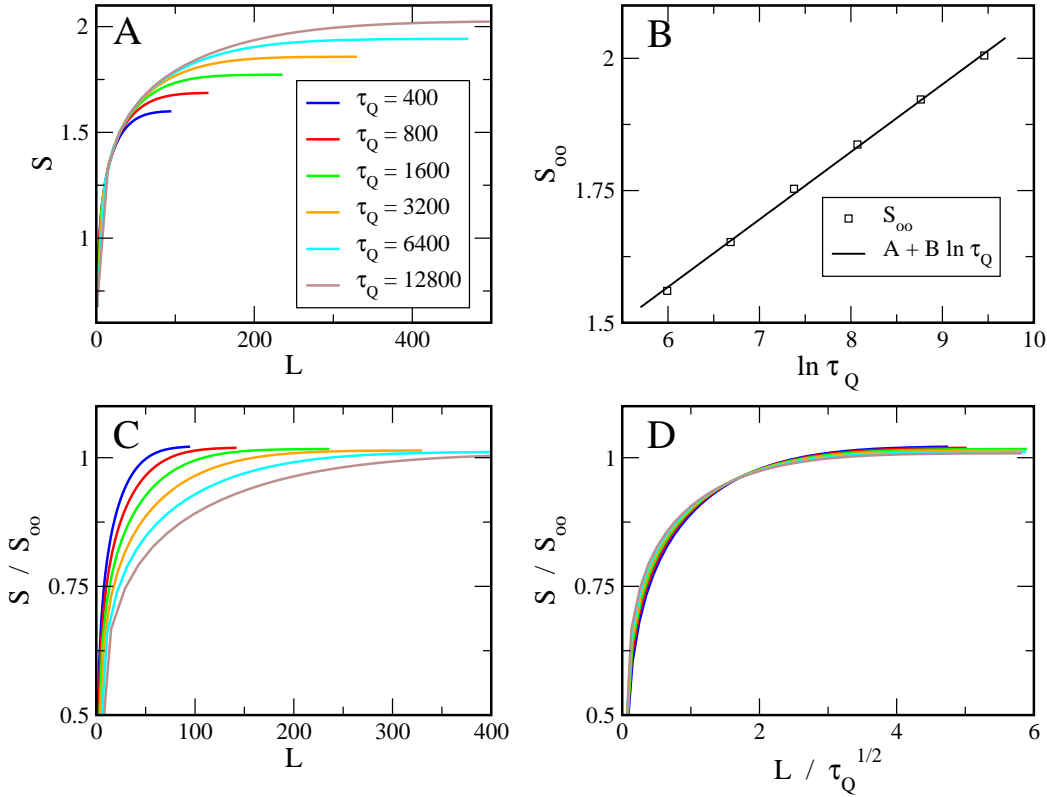


Figure 11. Panel A shows entropy of a block of L spins during the dynamical phase transition at the critical point $g = 1$ as a function of the block size L . The multiple plots correspond to different values of the quench time τ_Q . For all the quench times, the entropy grows with the block size L and saturates at a finite value $S_\infty(\tau_Q)$ for large enough L . In Panel B this asymptotic value of entropy is fitted with the function $S_\infty(\tau_Q) = A + B \ln \tau_Q$. The best fit has $B = 0.126 \pm 0.005$ and $A = 0.80 \pm 0.03$. This B is in reasonably good agreement with the expected value of $B = \frac{\ln 2}{12} = 0.120$. In Panels C and D, the entropy $S(L, \tau_Q)$ is rescaled by the best fit to its asymptotic value $S_\infty(\tau_Q) \approx A + B \ln \tau_Q$. With this rescaling one can focus on how the entropy depends on the block size L . In Panel D, rescaling the block size L by $\hat{\xi} = \sqrt{\tau_Q}$ makes the six plots collapse. (Figure from Ref. [38])

where $\alpha_j = \alpha_{j,0}$ and $\beta_j = \beta_{j,0}$. Further calculation as in Ref. [38] shows that at the final $g = 0$ the impurity saturates at

$$I_\infty \approx \frac{\ln \hat{\xi}}{\pi^2} \quad \text{when } L \gg l, \quad (144)$$

in analogy to the entropy in Eq. (140).

It is interesting to compare the dynamical impurity (144) with the impurity in the ground state near the critical point. A simple calculation gives the asymptote of impurity at the critical point

$$I^{\text{GS}}(L) \approx \frac{\ln L}{\pi^2}. \quad (145)$$

when $\ln L \gg 1$. Near the critical point, the asymptote is valid when the block is much shorter than the correlation length, $L \ll \xi$, and at larger L the impurity saturates at

$$I_\infty^{\text{GS}} \approx \frac{\ln \xi}{\pi^2}. \quad (146)$$

Again, in the same way as for the block entropy, the simple KZM replacement rule

$\xi \rightarrow \hat{\xi}$ applied to Eq. (146) gives the correct asymptotic value of the dynamical impurity in Eq. (144). As predicted by the adiabatic-impulse-adiabatic approximation in Section 2.3, the dynamical impurity is the same as the impurity in the ground state at \hat{c} .

2.13.6. Correlation functions after a quench

Correlation functions are of fundamental interest in the theory of phase transitions because they provide direct manifestation of their universal properties and are in general directly accessible experimentally. Here we present results for spin-spin correlation functions after a dynamical quantum phase transition, see Ref. [38, 58].

To begin with, we observe that for symmetry reasons the magnetization $\langle \sigma^x \rangle = 0$, but the transverse magnetization

$$\langle \sigma_n^z \rangle = \langle 1 - 2c_n^\dagger c_n \rangle = 2\alpha_0 - 1 \approx \frac{1}{2\pi\sqrt{2\tau_Q}} \quad (147)$$

when $\tau_Q \gg 1$. This is what remains of the initial magnetization $\langle \sigma_n^z \rangle = 1$ in the initial paramagnetic ground state at $g \rightarrow \infty$. As expected, when the linear quench is slow, then the final magnetization decays towards $\langle \sigma_n^z \rangle = 0$ characteristic of the ferromagnetic ground state at $g = 0$.

Final transverse spin-spin correlation function at $g = 0$ is

$$C_R^{zz} \equiv \langle \sigma_n^z \sigma_{n+R}^z \rangle - \langle \sigma_n^z \rangle \langle \sigma_{n+R}^z \rangle = 4(|\beta_R|^2 - |\alpha_R|^2) \approx \frac{e^{-\frac{\pi R^2}{2l^2}} \left(1 - e^{-\frac{\pi R^2}{4l^2}}\right)}{\pi \hat{\xi} l} - \frac{e^{-\frac{R^2}{\pi \hat{\xi}^2}}}{2\pi^2 \hat{\xi}^2}, \quad (148)$$

when $R > 1$ and $\ln \tau_Q \gg 1$. This correlation function depends on both $\hat{\xi}$ and the dephasing length l in Eq. (137), but its long range tail

$$C_R^{zz} \sim e^{-\frac{\pi R^2}{2l^2}} \quad (149)$$

decays on the scale l .

In contrast, the ferromagnetic spin-spin correlation function

$$C_R^{xx} = \langle \sigma_n^x \sigma_{n+R}^x \rangle - \langle \sigma_n^x \rangle \langle \sigma_{n+R}^x \rangle = \langle \sigma_n^x \sigma_{n+R}^x \rangle \quad (150)$$

cannot be evaluated so easily. As is well known, in the ground state C_R^{xx} can be written as a determinant of an $R \times R$ Toeplitz matrix whose asymptote for large R can be obtained with the Szegő limit theorem [82]. Unfortunately, in time-dependent problems the correlation function is not a determinant in general. However, below we circumvent this problem in an interesting range of parameters.

Using the Jordan-Wigner transformation, C_R^{xx} can be expressed as

$$C_R^{xx} = \langle b_0 a_1 b_1 a_2 \dots b_{R-1} a_R \rangle. \quad (151)$$

Here a_n and b_n are Majorana fermions defined as $a_n = (c_n^\dagger + c_n)$ and $b_n = c_n^\dagger - c_n$. Here a_n is hermitian and b_n is anti-hermitian. Using Eq. (134) and Eq. (135) we

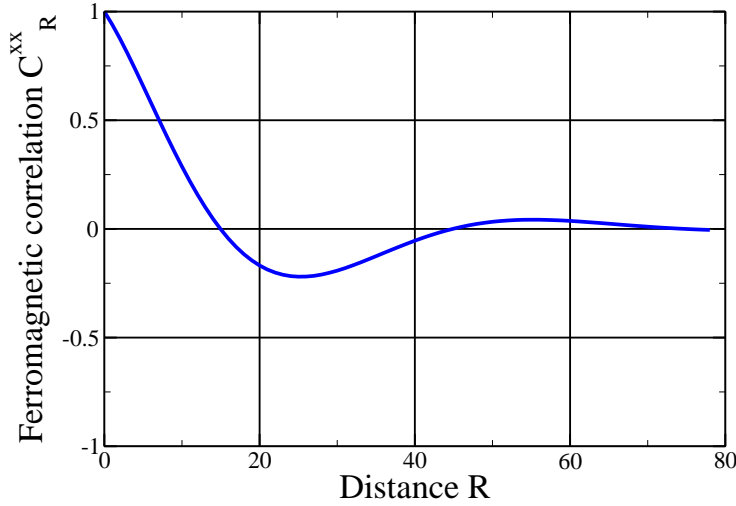


Figure 12. Ferromagnetic spin correlation in Eq. (153). The oscillatory term means that consecutive kinks are anti-correlated – they keep more or less the same distance $\simeq \hat{\xi}$ from each other forming something similar to a ...-kink-antikink-kink-antikink... regular lattice with a lattice constant $\simeq \hat{\xi}$. However, fluctuations in the length of bonds in this lattice are comparable to the average distance itself giving the exponential decay of the correlator C_R^{xx} on the same scale of $\simeq \hat{\xi}$.

obtain

$$\begin{aligned}
 \langle a_m b_n \rangle &= 2\alpha_{n-m} + 2\text{Re}\beta_{n-m} - \delta_{m,n} \\
 \langle b_m a_n \rangle &= \delta_{m,n} - 2\alpha_{n-m} + 2\text{Re}\beta_{n-m} \\
 \langle a_m a_n \rangle &= \delta_{m,n} + 2i\text{Im}\beta_{m-n} \\
 \langle b_m b_n \rangle &= \delta_{m,n} + 2i\text{Im}\beta_{m-n}
 \end{aligned} \tag{152}$$

Using Wick theorem, the average in Eq. (151) is a determinant of a matrix when $\langle a_m a_n \rangle = 0$ and $\langle b_m b_n \rangle = 0$ for $m \neq n$, or equivalently when $\text{Im}\beta_{m-n} = 0$ for $m \neq n$. Inspection of Eq. (136) shows that $\text{Im}\beta_{m-n} \approx 0$ when $|m-n| \ll l$. Consequently, when $R \ll l$ then we can neglect all $\text{Im}\beta_{m-n}$ assuming that $\langle a_m a_n \rangle = 0$ and $\langle b_m b_n \rangle = 0$ for $m \neq n$. The correlation function is a determinant of the Toeplitz matrix $[\langle b_m a_{n+1} \rangle]_{m,n=1,\dots,R}$ within the quasiparticle horizon where $R \ll l$. Asymptotic behaviour of this Toeplitz determinant can be obtained [38] using standard methods in Refs. [82] and [58, 83]:

$$C_R^{xx} \propto \exp\left(-0.174 \frac{R}{\hat{\xi}}\right) \cos\left(\sqrt{\frac{\ln 2}{2\pi}} \frac{R}{\hat{\xi}} - \varphi_0\right) \tag{153}$$

when $1 \ll R \ll l$ i.e. up to the dephasing length l , see Fig. 12.

The final ferromagnetic correlation function (153) exhibits decaying oscillatory behaviour on length scales much less than the scale l , but both the wavelength of these oscillations and their exponentially decaying envelope are determined by $\hat{\xi}$. As discussed in a similar situation by Cherng and Levitov [58], this oscillatory behaviour means that consecutive kinks keep more or less the same distance $\simeq \hat{\xi}$ from each other forming something similar to a ...-kink-antikink-kink-antikink... lattice with a lattice constant $\simeq \hat{\xi}$. However, fluctuations in the length of bonds are comparable to the lattice constant itself and they give the (marginally underdamped) exponential decay of the correlator C_R^{xx} on the same scale of $\simeq \hat{\xi}$.

The gaps in analytic knowledge of the correlation functions were filled by nu-

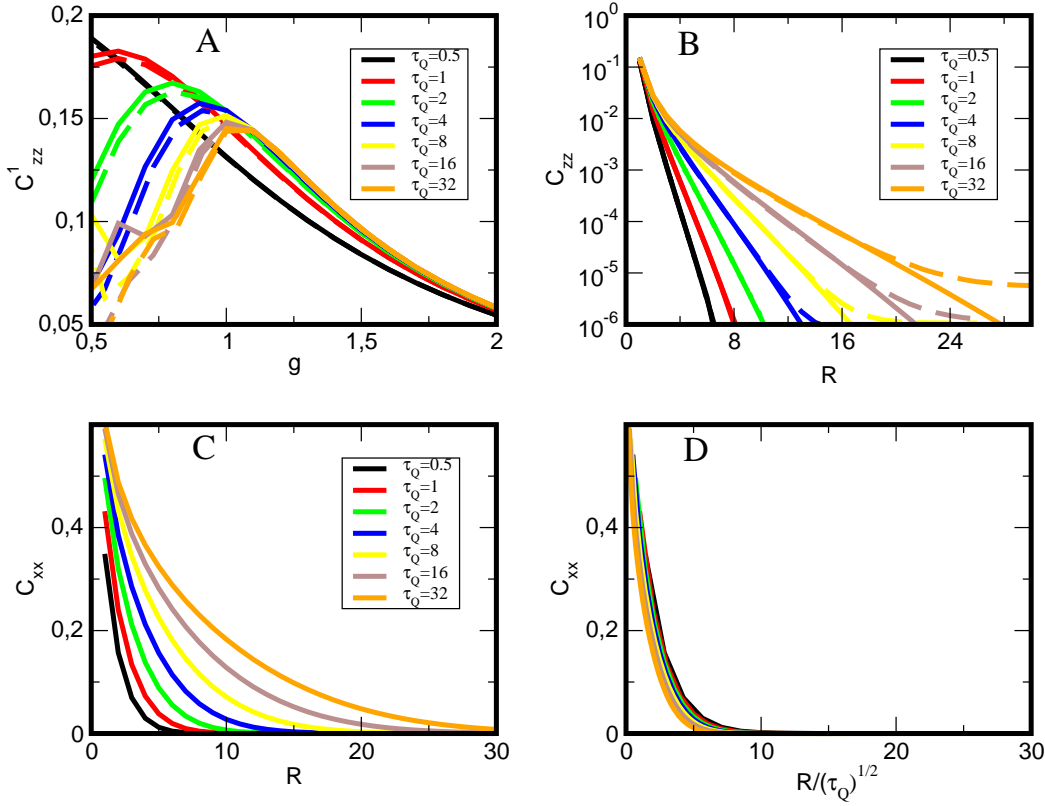


Figure 13. Panel A shows the dynamical transverse correlation C_1^{zz} as a function of magnetic field g in the linear quench. For each τ_Q , we show both numerical (dashed) and analytical (solid) result. The plots overlap near the critical point at $g = 1$ but diverge in the ferromagnetic phase when $g < 1$ indicating a breakdown of our numerical simulations in this regime. Panel B shows analytic and numerical results for the dynamical transverse correlation function at the moment when the quench crosses the critical point at $g = 1$. The transverse correlators overlap well confirming that our numerical simulations are still accurate at the critical point. Finally, in panel C, we show the dynamical ferromagnetic correlation function C_R^{xx} at $g = 1$ and in panel D, we show the same correlation function after rescaling $R/\hat{\xi}$. The rescaled plots overlap quite well supporting the idea that near the critical point the KZ correlation length $\hat{\xi} = \sqrt{\tau_Q}$ is the only relevant scale of length. (Figure from Ref. [38])

merical simulations with the real time TEDB (time evolving decimation block) algorithm [84] in Ref. [38]. As illustrated in panel A of Figure 13, the simulations were stable enough to cross the critical point and enter the ferromagnetic phase, but once in the ferromagnetic phase, the algorithm was breaking down due to the quasiparticle horizon effect, see Section 3.2. The numerics can be trusted at $g_c = 1$, but it is not reliable when $g < 1$. KZM can be tested at the critical point, but one cannot reliably follow the dephasing in the ferromagnetic phase.

Panel B of Figure 13 shows the transverse correlation C_R^{zz} at $g_c = 1$ for several values of τ_Q . For each τ_Q , both the numerical correlator and its analytic counterpart from Eq. (148) are plotted and they approximately coincide. Equation (148) can be also used to obtain analytically, but with some numerical integration, the exponential tail of the transverse correlator when $\tau_Q \gg 1$:

$$C_R^{zz} \approx \frac{0.44}{\tau_Q} \exp\left(-2.03 \frac{R}{\hat{\xi}}\right) \quad (154)$$

accurate when $R \gg \hat{\xi}$. This tail decays on the KZ correlation length $\hat{\xi}$ which proves to be the relevant scale of length.

Panel C shows the ferromagnetic spin-spin correlation functions at $g_c = 1$ for

the same values of τ_Q . They are roughly exponential and their correlation length seems to be set by $\hat{\xi} = \sqrt{\tau_Q}$. To verify this scaling hypothesis in panel D the same plots as in panel C are shown but with R rescaled by $\hat{\xi}$. The rescaled plots overlap reasonably well confirming the expected $\hat{\xi} = \sqrt{\tau_Q}$ scaling.

The correlation functions at the critical point $g_c = 1$ are consistent with the prediction of the adiabatic-impulse-adiabatic approximation in Section 2.3 that the state in the impulse stage is approximately the ground state at $\hat{\epsilon}$ with correlations decaying exponentially on the correlation length $\hat{\xi}$.

2.13.7. Fidelity between the state after a quench and the final ground state

A fidelity $F = |\langle \psi | \text{GS} \rangle|^2$ between the final state $|\psi\rangle$ and the desired final ground state $|\text{GS}\rangle$ is a very sensitive measure of the quality of adiabatic quantum computation or adiabatic quantum state preparation. In the quantum Ising chain, the fidelity can be obtained analytically from the exact solution, see Ref. [85]. The fidelity F is a probability that not a single pair of quasiparticles with opposite quasimomenta $(k, -k)$ is excited after a quench,

$$F = \prod_{k>0} (1 - p_k), \quad (155)$$

where the product runs over the positive half-integer quasimomenta in Eq. (106). It is more convenient to calculate its logarithm

$$\ln F = \sum_{k>0} \ln(1 - p_k) \approx \int_0^\pi dk \ln(1 - p_k), \quad (156)$$

accurate for $N \gg \hat{\xi}$. If the transition terminates at $g = 0$, then for $\tau_Q \gg 1$ we have $p_k = \exp(-2\pi\tau_Q k^2)$ and

$$\ln F = -\frac{N n_{\text{ex}}}{2} \frac{\int_0^\infty ds \ln[1 - e^{-s^2}]}{\int_0^\infty ds e^{-s^2}} = -1.3 n_{\text{ex}} N. \quad (157)$$

Here $n_{\text{ex}} = \int_{-\pi}^\pi \frac{dk}{2\pi} p_k = 1/2\pi \sqrt{2\tau_Q}$ is the density of excitations in Eq. (121). Thus, as might have been expected, the fidelity decays exponentially with the chain size N on the length scale $\hat{\xi} \simeq n_{\text{ex}}^{-1}$,

$$F = e^{-1.3 n_{\text{ex}} N}, \quad (158)$$

but with an unexpected coefficient 1.3 greater than 1.

It is instructive to compare the decay of fidelity in Eq. (158) to a simple Poissonian model where each of the N bonds is either excited (with probability n_{ex}) or not excited (with probability $1 - n_{\text{ex}}$) *independently* of other bonds. In this model the fidelity is a probability that none of the N independent bonds is excited:

$$F_{\text{Poisson}} = (1 - n_{\text{ex}})^N \approx e^{-n_{\text{ex}} N} \quad (159)$$

when $n_{\text{ex}} \ll 1$. Comparing Eqs. (158) and (159) we find that the decay in Eq. (158) is faster than in the model of independent bonds. The faster decay means anti-bunching correlations between the kinks randomly scattered along the spin chain in the final state. The same anti-bunching correlations are also responsible for the oscillations in the ferromagnetic correlation function in Eq. (153) and Fig. 12.

The anti-bunching in Eq. (158) contrasts with the bunching apparent in fidelity between the ferromagnetic ground state at $0 < |g| < 1$, which has finite density of kinks n_{ex} , and the fully polarized ferromagnetic ground state at $g = 0$:

$$F_{\text{ferro}} = e^{-\frac{1}{2}n_{\text{ex}}N}, \quad (160)$$

see Ref. [85]. Here the coefficient is $\frac{1}{2}$ meaning that the relevant density of uncorrelated excitations is one-half of the density of kinks. The kinks in the ferromagnetic ground state are bound into kink-antikink pairs randomly scattered along the chain. The bound pairs do not destroy the ferromagnetic long range order. This is most apparent when $g \ll 1$ is perturbatively small and the ground state is a fully polarized ferromagnet but with an admixture of a small density of reversed spins. Each reversed spin is a tightly bound pair of kink and antikink which, however, does not affect the long range ferromagnetic order.

2.13.8. Geometric phase after a quench

Connection between the geometric phase [86] and quantum phase transitions has been explored recently in Refs. [87]. The geometric phase can be used as a tool to probe quantum phase transitions in many body systems. It is a witness of a singular point in the energy spectrum arising in non-trivial geometric evolutions. In Ref. [88] the geometric phase of the final state at $g = 0$ was calculated as

$$\Gamma = 2\pi N(n_{\text{ex}} - 1) - 3\pi + \pi \left(\cos \pi n_{\text{ex}} + \sin \pi N \cot \frac{\pi}{2N} \right). \quad (161)$$

It depends on the density of excited kinks n_{ex} in Eq. (121).

2.13.9. Generalized entanglement in the final state

The generalized entanglement of a state $|\psi\rangle$ with respect to a Lie algebra h with hermitian, orthonormal basis of generators O_l enumerated by $l = 1, \dots, M$ can be characterised by a purity of $|\psi\rangle$ relative to h which is given by

$$P_h(|\psi\rangle) = \mathcal{N} \sum_{l=1}^M \langle \psi | O_l | \psi \rangle^2, \quad (162)$$

where \mathcal{N} is a normalisation factor chosen so that $0 \leq P_h \leq 1$.

A fermionic system, like e.g. the quantum Ising model in the representation of Jordan-Wigner fermions in Eq. (104), can be characterised by generalized entanglement with respect to the algebra h of number preserving bilinear fermionic operators spanned by $c_i^\dagger c_j$ with $1 \leq i, j \leq N$. In Ref. [89] it was shown that, near an isolated quantum critical point, the generalized entanglement of the ground state $|\text{GS}(\epsilon)\rangle$ scales like

$$P_h[|\text{GS}(\epsilon)\rangle] - P_h[|\text{GS}(0)\rangle] \sim \xi^{-1}, \quad (163)$$

where ξ is a correlation length in the ground state. The relative entanglement with respect to the critical point is inversely proportional to the diverging correlation length.

Moreover, as verified in Ref. [89], in a linear quench across an isolated critical point we have

$$P_h[|\psi(t)\rangle] - P_h[|\text{GS}[\epsilon(t)]\rangle] \sim \hat{\xi}^{-1} G(t/\hat{t}), \quad (164)$$

where $|\psi(t)\rangle$ is the state of the system during the transition, $|\text{GS}[\epsilon(t)]\rangle$ is the instantaneous ground state, and G is a scaling function. The relative amount of entanglement with respect to the instantaneous ground state is inversely proportional to the KZ length $\hat{\xi}$, which diverges in the adiabatic limit, and its time-dependence becomes universal when measured in units of \hat{t} in Eq. (14), as expected from KZM in Section 2.3.

In particular, the simple replacement rule $\xi \rightarrow \hat{\xi}$ applied to the generalized entanglement in the ground state (163) gives the correct dynamical result (164) in accordance with the adiabatic-impulse-adiabatic approximation in Section 2.3 where the state during the impulse stage is approximately the ground state at \hat{t} with correlation length $\hat{\xi}$.

2.13.10. Linear quench to $t \rightarrow +\infty$: quantum dephasing after KZM

As we could see in Section 2.13.6, near the critical point $g_c = 1$ the state of the system is close to the adiabatic ground state at \hat{t} which can be characterised by a single KZ correlation length $\hat{\xi} = \sqrt{\tau_Q}$, but in the following adiabatic evolution to $g = 0$ quantum dephasing develops the second longer scale $l = \sqrt{\tau_Q} \ln \tau_Q$. In this Section, as in Ref. [58], we extend the linear quench to $t \rightarrow +\infty$ to give the quantum dephasing enough time to complete its job, and see if there is any imprint of the KZ length $\hat{\xi}$ left in the final state at $t \rightarrow +\infty$ after the dephasing is completed.

The extended quench crosses both critical points $g_c = \pm 1$ and the quasiparticle excitation probability in Eq. (68) becomes a sum of two Gaussians localised near the two Fermi points $k_F = 0, \pi$:

$$p_k = e^{-2\pi\tau_Q \sin^2 k} \stackrel{\tau_Q \gg 1}{\approx} e^{-2\pi\tau_Q k^2} + e^{-2\pi\tau_Q (k-\pi)^2}. \quad (165)$$

Consequently, the average density of excitations in Eq. (69),

$$n_{\text{ex}} = \frac{1}{\pi\sqrt{2}} \tau_Q^{-1/2}, \quad (166)$$

is twice the density at $g = 0$ in Eq. (121). This n_{ex} is a density of \uparrow spins excited in the final ground state $|\downarrow\downarrow\downarrow \dots \downarrow\rangle$ at $g \rightarrow -\infty$.

Another consequence of crossing two critical points and Eq. (165) is a simplified quadratic correlator in Eq. (134),

$$\alpha_{m,n} = \frac{1}{2\pi} \int_{-\pi}^{\pi} dk p_k e^{ik(m-n)} = \frac{1 + (-1)^{m-n}}{2} \frac{1}{\sqrt{2}\pi \hat{\xi}} e^{-\frac{(m-n)^2}{8\pi \hat{\xi}^2}}, \quad (167)$$

which is zero when $m - n$ is odd. The other correlator $\beta_{m,n}$ in Eq. (135) is even simpler.

Indeed, the last adiabatic stage of the evolution, after crossing the second critical point at $g_c = -1$, leaves plenty of time for quantum dephasing. When $g \ll -1$ the eigenstates of the Bogoliubov-de Gennes Eqs. (109) are $(u_k, v_k) \approx (1, 0)$ and $(u_k, v_k) \approx (0, 1)$ with eigenvalues $-\omega_k$ and ω_k respectively, where $\omega_k \approx 2(g - \cos k)$. Consequently, the adiabatic solution of Eqs. (117) is

$$u_k \approx \sqrt{p_k} e^{i\frac{t^2}{\tau_Q} - 2it \cos k - i\varphi_k}, \quad v_k \approx \sqrt{1-p_k} e^{-i\frac{t^2}{\tau_Q} + 2it \cos k + i\varphi_k}. \quad (168)$$

As $t \rightarrow \infty$ the solutions (u_k, v_k) accumulate phase factors $\exp \mp i(2t \cos k - t^2/\tau_Q)$ which oscillate strongly with k . These oscillations “dephase” the integral in Eq.

(135) to zero:

$$\beta_{m,n} = \frac{1}{2\pi i} \int_{-\pi}^{\pi} dk \sqrt{p_k(1-p_k)} e^{2i\frac{t^2}{\tau_Q} - 4it \cos k - 2i\varphi_k} e^{ik(m-n)} \rightarrow 0 \quad (169)$$

when $t \rightarrow \infty$.

However, when t is large but finite, then the dephasing in Eq. (169) is effective only when $|m - n| \ll 4t$, where the 4 is twice the maximal group velocity of instantaneous quasiparticles when $|g| \gg 1$. This estimate means that the dephasing length l in Eq. (137) continues to grow like

$$l(t) = 4t \quad (170)$$

in the last adiabatic stage of the evolution after $g_c = -1$.

Notice that the correlator $\alpha_{m,n}$ depends on $\hat{\xi}$. Since in the absence of any non-zero $\beta_{m,n}$ the quadratic correlator $\alpha_{m,n} = \langle c_m c_n^\dagger \rangle$ contains all the information about the final Gaussian state, then we can conclude that $\hat{\xi}$ remains a permanent imprint of KZM which has not been washed out by quantum dephasing. This imprint has several interesting manifestations:

- Using Szegő limit theorem, the ferromagnetic correlator can be found as [58]

$$C_R^{xx} \propto \frac{1 + (-1)^R}{2} \exp\left(-0.174 \frac{R}{\hat{\xi}}\right) \cos\left(\sqrt{\frac{\ln 2}{2\pi}} \frac{R}{\hat{\xi}} - \varphi_\infty\right) \quad (171)$$

when $\tau_Q \gg 1$ and $1 \ll R \ll l(t)$. As a consequence of crossing two critical points instead of one, this correlator is zero for odd R . When $t \rightarrow \infty$ then $l(t) \rightarrow \infty$ and the correlator becomes accurate for all $R \gg 1$.

As we can see, during the linear quench the ferromagnetic correlator evolves from the pure exponential decay at $g_c = 1$, see Figs. 13C and D, to the oscillating exponential decay at $g \rightarrow -\infty$, see Eq. (171). These oscillations are gradually developed by quantum dephasing during the adiabatic stages of the evolution. At $g = 0$ the oscillations are limited to $R \ll \sqrt{\tau_Q} \ln \tau_Q$, but as $g \rightarrow -\infty$ they gradually extend to all (even) R . The dephasing relaxes the state to a crystal-like train of kinks and antikinks.

- The transverse magnetization is

$$\langle \sigma_n^z \rangle = 2\alpha_{0,0} - 1 = -1 + 2n_{\text{ex}}, \quad (172)$$

i.e., the magnetization -1 in the final ground state at $g \rightarrow -\infty$ plus twice the density of inverted spins in Eq. (166).

- The transverse correlator is

$$C_R^{zz} = -4|\alpha_{0,R}|^2 \approx -\frac{1 + (-1)^R}{2} \frac{2 e^{-\frac{R^2}{4\pi \hat{\xi}^2}}}{\pi^2 \hat{\xi}^2}, \quad (173)$$

compare Eqs. (148,166,167). This is roughly the $l \rightarrow \infty$ limit of the same correlator at $g = 0$, compare Eq. (148).

- The block impurity introduced in Section 2.13.5 is

$$I(\Pi) \equiv \text{Tr} \Pi(1 - \Pi) = 2\text{Tr}\alpha(1 - \alpha) \approx 2n_{\text{ex}}L \quad (174)$$

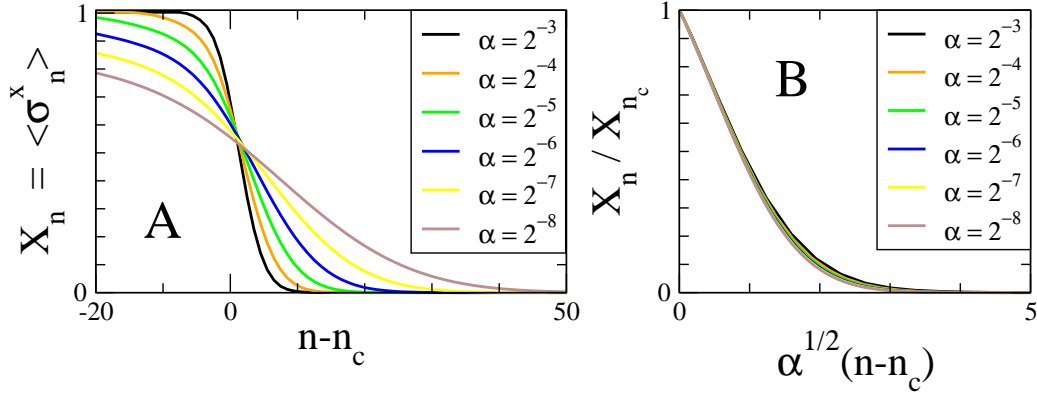


Figure 14. In A and B, spontaneous ferromagnetic magnetization as a function of $n - n_c$ and the rescaled $x = \sqrt{\alpha}(n - n_c)$ respectively. The collapse of the rescaled plots in panel B demonstrates that the penetration depth of the ferromagnetic order parameter into the paramagnetic phase is $\delta n \simeq \alpha^{-1/2}$ which is the same as the $\hat{\xi}$ predicted in Eq. (29). (Figure from Ref. [45])

when $L \gg \hat{\xi} \gg 1$ but $L \ll l(t)$. Here we used Eqs. (133,166,169,167).

- The extensive impurity in Eq. (174) implies that the block entropy is also extensive: $S(L, \tau_Q) = sL$ for $L \gg \hat{\xi}$. The entropy density s is most conveniently evaluated as the entropy of the whole chain $S(N, \tau_Q)$ divided by N , see Ref. [58]:

$$s = \lim_{N \rightarrow \infty} \frac{-2 \text{Tr} \alpha \log_2(1 - \alpha)}{N}$$

$$= -\frac{2}{\ln 2} \int_{-\pi}^{\pi} \frac{dk}{2\pi} [p_k \log_2 p_k + (1 - p_k) \log_2(1 - p_k)] \approx 0.11 n_{\text{ex}} \quad (175)$$

accurate when $n_{\text{ex}} \ll 1$. Here we used Eqs. (133,138,167,169) and evaluated the trace in the quasimomentum basis taking the continuous k limit for $N \rightarrow \infty$.

Notice that here the entropy of the whole chain sN appears finite while the actual quantum state of the isolated chain is pure. This is an artifact of sending $\beta_{m,n} \rightarrow 0$ in Eq. (169) which is accurate only when $|m - n| \ll l(t)$ at a finite t . This condition limits validity of the extensive entropy $S = 0.11 n_{\text{ex}} L$ to $L \ll l(t)$.

- Two site entanglement at $g \rightarrow -\infty$ was studied in Ref. [90]. Both concurrence \mathcal{C}^R and negativity \mathcal{N}^R are zero when the distance R between the two sites is odd. Only entanglement between even-neighbour sites can be non-zero. For large τ_Q , these two measures of entanglement scale as

$$\mathcal{C}^{2n} \sim \hat{\xi}^{-1}, \quad \mathcal{N}^{2n} \sim \hat{\xi}^{-2}, \quad (176)$$

when n is fixed, and they decay exponentially with $n/\hat{\xi}$ for large n . What is more, the concurrence and negativity are non-zero only when $\tau_Q > \tau_Q^{(2n)}$, where $\tau_Q^{(2n)}$ is a threshold that increases with n . When $\tau_Q \leq \tau_Q^{(2n)}$ there is no two-site entanglement and the entanglement is entirely multipartite.

2.13.11. Transition in space

In this Section we support the general discussion in Section 2.7 by a solution in the quantum Ising chain. We consider the ground state of an open Ising chain in an inhomogeneous transverse field g_n which can be linearised near the critical point at n_c where $g_c = 1$ as

$$g_n \approx 1 + \alpha (n - n_c), \quad (177)$$

compare Eq. (28). The open chain is in the ferromagnetic phase where $n < n_c$ and in the paramagnetic phase where $n > n_c$. We want to know if the non-zero spontaneous ferromagnetic magnetization $X_n = \langle \sigma_n^x \rangle$ in the ferromagnetic phase penetrates across the critical point into the paramagnetic phase and what is the depth of this penetration?

The quadratic Hamiltonian H^+ in Eq. (104) with open boundary conditions is diagonalised to $H^+ = \sum_m \omega_m \gamma_m^\dagger \gamma_m$ by a Bogoliubov transformation $c_n = \sum_{m=0}^{N-1} (u_{nm} \gamma_m + v_{nm}^* \gamma_m^\dagger)$ with m enumerating N eigenmodes of stationary Bogoliubov-de Gennes equations

$$\omega_m u_{n,m}^\pm = 2g_n u_{n,m}^\mp - 2u_{n\mp 1,m}^\mp \quad (178)$$

with $\omega_m \geq 0$. Here $u_{nm}^\pm \equiv u_{nm} \pm v_{nm}$. We make a long wavelength approximation $u_{n\mp 1,m}^\mp \approx u_{n,m}^\mp \mp \frac{\partial}{\partial n} u_{n,m}^\mp$ and obtain a long wavelength differential equation

$$\omega_m u_m^\pm = 2\alpha(n - n_c) u_m^\mp \pm 2\partial_n u_m^\mp . \quad (179)$$

Its eigenmodes with $\omega_m > 0$ are

$$\omega_m = \sqrt{8m\alpha} , u_m(n) \propto \psi_{m-1}(x) + \psi_m(x) , v_m(n) \propto \psi_{m-1}(x) - \psi_m(x) , \quad (180)$$

where

$$x = \sqrt{\alpha}(n - n_c) \quad (181)$$

is a rescaled distance from the critical point, $\psi_{m \geq 0}(x)$ are eigenmodes of a harmonic oscillator satisfying $\frac{1}{2}(-\partial_x^2 + x^2)\psi_m(x) = (m + 1/2)\psi_m(x)$, and $\psi_{-1}(x) \equiv 0$.

The modes in Eq. (180) are localised near $n = n_c$ where $x = 0$, in consistency with the linearisation in Eq. (177), and their typical width is $\delta x \simeq 1$, or equivalently

$$\delta n \simeq \alpha^{-1/2} . \quad (182)$$

When $\alpha \ll 1$ then $\delta n \gg 1$ and the long wavelength approximation in Eq. (179) is justified. As δn is the only scale of length in the solution (180), it must determine the penetration depth of the ferromagnetic magnetization into the paramagnetic phase, see Fig. 14. Note that this $\delta n \simeq \hat{\xi}$ in the general Eq. (29).

What is more, the analytic solution (180) implies a finite energy gap in the spectrum of H^+ ,

$$\hat{\Delta} = \omega_0 + \omega_1 = \sqrt{8\alpha} \simeq \alpha^{1/2} , \quad (183)$$

in agreement with the general scaling predicted in Eq. (30).

2.13.12. Inhomogeneous transition

The general argument in Section 2.8 can be also illustrated by a solution in the quantum Ising chain. Consider a time-dependent transverse field $g_n(t)$ which can be linearised near the critical point $g_c = 1$ as

$$g_n(t) \approx 1 + \alpha(n - vt) . \quad (184)$$

A critical point at $n = vt$ moving with a constant velocity $v > 0$ separates an expanding ferromagnetic phase for $n < vt$ from a shrinking paramagnetic phase

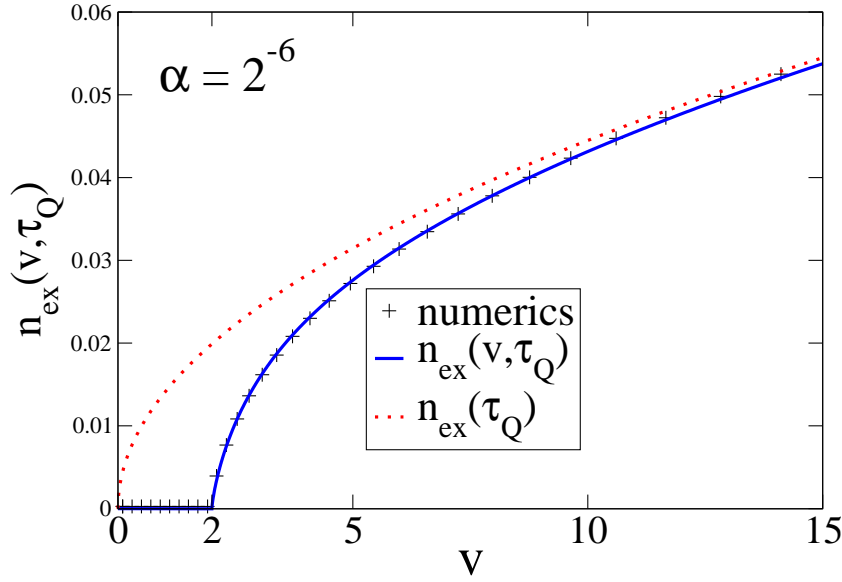


Figure 15. Comparison between the quasiparticle density predicted for an inhomogeneous transition in Eq. (187) (solid blue), the quasiparticle density after a homogeneous transition in Eq. (121) (dotted red), and numerical simulations on a lattice of $N = 1000$ spins (crosses) at a fixed inhomogeneity $\alpha = 2^{-6}$. (Figure from Ref. [45])

for $n > vt$. We want to know what is the density of quasiparticle excitations left behind the front in the ferromagnetic phase?

The time-dependent Bogoliubov-de Gennes equations are

$$i \frac{d}{dt} u_{n,m}^{\pm} = 2g_n(t) u_{n,m}^{\mp} - 2u_{n \mp 1, m}^{\mp}, \quad (185)$$

where $u_{nm}^{\pm} \equiv u_{nm} \pm v_{nm}$ are combinations of Bogoliubov modes in the transformation $c_n = \sum_{m=0}^{N-1} (u_{nm} \gamma_m + v_{nm}^* \gamma_m^{\dagger})$. A long wavelength approximation $u_{n \mp 1, m}^{\mp} \approx u_{n,m}^{\mp} \mp \frac{\partial}{\partial n} u_{n,m}^{\mp}$ leads to approximate long wavelength equations

$$i \partial_t \begin{pmatrix} u^+ \\ u^- \end{pmatrix} = [2\alpha(n - vt)\sigma^x + 2i\sigma^y \partial_n] \begin{pmatrix} u^+ \\ u^- \end{pmatrix}. \quad (186)$$

These equations were solved in Ref. [45]. Their analytic solution predicts the density of quasiparticle excitations

$$n_{\text{ex}}(v, \tau_Q) = \begin{cases} \left(1 - \frac{4}{v^2}\right)^{3/4} n_{\text{ex}}(\tau_Q) & \text{when } v > 2, \\ 0 & \text{otherwise,} \end{cases} \quad (187)$$

where $n_{\text{ex}}(\tau_Q) = \frac{1}{2\pi\sqrt{2\tau_Q}}$ is the density after a uniform transition in Eq. (121) with $\tau_Q = 1/\alpha v$. The analytic solution is not consistent with the long wavelength approximation in Eq. (186) near $v = 2$. This is why the exact equations (185) were also solved numerically. Figure 15 compares the analytic result (187), the numerical results, and the result for a homogeneous transition in Eq. (187).

As expected from the general scaling argument in 2.8, in the Ising chain there is a threshold velocity $\hat{v} \simeq 1$ below which excitation of quasiparticles is suppressed with respect to the homogeneous KZM. Analytic solution of the Ising chain gives the precise value $\hat{v} = 2$. Not incidentally, this is the fastest group velocity of quasiparticles at the critical point whose dispersion relation is $\epsilon_k \approx 2|k|$ for $|k| \ll$

π . As we have seen in Section 2.13.11, the spontaneous magnetization from the ferromagnetic phase behind the front penetrates into the paramagnetic phase ahead of the front, see Fig. 14. The paramagnetic spins near the critical front are biased to choose the same magnetization as in the ferromagnetic phase and in this way excitation of kinks (quasiparticles) behind the front is suppressed. The threshold $\hat{v} = 2$ is the fastest velocity at which the penetrating order parameter can catch up with the moving front. Indeed, the solution in Ref. [45] shows that when $v < 2$ the ferromagnetic magnetization penetrates into the paramagnetic phase to a depth

$$\delta n(v) \simeq \left(1 - \frac{v^2}{4}\right)^{1/4} \alpha^{-1/2} \quad (188)$$

which shrinks to zero when $v \rightarrow 2^-$. Above $\hat{v} = 2$ there is no bias to suppress kink excitations.

2.14. Quench across a multicritical point of the XY chain

The XY model is a generalisation of the Ising model (92)

$$H = - \sum_n (J_x \sigma_n^x \sigma_{n+1}^x + J_y \sigma_n^y \sigma_{n+1}^y + g \sigma_n^z) . \quad (189)$$

The Jordan-Wigner transformation (100) followed by a Fourier transform $c_n = \sum_k c_k e^{ikn} / \sqrt{N}$ maps the XY model to a one-dimensional quadratic fermionic Hamiltonian

$$H = \sum_k \left\{ 2[g - (J_x + J_y) \cos k] c_k^\dagger c_k + i(J_x - J_y) \sin k c_{-k} c_k + \text{h.c.} \right\} . \quad (190)$$

This Hamiltonian has the general form (59) with

$$H_k = 2 \begin{bmatrix} g - (J_x + J_y) \cos k & i(J_x - J_y) \sin k \\ -i(J_x - J_y) \sin k & -g + (J_x + J_y) \cos k \end{bmatrix} . \quad (191)$$

The multicritical point is located at $J_x = J_y = \frac{1}{2}g$, see Fig. 16, where the Hamiltonian (191) is $H_k = 2g(1 - \cos k)\sigma^z$ with a quasiparticle spectrum $\omega_k = 2g(1 - \cos k)$. This critical spectrum is quadratic in k for small k , hence $z = 2$ is the dynamical exponent.

We make a linear quench across this critical point along a line in the parameter space where $J_x = \frac{1}{2}g - \epsilon(t)$, $J_y = \frac{1}{2}g$ with the usual $\epsilon(t) = t/\tau_Q$, see Fig. 16. Along this quench line the Hamiltonian (191) is

$$H_k(t) = \epsilon(t) [2(\sigma^z \cos k + \sigma^y \sin k)] + [2g(1 - \cos k)\sigma^z] . \quad (192)$$

At $k = 0$ its spectrum is linear in $|\epsilon|$, $\omega_0 = 2|\epsilon|$, hence the critical exponents satisfy $\nu z = 1$ and, consequently, $z = 2, \nu = 1/2$. With these exponents the simple KZM estimate (17) predicts $n_{\text{ex}} \sim \tau_Q^{-1/4}$.

Equation (192) corresponds to the general Eq. (63). The orthonormalisation that follows Eq. (63) leads to Eq. (65) with functions

$$\Delta(k) = 2g(1 - \cos k) |\sin k| , \quad (193)$$

$$b(k) = 2g(1 - \cos k) \cos k . \quad (194)$$

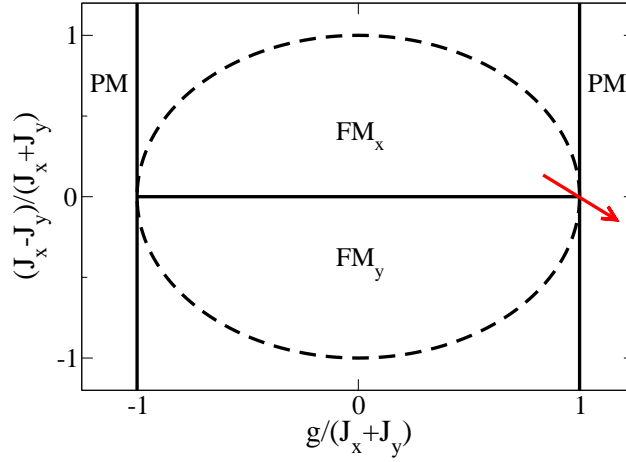


Figure 16. Phase diagram of the XY model (189) in the plane of anisotropy $(J_x - J_y)/(J_x + J_y)$ (vertical axis) and transverse field $g/(J_x + J_y)$ (horizontal axis). The vertical bold lines denote Ising transitions. The system is also gapless along the horizontal critical line. FM_x (FM_y) marks a ferromagnetic phase with long range order in the x (y) direction, and PM marks paramagnetic phases. The considered multicritical point is located at $(1, 0)$. The red arrow indicates direction of the linear quench near the multicritical point.

Near the Fermi point $k_F = 0$ we can expand $\Delta^2(k) \sim |k|^6$ and $b^2(k) \sim k^4$ and identify the exponents in Eqs. (71,77) as

$$z_\Delta = 6, \quad z_b = 4. \quad (195)$$

Here the inequality $z_\Delta \leq z_b$ in Eq. (78) is not satisfied and the exact density

$$n_{\text{ex}} \sim \tau_Q^{-1/z_\Delta} = \tau_Q^{-1/6} \quad (196)$$

decays with a different exponent than the $1/4$ predicted by the simple KZM estimate in Eq. (17). The anomalous scaling (196) was obtained for the first time in Ref. [60], see also [65]. More examples of multicritical anomalous scaling can be found in Ref. [61].

2.15. Kitaev model in 2D: quench across a gapless phase

The Kitaev model is a spin-1/2 model on a two-dimensional honeycomb lattice in Fig. 17 with a Hamiltonian [64]

$$H = \sum_{j+l=\text{even}} \left(J_1 \sigma_{j,l}^x \sigma_{j+1,l}^x + J_2 \sigma_{j-1,l}^y \sigma_{j,l}^y + J_3 \sigma_{j,l}^z \sigma_{j,l+1}^z \right), \quad (197)$$

where j and l are row and column indices of the lattice, see Fig. 17. It is an exactly solvable model with a gapless phase for $|J_1 - J_2| \leq J_3 \leq J_1 + J_2$. The model can be mapped onto a non-interacting fermionic model by a suitable Jordan-Wigner transformation [64],

$$H = i \sum_{\vec{n}} \left(J_1 b_{\vec{n}} a_{\vec{n}-\vec{M}_1} + J_2 b_{\vec{n}} a_{\vec{n}+\vec{M}_2} + J_3 D_{\vec{n}} b_{\vec{n}} a_{\vec{n}} \right), \quad (198)$$

where $a_{\vec{n}}$ and $b_{\vec{n}}$ are Majorana fermions sitting at the top and bottom sites respectively of a bond labelled \vec{n} , vectors $\vec{n} = \sqrt{3}\hat{i}n_1 + (\frac{\sqrt{3}}{2}\hat{i} + \frac{3}{2}\hat{j})n_2$ denote the midpoints of the vertical bonds shown in Fig. 17, and n_1, n_2 are integers. The vectors \vec{n} form

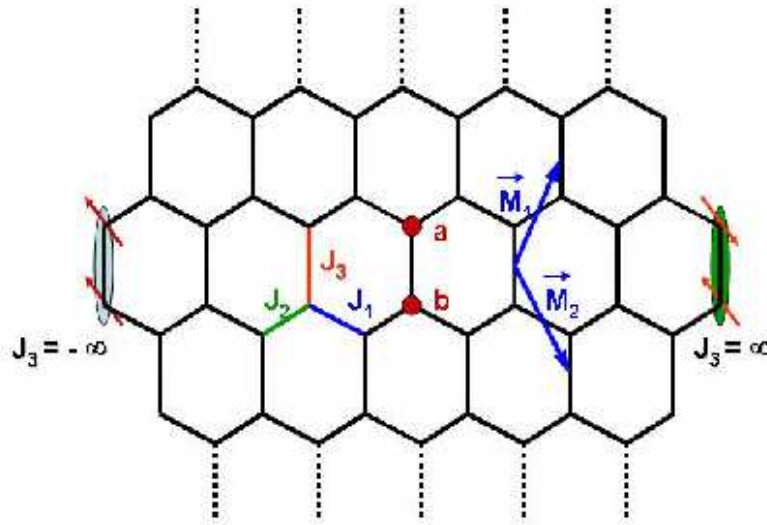


Figure 17. Schematic representation of the Kitaev model. (Figure from Ref. [63])

a triangular reciprocal lattice whose spanning vectors are $\vec{M}_1 = \frac{\sqrt{3}}{2}\hat{i} + \frac{3}{2}\hat{j}$ and $\vec{M}_2 = \frac{\sqrt{3}}{2}\hat{i} - \frac{3}{2}\hat{j}$. The operator $D_{\vec{n}}$ commutes with H and can take values ± 1 independently for each \vec{n} . The ground state corresponds to $D_{\vec{n}} = 1$ at every bond. Since $D_{\vec{n}}$ is a constant of motion, the dynamics of the model starting from the ground state will never take the system out of the subspace with $D_{\vec{n}} = 1$.

When $D_{\vec{n}} = 1$ a Fourier transform brings the fermionic Hamiltonian (198) to $H = \sum_{\vec{k}} \psi_{\vec{k}}^\dagger H_{\vec{k}} \psi_{\vec{k}}$, where $\psi_{\vec{k}}^\dagger = (a_{\vec{k}}^\dagger, b_{\vec{k}}^\dagger)$ are Fourier transforms of $a_{\vec{n}}$ and $b_{\vec{n}}$, and the sum over \vec{k} extends over half the first Brillouin zone of the triangular lattice formed by vectors \vec{n} . Here we quench

$$J_3(t) = \epsilon(t) = \frac{t}{\tau_Q} \quad (199)$$

from $t \rightarrow -\infty$ to $t \rightarrow +\infty$. The Hamiltonian $H_{\vec{k}}$ has the general form of Eq. (65) with

$$\Delta(\vec{k}) = 2[J_1 \sin(\vec{k}\vec{M}_1) - J_2 \sin(\vec{k}\vec{M}_2)] , \quad (200)$$

$$b(\vec{k}) = J_1 \cos(\vec{k}\vec{M}_1) + J_2 \cos(\vec{k}\vec{M}_2) , \quad (201)$$

$a(\vec{k}) = 2$, $\sigma(\vec{k}) = \sigma^y$, and $\sigma_\perp(\vec{k}) = \sigma^x$. The eigenvalues of $H_{\vec{k}}$ are $\pm\omega_{\vec{k}}$ and the quasiparticle spectrum $\omega_{\vec{k}} = \sqrt{4[\epsilon + b(\vec{k})]^2 + \Delta^2(\vec{k})}$ is gapless in the gapless phase where $|J_1 - J_2| \leq \epsilon \leq |J_1 + J_2|$. For each ϵ in this range there is a Fermi point \vec{k}_F such that $\Delta(\vec{k}_F) = 0$ and $\omega_{\vec{k}_F} = 0$.

The set of all Fermi points for different ϵ is a one dimensional Fermi line where $\sin(\vec{k}\vec{M}_1) = \sin(\vec{k}\vec{M}_2)$. When $\tau_Q \gg 1$ the excitation probability $p_{\vec{k}}$ in Eq. (68) is 1 on the Fermi line and exponentially small everywhere except near this line, see Figure 7. Expansion in $\vec{k} - \vec{k}_F$ near the Fermi line gives $z_\Delta = 2, z_b = 4$ when $J_1 = J_2$ and $z_\Delta = 2, z_b = 2$ otherwise. In any case, the integration in Eq. (69) gives

$$n_{\text{ex}} \simeq \tau_Q^{-\frac{d-m}{z_\Delta}} = \tau_Q^{-1/2} . \quad (202)$$

This result was obtained for the first time in Ref. [63]. A sudden quench from a topologically ordered Hamiltonian to a Hamiltonian that does not support topological order was considered in Ref. [91].

2.16. *The random Ising chain: logarithmic dependence of excitation density on transition rate*

An example of the random Ising chain is [92, 93]

$$H = - \sum_{n=1}^N (g \sigma_n^z + J_n \sigma_n^x \sigma_{n+1}^x) . \quad (203)$$

with periodic boundary conditions $\vec{\sigma}_{N+1} = \vec{\sigma}_1$. Here J_n 's are random ferromagnetic couplings which, without loss of generality, can be assumed positive, $J_n > 0$, and g is a uniform transverse magnetic field. This model has two quantum critical points at $g_c = \pm \exp(\overline{\ln J_n})$ separating a ferromagnetic phase, $|g| < g_c$, from two paramagnetic phases, $|g| > g_c$. The randomness is a relevant perturbation leading to a different universality class than the pure Ising model.

When ensemble averaged quantities are considered, the critical exponent is $\nu = 2$, instead of $\nu = 1$ in the pure case, and the dynamical parameter z diverges as

$$z \approx \frac{1}{2|\epsilon|} \quad (204)$$

near the critical point where $\epsilon \equiv (g - g_c)/g_c = 0$.

In a zero order approximation [85, 94, 95], one might take first the limit $\epsilon \rightarrow 0$ which implies $z \rightarrow \infty$. In this limit, the general KZM estimate (16) implies $\hat{\xi} \simeq 1$, i.e., neither the correlation length $\hat{\xi}$ nor the excitation density $n_{\text{ex}} \simeq \hat{\xi}^{-1}$ depend on the transition time τ_Q . No matter how slow the transitions is, the density of excitations remains the same. This approximation demonstrates that there is no usual *power law* KZ scaling in the random Ising model. However, it is too crude to exclude a weak logarithmic dependence.

A more accurate result is obtained with the adiabatic-impulse-adiabatic approximation which is central to KZM [85, 94], see Section 2.3. The energy gap depends on ϵ as $\Delta \simeq |\epsilon|^{z\nu} \simeq |\epsilon|^{1/|\epsilon|}$ while the transition rate is $|\dot{\epsilon}/\epsilon| = 1/|t| = 1/|\tau_Q \epsilon|$. The rate equals the gap at $\hat{\epsilon}$ when

$$\frac{\alpha}{\tau_Q \hat{\epsilon}} = \hat{\epsilon}^{1/\hat{\epsilon}} , \quad (205)$$

where $\alpha \simeq 1$ is a non-universal parameter. When $\ln \tau_Q \gg 1$ an approximate solution is

$$\hat{\xi} \sim \hat{\epsilon}^{-2} \sim (\ln \tau_Q)^2 . \quad (206)$$

This logarithmic dependence on τ_Q is very weak as compared to any power law scaling. It means that no matter how slow the transition is the ensemble-averaged density of defects in the final ferromagnetic phase,

$$n_{\text{ex}} \simeq \hat{\xi}^{-1} \sim (\ln \tau_Q)^{-2} , \quad (207)$$

remains roughly the same.

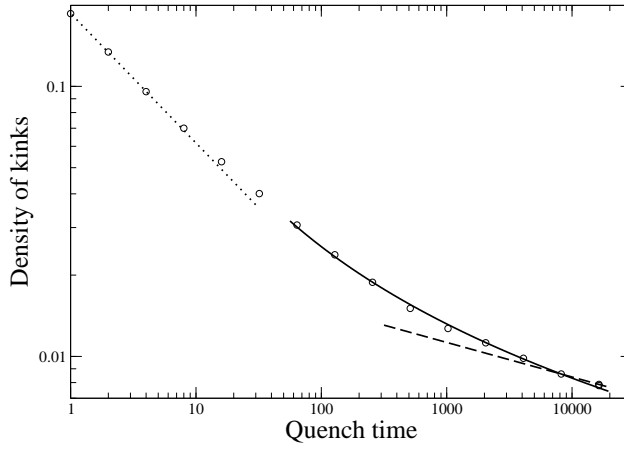


Figure 18. Density of kinks n_{ex} as a function of transition time τ_Q on a lattice of $N = 512$ sites. Circles are final kink densities averaged over 4 realizations of J_n . Error bars set the size of the circles. The solid line is the best fit $n_{\text{ex}}(\tau_Q) = \frac{0.15}{\hat{\epsilon}^2(\tau_Q/3.4)}$ where $\hat{\epsilon}(\tau_Q/\alpha)$ is the solution of Eq.(205). The dotted line is the best power law fit $d \sim \tau_Q^{-w}$ to the left-most 3 data points and the dashed line is the “fit” to the right-most 2 data points. The exponents are $w = 0.48$ and $w = 0.13$ respectively. The exponent $w = 0.48$ for the fastest transitions is consistent with the exponent $\frac{1}{2}$ in the pure Ising model. (Figure from Ref. [94])

The prediction (206) was tested by numerical simulation of the time-dependent Bogoliubov-de Gennes equations

$$i \frac{d}{dt} u_{n,m}^{\pm} = 2g(t)u_{n,m}^{\mp} - J_{n-\frac{1}{2} \mp \frac{1}{2}, m} u_{n \mp 1, m}^{\mp}. \quad (208)$$

Here $u_{n,m}^{\pm} = u_{n,m} \pm v_{n,m}$ are combinations of Bogoliubov modes in the transformation $c_n = \sum_{m=0}^{N-1} (u_{nm} \gamma_m + v_{nm}^* \gamma_m^{\dagger})$. The random J_n 's were uniformly distributed in $(0, 2)$ implying $g_c = 2e^{-1}$. $g(t) = -g_c t/\tau_Q$ was quenched from a large initial $g \gg g_c$ to the final $g = 0$ where density of kinks was calculated. The initial conditions were stationary modes of the Bogoliubov-de Gennes equations (208) at the initial large g corresponding to the ground state of the system.

Results of the simulations are collected in Fig. 18. They confirm the logarithmic dependence in Eq. (206) for large τ_Q . However, for relatively fast transitions that freeze out at relatively large $\hat{\epsilon}$, the scaling $n_{\text{ex}} \sim \tau_Q^{-1/2}$ characteristic for the pure Ising model is recovered, compare Eq. (121). These transitions cannot feel the effect of disorder that is appreciable only when $\hat{\epsilon}$ is close enough to the critical point.

The density of kinks scales as $n_{\text{ex}} \sim (\ln \tau_Q)^{-2}$. Since each kink contributes to the excitation energy, one might expect that the excitation energy density ε at the final $g = 0$ is proportional to n_{ex} . Contrary to this simple expectation, the ensemble-averaged energy density was found to scale as

$$\varepsilon \sim (\ln \tau_Q)^{-(3.4 \pm 0.2)} \quad (209)$$

with an exponent significantly greater than 2, see Ref. [95]. The origin of the steeper exponent can be traced back to the uniform distribution of $J_n \in (0, 2)$ which does not exclude arbitrarily weak bond strengths J_n . With increasing τ_Q the excited kinks tend to localize more and more on the weakest bonds, which are the easiest to excite, making the excitation energy decay faster than the kink density.

An alternative derivation of the scaling (207) from the Landau-Zener theory, taking into account distribution of minimal gaps at different values of g during the quench, can be found in Ref. [95]. This method originates from the theory of quantum annealing [12].

In summary, in the random Ising model, representing the infinite disorder universality class, density of excitations does not follow the usual KZM power law decay with the transition time, but the actual logarithmic dependence can still be obtained from the adiabatic-impulse-adiabatic approximation essential for KZM. This example and that in Ref. [96] suggest that disorder, when a relevant perturbation, makes excitation much easier than in the pure case, but we would need more evidence to support this claim as a general conclusion.

2.17. Topological insulators: anomalous excitation of edge states

Topological insulators are an intriguing state of matter where edge transport exists even in the presence of a bulk energy gap [97]. The edge states responsible for the transport are usually localised in the interface separating two topologically different insulators, the simplest example being an integer quantum Hall effect sample and the vacuum [98]. The topological edge states arise in a variety of systems such as one dimensional spin models [99], the integer and fractional quantum Hall effect [100], and have been experimentally realised in topological insulators [101]. They also include the anomalous half-integer quantum Hall effect in the honeycomb or square lattice [102] and the quantum Hall spin effect [103]. Depending on the symmetries of the Hamiltonian and the dimension of the system topological insulators can be classified in a periodic table [104]. One of the simplest systems is the one dimensional chain of Majorana fermions [105], where the edge states are the Majorana fermions localised at the ends of the chain. Isolation of Majorana fermions would be an important step towards topological quantum computation [106]. Various proposals include the vortex core of two dimensional $p + ip$ superconductor [107], tri-junctions of superconductor-topological insulator-superconductor [108], and many others [109].

Reference [110] considers the one dimensional fermionic chain [105]

$$H = \sum_j \left(-w a_j^\dagger a_{j+1} + \Delta a_j a_{j+1} - \frac{\mu}{2} a_j^\dagger a_j + \text{h.c.} \right) \quad (210)$$

where a_j are spinless fermionic lattice annihilation operators satisfying $\{a_i, a_j^\dagger\} = \delta_{ij}$. The fermions hopping between lattice sites with the tunnelling frequency w can be injected or removed from the wire in the form of Cooper pairs. In the following we assume $\mu = 0$ and imaginary $\Delta = i|\Delta|$ for simplicity.

In case of periodic boundary conditions, $a_{N+1} = a_1$, there are no edge states and the system is translationally invariant. In the quasimomentum representation $a_j = \frac{1}{\sqrt{N}} \sum_k a_k e^{-ikj}$ with $k \in (-\pi, \pi]$, the Hamiltonian becomes

$$H = \sum_k \begin{pmatrix} a_k^\dagger & a_{-k} \end{pmatrix} H_k \begin{pmatrix} a_k \\ a_{-k}^\dagger \end{pmatrix}, \quad H_k = \begin{pmatrix} -w \cos k & |\Delta| \sin k \\ |\Delta| \sin k & w \cos k \end{pmatrix} \quad (211)$$

with energies of Bogoliubov quasiparticle excitations $\epsilon_k = 2\sqrt{w^2 \cos^2 k + |\Delta|^2 \sin^2 k}$. These are the bulk excitations of the topological insulator. For a fixed $|\Delta| > 0$ they are gapless at a critical point $w = 0$ with the critical exponents $z = \nu = 1$.

Here we consider a linear quench

$$w(t) = \frac{t}{\tau_Q} \quad (212)$$

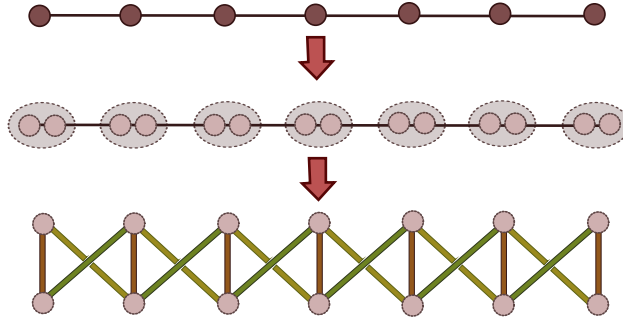


Figure 19. The fermionic chain (210) is mapped to a Majorana ladder by the transformation (214) which defines 2 Majorana fermions on each lattice site. (Figure from Ref. [110])

from $-|\Delta|$ to $|\Delta|$. Equation (211) becomes a set of independent Landau-Zener problems for each k like in Section 2.11. When $\tau_Q \gg |\Delta|^{-2}$, then only quasiparticles with $k \approx 0$ and $k \approx \pi$ get excited with probability $p_k = \exp(-\pi|\Delta|^2\tau_Q \sin^2 k / |\cos k|)$. In the thermodynamic limit density of bulk excitations becomes an integral

$$n_{\text{bulk}} = \int_{-\pi}^{\pi} \frac{dk}{2\pi} p_k \approx \frac{1}{\pi|\Delta|} \tau_Q^{-1/2}. \quad (213)$$

when $\tau_Q \gg |\Delta|^{-2}$. This is the usual KZ scaling expected for the critical exponents $z = \nu = 1$.

So far everything was standard and, probably, not worth a special Subsection. However, as expected from a *topological* insulator, an open chain is different from the periodic chain because there are localised edge states. In case of the open chain it is better to introduce hermitian Majorana fermions

$$c_{2j-1} = \frac{1}{\sqrt{2}} \left(e^{-i\pi/4} a_j^\dagger + e^{i\pi/4} a_j \right), \quad c_{2j} = \frac{i}{\sqrt{2}} \left(e^{-i\pi/4} a_j^\dagger - e^{i\pi/4} a_j \right), \quad (214)$$

satisfying $\{c_i, c_j\} = \delta_{i,j}$, which transform the Hamiltonian (210) into

$$H = i \sum_{j=1}^{N-1} [(w + |\Delta|)c_{2j}c_{2j+1} + (-w + |\Delta|)c_{2j-1}c_{2j+2}]. \quad (215)$$

The Majorana fermions live on a virtual ladder whose j -th rung contains two Majorana fermions c_{2j-1}, c_{2j} and corresponds to the j -th site of the original chain, see Fig. 19.

At the initial $w = -|\Delta|$ the Hamiltonian (215) is a sum of $N - 1$ products $2i|\Delta|c_{2j-1}c_{2j+2}$, each of them having two eigenvalues $\pm|\Delta|$. In addition to them, there are two Majorana operators c_2, c_{2N-1} which, in case of periodic boundary conditions, would couple through the term $2i|\Delta|c_{2N-1}c_2$ which is missing in the present open chain. Their Hilbert space has two states with zero energy. The paired and unpaired states are shown in Fig. 20a.

In a similar way, at the final $w = |\Delta|$ there are $N - 1$ products $2i|\Delta|c_{2j}c_{2j+1}$ with eigenenergies $\pm|\Delta|$ and two “unpaired” Majoranas c_1, c_{2N} with two zero energy states, see Fig. 20b. In both cases, the “paired” states are the gap-full bulk modes and the “unpaired” zero energy states are the edge states created by opening the periodic chain.

The bulk and edge states can be written in a compact form with the help of the BCS state $|\Omega\rangle = \prod_k \left(u_k + v_k a_{-k}^\dagger a_k^\dagger \right) |0\rangle$, where $|0\rangle$ is a Fock vacuum for a_j

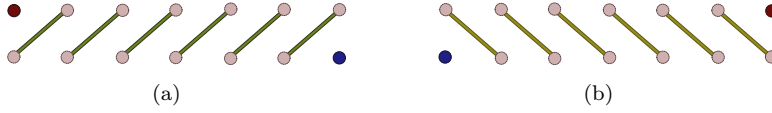


Figure 20. The gap-full paired bulk states and the unpaired edge zero modes for the initial $w = -|\Delta|$ (panel a) and the final $w = |\Delta|$ (panel b). (Figure from Ref. [110])

and the Bogoliubov coefficients are $u_k = \frac{1}{\sqrt{2}} \sqrt{1 - \frac{w \cos k}{\epsilon_k}}$, $v_k = \frac{\text{sign}(k)}{\sqrt{2}} \sqrt{1 + \frac{w \cos k}{\epsilon_k}}$. This state is a zero energy state of the periodic chain with a Hamiltonian $\bar{H} = \sum_{k>0} \epsilon_k \left(\gamma_{k,+}^\dagger \gamma_{k,+} - \gamma_{k,-}^\dagger \gamma_{k,-} \right)$, where $\gamma_{k,+} = u_k^* a_k + v_k a_{-k}^\dagger$ and $\gamma_{k,-} = -v_k^* a_k + u_k a_{-k}^\dagger$. In case of the open chain and the initial $w = -|\Delta|$ the edge zero modes are $c_2|\Omega\rangle$ and $c_{2N-1}|\Omega\rangle$, and the bulk eigenstates of energies $\pm|\Delta|$ are $(\pm i c_{2j-1} + c_{2j+2})|\Omega\rangle$. At the final $w = |\Delta|$ the zero energy edge states are $c_1|\Omega\rangle$ and $c_{2N}|\Omega\rangle$, and the bulk eigenstates of energies $\pm|\Delta|$ are $(\pm i c_{2j} + c_{2j+1})|\Omega\rangle$.

We assume that the initial state at $w = -|\Delta|$ is one of the two unpaired edge states: the left zero mode $|L(-|\Delta|\rangle) = c_2|\Omega\rangle$ or the right one $|R(-|\Delta|\rangle) = c_{2N-1}|\Omega\rangle$. In adiabatic transition the left and right zero modes would evolve with increasing w into [105, 110]

$$|L(w)\rangle \propto \left(c_2 + r c_6 + \cdots + r^{\frac{N+1}{2}} c_{2N} \right) |\Omega\rangle, \quad (216)$$

$$|R(w)\rangle \propto \left(c_{2N-1} + r c_{2N-5} + \cdots + r^{\frac{N+1}{2}} c_1 \right) |\Omega\rangle, \quad (217)$$

where $r = (|\Delta| + w)/(|\Delta| - w)$ increases with w from $r = 0$ at the initial $w = -|\Delta|$, through $r = 1$ at the critical $w = 0$, to $r \rightarrow \infty$ at the final $w = |\Delta|$. As w increases, the edge states get increasingly de-localised until they become uniformly spread along the whole ladder at the critical point. These de-localised states can be also written as

$$|L(0)\rangle \propto \left(\gamma_{-\pi,-}^\dagger + \gamma_{0,+}^\dagger \right) |\Omega\rangle, \quad |R(0)\rangle \propto \left(\gamma_{-\pi,-}^\dagger - \gamma_{0,+}^\dagger \right) |\Omega\rangle. \quad (218)$$

Each of these two states is an equal superposition of two gapless bulk modes from the positive and negative energy branch. Thus no matter how slow, the evolution at this point cannot be adiabatic and any further increase of w above 0 will not connect these states to the edge states at the final $w = |\Delta|$. An initial edge state will end with probability 1/2 in either the positive or negative energy band. Thus the probability to excite a defect is 1/2 and does not depend on τ_Q .

A similar analysis in Ref. [111] in another topological insulator - the Creutz ladder [112] - concludes that, while the density of bulk excitations decays like $\tau_Q^{-1/2}$, the edge modes are excited with a probability scaling as $\tau_Q^{-1.35}$. This is much steeper decay than for the bulk excitations in contrast to the Majorana chain, where the edge modes are excited with the probability 1/2 independent of τ_Q . Unlike in the Majorana chain, the edge modes of the Creutz ladder remain localised at the critical point. These two examples demonstrate that the edge modes, whose existence is ensured by topology, need special treatment in dynamical phase transitions.

2.18. The Lipkin-Meshkov-Glick model: KZM and infinite coordination number

Most examples in this review are in one or at most two spatial dimensions, but in this Section we follow Ref. [113] and consider the opposite extreme of infinite coordination number. In this limit it is hard to identify an analogue of the KZ correlation length $\hat{\xi}$ but, nevertheless, the density of excitations can still be obtained from KZM.

The specific model that we consider is the exactly solvable Lipkin-Meshkov-Glick model,

$$H = -\frac{2}{N} \sum_{i<j} \left(\sigma_i^x \sigma_j^x + \gamma \sigma_i^y \sigma_j^y \right) - g \sum_{i=1}^N \sigma_i^z . \quad (219)$$

It was introduced for the first time in the context of nuclear physics [114] and then thoroughly studied in a number of papers [115]. Here $N \rightarrow \infty$ is a number of spins in the system, $\gamma \leq 1$ is the anisotropy parameter, and g is the transverse field. In a sense, the model is the infinite coordination number limit of the XY model or, when $\gamma = 0$, the quantum Ising chain.

The model has a second order quantum phase transition at $g_c = 1$ with mean-field critical exponents. The magnetization in the x -direction (or the xy -plane in the isotropic case of $\gamma = 1$) is

$$m = (1 - g^2)^{1/2} \quad (220)$$

in the ferromagnetic phase when $g \leq 1$ and zero otherwise. The energy gap vanishes at the transition as

$$\Delta = \sqrt{(g-1)(g-\gamma)} \quad (221)$$

for $g > 1$. The ferromagnetic ground state below $g = 1$ is doubly degenerate for any $\gamma < 1$.

A sudden quench in the Ising version of this model, when $\gamma = 0$, was considered in Ref. [116]. Here we follow Ref. [113] and consider a linear quench

$$g(t) = -\frac{t}{\tau_Q} \quad (222)$$

from the ground state at $g \rightarrow \infty$ to $g = 0$. In the adiabatic limit we would expect final magnetization $m = 1$ with all spins pointing in the same direction. After a transition with a finite rate a fraction m_{inc} of spins is reversed and the magnetization is *incomplete*

$$m = 1 - m_{\text{inc}} . \quad (223)$$

This reduced magnetization costs a finite residual excitation energy per site $\frac{E_{\text{res}}}{N}$. When $m_{\text{inc}} \ll 1$ then $\frac{E_{\text{res}}}{N} \simeq m_{\text{inc}}$.

In Ref. [113] the linear quench was evolved numerically with the results collected in Fig. 21a. When $\tau_Q \lesssim 1$ we can see saturation at $m_{\text{inc}} \approx 1$. These quenches are effectively instantaneous as there is simply not enough time to build up any ferromagnetic magnetization. However, when $\tau_Q \gg 1$ then we observe a scaling

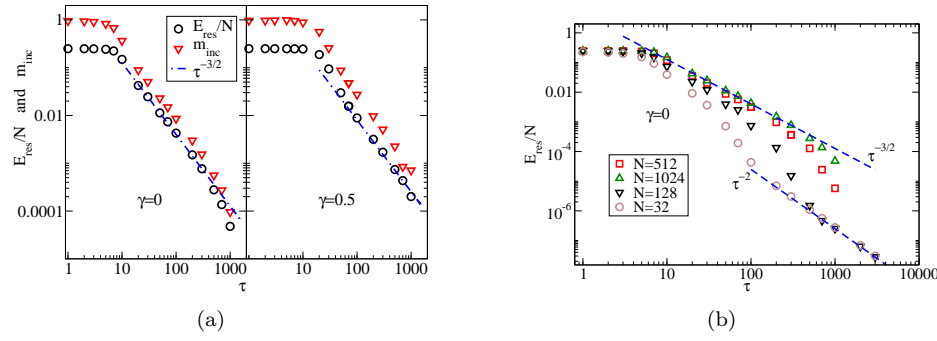


Figure 21. In a, residual energy per spin and m_{inc} as a function of τ_Q in a system of $N = 1024$ sites. For slow enough quenches the data are consistent with the $\tau_Q^{-3/2}$ scaling. In b, residual energy per spin as a function of τ_Q for different system sizes ranging from $N = 32$ to $N = 1024$. For very large τ_Q the dependence of energy on the transition rate crosses over to a steeper power law τ_Q^{-2} , as explained in Ref. [113] by incomplete LZ anti-crossings. (Figure from Ref. [113])

consistent with

$$\frac{E_{\text{res}}}{N} \sim m_{\text{inc}} \sim \tau_Q^{-3/2}. \quad (224)$$

The exponent can be explained as follows.

Since the parity operator $\prod_{n=1}^N \sigma_n^z$ is a good quantum number and the initial ground state at large g is the even-parity state fully polarized along the z -axis, then we can confine to the subspace of even parity. In this subspace, when $g \gg 1$ then the instantaneous gap to reverse two spins is $4g \approx \frac{4|t|}{\tau_Q}$. On the other hand, the gap at the critical $g_c = 1$ scales as

$$\Delta_c \simeq N^{-1/3} \quad (225)$$

when $N \rightarrow \infty$. Consequently, the transition between the ground state and the first excited state can be described by an effective LZ model with a time-dependent Hamiltonian

$$H_{\text{LZ}} = \begin{pmatrix} -4\left(\frac{t}{\tau_Q} + g_c\right) & \Delta_c \\ \Delta_c & 4\left(\frac{t}{\tau_Q} + g_c\right) \end{pmatrix} \quad (226)$$

and the LZ excitation probability is

$$P = \exp\left(-\frac{\pi}{4}\Delta_c^2\tau_Q\right) \simeq \exp\left(-\frac{\pi}{4}N^{-2/3}\tau_Q\right) \quad (227)$$

From this probability we can read that, for a given τ_Q , the maximal size of a defect-free system is $N_{\text{free}} \simeq \tau_Q^{3/2}$. In a similar way as in Section 2.13.2 and Ref. [36], we can use its inverse N_{free}^{-1} as an estimate of the density of reversed spins,

$$m_{\text{inc}} \simeq N_{\text{free}}^{-1} \simeq \tau_Q^{-3/2}. \quad (228)$$

This estimate explains the $\frac{3}{2}$ -scaling observed in Fig. 21a.

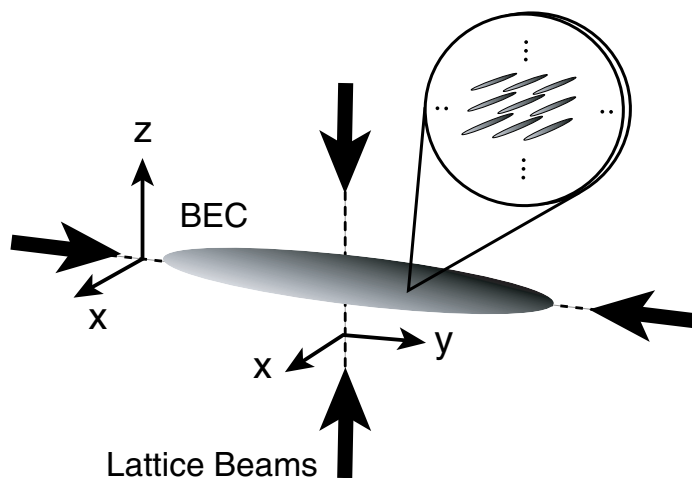


Figure 22. Schematic set up of the experiment in Refs. [2, 19]. A 2D lattice is formed by overlapping two optical standing waves along the y -axis and the z -axis with a Bose-Einstein condensate in a harmonic trap. The condensate is then confined to an array of several thousand narrow potential tubes. (Figure from Ref. [19])

2.19. *Bose-Hubbard model: transition between gapped Mott insulator and gapless superfluid*

The non-integrable Bose-Hubbard model is one of the two paradigmatic examples of systems with a quantum phase transition [15], the other being the already described integrable quantum Ising chain. What may be even more important, the model was realised experimentally with ultracold atomic gases [2, 13, 19], see Fig. 22. Here we consider mainly its one-dimensional version

$$H = -J \sum_{s=1}^N (a_{s+1}^\dagger a_s + \text{h.c.}) + \frac{U}{2} \sum_{s=1}^N n_s(n_s - 1), \quad (229)$$

where a_s are bosonic annihilation operators, $n_s = a_s^\dagger a_s$ are number operators, and J is the tunnelling rate between nearest-neighbour lattice sites. For the sake of convenience, we will use dimensionless units such that the on-site interaction strength is $U = 1$, and assume periodic boundary conditions. In a realistic experiment with a few tens of lattice sites the dynamics should not be affected by the boundary conditions, if not to mention that the periodic boundary conditions should be directly accessible in a ring-shaped optical lattice [117] or by painting arbitrary and time-dependent potentials [7], see Fig. 23.

The model is especially interesting in the thermodynamic limit when the number of lattice sites $N \rightarrow \infty$ and a number of particles is commensurate with N , i.e., average number of particles per site is an integer n . In this limit it has a quantum Berezinski-Kosterlitz-Thouless transition [118] at $J_c \simeq n^{-1}$, see Ref. [119]. When $J > J_c$ the system is in the gapless superfluid phase with (algebraically decaying) quasi-long-range order, and when $J < J_c$ it is in the gapfull Mott insulator phase. Here we consider dynamical transitions both from Mott insulator to superfluid and back.

We begin with a linear ramp from Mott insulator to superfluid,

$$J = \frac{t}{\tau_Q} \quad (230)$$

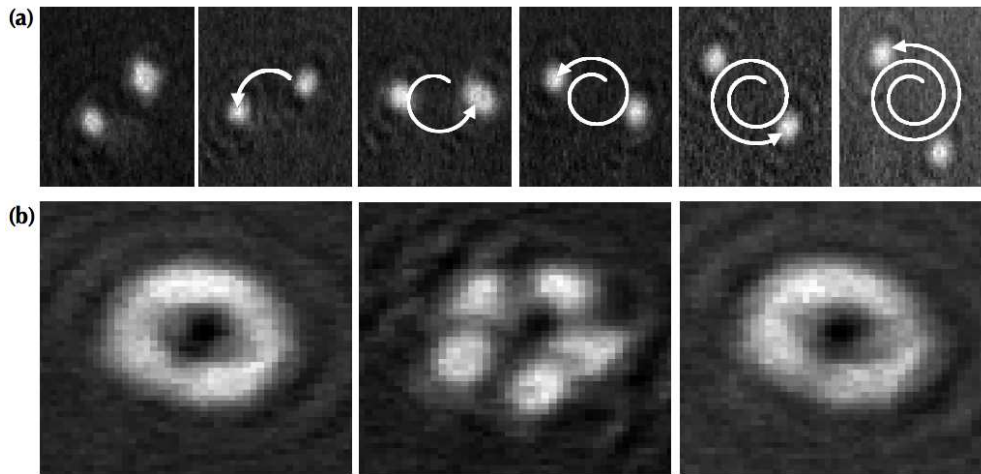


Figure 23. Painting an arbitrary and time-dependent potential by a rapidly moving laser beam. In a) a rotating two-site potential with Bose-Einstein condensates (BEC's), and in b) a toroidal BEC which is adiabatically converted into 5 disconnected spots and then back into toroidal form. (Figure from Ref. [7])

where τ_Q is the usual quench time. The evolution begins at $t = 0$ from the ground state of the Hamiltonian (229) at $J = 0$ which is the Mott state

$$|n, n, n, \dots\rangle \quad (231)$$

with a definite number of n particles per site. Experimentally, a perfect linear ramp of the tunnelling rate can be obtained by logarithmically reducing amplitude of optical lattice with an (optional) minor adjustment of interaction strength via the Feshbach resonance [55], see Figure 5, or by painting a time-dependent potential [7], see Figure 23.

In a transition to the superfluid phase we are interested in correlation functions

$$C_R(t) = \frac{1}{2} \langle \psi(t) | a_{i+R}^\dagger a_i + \text{h.c.} | \psi(t) \rangle . \quad (232)$$

The correlations are related to the momentum distribution of atoms n_k by a Fourier transform $n_k = \frac{1}{N} \sum_R \exp(ikR) C_R$. They are also good observables because C_R 's are conserved by the hopping term in the Hamiltonian (229) and by the end of time evolution at large J , when the interaction is just a small perturbation to the hopping term, they take stable final values. In particular,

$$K_1 = 1 - C_1 = \sum_k (1 - \cos k) n_k \quad (233)$$

is a (normalized) kinetic hopping energy. Both the hopping energy in particular and the momentum distribution in general depend on the transition time τ_Q .

Since the model is not integrable, in the following Sections we review approximate solutions in different regimes of parameters.

2.19.1. Slow transition from Mott insulator to superfluid

We begin with the limit of slow transitions in infinite system. Numerical studies in this regime are extremely time consuming, therefore we concentrate mainly on KZM predictions. According to KZM, the state of the system after a slow transition has the characteristic length-scale $\hat{\xi}$ in Eq. (16), where z and ν are critical exponents. For the Bose-Hubbard model the dynamical exponent $z = 1$.

The Mott insulator-superfluid transition (at an integer density of particles) in a d -dimensional Bose-Hubbard model belongs to the universality class of the $(d+1)$ -dimensional XY spin model [120]. Therefore:

- In one dimension this mapping implies that $\nu \rightarrow \infty$ as in the Berezinski-Kosterlitz-Thouless transition and

$$\hat{\xi} \sim \tau_Q. \quad (234)$$

As a result, the hopping energy of excitations should scale as

$$K_1 \sim \xi^{-2} \sim \tau_Q^{-2}. \quad (235)$$

The exponent -2 means a steep dependence of the hopping energy on the quench time τ_Q , which should make it easily discernible experimentally.

- In two dimensions $\nu = 0.67$ and

$$\xi \sim \tau_Q^{0.40}, \quad K_1 \sim \tau_Q^{-0.80}. \quad (236)$$

- In three dimensions we have the mean-field exponent $\nu = 1/2$ and

$$\xi \sim \tau_Q^{1/3}, \quad K_1 \sim \tau_Q^{-2/3}. \quad (237)$$

This scaling was confirmed in Ref. [70] by analytic calculations in the Bogoliubov theory of Ref. [121].

The non-mean-field scalings predicted in 1D and 2D have not been verified numerically, but see Ref. [122].

Slow transitions probe the universal critical exponents, but they require stability of experimental set-up over long transition time τ_Q . This is why it may be more practical to experiment first with faster transitions, where the point of freeze-out \hat{e} may be not close enough to the critical point to capture the universal scalings predicted in this Section, but there are nevertheless (non-universal) scaling relations bearing witness to non-adiabaticity of the transition. In the following two Sections we consider two tractable regimes of parameters where such non-universal predictions can be made. In the next Section 2.19.2 we assume the density of one particle per site. This minimal commensurate density makes direct numerical simulations possible for fast quenches and limited lattice sizes. Numerical results can be further corroborated by approximate analytic solutions. In Section 2.19.3 we take the opposite extreme of large density when semiclassical methods become applicable and, finally, in Section 2.19.4 we analyse a reverse transition from superfluid to Mott insulator.

2.19.2. Fast transition from Mott insulator to superfluid at small density

In this Section we follow Ref. [123] and consider $n = 1$ particle per site. This minimal commensurate density allows for some exact numerical simulations. For fast quenches it is enough to consider short times when the wave function remains close to the initial Mott state (231) and can be approximated by a variational state

$$|\psi(t)\rangle = a(t)|1, 1, \dots\rangle + b(t)(|0, 2, 1, 1, \dots\rangle + |2, 0, 1, 1, \dots\rangle + \dots) / \sqrt{2N}, \quad (238)$$

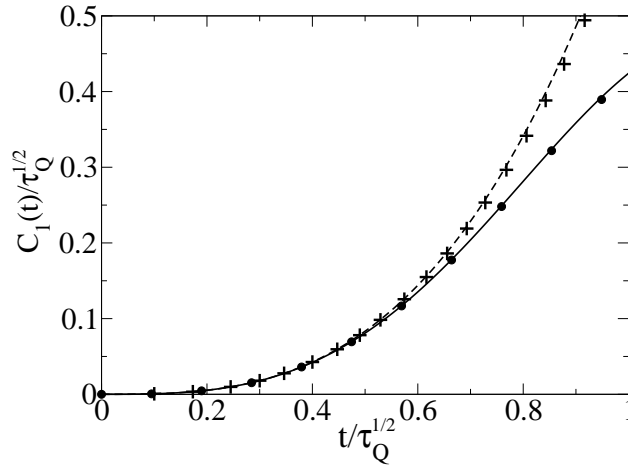


Figure 24. Short time dynamics of $C_1(t)$. Numerics for $N = 10$ lattice sites is given by the solid line ($\tau_Q = 0.001$) and the large dots ($\tau_Q = 0.1$). The dashed line presents Eq. (242). (Figure from Ref. [123])

where $|a|^2 + |b|^2 = 1$ and dynamics of $a(t), b(t)$ is governed by

$$i \frac{\partial}{\partial t} \begin{pmatrix} a \\ b \end{pmatrix} = \begin{pmatrix} 0 & -t \frac{2\sqrt{N}}{\tau_Q} \\ -t \frac{2\sqrt{N}}{\tau_Q} & 1 \end{pmatrix} \begin{pmatrix} a \\ b \end{pmatrix}. \quad (239)$$

A change of basis $(a', b') = e^{it/2}(a - b, -a - b)/\sqrt{2}$ yields

$$i \frac{\partial}{\partial t} \begin{pmatrix} a' \\ b' \end{pmatrix} = \frac{1}{2} \begin{pmatrix} \frac{t}{\tau} & 1 \\ 1 & -\frac{t}{\tau} \end{pmatrix} \begin{pmatrix} a' \\ b' \end{pmatrix}, \quad \tau = \frac{\tau_Q}{4\sqrt{N}}. \quad (240)$$

Here the time-dependent Hamiltonian is precisely the Landau-Zener Hamiltonian in Eq. (39) but, unlike in the standard LZ model where $t \in (-\infty, \infty)$, here the time evolution begins at $t = 0$ from the instantaneous ground state right in the middle of the anti-crossing. This is the case (ii) considered in Section 2.9.

The quantity of interest is

$$C_1(t) = \frac{|b'(t)|^2 - |a'(t)|^2}{\sqrt{N}}. \quad (241)$$

An expansion of the exact solution in Eq. (56) for small τ_Q gives

$$\frac{C_1(t)}{\sqrt{\tau_Q}} = \frac{2}{3} \left[\frac{t}{\sqrt{\tau_Q}} \right]^3 \quad (242)$$

to leading order in $t/\sqrt{\tau_Q}$. The expression (242) suggests that simple rescalings make the dependence of rescaled $C_1/\sqrt{\tau_Q}$ on rescaled time $t/\sqrt{\tau_Q}$ independent of the transition time τ_Q . This prediction is confirmed in Fig. 24 where the numerical solutions $C_1(t)$ for two widely different $\tau_Q = 0.001, 0.1$ collapse on each other. That a similar collapse in Fig. 25 extends also to large t comes as a bit of surprise.

The variational Ansatz (238) is accurate under two assumptions:

- Fluctuations of occupation numbers around the average $n = 1$ are small;
- Particles can be displaced with respect to the initial Mott state (231) not more than to nearest-neighbour sites.

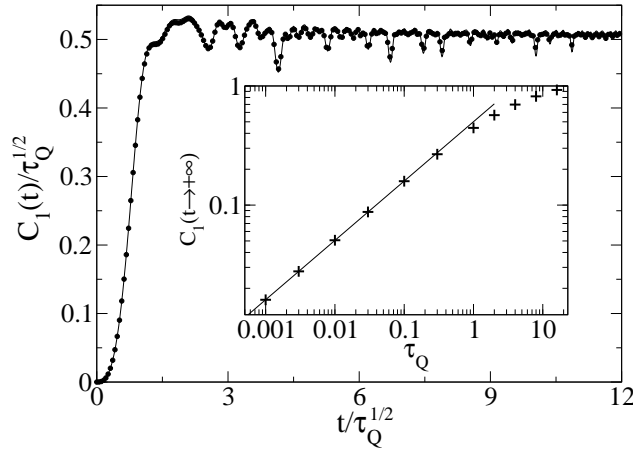


Figure 25. Scaling properties of C_1 obtained numerically. Solid line: $\tau_Q = 0.001$, dots: $\tau_Q = 0.03$. Inset: the solid line is a power law fit to data for $0.001 \leq \tau_Q \leq 0.1$ giving $C_1(\infty) = 0.501\tau_Q^{0.498}$. All data is for $N = 10$ and $J_{max} = 600$. (Figure from Ref. [123])

The former assumption is self-consistent up to

$$\hat{t} \simeq \tau_Q^{1/2} \quad (243)$$

when significant number fluctuations begin to develop. This time corresponds to

$$\hat{J} \simeq \tau_Q^{-1/2} \quad (244)$$

which is large, $\hat{J} \gg 1$, for fast transitions with $\tau_Q \ll 1$. In a fast transition, the number fluctuations do not have enough time to develop before J enters the regime of strong tunnelling, $J \gg 1$. In this regime, the correlators C_R are approximately constant, see Fig. 25, so the asymptotic $C_R(\infty)$ can be accurately approximated by $C_R(\hat{t})$ at \hat{J} when the number fluctuations are still sufficiently small for the ansatz (238) to be accurate. Indeed, $C_1(\hat{t}) \simeq \frac{2}{3}\sqrt{\tau_Q}$ in Eq. (242) gives the correct scaling of the asymptotic $C_1(\infty) \sim \sqrt{\tau_Q}$, as confirmed by the numerical data in Fig. 25.

The latter assumption, which makes all correlators C_R with $R > 1$ vanish, is relaxed in the Bogoliubov theory developed in Refs. [121] and [123]. In consistency with the former assumption, the theory truncates the Hilbert space to states with 0, 1 or 2 particles per site only. The Mott state (231) is a vacuum, a site with 2 particles is occupied by a quasiparticle and an empty site by a quasihole. The quasiparticles and quasiholes are hard-core bosons, but the hard-core constraint is relaxed to make their Hamiltonian quadratic. After solving corresponding time-dependent Bogoliubov-de Gennes equations and making the approximation $C_R(\infty) = C_R(\hat{t})$ we obtain

$$\begin{aligned} C_1(\infty) &\approx 3.9 \times 10^{-1} \sqrt{\tau_Q}, \\ C_3(\infty) &\approx -3.5 \times 10^{-3} \sqrt{\tau_Q}, \\ C_5(\infty) &\approx 1.4 \times 10^{-5} \sqrt{\tau_Q}, \end{aligned}$$

and $C_{2l} \sim \tau_Q$ for small $\tau_Q \ll 1$. Bogoliubov theory predicts that dominant odd correlations $C_{2l+1} \sim \sqrt{\tau_Q}$ decay quickly with the distance $R = 2l + 1$.

2.19.3. Fast transition from Mott insulator to superfluid at large density

In this Section we follow Ref. [34] and consider the opposite limit of large particle density, $n \gg 1$, in the initial Mott state (231). The large density regime is tractable by semiclassical methods, but it also makes the tight binding approximation leading to the Hubbard model (229) more problematic. For this reason most experiments simulating Bose-Hubbard model are carried out at densities close to unity [2], but experiments on number squeezing at large filling have been performed as well already at the early stage of research into possible occurrence of the Mott transition [13]. Apart from this, for slow enough quenches high energy degrees of freedom neglected in the Hubbard model are likely to remain adiabatic during the transition. In this sense, the model is a first low energy approximation to a ring of initially disconnected Bose-Einstein condensates being merged into a toroidal trap as in the experiment in Fig. 23 b. In this Section we will attempt to answer the question how does a winding number around the final toroidal condensate depend on the transition rate? The first experiment along these lines was done in Ref. [124] where 3 initially disconnected condensates were suddenly merged into one by removing a “Mercedes” potential separating them. In many realisations of that experiment vortices were detected in the final condensate, see Fig. 26.

For the sake of convenience, in this Section we rescale variables in the Bose-Hubbard Hamiltonian (229) so that

$$H = -J \sum_{s=1}^N \left(a_{s+1}^\dagger a_s + \text{h.c.} \right) + \frac{1}{2n} \sum_{i=1}^N n_s (n_s - 1) \quad (245)$$

and the phase transition is at $J_c \simeq n^{-2}$. In the truncated Wigner method [125] employed in Ref. [34] the annihilation operators a_s are represented by a complex field ϕ_s , $a_s \approx \sqrt{n} \phi_s$, which is normalised as $\sum_{s=1}^N |\phi_s|^2 = N$, and evolves with the time-dependent Gross-Pitaevskii equation

$$i \frac{d\phi_s}{dt} = -J (\phi_{s+1} - 2\phi_s + \phi_{s-1}) + |\phi_s|^2 \phi_s. \quad (246)$$

These approximations become accurate as $n \rightarrow \infty$ and the critical point $J_c \simeq n^{-2} \rightarrow 0$. Quantum expectation values are estimated by averages over stochastic realisations of the field $\phi_s(t)$. For example, the correlation function (232) becomes

$$C_R = \frac{1}{2n} \langle \psi(t) | a_{s+R}^\dagger a_s + \text{h.c.} | \psi(t) \rangle \approx \frac{1}{2} \overline{(\phi_s^* \phi_{s+R} + \text{c.c.})}. \quad (247)$$

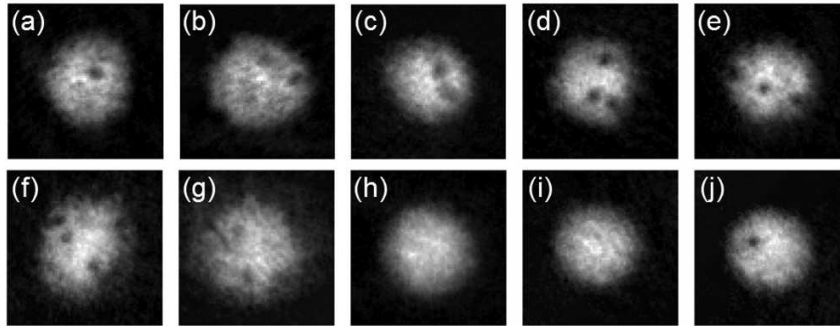


Figure 26. Images of a Bose-Einstein condensate taken after sudden merging of 3 initially disconnected condensates. The dark spots are vortices created in the process (Figure from Ref. [124]).

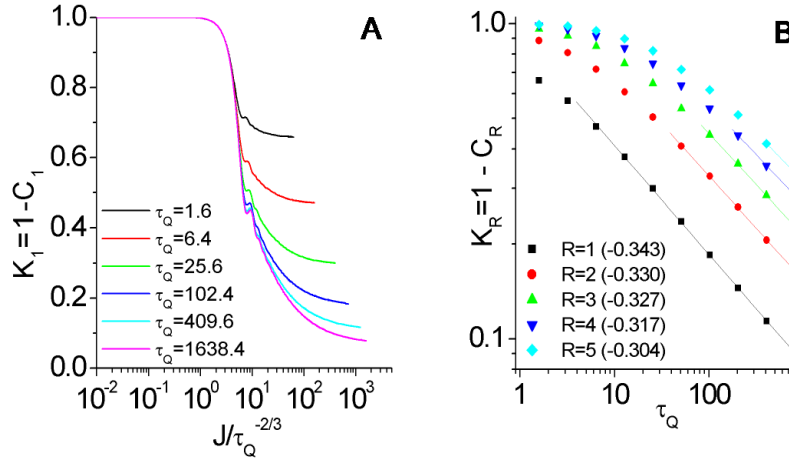


Figure 27. Kinetic hopping energy $K_1 = 1 - C_1 \approx \overline{1 - \cos \Delta\theta_s} \approx \frac{1}{2} \overline{\Delta\theta_s^2}$ as a function of rescaled J/\hat{J} for different τ_Q is seen in A. When $J \ll 1$, all the plots overlap demonstrating that $\hat{J} = \tau_Q^{-2/3}$ is the relevant scale for $J \ll 1$. Individual plots depart from this small- J “common bundle” at $J \simeq 1$, or equivalently $J/\tau_Q^{-2/3} \simeq \tau_Q^{2/3}$, when $K_1 = 1 - C_1$ is expected to stabilise. In B, we show $K_R \equiv 1 - C_R$ at $J = 10$ as a function of τ_Q for $R = 1, \dots, 5$. Data points for each R were fitted with lines, their slopes giving exponents close to the $\frac{1}{3}$ -scaling predicted in Eq. (253) with error bars on their last digits. (Figure from Ref. [34])

Here the overline means average over stochastic realisations. All realisations of $\phi_s(t)$ evolve with the same deterministic Gross-Pitaevskii equation (246), but they start from different random initial conditions distributed according to Wigner distribution of an initial quantum state. The initial Mott state (231) translates into initial fields

$$\phi_s(0) = e^{i\theta_s} \quad (248)$$

with independent random phases $\theta_s \in [-\pi, \pi)$. The Mott state has the same fixed number of n particles at each site, translating into constant modulus $|\phi_s(0)|^2 = 1$ and indeterminate quantum phases translating into random θ_s .

Our goal is to estimate average size of a random phase step $\Delta\theta_s = \theta_{s+1} - \theta_s$ between nearest-neighbour sites in a final state after transition. A random walk of phase around a chain of N sites generates a net winding number whose average magnitude scales as \sqrt{N} times the average size of a phase step. We begin with a KZM-like estimate in a linearised Gaussian theory.

The Gross-Pitaevskii equation (246) can be linearised in small fluctuations $\delta\phi_s$ around a uniform large background, $\phi_s = 1 + \delta\phi_s$, and $\delta\phi_s$ can be expanded in Bogoliubov modes as $\delta\phi_s = \sum_k (b_k u_k e^{iks} + b_k^* v_k^* e^{-iks})$ with pseudomomentum k . For a constant J we have $b_k(t) = b_k(0)e^{-i\omega_k t}$ with Bogoliubov frequencies

$$\omega_k = 2\sqrt{J(1 - \cos k)[1 + J(1 - \cos k)]} \quad (249)$$

and stationary Bogoliubov modes

$$u_k = -\mathcal{N}_k [1 + 2J(1 - \cos k) + \omega_k], \quad v_k = \mathcal{N}_k. \quad (250)$$

Here \mathcal{N}_k is such that $u_k^2 - v_k^2 = 1$. In the Josephson regime, when $J \ll 1$, we have $v_k \approx -u_k$ and a purely imaginary $\delta\phi_s$ in $\phi_s = 1 + \delta\phi_s$ is a phase fluctuation. However, for our random initial conditions (248), this linearisation is justified only for short wavelength modes of ϕ_s , with $k \approx \pm\pi$, for whom the modes with longer

wavelength appear to be the (locally) uniform large background. From now on we concentrate on the short wavelength modes because they determine the variance of the nearest-neighbour phase step $\Delta\theta_s$.

When $k \approx \pm\pi$ and $J \ll 1$ then $\omega_k \approx 2\sqrt{2J}$. Early in the linear quench (230) this ω_k is so small that the early evolution of the short wavelength modes is approximately impulsive, i.e., their magnitude remains the same as in the initial Mott state and, consequently, $\overline{\Delta\theta_s^2} \simeq 1$ in this impulse stage. The impulse approximation breaks down at \hat{J} when the transition rate $\dot{\omega}_k/\omega_k$ equals ω_k , and the evolution becomes adiabatic. This happens at

$$\hat{J} \simeq \tau_Q^{-2/3} \quad (251)$$

which is self-consistent with the assumption of $J \ll 1$ when $\tau_Q \gg 1$.

The crossover from impulse to adiabatic evolution at \hat{J} is the key ingredient of KZM. In the following adiabatic evolution after \hat{J} , but before $J \approx 1$, short wavelength phase fluctuations scale as $\delta\phi_s \sim J^{-1/4}$ because the amplitudes $|b_k|$ do not change and the modes u_k, v_k follow instantaneous stationary Bogoliubov modes $u_k \approx -v_k \approx -1/2(2J)^{1/4}$. Consequently, $\Delta\theta_s$ has variance scaling as $\overline{\Delta\theta_s^2}|_J \simeq \overline{|\delta\phi_s|^2} \sim J^{-1/2}$. Given the initial condition for the adiabatic stage at \hat{J} that $\overline{\Delta\theta_s^2}|_{\hat{J}} \simeq 1$, the phase fluctuations must shrink as $\overline{\Delta\theta_s^2}|_J \simeq \overline{\Delta\theta_s^2}|_{\hat{J}} (J/\hat{J})^{-1/2} \simeq \tau_Q^{-1/3} J^{-1/2}$ while $J \ll 1$.

On the other hand, when $J \gg 1$ then stationary modes $u_k \approx 1$ and $v_k \approx 0$ do not depend on J and $\overline{\Delta\theta_s^2}$ does not depend on J either. This means that $\overline{\Delta\theta_s^2}$ must stabilise between the regimes of $J \ll 1$ and $J \gg 1$, i.e., around $J \simeq 1$ where it saturates at its final value

$$\overline{\Delta\theta_s^2}|_{J \gg 1} \approx \overline{\Delta\theta_s^2}|_{J \simeq 1} \simeq \tau_Q^{-1/3} \quad (252)$$

scaling with a power of $-1/3$. This variance determines e.g. the correlator C_1 in

$$K_1 = 1 - C_1 = 1 - \overline{\cos \Delta\theta_s} \simeq \tau_Q^{-1/3}, \quad (253)$$

for $\tau_Q \gg 1$. The kinetic hopping energy per particle K_1 is expected to stabilise for $J \gg 1$, when the hopping term dominates over the non-linearity in Eq. (246) and K_1 becomes an approximate constant of motion, see Fig. 27.

The integer winding number is a phase accumulated after N steps (divided by 2π)

$$W_N = \frac{1}{2\pi} \sum_{s=1}^N \text{Arg}(\phi_{s+1}\phi_s^*), \quad (254)$$

where $\text{Arg}(\dots) \in (-\pi, \pi]$. A random walk of phase, with the variance of nearest neighbour phase differences scaling as in Eq. (252), gives winding numbers with a variance

$$\overline{W_N^2} \simeq N \tau_Q^{-1/3}. \quad (255)$$

There are two limits where this scaling must fail. For very fast quenches with $\tau_Q \ll 1$ phases are completely random between neighbouring sites, so $\overline{\Delta\theta_s^2} = \pi^2/3$,

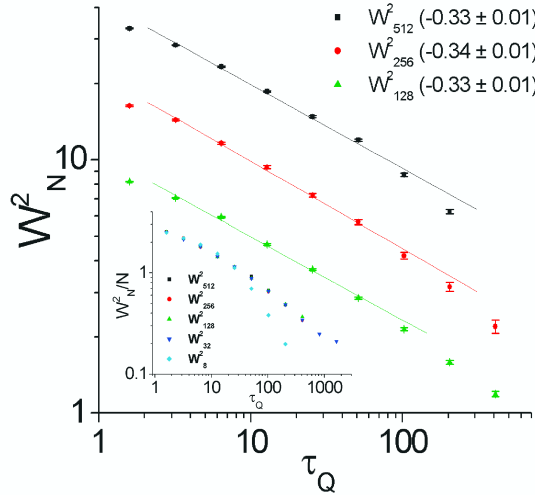


Figure 28. Variance of winding number $\overline{W_N^2}$ measured at $J = 10$ as a function of τ_Q for lattice sizes $N = 512, 256, 128$. Here point sizes equal error bars. The data points with $\tau_Q > 2$ and $\overline{W_N^2} > 2$ were fitted with the solid lines giving slopes close to the predicted $-\frac{1}{3}$ in Eq. (255). $\overline{W_N^2}$ is shown over a wider range of τ_Q to show the saturation for nearly instantaneous quenches, when $\tau_Q < 2$, and the crossover to steeper slope when $\overline{W_N^2} < 2$. The inset shows a rescaled $\overline{W_N^2}/N$ for $N = 512, 256, 128, 32, 8$ to demonstrate that $\overline{W_N^2} \sim N$ in the KZ regime of $\tau_Q > 2$ and $\overline{W_N^2} > 2$. (Figure from Ref. [34])

and $\overline{W_N^2} = N/12$. For quenches so slow that $\overline{W_N^2} < 1$ the nature of the problem changes, leading to steeper falloff of $\overline{W_N^2}$ with τ_Q . Between these two limits the $\frac{1}{3}$ -scaling in Eq. (255) for the winding number is confirmed by numerical results in Fig. 28.

On one hand, the predicted $1/3$ -scaling of the winding number is limited to relatively slow transitions with $\tau_Q \gg 1$ so that $\hat{J} \ll 1$ but, on the other hand, the transition must be fast enough for the truncated Wigner method to remain accurate. This means that the crucial \hat{J} in Eq. (251) must be much greater than the critical $J_c \simeq n^{-2}$, or equivalently $\tau_Q \ll n^3$. For density of, say, $n \simeq 100$ atoms per site τ_Q can range over 6 orders of magnitude.

2.19.4. Fast transition from superfluid to Mott insulator at large density

A reverse transition from the gapless superfluid to the gapped Mott insulator was analysed in Refs. [126, 127]. Since at the final tunnelling rate $J = 0$ site occupation numbers n_s are good quantum numbers, we will concentrate on time evolution of the occupation numbers and their conjugate phase fluctuations. An initial superfluid ground state at large $J \gg n$ has large Poissonian number fluctuations $\sim \sqrt{n}$ at each site and small $\sim 1/\sqrt{n}$ fluctuations of phase. By contrast, in the Mott ground state (231) at the final $J = 0$ the number fluctuations are zero and the phases are random. We can expect that a non-adiabatic transition from large $J \gg n$ to $J = 0$ will end in an excited state with finite number fluctuations. The conserved magnitude of these final number fluctuations will depend on transition rate.

In this Section we assume large density of $n \gg 1$ particles per site when a polar decomposition $a_s = \sqrt{n_s} \exp(i\theta_s)$ with a phase operator θ_s makes sense. Deep in the superfluid regime we can define $n_s = n + \delta n_s$ and $\theta_s = \delta\theta_s$, where the c -number n is the large particle density, while $\delta n_s \ll n$ and $\delta\theta_s$ are mutually conjugate small number and phase fluctuations respectively. Inserting the polar decomposition into an equation of motion $i\partial_t a_s = J(t)(a_{s+1} + a_{s-1}) + n_s a_s$, expanding to leading order

in the small quantum fluctuations, eliminating $\delta\theta_s$, and making Fourier transform of δn_s , we obtain a linearised Bogoliubov equation

$$\left(\frac{\partial}{\partial t} \frac{1}{J(t)} \frac{\partial}{\partial t} + 4(1 - \cos k)[n + J(t)(1 - \cos k)] \right) \delta n_k = 0 \quad (256)$$

with a time-dependent $J(t)$.

Notice that in case of constant J we obtain the Bogoliubov spectrum of quasiparticle excitations $\omega_k = \sqrt{4J(1 - \cos k)[n + J(1 - \cos k)]}$ which is identical with Eq. (249) up to rescaled units. Here we are interested mainly in the Josephson regime, $J \gg J_c \simeq 1/n$ and $J \ll n$, where the ground state is a number-squeezed state with a number variance

$$\Delta n_{\text{GS}}^2(J) \simeq \sqrt{nJ} \quad (257)$$

and a phase variance $\Delta\theta_{\text{GS}}^2 \simeq 1/\Delta n_{\text{GS}}^2$. In this regime

$$\omega_k \approx \sqrt{4nJ(1 - \cos k)} \sim (nJ)^{1/2}. \quad (258)$$

We assume that the transition is slow enough for most Bogoliubov modes to remain unexcited before they enter the Josephson regime, except for a narrow range of low frequency modes with small $|k|$ which becomes negligible with increasing transition time.

In the Josephson regime, a mode k becomes excited at a \hat{J} when the transition rate \dot{J}/J equals ω_k . We consider two different functions $J(t)$:

- Like in the previous Sections on the Mott to superfluid transition and in Ref. [126], we consider a linear

$$J(t) = -\frac{t}{\tau_Q}, \quad (259)$$

where t runs from $-\infty$ to 0. The transition rate $\dot{J}/J = 1/|t|$ equals ω_k in Eq. (258) at

$$\hat{J} \sim n^{-1/3} \tau_Q^{-2/3}. \quad (260)$$

After \hat{J} the evolution becomes impulse and the final variance at $J = 0$ remains the same as in the ground state at \hat{J} :

$$\Delta n^2 \sim \Delta n_{\text{GS}}^2(\hat{J}) \sim n^{1/3} \tau_Q^{-1/3}. \quad (261)$$

Self-consistency requires \hat{J} in the Josephson regime or, equivalently, $\frac{1}{n^2} \ll \tau_Q \ll n$. The transition has to be fast enough, $\tau_Q \ll n$, for the crossover to the impulse stage to take place much above the critical point J_c where the Bogoliubov approximation would break down.

- Since the tunnelling rate J depends exponentially on the strength of an optical lattice, we also consider an exponential

$$J(t) = J_0 e^{-t/\tau_Q}, \quad (262)$$

where $t \in (0, \infty)$, like in Ref. [127]. The transition rate $\dot{J}/J = 1/\tau_Q$ equals ω_k in Eq. (258) at

$$\hat{J} \sim n^{-1}\tau_Q^{-2} . \quad (263)$$

The final variance

$$\Delta n^2 \sim \Delta n_{\text{GS}}^2(\hat{J}) \sim \tau_Q^{-1} \quad (264)$$

does not depend on n and its dependence on τ_Q is steeper than after a linear transition, but \hat{J} in the Josephson regime requires $n^{-1} \ll \tau_Q \ll 1$, i.e., a more narrow range of τ_Q .

The adiabatic-impulse scaling argument above has two limitations: as usual, it does not predict any numerical pre-factors and, what is potentially more dangerous, it ignores any dependence of \hat{J} on k . This is why we follow a more detailed calculation in Ref. [127] in the case of exponential transition.

A new k -dependent time variable $\tau = -2(1 - \cos k)J(t)\tau_Q$, running from $\tau \rightarrow -\infty$ to $\tau = 0$, transforms Eq. (256) into a more universal

$$\left[\frac{\partial^2}{\partial \tau^2} + \left(1 - \frac{2n\tau_Q}{\tau} \right) \right] \delta n_k = 0 . \quad (265)$$

This equation demonstrates that, after proper rescaling of time, different modes δn_k evolve in the same way. Their evolution changes qualitatively at $\tau \simeq 2n\tau_Q$ when it crosses over from pure oscillations with constant frequency, $\sim \exp(\pm i\tau)$, to damped oscillations with increasing frequency. This crossover corresponds roughly to entering the Josephson regime near $J \simeq n$. After the crossover the damping makes number fluctuations Δn shrink from the initial $\Delta n \simeq \sqrt{n}$ to its final value at $J = 0$.

More precisely, see Ref. [127],

$$\delta n_k = \sqrt{n} e^{-\pi n \tau_Q / 2} W_{in\tau_Q, 1/2}(2i\tau) b_k + \text{h.c.} , \quad (266)$$

where W is the Whittaker function and b_k are bosonic Bogoliubov quasiparticles. Here we work in the Heisenberg picture, where the state is a vacuum $|0\rangle$ annihilated by all b_k . The number fluctuations at the final $\tau = 0$, corresponding to $J = 0$, are

$$\langle (\delta n_k)^2 \rangle \equiv \langle 0 | (\delta n_k)^2 | 0 \rangle = \frac{1 - e^{-2\pi n \tau_Q}}{2\pi \tau_Q} + \mathcal{O} \left[t e^{-t/\tau_Q} (1 - \cos k) \right] . \quad (267)$$

This limit is saturated and the number fluctuations freeze out when $t \gg \tau_Q$. Since the frozen $\langle (\delta n_k)^2 \rangle$ is independent of k , we obtain non-zero frozen on-site variations

$$\langle n_s^2 \rangle - \langle n_s \rangle^2 = \langle (\delta n_s)^2 \rangle = \frac{1 - e^{-2\pi n \tau_Q}}{2\pi \tau_Q} , \quad (268)$$

but vanishing two-site correlations between δn_s at different sites. After a very fast quench with $n\tau_Q \ll 1$ the final variance is equal to n like in the initial Poissonian ground state at $J \gg n$. These quenches are effectively impulse right from an initial $J \gg n$ and all the way down to $J = 0$ - they are too fast for the initial state to adapt to the rapidly shrinking J . In the more interesting regime of $n\tau_Q \gg 1$ the

final frozen number fluctuations are

$$\Delta n^2 = \frac{1}{2\pi\tau_Q} \quad (269)$$

in agreement with the scaling prediction in Eq. (264). The pre-factor missing in Eq. (264) is $\frac{1}{2\pi}$.

When $J \approx 0$ these uncorrelated number fluctuations evolve with evolution operator

$$e^{-in_s(n_s-1)t/2} \approx e^{-in^2t/2} e^{-in \delta n_s t} . \quad (270)$$

and gradually translate into increasing phase fluctuations with a variance [127]

$$\Delta\theta^2 = \frac{t^2}{2\pi\tau_Q} . \quad (271)$$

These phase fluctuations determine relative quantum depletion from the condensate, i.e., fraction of particles that are not condensed into a uniform condensate wave function with a site-independent phase. For our Bogoliubov approximation to be self-consistent they need to remain small, $\Delta\theta^2 \ll 1$, at least down to \hat{J} when the ground state phase fluctuations are $\Delta\theta^2 \simeq \tau_Q$. Thus the range of validity of the scaling in Eq. (269) is limited to

$$n^{-1} \ll \tau_Q \ll 1 . \quad (272)$$

Notice that in the simple scaling argument leading to Eq. (264) the condition (272) is equivalent to \hat{J} in the Josephson regime.

We can conclude that the detailed calculation confirms the scaling $\Delta n^2 \sim \tau_Q^{-1}$ predicted in Eq. (264), provides the missing pre-factor of $1/2\pi$, justifies *a posteriori* ignoring the non-adiabaticity in a narrow range of long wavelength modes, and limits validity of the scaling to the same range of τ_Q as the simple scaling argument based on the adiabatic-impulse approximation.

The vanishing final two-site correlator between different δn_s has observable implications for a two-site correlation function C_R . In the Heisenberg picture at the final $J = 0$, the annihilation operators evolve as $a_s(t) = \exp(-in_s t) a_s(0)$ and the correlation function

$$C_R(t) = \langle a_{s+R}^\dagger(t) a_s(t) \rangle = C_R(0) \langle \exp[it(n_{s+R} - n_s)] \rangle \quad (273)$$

decays to zero after a dephasing time $\simeq (\Delta n)^{-1}$. When the final J is precisely zero, then the decay is followed by periodic revivals every 2π , but when the final J is small but non-zero, then the revivals disappear after a dephasing time proportional to the width $\simeq J^{-1}$ of the quasiparticle band at small J , see Ref. [128] for more details. The (disappearing) periodic revivals of the initial superfluid state were observed in the experiment [2] after a sudden quench to the Mott phase, see Fig. 29.

In the following Section we continue with bosonic atoms in a quasi-1D trap, but this time without the tight-binding approximation leading to the Bose-Hubbard model (229).

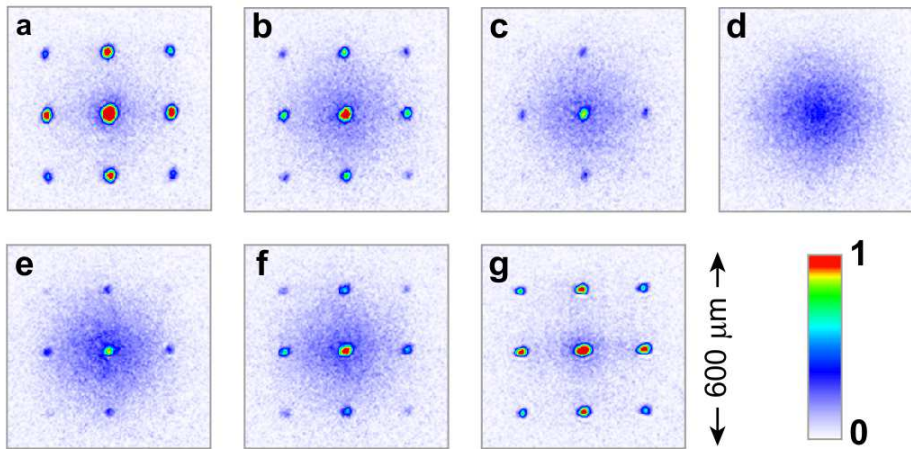


Figure 29. Dynamical evolution of the multiple matter wave interference pattern observed after sudden reduction of the tunnelling rate from the superfluid to the Mott phase. Panels a...g are absorption images taken after hold times: $0\mu s$, $100\mu s$, $150\mu s$, $250\mu s$, $350\mu s$, $400\mu s$ and $550\mu s$ respectively. A first distinct interference pattern is visible (a), showing that initially the system can be described by a macroscopic condensate wave function. After $250\mu s$ the pattern is lost (d) and after $550\mu s$ hold time it is almost perfectly restored. (Figure from Ref. [2])

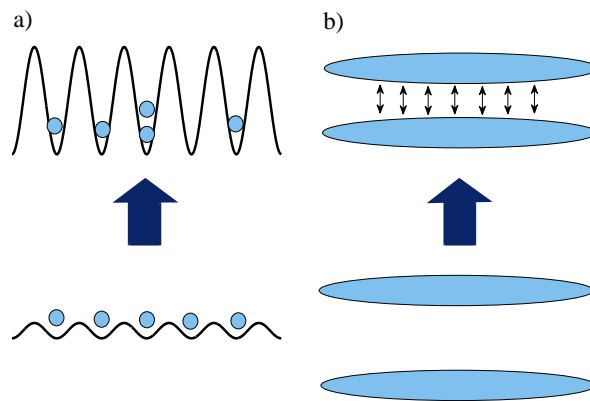


Figure 30. The two scenarios considered in Ref. [42]. Here we review case a) when a one dimensional Bose gas is loaded into an optical lattice potential. A similar experiment was done in Ref. [8]. (Figure from Ref. [42])

2.20. Loading a 1D Bose gas into an optical lattice: transition into the gapped phase of the sine-Gordon model

The parameter that defines properties of a Bose gas in one dimension [129] is its interaction strength $\gamma = mg/\hbar^2\rho$, where m is the mass of a particle, g is the interaction strength in the contact interaction $g\delta(x_1 - x_2)$, and ρ is the linear density of particles. In a spatially uniform system the spectrum of excitations is gapless for any γ and the low energy physics is described by the Luttinger liquid [130]. The parameter K of the Luttinger theory is $K \approx 1 + 4/\gamma$ for strong and $K \approx \pi/\sqrt{\gamma}$ in for weak repulsion γ [129, 131]. In the extreme Tonks-Girardeau limit $\gamma \rightarrow \infty$ of strong repulsive interactions [132], realised experimentally in Refs. [3–5], the particles behave like hard-core bosons which cannot occupy the same position in space.

In Refs. [39, 42] the experimental set-up in Fig. 30a was considered, where by slowly turning on an optical lattice the initial zero temperature Bose gas is loaded

into a lattice potential. The lattice potential of increasing strength $\epsilon(t)$ results in a sine-Gordon Hamiltonian [133]

$$H = \frac{1}{2} \int dx \left[\Pi^2 + (\partial_x \phi)^2 - 4\epsilon(t) \cos(2\sqrt{\pi K} \phi) \right], \quad (274)$$

where $\Pi(x)$ and $\phi(x)$ are mutually conjugate, and K is the parameter of the Luttinger liquid before turning on the perturbation. When $K < 2$ the cosine term is a relevant perturbation opening an energy gap in the spectrum of the gapless Luttinger liquid. In the repulsive regime when $1 < K < 2$, the massive excitations are solitons of mass

$$\Delta \simeq \epsilon^{\frac{1}{2-K}}, \quad (275)$$

for small ϵ , see Refs. [42] and [134]. Since in a translationally invariant system the solitons can be excited only as topologically trivial pairs of solitons and antisolitons with opposite momenta $(k, -k)$, the spectrum of relevant excitations is $2\sqrt{\Delta^2 + k^2}$. In the attractive regime when $K < 1$, the spectrum includes also breathers that can be interpreted as soliton-antisoliton bound states.

Since at the critical point $\Delta = 0$ the excitation spectrum $2\sqrt{\Delta^2 + k^2}$ is linear in $|k|$, the dynamical critical exponent is

$$z = 1. \quad (276)$$

Consequently, the finite gap Δ translates into a finite correlation length $\xi \sim \Delta^{-1}$ in the ground state of the system. Given the scaling in Eq. (275), we identify the critical exponent

$$\nu = \frac{1}{2-K} \quad (277)$$

in $\xi \sim \epsilon^{-\nu}$.

A linear ramp of the lattice amplitude,

$$\epsilon(t) = \frac{t}{\tau_Q}, \quad (278)$$

with the time running from $t = 0$ to $t \rightarrow \infty$, drives the system from the critical point at $\epsilon = 0$ into the gapped phase with $\epsilon > 0$. This is an example of the general half-quench analysed in Section 2.6. Given the exponents z and ν , we can use Eq. (26) to obtain the density of excited solitons and antisolitons

$$n_{\text{ex}} \simeq \hat{\xi}^{-1} \simeq \hat{\epsilon}^\nu \simeq \tau_Q^{-1/(3-K)}. \quad (279)$$

The result (279) is corroborated by the calculation in Ref. [42] along the general lines of Section 2.12.

The non-adiabaticity of condensate loading into an optical lattice was also studied in Ref. [96] in presence of a harmonic trap potential and quasi-disorder. The disorder makes the transition much less adiabatic than in the pure case, in coherence with the example of the random Ising model in Refs. [85, 94, 95] and Section 2.16.

This Section completes our review of spinless bosons. In the next Section we consider spin-1 Bose-Einstein condensates.

2.21. Spin-1 Bose-Einstein condensate: transition from paramagnetic to ferromagnetic phase

A sudden quench in a spin-1 ferromagnetic Bose-Einstein condensate was realised in the experiment of Ref. [135], see Fig. 31, and analysed in Refs. [136–138]. Here, following Ref. [138], we consider for simplicity a one-dimensional homogeneous condensate in a finite box. Since the following analysis is on the mean-field level, most conclusions can be easily generalised to higher dimensions. In dimensionless variables, a system placed in a magnetic field B along the z -axis has a mean-field energy functional

$$E[\Psi] = \int_{\text{box}} dz \left[\frac{1}{2} \frac{d\Psi^\dagger}{dz} \frac{d\Psi}{dz} + \frac{c_0}{2} (\Psi^\dagger \Psi)^2 + Q \Psi^\dagger F_z^2 \Psi + \frac{c_1}{2} \sum_{\alpha} (\Psi^\dagger F_{\alpha} \Psi)^2 \right]. \quad (280)$$

Here $\Psi^T = (\psi_1, \psi_0, \psi_{-1})$ describes the $m = 0, \pm 1$ condensate components, the wave function is normalised $\int_{\text{box}} dz \Psi^\dagger \Psi = 1$, and $F_{x,y,z}$ are spin-1 matrices. The first term in (280) is the kinetic energy, the second and the fourth term describe spin-independent and spin-dependent atom interactions respectively, and the third term is a quadratic Zeeman shift originating from atom interactions with the magnetic field B .

A phase diagram of the model (280) is interesting when $c_1 < 0$, like for e.g. ^{87}Rb atoms, and there is competition between the last two terms in Eq. (280). When we assume zero longitudinal magnetisation, $f_z \equiv \Psi^\dagger F_z \Psi = 0$, whose integral is a

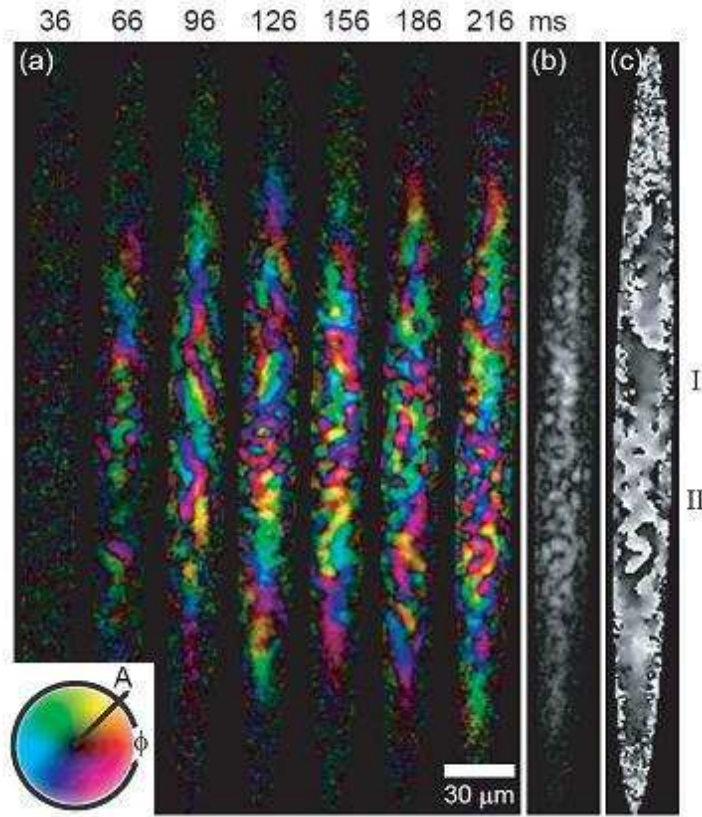


Figure 31. Images of a cigar-shaped spin-1 Bose-Einstein condensate after a sudden quench from the paramagnetic to the ferromagnetic phase. In a) transverse magnetization with magnetization density shown by brightness and its orientation by colour. In b) magnetization density and in c) magnetization orientation respectively shown in grey scale. (Figure from Ref. [135]).

constant of motion, then the relevant parameter is

$$\epsilon = \frac{Q}{n|c_1|} - 2, \quad (281)$$

where $n = \Psi^\dagger \Psi$ is the density. At $\epsilon = 0$ there is a transition between the symmetric polar phase for $\epsilon > 0$, where the ground state wave function is

$$\Psi_P^T \sim (0, 1, 0), \quad (282)$$

and the broken-symmetry ferromagnetic phase for $\epsilon < 0$, where the degenerate ground states are

$$\Psi_F^T \sim \left(e^{i\chi_1} \sqrt{-2\epsilon}, e^{i(\chi_1 + \chi_{-1})/2} 2\sqrt{4 + \epsilon}, e^{i\chi_{-1}} \sqrt{-2\epsilon} \right). \quad (283)$$

The relative phase $\chi_1 - \chi_{-1}$ determines orientation of the transverse magnetisation $(f_x, f_y) = (\Psi^\dagger F_x \Psi, \Psi^\dagger F_y \Psi)$ in the $x - y$ plane. The ground state is degenerate with respect to this orientation allowing topological defects like textures in 1D, point vortices in 2D, and vortex lines in 3D.

In the symmetric phase there are small thermal or at least quantum fluctuations around the ground state (282) which can be expanded into Bogoliubov modes [139]. Near the critical point the gap in the quasiparticle spectrum scales as

$$\Delta \sim \epsilon^{1/2}. \quad (284)$$

Since by definition $\Delta \sim \epsilon^{\nu z}$ for small ϵ , we can identify $\nu z = 1/2$. On the mean field level considered here the critical exponent $\nu = 1/2$ and KZM predicts

$$\hat{\xi} \simeq \tau_Q^{1/3}, \quad (285)$$

compare Eq. (16), after a linear quench to the ferromagnetic phase.

More precisely, see Refs. [136–138], what happens is that when the linear quench crosses the critical point $\epsilon = 0$ the initial paramagnetic ground state (282) becomes a dynamically unstable false vacuum. The frequency of the $k = 0$ Bogoliubov mode (contributing to the initial small fluctuations around this false vacuum) given by the gap in Eq. (284) becomes imaginary and the mode begins to grow quasi-exponentially on the timescale of $\hat{t} \simeq \tau_Q^{1/3}$ in a similar way as in the classical transitions considered in Section 2.2. As ϵ enters deeper into the ferromagnetic phase, more long wavelength modes become unstable. This linear instability grows until time \hat{t} when its growth is halted by the quartic term in the energy functional (280) and the linearisation in small fluctuations around the initial paramagnetic state breaks down. By this time, the long wavelength modes with $|k|$ up to $\hat{\xi}^{-1}$ have become unstable and exponentially amplified with respect to the initial small fluctuations back in the symmetric phase. This exponential amplification promotes $\hat{\xi}$ to the only relevant scale of length characterising the wave function Ψ after the transition.

In the spirit of the truncated Wigner method, in the numerical simulations of Ref. [138] the wave function Ψ was initialised in the symmetric phase in the ground state (282) plus small Gaussian noise uncorrelated in space. The noise provides seed quantum/thermal fluctuations. Then the wave function was evolved by a linear quench $\epsilon(t) = -t/\tau_Q$ to the symmetry-broken phase. Figure [139] shows two

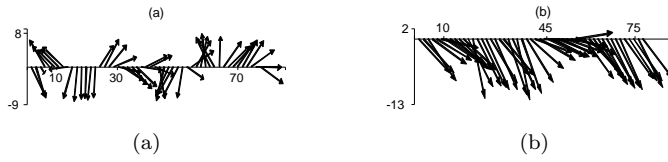


Figure 32. Vector representation of the (magnified) transverse magnetisation $(f_x, f_y) \times 10^3$ at a) $\epsilon = -0.28$ and b) $\epsilon = -2$ during a transition with $\tau_Q = 10$. (Figure from Ref. [138])

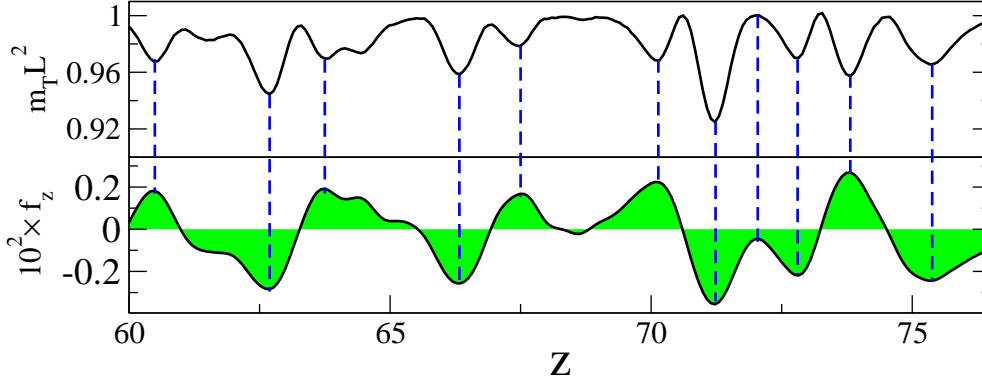


Figure 33. Snapshot of a magnetisation of the system at $t = 2\tau_Q$ when $\epsilon = -2$ after a transition with $\tau_Q = 10$. The top part shows transverse magnetisation $m_T = \sqrt{f_x^2 + f_y^2}$ (times the box size squared L^2). The bottom part shows the measurable longitudinal magnetisation f_z (magnified by a factor of 10^2). The vertical dashed lines help to see coincidences between minima of the transverse magnetisation and extrema of the longitudinal magnetisation. Average size of the longitudinal domains was verified in Ref. [138] to scale as $\hat{\xi} \simeq \tau_Q^{1/3}$. (Figure from Ref. [138])

snapshots of the transverse magnetisation (f_x, f_y) in the ferromagnetic phase. The magnetisation has orientation which is random, but correlated on the length scale $\hat{\xi}$. Topological textures in this random transverse magnetisation can be characterised by a winding number

$$\frac{1}{2\pi} \int_{\text{box}} dz \frac{d}{dz} \text{Arg}(f_x + if_y) . \quad (286)$$

Density of textures scales as $\hat{\xi}^{-1}$. Reference [137] considers formation of topological textures in more than one dimension.

Another quantity measured in Ref. [135] was the longitudinal magnetisation. Both in the experiment and in the numerical simulations of Ref. [138] the net longitudinal magnetisation was initially zero, $\int_{\text{box}} dz f_z = 0$, and fluctuations of local magnetisation f_z were small. Conservation of the net longitudinal magnetisation allows for creation of a network of magnetic domains with opposite f_z . The domains begin to form at the time $\simeq \hat{t}$ of the quasi-exponential growth of the dynamical instability. The bottom part of Figure 33 shows one realisation of longitudinal domains. The top part of the same figure demonstrates anti-correlation between transverse magnetisation $m_T = \sqrt{f_x^2 + f_y^2}$ and the longitudinal magnetisation. Both are correlated in space on the length scale $\hat{\xi} \simeq \tau_Q^{1/3}$.

The model (280) provides also another illustration of KZM in space, see Sections 2.7 and 2.13.11. Reference [46] considers a transition in space with

$$\epsilon(z) = \alpha z \quad (287)$$

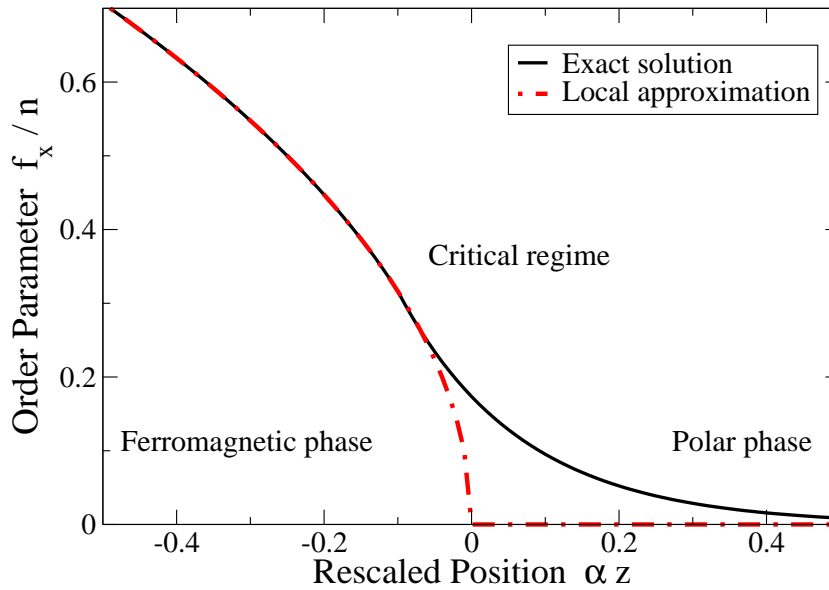


Figure 34. Typical condensate magnetisation f_x (order parameter) in a spatial transition (287). The solid line is the exact solution and the dashed line is the local approximation. In the critical regime near the critical point the exact solution deviates from the local approximation and penetrates into the symmetric polar phase to a depth of $\hat{\xi} \simeq \alpha^{1/3}$. (Figure from Ref. [138])

from the symmetry-broken phase where $z < 0$ to the symmetric polar phase where $z > 0$. Figure 34 shows the transverse magnetisation $f_x(z)$ which is the order parameter. The dashed line is the magnetisation in the local approximation. It is non-zero in the broken-symmetry phase and vanishes as $f_x \sim \sqrt{-\epsilon} = \sqrt{\alpha z}$ when the critical point is approached, $z \rightarrow 0^-$. The solid line is the exact solution which deviates from the local approximation at $\hat{\epsilon} \sim \alpha^{2/3}$ and penetrates into the symmetric polar phase to a depth $\hat{\xi} \simeq \alpha^{-1/3}$. These scalings were verified in Ref. [46] to be accurate for $\alpha \ll 1$, as expected from the general argument in Section 2.7.

2.22. Adiabatic sweep across a gapless regime

The main result of KZM is that, in the thermodynamic limit, a sweep across a second order phase transition cannot be adiabatic, no matter how slow is the transition rate

$$\delta = \tau_Q^{-1}, \quad (288)$$

because the system is gapless at the critical point and the adiabatic theorem cannot apply. Consequently, there is a finite density of excitations n_{ex} (or density of excitation energy ϵ) which scales with a power of the transition rate δ . The power generally increases with the dimensionality of the system making the density of excitations in higher dimensions decay faster in the adiabatic limit of $\delta \rightarrow 0$, compare e.g. Eq. (17). Lower dimensional systems are generally less adiabatic because they have more low energy states available for excitation. As pointed out in the seminal paper [140], the same observations must necessarily apply to all gapless systems, no matter what is their dimensionality, but their non-adiabaticity can be expected to be more dramatic in lower dimensions. Gapless systems are quite generic as most systems with broken symmetries have gapless excitations like e.g. phonons, magnons, or spin waves.

In the zero temperature quantum limit, we can consider a linear sweep of a parameter κ in a Hamiltonian,

$$\kappa(t) = \kappa_i + \delta t , \tag{289}$$

starting from the ground state at an initial κ_i and terminating at a final κ_f . The final density of the positive excitation energy depends on the transition rate, $\varepsilon(\delta) > 0$. According to Ref. [140], response of the system to the adiabatic sweep may fall into one of the following three regimes:

A When $\varepsilon(\delta)$ is an analytic function of δ , then to leading order in δ we have

$$\varepsilon(\delta) \sim \delta^2 . \tag{290}$$

Here the linear term is zero because the positive excitation energy cannot be made negative by a sweep in the opposite direction. This regime can be called *mean field* or *analytic*. Since $\varepsilon(\delta \rightarrow 0) = 0$, there is adiabatic limit in this regime. On a more microscopic level, the origin of the quadratic scaling lies in the Landau-Zener transition in Section 2.9, see cases (ii,iii,iv) and Eq. (49) where the parameter driving the transition has a discontinuous time derivative just like Eq. (289). The discontinuity makes the excitation probability scale with a square of a transition rate $\tau_Q^{-2} \sim \delta^2$ instead of the usual exponential decay, see a more detailed discussion in Ref. [39].

B Even when $\varepsilon(\delta)$ is not analytic, it is still possible to approach the adiabatic limit as

$$\varepsilon(\delta) \sim |\delta|^a \tag{291}$$

where $a > 0$ but $a \neq 2$. This regime can be termed *non-analytic*. On the microscopic level it originates from a combination of the δ^2 scaling like in case A and large density of low energy excitations, see Ref. [39].

C Finally, in a *non-adiabatic* regime we have

$$\varepsilon(\delta) \sim |\delta|^a L^b , \tag{292}$$

where $a, b > 0$ and L is the system size. Here the adiabatic limit does not exist for infinite system size. Notice that it is not just the excitation energy, but the excitation *energy density* that diverges in the thermodynamic limit.

In a system with well defined quasiparticles the non-adiabaticity of the transition can be alternatively classified by scaling of the density of excitations $n_{\text{ex}}(\delta)$ when $|\delta| \rightarrow 0$. In general, the two classifications are different because the dominant low energy quasiparticles have a non-trivial dispersion relation.

The existence of regimes B and C in the quantum limit was supported in Ref. [140] by solution of a generic low energy quadratic Hamiltonian,

$$H = \frac{1}{2} \sum_q (q^2 \phi_q^2 + \kappa_q \Pi_q^2) , \tag{293}$$

where ϕ_q and Π_q are conjugate coordinates and momenta respectively. In the context of superfluidity κ_q is a compressibility. Here we choose

$$\kappa_q = \kappa + \lambda q^2 \tag{294}$$

to cover all three regimes defined above. κ is ramped as in Eq. (289). For a large initial κ_i , the response of the system belongs to regime A with $\epsilon(\delta) \sim \delta^2$, but when $\kappa_i = 0$ then

$$\epsilon \sim \frac{|\delta|^{(d+1)/4}}{\lambda^{(d+1)/8}}, \quad (295)$$

and the response belongs to regime B. Here d is the number of dimensions. The density of excitations $n_{\text{ex}}(\delta)$ leads to a different classification. When κ_i is large, then the non-analytic regime B is realised for $d = 1$ and the analytic regime A when $d \geq 2$. However, when $\kappa_i = 0$, then the system is non-analytic (B) when $d = 2, 3$, but *non-adiabatic* (C) in 1D.

The crossover between different scalings can be further illustrated by e.g. Ref. [141] where a near-adiabatic parameter change within a gapless metallic or gapped insulating phase of the Falicov-Kimball model is studied by the dynamical mean field theory [142]. The excitation energy density scales with a power of the quench rate δ whose exponent depends in general both on energy spectrum of the system and smoothness of the quench protocol. However, in the gapped insulator the exponent depends on the smoothness of the ramp only. By contrast, for a sufficiently smooth ramp protocol in the gapless metallic phase the exponent depends on the intrinsic spectrum of the system only, but this intrinsic behaviour is not observable when the ramp is not smooth enough. For instance, for a linear ramp there is a crossover to the δ^2 scaling in case A. The quadratic scaling for energy density was also derived in Ref. [143].

2.23. Many-particle Landau-Zener problem: adiabatic passage across a Feshbach resonance

Non-adiabatic dynamics of a single-particle quantum system can often be described by the Landau-Zener problem where a probability of the transition from the initially occupied ground state to the excited state is exponentially small in the sweeping rate δ . With more particles one generally encounters more LZ anti-crossings whose cumulative effect describes the behaviour of the system during the driving process. However, in many-body systems there is exponential density of energy levels and it is not possible to divide the evolution into a series of independent LZ anti-crossings: every anti-crossing takes finite time, but the frequency of anti-crossings increases exponentially. In experiments with ultracold quantum gases, where macroscopically large numbers of particles are involved, the microscopic (LZ) treatment is not practical, but it is often justified to use semiclassical treatments like the truncated Wigner method [125]. In this context, non-adiabaticity in the semiclassical models has been discussed recently in Refs. [34, 46, 136, 138, 144–152] and Sections 2.19.4 and 2.21.

In this Section we consider a time-dependent Dicke model in dimensionless units with a time-dependent Hamiltonian

$$H = -\delta t b^\dagger b + \delta t S^z + \frac{1}{\sqrt{N}}(b^\dagger S^- + \text{h.c.}), \quad (296)$$

where $S^\pm = S_x \pm iS_y$ are spin operators, the spin $S = N/2$, b is a bosonic annihilation operator, and δ is the sweep rate. When $N = 1$ we recover the standard LZ model in Eq. (39) and the excitation probability $P = \exp(-\pi/\delta)$ is exponentially small in the adiabatic regime $\delta \ll 1$. However, here we are interested in the opposite extreme of a macroscopically large spin when $N \gg 1$.

In the context of the adiabatic passage across a Feshbach resonance [55] the Hamiltonian (296) is equivalent to

$$H = -\delta t b^\dagger b + \frac{\delta t}{2} \sum_{i=1}^N \left(c_{i,\uparrow}^\dagger c_{i,\uparrow} + c_{i,\downarrow}^\dagger c_{i,\downarrow} \right) + \frac{1}{\sqrt{N}} \sum_{i=1}^N (b^\dagger c_{i,\downarrow} c_{i,\uparrow} + \text{h.c.}), \quad (297)$$

where $c_{i\sigma}$ are fermionic annihilation operators, and $\sigma = \uparrow, \downarrow$ represents internal states of fermions, see the caption of Figure 5. Initially at $t \rightarrow -\infty$ the system is prepared in the ground state with $2N$ fermionic atoms, and when $t \rightarrow +\infty$ its instantaneous ground state becomes the state with N bosonic molecules. In the adiabatic limit, the time-dependent Hamiltonian (297) is meant to convert all atoms into molecules. However, as shown in Refs. [147, 149, 150] and outlined below, the sweep is never truly adiabatic, because it leaves behind a fraction of fermions which scales with a power of δ .

In a semiclassical approximation to Eq. (296), we use the number-phase decomposition of the boson field, $b = \sqrt{Nn} e^{i\varphi}$, and the polar representation of the spin variables: $S_z = \frac{N}{2} \cos \theta$, $S_x = \frac{N}{2} \sin \theta \cos \xi$, and $S_y = \frac{N}{2} \sin \theta \sin \xi$. Combining the angles as $\xi - \varphi + \pi \equiv \phi$, and using a conservation law $Nn = \frac{N}{2}(1 - \cos \theta)$ to eliminate θ , we obtain $H = -2N (\delta t n + n\sqrt{1-n} \cos \phi)$. Finally, we rescale the Hamiltonian as

$$H' = H/N = -\gamma n - 2n\sqrt{1-n} \cos \phi, \quad (298)$$

where

$$\gamma = 2\epsilon t', \quad (299)$$

$\epsilon = \delta/N$, and $t' = Nt$. Here n and ϕ are mutually conjugate variables and $n \in [0, 1]$ is a fraction of bosons. In the following we skip the primes.

The equations of motion that follow from the Hamiltonian (298) are $\dot{n} = -\partial_\phi H$ and $\dot{\phi} = \partial_n H$. Given an initial $n = n_-$ at $t \rightarrow -\infty$, we want to find $n = n_+$ after the sweep to $t \rightarrow \infty$. These two asymptotic values n_\mp are related to an adiabatic invariant given by the action

$$I = \int \frac{d\phi}{2\pi} n, \quad (300)$$

where the integral is along a closed trajectory $n(t), \phi(t)$ in the phase space. More precisely, I is the area (divided by 2π) of the phase space enclosed by the trajectory $n(t), \phi(t)$ with the convention that, when moving along the trajectory, the enclosed area is on the left. For a fixed $\gamma \rightarrow \mp\infty$, the trajectories become $\phi = \phi_0 - \gamma t, n = n_\mp$ and the action is

$$I_- = n_-, \quad I_+ = 1 - n_+, \quad (301)$$

compare Figs. 35a and 35c respectively, where the I 's are the shaded areas (divided by 2π).

In the adiabatic limit of $\epsilon \rightarrow 0$ we expect the invariant I to be conserved, $I_+ = I_-$, and an initial state with $n_- = I_-$ bosons to be adiabatically converted into a final state with $n_+ = 1 - I_+ = 1 - I_- = 1 - n_-$ bosons. However, in a sweep with a finite rate ϵ we expect that I changes by $\Delta I = I_+ - I_- > 0$ and the final number

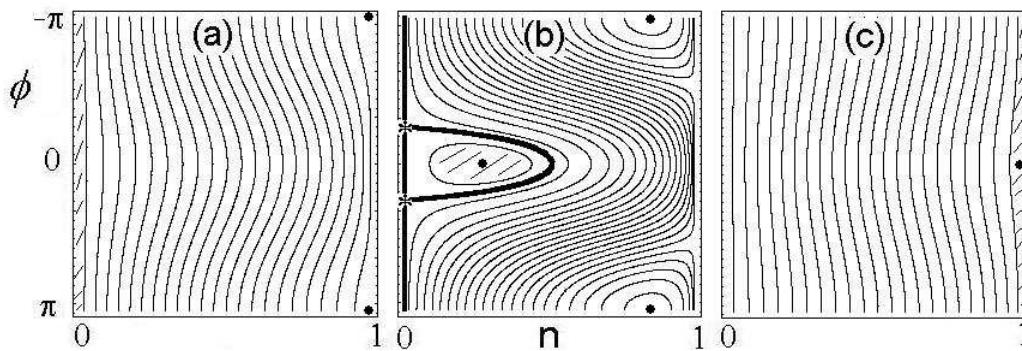


Figure 35. Phase portraits of the Hamiltonian (298). Panels a,b,c correspond to $\gamma = -6, -1.7, 20$ respectively. The solid dots are the fixed points, the asterisks mark the saddle points, the solid line is the separatrix, and the shaded areas illustrate the definition of the classical action, i.e., the area enclosed by the integral in Eq. (300). (Figure from Ref. [150])

of bosons,

$$n_+ = 1 - n_- - \Delta I, \quad (302)$$

is less than in the adiabatic limit by ΔI .

The change of the adiabatic invariant ΔI depends on n_- . In the truncated Wigner method [125], the final $\Delta I(n_-)$ in Eq. (302) has to be averaged over the initial Wigner function $W_-(n_-, \phi)$. Even in the initial ground state with no bosons the function $W_-(n_-) = 2N \exp(-2Nn_-)$ has a finite spread $n_- \simeq 1/N$. Thus we need to consider not only $n_- = 0$, but also small finite n_- .

The classical phase space portrait of the Hamiltonian (298) depends on a fixed γ . When $\gamma < -2$ or $\gamma > 2$, there is only one fixed point where $\partial_n H = 0 = \partial_\phi H$, see Figs. 35a and b. At $\gamma = -2$ there is a bifurcation and in the range $-2 < \gamma < 2$ there are two fixed points. In the same regime, there are two saddle points located where $n = 0$ and $\cos \phi = -\gamma/2$, see Fig. 35b. The trajectory connecting these two saddles, called separatrix, separates rotating from oscillating motions. In the adiabatic limit, the major part of the total change of the classical action ΔI is generated near the separatrix and especially near the saddle points when they arise during the bifurcation at $\gamma = -2$.

The initial n_- is subject to quantum fluctuations $\simeq N^{-1}$ so we need to consider finite but very small $n \simeq N^{-1}$. Approximating $\gamma = -2$ near the bifurcation, expanding to leading order in small n , introducing new canonically conjugate variables P, Y and a new time variable s , we obtain an effective Hamiltonian

$$H = \frac{P^2}{2} - s \frac{Y^2}{2} + \frac{Y^4}{2}, \quad (303)$$

see Ref. [150] for more details. The Hamiltonian implies the Panleve equation $\frac{d^2 Y}{ds^2} = sY - 2Y^3$ whose asymptotes were found in Ref. [153]:

$$Y(s \rightarrow -\infty) = \alpha(-s)^{-\frac{1}{4}} \sin \left(\frac{2}{3}(-s)^{3/2} + \frac{3}{4}\alpha^2 \ln(-s) + \text{const} \right), \quad (304)$$

$$Y(s \rightarrow +\infty) = \pm \sqrt{\frac{s}{2}} \pm \rho(2s)^{-\frac{1}{4}} \cos \left(\frac{2\sqrt{2}}{3}s^{3/2} - \frac{3}{2}\rho^2 \ln(s) + \text{const} \right). \quad (305)$$

As $s \rightarrow \pm\infty$ the adiabatic invariant of the Panleve equation tends to $I_+ = \frac{\alpha^2}{2}$ and $I_- = \frac{\rho^2}{2}$ respectively. Using a relation between the constants α and ρ in Ref. [150]

and going back to the variables of the Hamiltonian (298) we obtain

$$\Delta I(n_-) = n_- - \frac{\epsilon}{\pi} \ln \left(e^{\pi n_- / \epsilon} - 1 \right) - \frac{2\epsilon}{\pi} \ln(2 \sin(\pi \xi)) , \quad (306)$$

where $\xi \in [0, 1)$ is a quasi-random variable. For a given initial n_- , the final fraction of bosons is $n_+ = 1 - n_- - \Delta I(n_-)$.

There are two physically interesting ways of taking the adiabatic limit:

- When $\epsilon \rightarrow 0$ before $N \rightarrow \infty$, or more precisely $\epsilon \ll 1/N$, we obtain the asymptote

$$n_+ \approx 1 - n_- + \frac{2\epsilon}{\pi} \ln[2 \sin(\pi \xi)] . \quad (307)$$

This final n_+ is a random variable because the random variable n_- comes from the initial Wigner function $W_-(n_-) = 2N \exp(-2Nn_-)$ and ξ from a uniform distribution between 0 and 1. The last ξ -term is zero on average, so it does not contribute to the average of n_+ , but it increases its variance. The amplification is relatively weak because $\epsilon \ll 1/N$.

- When $N \rightarrow \infty$ before $\epsilon \rightarrow 0$, or more precisely $1/N \ll \epsilon \ll 1$, we have

$$n_+ \approx 1 - \frac{\epsilon}{\pi} \ln \left(\frac{\epsilon}{\pi n_-} \right) . \quad (308)$$

Average of n_+ over the initial distribution $W_-(n_-) = 2N \exp(-2Nn_-)$ is

$$\langle n_+ \rangle \approx 1 - \frac{1}{2} \epsilon \ln \epsilon . \quad (309)$$

The small initial quantum fluctuations of $n_- \simeq 1/N$ are amplified to much stronger fluctuations $\frac{1}{2}\epsilon \ln \epsilon$.

In both cases we find that, unlike in the two-level LZ problem, the leading non-adiabatic effect scales with a power of ϵ . There exists adiabatic *limit* when $\epsilon \rightarrow 0$, but there is no adiabatic *regime* below any threshold value of ϵ .

2.24. Summary

In Section 2 we reviewed accumulated evidence that adiabatic dynamics in a gapless isolated quantum system results in excitation which scales with a power of the transition rate (but with an exception of a disordered system where the excitation is only logarithmic in the rate). The leading motif was the adiabatic-impulse approximation essential for KZM. The main story left over some less universal features of the considered models, quite as well as some interesting ideas and problems that did not quite fit into the main narrative. Below we briefly mention three recent examples.

In Ref. [154] the adiabaticity of the linear quench across a quantum phase transition was readdressed within the adiabatic perturbation theory. There turns out to be an upper estimate on the excitation probability of the system in terms of an adiabatic dimension d_a . The adiabatic dimension is the dimension of the fidelity susceptibility of the driving Hamiltonian [155]. In the critical region, the quantum adiabatic dimension $d_a = 2d + 2z - 2\Delta_V$, where d is the dimension of the system, z is the dynamical exponent, and Δ_V is the scaling dimension of the driving Hamiltonian [156]. The upper estimate implies that the excitation is negligible when the

linear quench time $\tau_Q \gg L^{d_a}$, where L is the linear size of the system. For instance, in the quantum Ising chain $d_a = 2$ and the upper bound implies adiabaticity when $\tau_Q \gg L^2$, in agreement with the exact Eq. (124) where $L = N$ is the number of spins. By contrast, in the Lipkin-Meshkov-Glick model the upper bound implies $\tau_Q \gg N^{4/3}$, while the exact adiabaticity condition in Eq. (227) is a weaker $\tau_Q \gg N^{2/3}$, so in this model the upper bound is correct, but it overestimates the minimal τ_Q required to make the transition adiabatic. Reference [39] introduces a family of generalized adiabatic susceptibilities χ_m enumerated by their order m . Their χ_2 is the susceptibility considered in Ref. [154], but they argue that it is χ_4 that describes the excitation probability and density of excitations n_{ex} for slow linear quenches. In the Lipkin-Meshkov-Glick model they obtain an accurate adiabatic condition $\tau_Q \gg N^{2/3}$ - the same as the exact Eq. (227). Both Refs. [154] and [39] make a very interesting connection between the adiabaticity and the fidelity susceptibility.

This review is limited to isolated quantum systems, but it would not be quite physical to ignore the problem of adiabatic dynamics in open quantum systems. This problem has already been studied in some detail [85, 157–160], but it is certainly far from being completely explored. The effect of classical and quantum noise acting uniformly on the quantum Ising chain was considered in Refs. [157] and [158] respectively. Numerical simulations for a model of local noise acting on the disordered Ising chain were performed in Ref. [159], and the effect of a static spin bath coupled locally to the ordered Ising chain was considered in Ref. [85]. The static spin bath was found to change the universality class of the quantum phase transition to that of the disordered Ising chain in Section 2.16. For weak coupling to the spin bath and not too slow quenches the density of excitations scales like in the pure Ising chain in Eq. (121), but for very slow transitions the scaling is replaced by a much slower logarithmic dependence like in Eq. (206). Finally, in Ref. [160] the scaling theory was generalised to an open critical system and a quantum kinetic equation approach was formulated for adiabatic dynamics in the quantum critical region. It was found that for weak coupling and not too slow quenches the density of excitations is universal also in the presence of the external bath. Given the evidence at hand, we can conclude that a weak coupling to environment does not alter KZM for not too slow quenches, but in the adiabatic limit we have $\hat{\epsilon} \rightarrow 0$ and the KZM happens very close to the critical point, where the system is very susceptible to the influence of the environment. Moreover, thermalisation dynamics close to a quantum critical point was considered in Ref. [161].

An opposite situation is considered in Ref. [162], where a central spin couples globally to the environment of the transverse Ising model subject to the linear quench like in Section 2.13. The quenched environment monitors the state of the central spin and its sensitivity is amplified by closeness to the phase transition. Decoherence of the central spin happens almost exclusively when the critical point of the environment is traversed and is significantly enhanced by the non-equilibrium dynamics.

In the next part 3 we consider relaxation of the excited state in the last adiabatic stage of the evolution.

3. Apparent relaxation of an isolated quantum system after a sudden quench

3.1. Introduction

Once a system got excited, the question is what is going to be the fate of the excited state? Does it relax to any stationary state or, maybe, even thermal state? This question has not been thoroughly investigated in the context of adiabatic linear quenches, but with the exception of Section 2.13.10 above where some of the consequences of quantum dephasing have been worked out in the integrable quantum Ising chain. The reason partially is that in a linear quench it is hard to make a clear-cut distinction between the non-adiabatic process of exciting the system and the process of relaxation, because the relaxation begins already during the non-adiabatic excitation.

Nevertheless, the relaxation problem itself can be formulated in a clear-cut way when we assume that a system is initially prepared in the ground state of an initial Hamiltonian H_0 and then, at $t = 0$, a *sudden* quench, faster than any time scale of the system, is made to a final Hamiltonian H :

$$H_0 \xrightarrow{t=0} H . \quad (310)$$

In this way, the ground state of H_0 all of a sudden becomes the excited initial state for adiabatic evolution with a time-independent H . At first sight, the discontinuous sudden quench may appear very different from the smooth linear quench: a slow linear quench makes an effort to be adiabatic, while the sudden quench does not even pretend to be anything like adiabatic. In spite of this first impression, the difference is more quantitative than qualitative. As we know from Section 2.3, even in the linear quench one can often use the adiabatic-impulse-adiabatic approximation. In this approximation the state of the system does not change during the impulse stage, when the parameter ϵ in the Hamiltonian evolves from $\hat{\epsilon}$ to $-\hat{\epsilon}$, but the ground state at $\hat{\epsilon}$ survives to become the excited initial state for the adiabatic evolution after $-\hat{\epsilon}$. In this approximation the linear quench is effectively a sudden quench between $\hat{\epsilon}$ and $-\hat{\epsilon}$. The quantitative difference is that in a slow linear quench the effective parameter jumps from $\hat{\epsilon}$ across a critical point $\epsilon = 0$ to $-\hat{\epsilon}$ is small, while in a sudden quench it does not need to be small just as it does not need to cross any critical point. The relaxation after a sudden quench has been studied in many different integrable and non-integrable models. Section 3 is an attempt to review some well established concepts as well as more controversial conjectures that were formulated in this relatively new area of research.

The first question that comes to mind is what is meant by relaxation in an isolated quantum system at zero temperature? After all, the evolution of the initial pure state is unitary so the state cannot relax to any mixed steady state. However, even when the state $|\psi\rangle$ of the whole system is pure, a state of its subsystem Ω is in general mixed because the subsystem is entangled with the rest of the system Ω^\perp . The state of the subsystem must be described by a reduced density matrix $\rho_\Omega = \text{Tr}_{\Omega^\perp} |\psi\rangle\langle\psi|$ which is in general a mixed state. Thus a subsystem can be mixed even though the system as a whole remains pure.

Having thus introduced mixedness, we can now attempt a definition of relaxation. A well defined question is: is there a mixed stationary state ρ_∞ of the whole system such that

$$\lim_{t \rightarrow \infty} \rho_\Omega(t) = \text{Tr}_{\Omega^\perp} \rho_\infty \quad (311)$$

for a finite subsystem Ω ? If yes, then expectation values of *local* observables, with a finite support in the subsystem Ω , relax to their expectation values in the steady state ρ_∞ . Even though the actual pure state of the whole system $\rho(t) = |\psi(t)\rangle\langle\psi(t)|$ cannot relax, it appears to relax for local observables. There is no global relaxation, but there appears to be relaxation for local observers.

The local relaxation is not the most general way a relaxation of a pure state can be defined. Suppose that we want the steady state ρ_∞ to be a statistical description of a system like, e.g., a canonical or microcanonical ensemble. Even in classical physics a statistical description is not meant to capture all fine details of a state but only its most “coarse-grained” properties mainly because a too detailed description would not be tractable and thus not useful. From the point of view of observables, we expect good statistical description of a state to give accurate predictions of sufficiently coarse-grained observables, but we will not be surprised when a measurement of a complicated fine-detailed observable reveals a difference between the actual state and, say, a canonical ensemble. The same is true for an isolated quantum system: we expect that coarse-grained observables O can relax,

$$\lim_{t \rightarrow \infty} \langle \psi(t) | O | \psi(t) \rangle = \text{Tr } \rho_\infty O, \quad (312)$$

but a measurement of a sufficiently fine-detailed observable can reveal a difference between the statistical ρ_∞ and the actual pure state $|\psi(t)\rangle$. In a many-body system, for instance, simple few-body observables may be accurately described by ρ_∞ , while a complicated many-body observable can reveal that the statistical ρ_∞ is not accurate. Thus the pure state $|\psi(t)\rangle$ does not relax, but its approximate coarse-grained description appears to relax.

Having established what is meant by relaxation in an isolated quantum system, we can ask what is the relaxed state ρ_∞ ? A quick and in principle correct answer is: a diagonal ensemble. If a system does relax, then a diagonal infinite time average of its density matrix

$$\bar{\rho} \equiv \lim_{T \rightarrow \infty} \frac{1}{T} \int_0^T dt |\psi(t)\rangle\langle\psi(t)| = \sum_{\alpha} p_{\alpha} |\alpha\rangle\langle\alpha|, \quad (313)$$

is the first candidate for ρ_∞ . Here α enumerates eigenstates of a non-degenerate H and

$$p_{\alpha} = |\langle\alpha|\psi(0)\rangle|^2 = |\langle\alpha|\psi(t)\rangle|^2 \quad (314)$$

is a conserved probability that the isolated system is in the eigenstate α . Indeed, if a system relaxes to a steady state, then expectation values in the steady state must be the same as in the infinite time average $\bar{\rho}$. Unfortunately, the diagonal ensemble $\bar{\rho}$ may be disappointing as a statistical description, because it contains a lot of information about the initial state $|\psi(0)\rangle$ encoded in the microscopic initial probabilities p_{α} . Thus $\bar{\rho}$ itself may be not the desired tractable statistical description ρ_∞ , but it is a good starting point to look for a more tractable ρ_∞ as a coarse-grained description of $\bar{\rho}$.

By analogy to classical statistical physics, one can hypothesise that the steady state ρ_∞ is the state of maximal entropy subject to the constraints imposed by integrals of motion I_m , where the integrals I_m commute with H and between

themselves. The entropy is maximised by a generalised Gibbs ensemble (GGE)

$$\rho^{\text{GGE}} = \mathcal{N} \exp \left(- \sum_m \lambda_m I_m \right), \quad (315)$$

where the numbers λ_m are fixed by the conserved expectation values $\text{Tr} \rho^{\text{GGE}} I_m = \langle \psi(0) | I_m | \psi(0) \rangle$. The special case of only one integral $I_1 = H$ is the canonical ensemble. However, unlike a classical system, any quantum system has as many integrals of motion as the dimension of its Hilbert space. Indeed, we can always choose the integrals to be projectors $I_\alpha = |\alpha\rangle\langle\alpha|$ on the eigenstates of H , or as integer powers of a finite Hamiltonian $I_m = H^m$ with $m = 1, \dots, \dim(H)$. With the former choice the GGE becomes the microscopic diagonal ensemble $\bar{\rho}$, which may be too accurate to be tractable. The latter choice is also equivalent to the diagonal ensemble $\bar{\rho}$, but it may be a better starting point for further coarse-graining approximations, at least in the model considered in Section 3.9 below, where the sum over H^m can be accurately truncated to a few lowest powers. Thus, unlike in a classical system, the problem with GGE is not how to find any integrals of motion, but how to find a subset of the abundant integrals of motion leading to a sufficiently accurate but still tractable GGE. Nevertheless, there is a wide class of quadratic bosonic/fermionic Hamiltonians, where the number operators n_α of bosonic/fermionic quasiparticles provide such a small subset, see Sections 3.3 and 3.4 below, where these non-interacting systems are shown to relax to GGE for local observables O . The absence of relaxation to a thermal state was experimentally observed in the seminal experiments on one-dimensional hard-core bosons [3, 4], see Fig. 3.1.

Thus the integrable quadratic Hamiltonians relax locally to a GGE, but what happens with an interacting system that cannot be mapped to any non-interacting Hamiltonian? It turns out that in certain circumstances a non-integrable system may relax to a microcanonical ensemble. This scenario requires two conditions to be met: the *eigenstate thermalisation hypothesis* (ETH) proposed in Ref. [163] and a narrow energy distribution p_α of the initial state in the eigenbasis of the final H . The narrow distribution often happens to be the case, see the examples in Sections 3.9 and 3.10. The ETH asserts that any few-body observable O has the same expectation value in each eigenstate $|\alpha\rangle$ of a many-body Hamiltonian H in a narrow energy window ΔE . This not-quite-intuitive hypothesis is shown to be the case in the examples of non-integrable systems considered in Section 3.10 while it is not true for the integrable models considered there. When we assume these two conditions, then for any few-body observable the diagonal ensemble (313) is indistinguishable from a microcanonical ensemble

$$\rho_\infty = \mathcal{N} \sum_{\alpha, |E_\alpha - \langle H \rangle| < \Delta E} |\alpha\rangle\langle\alpha| \quad (316)$$

where ΔE is a narrow energy window around average energy $\langle H \rangle$. A coarse-grained few-body observable has the same expectation value in $\bar{\rho}$ as in ρ_∞ because, thanks to ETH, it actually has the same expectation value in any eigenstate in the energy window. In fact, assuming that ETH is exactly true, we can push it to its logical limit and claim that for any few-body observable the state

$$\rho_\infty = |\alpha\rangle\langle\alpha|, \quad (317)$$

with $|\alpha\rangle$ being any individual eigenstate in the energy window ΔE , is as good an

approximation to the actual diagonal ensemble $\bar{\rho}$ as the microcanonical ensemble. Indeed, since all expectation values $\langle \alpha | O | \alpha \rangle$ in the window are the same, there is no need to average over the window as in the microcanonical ensemble (316). Thus each individual many-body eigenstate in the window provides a thermal (microcanonical) average for a few-body observable O . This thermal character of the individual eigenstates is hidden by their initial coherent superposition $|\psi(0)\rangle$, but it is revealed after the initial phase coherence is destroyed by relaxation or, more precisely, it appears to be destroyed for the simple (coarse-grained) few-body observables.

The ETH is argued to hold in non-integrable quantum systems, while the GGE often is an accurate description of the relaxed state in integrable quadratic systems, see Sections 3.3, 3.4, 3.5, 3.6, and 3.7 below. This is similar to classical physics, where integrable systems constrained by their conservation laws do not thermalise, but non-integrable chaotic systems do thermalise [164]. However, this mechanism of quantum thermalisation is qualitatively different than that of classical thermalisation. According to ETH, each many-body eigenstate is a thermal ensemble, while the ergodicity means that classical thermalisation requires probing essentially all states on a manifold of definite energy. A classical integrable system becomes chaotic when a non-integrable perturbation is stronger than certain threshold. A good example is the classic Fermi-Pasta-Ulam numerical experiment, where the perturbation is too weak to make the system chaotic [164]. An interesting question, addressed in Section 3.10, is if a similar threshold exists in a quantum system. Numerical simulations in small systems suggest that turning-off a non-integrable perturbation to an integrable model results in a smooth departure from ETH, but it is not clear what happens in the thermodynamic limit.

The microcanonical steady state required both ETH and a narrow initial energy distribution p_α . Since in an isolated system the distribution is constant, there is no way it could relax to a canonical distribution $p_\alpha \sim \exp(-\beta E_\alpha)$ unless it happened to be canonical from the very beginning. Thus there is no global thermalisation, but one can still try to identify local or coarse-grained observables O for which the global state appears to relax to the canonical ensemble. For instance, in a system of many identical particles one is often interested in a single particle momentum distribution $n_{\vec{k}}$. This interest is well motivated by current ultracold atoms experiments, where it is routine to measure the momentum distribution in an atomic cloud expanding after opening a trap, see the example in the right panel of Fig. 3.1. Thermalisation of $n_{\vec{k}}$ is inhibited by integrability of the system like e.g. for quadratic Hamiltonians which relax locally to a non-thermal GGE. It can also be inhibited for particles interacting by two-body interactions in one dimension, where the conservation of momentum and kinetic energy in a collision of two particles does not allow for any changes in the momentum distribution. A spectacular recent quantum Newton cradle experiment [4] demonstrates this inhibited relaxation in a quasi-one-dimensional regime, see Fig. 3.1. Integrability is also responsible for such phenomena as the ballistic character of transport [165] or the meta-stability of solitons [166].

Another interesting question, in addition to the nature of the final relaxed state, is the dynamics of relaxation to this state. Since the ground state of an initial H_0 may contain highly excited eigenstates of a final Hamiltonian H , the answer to this question is not universal, because the usual universal low energy theories may not describe the relaxation accurately. This non-universality is illustrated by examples in Section 3.11, where it is shown that the relaxation can be actually the fastest when H is either at a critical point or close to it. This is contrary to the usual notion of critical slowing down derived from a universal low energy theory. In spite

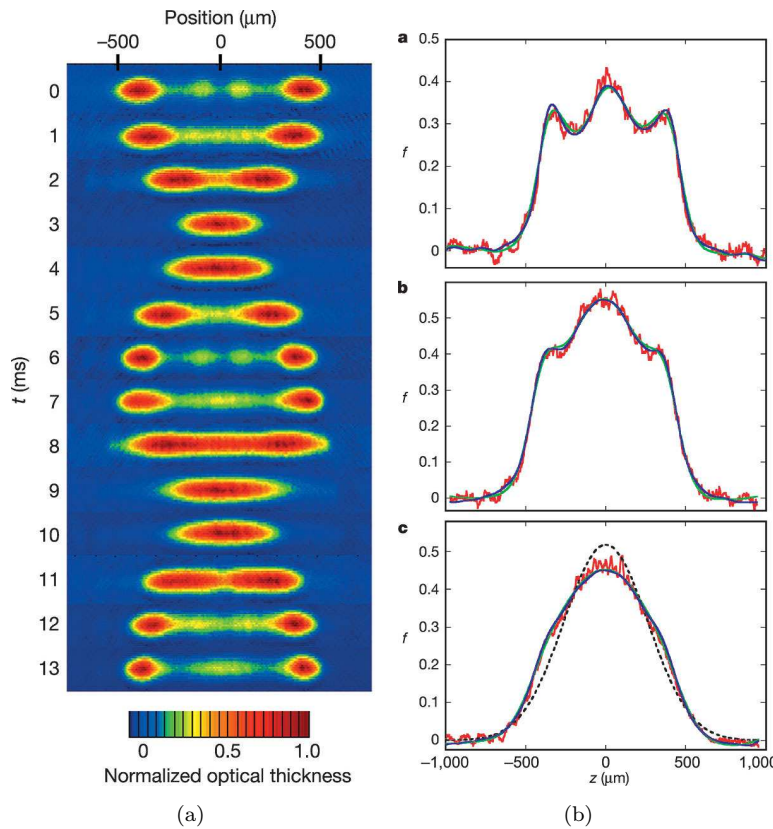


Figure 36. Left panel: The Newton cradle experiment in Ref. [4]. An atomic cloud of effectively one-dimensional bosons confined in a harmonic trap is initially split into two clouds with opposite momenta. Then the two halves keep oscillating in the trap and pass through each other without thermalisation of momentum distribution, see the right panel. (Figure from Ref. [4]) Right panel: The red curves in panels a,b,c are the actual momentum distributions measured for different interaction strengths of one-dimensional hard-core bosons in Ref. [4]. The dashed line in panel c is the best Gaussian fit to the actual distribution. To the extent the actual distribution does not conform to a Gaussian, the atoms have not thermalised. (Figure from Ref. [4])

of that, there are some remarkable universal features, like the quasiparticle horizon effect described in Section 3.2.

Section 3 is organised as follows. In Section 3.2 we review the quasiparticle horizon effect. In Section 3.3 the generalised Gibbs ensemble is introduced for quadratic Hamiltonians, and in Section 3.4 it is shown how a quadratic Hamiltonian prepared in an initial Gaussian pure state relaxes locally to GGE. The following Sections 3.5, 3.6, and 3.7 describe examples of quadratic systems relaxing to GGE, and discuss applicability of the GGE to different observables. In Section 3.8 we consider the non-integrable Bose-Hubbard model in different limits when it is close to integrability and GGE is an accurate steady state, but we also cite some evidence that it thermalises away from these integrable limits. Section 3.9 provides an example of a system integrable by Bethe ansatz, where an accurate non-thermal GGE can be constructed out of integer powers of the Hamiltonian. In Section 3.10 we review the microcanonical ensemble in connection with the eigenstate thermalisation hypothesis (ETH). Finally, in Section 3.11 we mention some aspects of the dynamics of relaxation. We conclude in Section 3.12.

3.2. Quasiparticle light cone effect in dephasing after a sudden quench

At $t = 0$ a system is prepared in the ground state $|\psi_0\rangle$ of a Hamiltonian H_0 and then, after a sudden quench, it evolves unitarily with a different Hamiltonian H at $t > 0$. The initial H_0 is non-critical and it has a finite correlation length ξ_0 and a finite gap Δ_0 . The sudden quench is faster than Δ_0^{-1} . The question is how do the correlations evolve in time? As shown in Ref. [167], the answer to this question is quite universal when H is at a critical point. Particularly powerful analytic results can be obtained in one dimension when the dynamical exponent is $z = 1$ or, equivalently, there is a linear quasiparticle dispersion relation $\epsilon_k = v|k|$ with quasiparticle velocity v . This $1 + 1$ dimensional problem can be described asymptotically by a boundary conformal field theory [168], where the initial state is a boundary condition.

The results from the conformal field theory suggest a simple physical picture. The initial state $|\psi_0\rangle$ is a highly excited state as compared to the ground state of the final Hamiltonian H . It is a source of quasiparticle excitations. Quasiparticles originating from closely separated points, within the correlation length ξ_0 in the ground state of H_0 , are quantum entangled. Once they are emitted, they behave semi-classically travelling at speed v . This simple picture has several important implications:

- Incoherent quasiparticles arriving at a given point from well separated sources cause relaxation of most local observables at this point to their expectation values in the ground state of H . There are exceptions like the local energy density which is conserved. This relaxation is exponential $\sim \exp(-\pi xvt/2\tau_0)$, where $\tau_0 \sim \Delta_0^{-1}$ is not universal, but x is the bulk scaling dimension of a given observable.
- Entangled quasiparticles arriving at the same time t at points with separation $R \gg \xi_0$ induce correlations between local observables at these points. Since they travel at a definite speed v , there is a sharp light-cone effect, i.e., the connected correlation functions do not change significantly from their initial values until time $t \simeq R/2v$. The light-cone effect is rounded off over the region $t - R/2v \simeq \tau_0$ because quasiparticles remain entangled over this time scale. After $t \simeq R/2v$ the connected correlations rapidly relax to time-independent values. At asymptotically large separations R , but well within the light cone where $R \ll 2vt$, they decay exponentially $\sim \exp(-\pi xR/2v\tau_0)$. This decay is qualitatively different from the power law decay in the ground state of H which is at the critical point.
- Entangled quasiparticles arriving at the same time $t \simeq R/2v$ at points separated by $R \gg \xi_0$ induce entanglement between these points. The entropy of a subsystem of size L , which is dominated by pairs of quasiparticles entangled across the boundary of the subsystem, initially grows linearly with time as more and more quasiparticles cross the subsystem boundary until it saturates at $t \simeq L/v$. In the thermodynamic limit, in a system with periodic boundary conditions the saturation time is $t \simeq L/2v$, and in an open system the entropy saturates at $t \simeq L/v$. In a conformal field theory the saturation time is rounded off on the time scale Δ_0^{-1} .
- In the thermodynamic limit, the saturated entropy of the subsystem of size L is linear in L because the number of quasiparticles in the subsystem is linear in L and, after the saturation at $t = \mathcal{O}(L/v)$, every quasiparticle which happens to be in the subsystem is more likely to be entangled with a quasiparticle outside than a quasiparticle inside the subsystem. Thus, there is no area law for the entropy, so the relaxation process cannot be efficiently simulated by, say, the DMRG algorithm [169] on a classical computer.

The light cone effect is even more rounded off when the critical H is a lattice system. The saturation begins at $t_0 \simeq R/2v_0$, where $v_0 = \frac{\partial \epsilon_k}{\partial k}(k=0)$ is a long wavelength quasiparticle group velocity, but after t_0 the entropy (or correlation function) keeps varying slowly with time because on a lattice there are quasiparticles slower than v_0 .

Beyond the conformal field theory, the light cone effect was confirmed in the quantum Ising model [167], the chain of coupled harmonic oscillators [167], the Heisenberg chain [170], and a number of other systems, see Ref. [171] and the following Sections. It was also confirmed away from criticality, where v_0 becomes the maximal group velocity of quasiparticles, see e.g. Ref. [172]. In general, a maximal velocity of propagation of information in non-relativistic systems is guaranteed by the Lieb-Robinson theorem [173].

By contrast, in a disordered Heisenberg chain the entropy seems to grow logarithmically with time, at least as far as it can be inferred from numerical results [170]. This effect cannot be explained by diffusion of quasiparticles replacing the ballistic motion in the pure case.

The light cone effect is the dominant feature of quantum relaxation after a sudden quench. The question what is the final relaxed state is the topic of the following Sections.

3.3. Generalised Gibbs ensemble (GGE) for a quadratic Hamiltonian

Integrals of motion I_α mutually commute, $[I_\alpha, I_\beta] = 0$, and commute with the Hamiltonian, $[I_\alpha, H] = 0$. In a unitary evolution of an isolated quantum system, $|\psi(t)\rangle = e^{-itH}|\psi(0)\rangle$, all moments of the integrals of motion are conserved,

$$\langle \psi(t) | I_1^{r_1} I_2^{r_2} \dots | \psi(t) \rangle = \langle \psi(0) | I_1^{r_1} I_2^{r_2} \dots | \psi(0) \rangle, \quad (318)$$

because each product $I_1^{r_1} I_2^{r_2} \dots$ is also an integral of motion.

When degeneracies in the spectrum of the Hamiltonian can be ignored, then the infinite time average of the density matrix of the system $\rho(t) = |\psi(t)\rangle\langle\psi(t)|$ is diagonal in the eigenbasis of the integrals of motion,

$$\bar{\rho} \equiv \lim_{T \rightarrow \infty} \frac{1}{T} \int_0^T dt \rho(t) = \sum_{n_1, n_2, \dots} p_{n_1, n_2, \dots} |n_1, n_2, \dots\rangle \langle n_1, n_2, \dots|, \quad (319)$$

where $I_\alpha |n_1, n_2, \dots\rangle = n_\alpha |n_1, n_2, \dots\rangle$. The diagonal $\bar{\rho}$ conserves all moments $I_1^{r_1} I_2^{r_2} \dots$,

$$\begin{aligned} \text{Tr } \bar{\rho} I_1^{r_1} I_2^{r_2} \dots &= \lim_{T \rightarrow \infty} \frac{1}{T} \int_0^T dt \text{Tr } \rho(t) I_1^{r_1} I_2^{r_2} \dots \\ &= \lim_{T \rightarrow \infty} \frac{1}{T} \int_0^T dt \langle \psi(t) | I_1^{r_1} I_2^{r_2} \dots | \psi(t) \rangle \\ &= \langle \psi(0) | I_1^{r_1} I_2^{r_2} \dots | \psi(0) \rangle, \end{aligned} \quad (320)$$

as expected from a candidate for a stationary state of an integrable system.

The diagonal average $\bar{\rho}$ can be rewritten in an equivalent form

$$\bar{\rho} = \mathcal{N} \exp \left[- \sum_{\alpha} \lambda_{\alpha} I_{\alpha} - \sum_{\alpha \leq \beta} \lambda_{\alpha \beta} I_{\alpha} I_{\beta} - \sum_{\alpha \leq \beta \leq \gamma} \lambda_{\alpha \beta \gamma} I_{\alpha} I_{\beta} I_{\gamma} - \dots \right], \quad (321)$$

where the λ 's and the normalisation \mathcal{N} are chosen so that $\text{Tr } \bar{\rho} I_1^{r_1} I_2^{r_2} \dots = \langle \psi(0) | I_1^{r_1} I_2^{r_2} \dots | \psi(0) \rangle$ and $\text{Tr } \bar{\rho} = 1$. The density matrix (321) has a form of a most general Gibbs ensemble and as such it is manifestly the density matrix that maximises the von Neumann entropy subject to the constraints imposed by all the conserved moments $\langle \psi(0) | I_1^{r_1} I_2^{r_2} \dots | \psi(0) \rangle$. However, this exact representation of $\bar{\rho}$ may be not a useful coarse-grained *statistical* description because it contains as much information as the diagonal ensemble (319) itself.

Nevertheless, the exact form (321) is a good starting point for more tractable approximations. The crudest but still non-trivial approximation is known as a *generalised Gibbs ensemble* (GGE) [174]

$$\bar{\rho} \approx \mathcal{N} \exp \left[- \sum_{\alpha} \lambda_{\alpha} I_{\alpha} \right] \equiv \rho_{\text{GGE}} , \quad (322)$$

where the λ 's are fixed by conservation of the first moments only: $\text{Tr } \bar{\rho} I_{\alpha} = \langle \psi(0) | I_{\alpha} | \psi(0) \rangle$. The mixed state ρ_{GGE} is the maximal entropy state subject to these constraints. The drastic approximation has a price of course: there are observables O for which $\text{Tr } \rho_{\text{GGE}} O$ is a very bad approximation to the exact $\text{Tr } \bar{\rho} O$. However, this is expected in statistical physics, where a sufficiently complex observable O can reveal a difference between a coarse grained state like ρ_{GGE} and a microscopic state like $\bar{\rho}$, but there is practically no difference for sufficiently coarse grained observables. In the following we attempt to figure out what are the conditions for an observable to be “sufficiently coarse grained” in case of the generalised Gibbs ensemble.

To be more specific, we assume that the integrals are numbers of bosonic or fermionic quasiparticles [175, 176], $I_{\alpha} = n_{\alpha} = \gamma_{\alpha}^{\dagger} \gamma_{\alpha}$. Since I_{α} 's mutually commute we can factorise (322)

$$\rho_{\text{GGE}} = \left(\prod_{\alpha} \mathcal{N}_{\alpha} \exp [-\lambda_{\alpha} n_{\alpha}] \right) |n_1, n_2, \dots\rangle \langle n_1, n_2, \dots| . \quad (323)$$

This diagonal matrix is a classical ensemble for the set of *independent* random variables n_{α} with a product joint probability distribution

$$p_{n_1, n_2, \dots}^{\text{GGE}} = \prod_{\alpha} \mathcal{N}_{\alpha} \exp [-\lambda_{\alpha} n_{\alpha}] . \quad (324)$$

In the GGE the occupation numbers n_{α} are independent and, in particular, uncorrelated. For an observable O to have an accurate expectation value in GGE the observable cannot depend on correlations between different n_{α} 's.

In case of fermions, when n_{α} is either 0 or 1, this is also a sufficient condition because the expectation value $\langle n_{\alpha} \rangle$ plus normalisation determine completely the probability distribution for n_{α} . The distribution can be written in e.g. the GGE form $\mathcal{N}_{\alpha} \exp [-\lambda_{\alpha} n_{\alpha}]$ with the coefficients \mathcal{N}_{α} and λ_{α} determined by the two constraints.

In case of bosons, when $n_{\alpha} = 0, 1, 2, \dots$, the expectation value $\langle n_{\alpha} \rangle$ and normalisation are not sufficient to determine the probability distribution for n_{α} . Thus the GGE ansatz $\mathcal{N}_{\alpha} \exp [-\lambda_{\alpha} n_{\alpha}]$ may have wrong variance and higher moments even though it has the correct expectation value.

Thus we can conclude, that GGE is an accurate statistical description for observables which do not depend on correlations between quasiparticle occupation

numbers and, in case of bosons, higher moments of individual occupation numbers. This is the meaning of the mathematical conditions given in Ref. [175].

The GGE is an accurate statistical description of $\bar{\rho}$ for observables O that do not depend on correlations between n_α . Some correlations between n_α 's are allowed provided that their contribution is negligible in the thermodynamic limit. A good example are 1D hard core bosons which can be represented equivalently by non-interacting fermions. When perturbed by an alternating potential, as in Ref. [174], the initial state contains correlations between pairs of occupation numbers n_k and $n_{k+\pi}$ only. These sparse correlations make negligible contribution to *local* observables restricted to a finite region of real space. Another example is the Luttinger model equivalent to non-interacting bosons, see Ref. [177] and Section 3.6. A quench of interaction strength in this translationally invariant Hamiltonian prepares an initial state with correlations between pairs of bosonic occupation numbers n_k and n_{-k} only. Again, in the thermodynamic limit these sparse correlations have negligible contribution to local observables.

Moreover, with an additional assumption that the initial pure state is Gaussian and the Hamiltonian is quadratic in bosonic/fermionic annihilation operators, GGE can be shown to be the unique steady state for local observables. This and the dynamics of local relaxation to this stationary state is the subject of the next Section.

3.4. Local relaxation to GGE after a quench in a quadratic Hamiltonian

In the last Section we discussed for what observables the time-averaged diagonal density matrix $\bar{\rho}$ in Eq. (319) can be accurately represented by the generalised Gibbs ensemble (GGE) in Eq. (322). Our interest in the time-averaged density matrix was motivated by the fact that *if* the long time limit of an expectation value $\text{Tr } \rho(t) O$ exists, then it is equal to the expectation value in the time-averaged density matrix,

$$\lim_{t \rightarrow \infty} \text{Tr } \rho(t) O = \text{Tr } \bar{\rho} O . \tag{325}$$

However, in an isolated quantum system a limit $\rho(t \rightarrow \infty)$ does not exist¹, so the existence of the limit on the left hand side of (325) should not be taken for granted for an arbitrary observable O . This is why in this Section we investigate a more refined question if we can define a subset of observables O for which

$$\lim_{t \rightarrow \infty} \text{Tr } \rho(t) O = \text{Tr } \rho^{\text{GGE}} O ? \tag{326}$$

In other words, we are looking for a subset of observables for which a pure state $\rho(t)$ appears to relax to a mixed steady state ρ^{GGE} .

Following Ref. [176], we consider a general quadratic lattice Hamiltonian

$$H = \sum_{mn} \left[c_m^\dagger V_{mn} c_n + \frac{1}{2} \left(c_m^\dagger W_{mn} c_n^\dagger + \text{h.c.} \right) \right] \tag{327}$$

where c_m are bosonic or fermionic annihilation operators. The Hamiltonian is di-

¹Except for the trivial case of a time-independent ρ diagonal in the eigenbasis of the Hamiltonian.

agonalised to $H = \sum_k \omega_k \gamma_k^\dagger \gamma_k \equiv \sum_k \omega_k I_k$ by a Bogoliubov transformation

$$c_m = \sum_k \left(u_{mk} \gamma_k + v_{m,k}^* \gamma_k^\dagger \right), \quad (328)$$

where the index k enumerates quasiparticle states. The quadratic Hamiltonian (327) has a Gaussian Bogoliubov vacuum ground state annihilated by all quasiparticle annihilation operators γ_k . Any Gaussian state ρ is fully determined by its quadratic correlators

$$\alpha_{mn} = \text{Tr } \rho c_m c_n^\dagger, \quad \beta_{mn} = \text{Tr } \rho c_m c_n. \quad (329)$$

Here we assume that the initial pure state $\rho(0)$ is Gaussian. It can be prepared as a ground state of a different quadratic Hamiltonian H_0 before the Hamiltonian is suddenly quenched to the final H . The quadratic H evolves $\rho(0)$ into a pure state $\rho(t)$ which is also Gaussian.

The lattice can be divided into a finite subsystem Ω and its environment Ω^\perp . We are interested in *local* observables O with a finite support in Ω . To find expectation values of the local observables it is enough to know a reduced density matrix

$$\rho_\Omega(t) = \text{Tr}_{\Omega^\perp} \rho(t). \quad (330)$$

We want to show that, under certain conditions, the reduced density matrix tends to a steady state,

$$\lim_{t \rightarrow \infty} \rho_\Omega(t) = \text{Tr}_{\Omega^\perp} \rho^{\text{GGE}}, \quad (331)$$

obtained by reduction of a *Gaussian* GGE

$$\rho^{\text{GGE}} = \mathcal{N} \exp \left[- \sum_k \lambda_k \gamma_k^\dagger \gamma_k \right]. \quad (332)$$

Here λ 's are fixed by initial conditions $\text{Tr} \rho^{\text{GGE}} \gamma_k^\dagger \gamma_k = \text{Tr} \rho(0) \gamma_k^\dagger \gamma_k \equiv n_k$ for the integrals of motion $I_k = \gamma_k^\dagger \gamma_k$. If the limit exists, then for all *local* observables O in the finite Ω the state appears to relax to GGE. This is *apparent local relaxation* which should not be mistaken with any global relaxation of the pure state $\rho(t)$.

When ρ is a Gaussian state fully characterized by the correlators (329), then the reduced density matrix ρ_Ω is also a Gaussian state fully characterised by a subset of the same correlators (329) with indices m, n restricted to the subsystem Ω . Thus all that we need to show for a Gaussian initial state is that

$$\lim_{t \rightarrow \infty} \alpha_{mn}(t) = \alpha_{mn}^{\text{GGE}}, \quad \lim_{t \rightarrow \infty} \beta_{mn}(t) = \beta_{mn}^{\text{GGE}}, \quad \text{for } m, n \in \Omega. \quad (333)$$

Here

$$\alpha_{mn}(t) = \sum_{k, k'} \text{Tr } \rho(t) \left(u_{mk} \gamma_k + v_{m,-k}^* \gamma_{-k}^\dagger \right) \left(u_{nk'} \gamma_{k'}^\dagger + v_{n,-k'} \gamma_{-k'} \right), \quad (334)$$

$$\beta_{mn}(t) = \sum_{k, k'} \text{Tr } \rho(t) \left(u_{mk} \gamma_k + v_{m,-k}^* \gamma_{-k}^\dagger \right) \left(u_{nk'} \gamma_{k'} + v_{n,-k'}^* \gamma_{-k'}^\dagger \right), \quad (335)$$

while the correlators in the GGE are “diagonal” in k

$$\alpha_{mn}^{\text{GGE}} = \sum_k [u_{mk} u_{nk}^* (1 \pm n_k) + v_{mk}^* v_{nk} n_k] , \quad (336)$$

$$\beta_{mn}^{\text{GGE}} = \sum_k [u_{mk} v_{nk}^* (1 \pm n_k) + v_{mk}^* u_{nk} n_k] , \quad (337)$$

with the upper/lower sign for bosons/fermions. They follow from diagonal expectation values in GGE:

$$\text{Tr} \rho^{\text{GGE}} \gamma_k \gamma_{k'} = 0 , \quad (338)$$

$$\text{Tr} \rho^{\text{GGE}} \gamma_k \gamma_{k'}^\dagger = \delta_{k,k'} (1 \pm n_k) . \quad (339)$$

Equations (333) are satisfied if a contribution of quasiparticle correlators

$$\text{Tr} \rho(t) \gamma_k \gamma_{k'} = e^{-it(\omega_k + \omega_{k'})} \text{Tr} \rho(0) \gamma_k \gamma_{k'} , \quad (340)$$

$$\text{Tr} \rho(t) \gamma_k \gamma_{k'}^\dagger = e^{-it(\omega_k - \omega_{k'})} \text{Tr} \rho(0) \gamma_k \gamma_{k'}^\dagger \quad \text{for } k \neq k' \quad (341)$$

to correlators (334,335) vanishes when $t \rightarrow \infty$.

This seems to be quite generic. Indeed, given that the indices m, n are bounded to a finite Ω , we need to consider a finite number of Bogoliubov coefficients u_{mk}, v_{mk} enumerated by $m \in \Omega$. In the thermodynamic limit of infinite lattice, when $t \rightarrow \infty$ then the phase factor $e^{-it(\omega_k + \omega_{k'})}$ in (340) oscillates with k and k' fast enough to average out to zero the contribution of this term to the infinite sum over k, k' . The same is generically true for Eq. (341) when $k \neq k'$. More rigorous mathematical conditions, and some important exceptions, can be found in Ref. [176].

After the dephasing in a finite subsystem Ω is completed, then for local observables in Ω the quadratic quasiparticle correlators appear to be equal to quadratic correlators (339) in GGE (332). Since GGE is Gaussian and quadratic correlators determine a Gaussian state uniquely, then GGE is the unique (apparent) stationary state for local observables in Ω .

Returning to the issue of relaxation, we can refine the above argument in a translationally invariant case, when $V_{mn} = V_{m-n}$ and $W_{mn} = W_{m-n}$ in the quadratic Hamiltonian (327) and the Bogoliubov modes in Eq. (328) become $u_{mk} = e^{ikm} u_k$ and $v_{mk} = e^{ikm} v_k$ with definite quasimomenta k (we suppress vector notation in more than one dimension). A quench from a different translationally invariant quadratic Hamiltonian H_0 prepares an initial state $\rho(0)$ such that

$$\text{Tr} \rho(0) \gamma_k \gamma_{k'} = \delta_{-k,k'} \Delta_k , \quad \text{Tr} \rho(0) \gamma_k \gamma_{k'}^\dagger = \delta_{k,k'} (1 \pm n_k) . \quad (342)$$

After simple algebra using the symmetry $\omega_k = \omega_{-k}$ we obtain

$$\alpha_{mn}(t) = \alpha_{mn}^{\text{GGE}} + \int_{-\pi}^{\pi} \frac{dk}{2\pi} e^{ik(m-n)} (e^{-2it\omega_k} u_k v_{-k} \Delta_k + \text{c.c.}) , \quad (343)$$

$$\beta_{mn}(t) = \beta_{mn}^{\text{GGE}} + \int_{-\pi}^{\pi} \frac{dk}{2\pi} e^{ik(m-n)} (e^{-2it\omega_k} u_k u_{-k} \Delta_k + e^{2it\omega_k} v_k^* v_{-k}^* \Delta_k^*) \quad (344)$$

In a small neighbourhood $(k_0 - \delta k, k_0 + \delta k)$ of a generic k_0 we can linearise in

$(k - k_0)$ as $\omega_k \approx \omega_{k_0} + v_{k_0}(k - k_0)$, where $v_{k_0} = \frac{d\omega_k}{dk}(k_0)$ is a group velocity¹. Contributions to the above integrals from this neighbourhood are proportional to

$$\int_{-\delta k}^{\delta k} \frac{d(k - k_0)}{2\pi} e^{i(k - k_0)[m - n \pm 2v_{k_0}t]}, \quad (345)$$

provided that δk is much less than the shortest scale on which the functions u_k, v_k, n_k can vary in k . If u_k, v_k, n_k are not singular¹, then for $t \rightarrow \infty$ this integral decays like $\mathcal{O}(\delta k/t)$ except when

$$|m - n| \approx 2 v_{k_0} t. \quad (346)$$

The distance $2v_{k_0}t$ is a separation of a pair of quasiparticles with opposite momenta $(k_0, -k_0)$ created by the quench, see the quasiparticle horizon effect in Section 3.2. When t is long enough this separation becomes much longer than the subsystem Ω and the exception (346) does not apply to any $m, n \in \Omega$. This is another example of the quasiparticle horizon effect in Section 3.2.

Thus the relaxation in Eqs. (333) seems to be generic and the quadratic correlators tend to the quadratic correlators in the GGE (332). Since both $\rho_\Omega(t \rightarrow \infty)$ and $\text{Tr}_{\Omega^\perp} \rho^{\text{GGE}}$ are Gaussian, the equality of their quadratic correlators implies that both states are the same and, in particular, *all* local observables $O \in \Omega$ (and not only quadratic correlators) have the same expectation values in the two states. The GGE (332) is determined uniquely by the quadratic correlators plus the requirement that GGE is Gaussian.

The Gaussian GGE (332) is determined by the initial quasiparticle occupation numbers n_k , so it is not surprising that it correctly “predicts” the conserved n_k . The free lunch is that after the local relaxation GGE also correctly describes all local observables $O \in \Omega$. Thus we need to invest all n_k to predict all local observables. This is lesser return than in the Gaussian canonical ensemble

$$\rho^{\text{canonical}} = \mathcal{N} \exp[-\beta H] = \mathcal{N} \exp \left[-\beta \sum_k \omega_k \gamma_k^\dagger \gamma_k \right], \quad (347)$$

which is a special case of GGE (332) with $\lambda_k = \beta \omega_k$ and only one adjustable parameter β that we need to fix. However, this is the price for the integrability of the quadratic Hamiltonian. In a sense, in the GGE (332) each non-interacting quasiparticle has its own inverse temperature $\beta_k = \lambda_k / \omega_k$.

We can conclude that in general a quadratic Hamiltonian initially prepared in a pure Gaussian state relaxes locally to GGE. More precisely, expectation values of observables within a quasiparticle horizon relax to their expectation values in GGE.

3.5. GGE and the transverse quantum Ising chain

The argument in Section 3.4 applies to the transverse field quantum Ising chain (92). A Jordan-Wigner transformation maps the Hamiltonian (92) to a translationally invariant quadratic Hamiltonian (104). A sudden quench from an initial

¹When $v_{k_0} = 0$, then we can expand $\epsilon_k = \epsilon_{k_0} + A(k - k_0)^2$ and, when u_k, v_k, n_k are not singular, the integrals decay like $\mathcal{O}(\delta k/\sqrt{t})$ for $t \rightarrow \infty$.

¹The u_k, v_k, n_k cannot be singular for fermions, when they are bounded by the constraints $|u_k|^2 + |v_k|^2 = 1$ and $0 \leq n_k \leq 1$, but they can in principle be singular for bosons because the bosonic constraints $|u_k|^2 - |v_k|^2 = 1$ and $0 \leq n_k < \infty$ do not provide any upper bounds.

transverse field g_i to a final $g_f > 0$ prepares an initial Gaussian state which later relaxes *locally* to the GGE (332), where γ_k is an annihilation operator for a Bogoliubov quasiparticle at the final g_f , see Eqs. (108,109,110,111), and λ_k are such that $\text{Tr } \rho^{\text{GGE}} \gamma_k^\dagger \gamma_k = \text{Tr } \rho(0) \gamma_k^\dagger \gamma_k$.

When expressed in terms of fermions, the quantum Ising model relaxes locally to GGE. However, since the Jordan-Wigner transformation (100) between the original spin operators and the fermions is non-local, there are local spin operators which are not local in fermionic representation, the simplest example being σ_n^x . Thus in general only spin observables with a finite *fermionic* support relax to GGE.

The dephasing to GGE (332) was studied in Refs. [83, 178], although without any explicit reference to GGE for good chronological reasons. In particular, in Ref. [83] ferromagnetic correlation functions $C_R^{xx} = \text{Tr } \rho^{\text{GGE}} \sigma_{n+R}^x \sigma_n^x$ were found in the final dephased state in the two limiting cases of $g_i = 0$ and $g_i = \infty$. Here we list their tails for large R only:

- When $g_i = 0$

$$C_R^{xx} = \begin{cases} \left(\frac{1 + \sqrt{1 - g_f^2}}{2} \right)^{R+1} & , \text{ when } g_f < 1 , \\ \left(\frac{1}{2} \right)^R & , \text{ when } g_f > 1 , \end{cases} \quad (348)$$

- When $g_i = \infty$

$$C_R^{xx} = \begin{cases} \left(\frac{1}{2} \right)^R \cos [R \arccos(g_f)] & , \text{ when } g_f < 1 , \\ \left(\frac{1}{2g_f} \right)^R & , \text{ when } g_f > 1 , \end{cases} \quad (349)$$

The oscillatory correlation function in the ferromagnetic phase, $g_f < 1$, obtained after dephasing from a fully disordered initial state, $g_i = \infty$, is a clear qualitative indication of a non-thermal steady state. Notice similarity of this oscillatory correlation function to the correlators (153,171) obtained after a linear quench.

Dephasing to the GGE instead of a thermal state does not mean that some quantities, which are not very sensitive to fine details of GGE, cannot behave like in a thermal state. For instance, as shown in Ref. [179], time correlations of the order parameter decay exponentially at the same rate as in a canonical ensemble with an effective temperature determined by energy density pumped to the system by the sudden quench.

We can conclude that after a sudden quench in the quantum Ising chain observables which are local in fermionic representation relax to GGE.

3.6. GGE and Luttinger model (LM)

In this Section, following Ref. [177], we consider local relaxation to GGE in the integrable Luttinger model (LM) [180]. This model describes low energy properties of a wide class of 1D Tomonaga-Luttinger liquids [181]. The Hamiltonian of the

LM is

$$H_{\text{LM}} = H_0 + H_2 + H_4, \quad (350)$$

$$H_0 = v_F p \sum_{p,\alpha} : \psi_\alpha^\dagger(p) \psi_\alpha(p) : , \quad (351)$$

$$H_2 = \frac{2\pi}{L} \sum_q g_2(q) J_R(q) J_L(q) , \quad (352)$$

$$H_4 = \frac{\pi}{L} \sum_{q,\alpha} : J_\alpha(q) J_\alpha(-q) : , \quad (353)$$

where the Fermi operators satisfy $\{\psi_\alpha(p), \psi_\beta^\dagger(p')\} = \delta_{p,p'} \delta_{\alpha,\beta}$ with $\alpha, \beta = L, R$ and anticommute otherwise. Anti-periodic boundary conditions $\psi_\alpha(x+L) = -\psi_\alpha(x)$, where $\psi_\alpha(x) = \sum_p e^{is_\alpha p} \psi_\alpha(p) / \sqrt{L}$ with $s_R = -s_L = 1$, result in a non-degenerate ground state. The quantised momentum $p = 2\pi(n-1/2)/L$ with integer n is “half-integer”. The current operators $J_\alpha(q) = \sum_p : \psi_\alpha^\dagger(p+q) \psi_\alpha(p) :$, where $q = 2\pi m/L$ with integer m .

The currents obey the Kac-Moody algebra $[J_\alpha(q), J_\beta(q')] = \frac{qL}{2\pi} \delta_{q+q',0} \delta_{\alpha\beta}$ which allows one to introduce bosonic operators

$$b_0(q) = -i(2\pi/|q|L)^{1/2} [\theta(q) J_R(-q) - \theta(-q) J_L(q)] , \quad (354)$$

$$b_0^\dagger(q) = i(2\pi/|q|L)^{1/2} [\theta(q) J_R(q) - \theta(-q) J_L(-q)] \quad (355)$$

for $q \neq 0$. Moreover, there are two conserved operators $N = N_R + N_L$ and $J = N_R - N_L$, where $N_\alpha = J_\alpha(0)$. The Hamiltonian H_{LM} is quadratic in b_0, b_0^\dagger but not diagonal. It is diagonalised by the Bogoliubov transformation

$$b(q) = b_0(q) \cosh \varphi(q) + b_0^\dagger(-q) \sinh(q) , \quad (356)$$

$$b^\dagger(q) = b_0(-q) \sinh \varphi(q) + b_0^\dagger(q) \cosh(q) \quad (357)$$

with $\tanh \varphi(q) = g_2(2)/[v_F + g_4(q)]$ and becomes

$$H_{\text{LM}} = \sum_{q \neq 0} v(q) |q| b^\dagger(q) b(q) + \pi v_N \frac{N^2}{L} + \pi v_J \frac{J^2}{L} , \quad (358)$$

where $v(q) = [(v_F + g_4(q))^2 - g_2^2(q)]^{1/2}$, $v_N = v(0)e^{2\varphi(0)}$, $v_J = v(0)e^{-2\varphi(0)}$. The integrals of motion are N, J , and the bosonic occupation numbers $b^\dagger(q)b(q)$.

We consider an interaction quench where both couplings $g_2(q)$ and $g_4(q)$ are suddenly switched on at $t = 0$. Before the quench $H_{\text{LM}} = H_0$ is a non-interacting Fermi liquid and its ground state is a vacuum for the operators $b_0(q)$. After some algebra, see Ref. [177], one obtains a one-body correlation function

$$C_{\psi_R}(x, t) \equiv \langle 0 | e^{itH_{\text{LM}}} \psi_R^\dagger(x) \psi_R(0) e^{-itH_{\text{LM}}} | 0 \rangle . \quad (359)$$

It is interesting to compare two asymptotes of the function in the thermodynamic limit:

$$C_{\psi_R}(x, t) \approx \frac{i(R_0/2vt)^{\gamma^2}}{2\pi(x+ia)} , \quad \text{when } |x| \ll 2v(0)t , \quad (360)$$

and

$$C_{\psi_R}(x, t) \approx \frac{i|R_0/x|^{\gamma^2}}{2\pi(x+ia)}, \quad \text{when } |x| \gg 2v(0)t, \quad (361)$$

where $\gamma = \sinh 2\varphi(0)$. The correlation function relaxes from the initial Fermi liquid form for $|x| \gg 2v(0)t$ to a final non-Fermi liquid form when $|x| \ll 2v(0)t$, but the limiting form $C_{\psi_R}(x, t \rightarrow \infty)$ has a different exponent γ^2 than in the ground state of the LM.

Thus in any bounded region Ω within the quasiparticle horizon,

$$|x| \ll 2v(0)t, \quad (362)$$

the correlation functions are relaxed to a steady state. Given the quadratic form of the bosonic Hamiltonian (358) and the general discussion in Section 3.4, it is not quite surprising to find that the correlators in the steady state can be obtained from a GGE

$$\rho^{\text{GGE}} = \mathcal{N} \exp \left[- \sum_q \lambda(q) b^\dagger(q)b(q) \right], \quad (363)$$

where $\lambda(q)$ are fixed by initials conditions. We can conclude that any finite subsystem within the quasiparticle horizon appears relaxed to GGE.

3.7. GGE and hard-core bosons

The integrable hard-core bosons in one dimension [182] were realised experimentally in the seminal experiment [3], where the momentum distribution in an expanding cloud of atoms was observed to have a stationary but non-thermal distribution. Relaxation in this system was considered in Ref. [174], where it was shown that the correct momentum distribution f_k for one-dimensional hard-core bosons can be obtained from a GGE for an equivalent fermionic representation of the hard-core bosons. However, in a subsequent paper [183] it was demonstrated that the stationary state preserves information not only on momentum distribution, but also on momentum correlations which are missing in the GGE description. Here we outline the argument of Ref. [183].

For $t < 0$ a system of N hard-core bosons was in the ground state in a harmonic trap potential,

$$H_0 = H + V_{\text{trap}}, \quad (364)$$

where $V_{\text{trap}} = \int dx V(x)\rho(x)$, $\rho(x)$ is a density operator, and

$$V(x) = \frac{1}{2}m\omega_0^2x^2 \quad (365)$$

is the trap potential. At $t = 0$ the trap potential $V(x)$ is switched off,

$$\omega_0 \xrightarrow{t=0} 0, \quad (366)$$

and the bosons expand with the translationally invariant Hamiltonian H .

It is convenient to make a Jordan-Wigner transformation

$$\psi(x) = \exp \left[i\pi \int_{-\infty}^x dy \rho(y) \right] \varphi(x) , \quad (367)$$

where the operators $\psi(x)$ and $\varphi(x)$ correspond to spinless fermions and bosons respectively: $\{\psi(x), \psi^\dagger(y)\} = [\varphi(x), \varphi^\dagger(y)] = \delta(x-y)$. The free Hamiltonian becomes

$$H = \int dx \psi^\dagger(x) \left[-\frac{1}{2m} \frac{\partial^2}{\partial x^2} \right] \psi(x) , \quad (368)$$

but the density operator retains its form

$$\rho(x) = \varphi^\dagger(x)\varphi(x) = \psi^\dagger(x)\psi(x) . \quad (369)$$

Since the fermionic occupation numbers in momentum space

$$n_k = \psi_k^\dagger \psi_k , \quad (370)$$

where $\psi_k = (2\pi)^{-1/2} \int dx e^{-ikx} \psi(x)$, mutually commute and commute with $H = \int dk \frac{k^2}{2m} n_k$, they are the integrals of motion to be included in GGE, see the discussion in Section 3.3. Neither their expectation values $\langle n_k \rangle$ nor expectation values of their products depend on t . In particular, for $\delta n_k = n_k - \langle n_k \rangle$ the Wick theorem gives a correlator

$$\langle \delta n_k \delta n_{k'} \rangle_t = - |\langle \psi_k^\dagger \psi_{k'} \rangle_0|^2 \neq 0 . \quad (371)$$

Since the initial ground state in a harmonic trap is not translationally invariant, the right hand side is generally non-zero when $k' \neq k$.

For a harmonic trap $V(x) = \frac{x^2}{2ml^4}$ with $l = (m\omega_0)^{-1/2}$ the correlation function can be written as

$$\langle \psi_k^\dagger \psi_{k'} \rangle = \sum_{n=0}^{N-1} \phi_n^*(k) \phi_n(k') , \quad (372)$$

where $\phi_n(k)$ are eigenfunctions of the harmonic oscillator in momentum representation. When $N \gg 1$ we can approximate, see Ref. [183],

$$\langle n_k \rangle = \frac{R}{\pi} \sqrt{1 - \frac{k^2}{k_F^2}} , \quad \langle \delta n_k \delta n_{k'} \rangle = - \frac{\sin^2[(k-k')R]}{\pi^2(k-k')^2} , \quad (373)$$

where $k_F l = R/l = \sqrt{2N}$ and $|k|, |k'| \ll k_F$. There are non-negligible correlators between different fermionic occupation numbers. They originate from the broken translational invariance of the initial state and are conserved after the opening of the trap (366).

In an experiment like Ref. [3] one can in principle measure *bosonic* correlation functions. Since the Jordan-Wigner transformation between bosons and fermions is non-local, the bosonic correlations are in general different than their fermionic counterparts. However, Ref. [183] demonstrates that bosonic occupation numbers f_k tend to the conserved fermionic occupation numbers: $f_k(t \rightarrow \infty) = n_k$. Thus

when $t \rightarrow \infty$ all the non-trivial initial correlations between the integrals of motion can be measured as bosonic momentum correlations.

When $t \rightarrow \infty$ GGE becomes $\rho^{\text{GGE}} = \mathcal{N} \exp(-\int dk \lambda_k f_k)$. By construction, this ensemble “predicts” correct expectation values $\text{Tr} \rho^{\text{GGE}} f_k = n_k$, but it ignores any momentum correlations. Thus, in accordance with the discussion in Section 3.3, GGE cannot be used to predict occupation numbers in momentum space. However, the general argument in Section 3.4 proves that, after dephasing for $t \rightarrow \infty$, $\rho^{\text{GGE}} = \mathcal{N} \exp(-\int dk \lambda_k f_k)$ accurately predicts observables within a finite fermionic support Ω in real space.

The local relaxation in Section 3.4 cannot always be taken for granted as demonstrated by another example in Ref. [184]. In that paper, instead of switching off the trapping potential, they consider a sudden quench of the trap frequency in Eq. (365) from an initial ω_0 to a lower frequency ω_1 :

$$\omega_0 \xrightarrow{t=0} \omega_1 . \quad (374)$$

This problem is solved exactly by a scaling transformation of the initial wave function. The wave function is coherently breathing with frequency $\omega_1/2$. There are periodic revivals of the initial state every π/ω_1 demonstrating the absence of dephasing at the revivals. This anomaly originates from the fact that the non-interacting Jordan-Wigner fermions in a harmonic potential have commensurate eigenenergies being integer multiples of ω_1 , so there is no way anything could irreversibly dephase when $t \rightarrow \infty$. Thus one of the basic assumptions in Section 3.4 is not satisfied and there is no local relaxation to any GGE. However, one could argue that a small anharmonicity of the trapping potential would alter this conclusion ¹.

3.8. GGE and the Bose-Hubbard model

The Bose-Hubbard model (229) is not integrable, but it is close to integrability in some regimes or limits of parameters. It seems to relax to a non-thermal steady state when close to integrability, and thermalise otherwise.

For instance, Ref. [185] considers a quench from $J = 0$ to a large $J \gg n$ well in the superfluid phase. This quench jumps between two limits of the model where it is integrable. The state after the quench relaxes *locally* to a non-thermal steady state. It will be shown below that the steady state is a GGE. This is an example that even a non-integrable model can locally relax to a non-thermal steady state when it is close to integrability.

Before the quench, when the Hamiltonian is $H_0 = \frac{1}{2} \sum_j n_j(n_j - 1)$, the initial state is the non-Gaussian Mott ground state $|n, n, \dots\rangle$ with exactly n bosons at each site. Suddenly, at $t = 0$ a finite hopping rate J is switched on. We assume $J \gg n$ so large that the interaction term can be neglected and

$$H \approx -J \sum_{j=1}^N (a_{j+1}^\dagger a_j + a_j^\dagger a_{j+1}) = -2J \sum_k \cos(k) a_k^\dagger a_k \quad (375)$$

¹The limiting case of $\omega_1 = 0$, i.e. the opening of the trap (366) considered in this Section, results in a continuous dispersion $k^2/2m$ of the non-interacting Jordan-Wigner fermions. The integration over the continuous k yields irreversible local relaxation when $t \rightarrow \infty$.

This limiting case suggests that even for $\omega_1 > 0$ there may be local relaxation in between the periodic revivals such that a local state $\rho_\Omega(t)$ oscillates between the initial $\rho_\Omega(0)$ at the revivals and $\text{Tr}_\Omega \rho^{\text{GGE}}$ in between. When $\omega_1 \rightarrow 0$ then the revival period π/ω_1 stretches to infinity allowing enough time for irreversible local relaxation.

is just the hopping term, where $a_k = \sum_{j=1}^N a_j e^{-ikj} / \sqrt{N}$ is an annihilation operator in pseudomomentum representation. $n_k = a_k^\dagger a_k$ are the integrals of motion of this quadratic H . Since before the quench bosons were localised in the Mott state, their conserved occupation numbers are the same for all quasimomenta, $\text{Tr} \rho(t) n_k = n$.

We are interested in local observables with support in a finite subsystem Ω of the lattice. The Hamiltonian (375) is quadratic as assumed in Section 3.4, but the initial Mott state is not Gaussian. Nevertheless, Ref. [185] shows that in the thermodynamic limit $N \rightarrow \infty$ and $t \rightarrow \infty$ (here the order of limits is important) the reduced density matrix of a block Ω of S sites converges to a product of Gaussian states

$$\lim_{t \rightarrow \infty} \lim_{N \rightarrow \infty} \rho_\Omega(t) = \prod_{j=1}^S \frac{e^{-\lambda a_j^\dagger a_j}}{1+n} \quad (376)$$

and $\lambda = \ln(1 + 1/n)$. This limiting steady state can be also obtained by reduction of the generalised Gibbs ensemble,

$$\lim_{t \rightarrow \infty} \lim_{N \rightarrow \infty} \rho_\Omega(t) = \text{Tr}_{\Omega^\perp} \rho^{\text{GGE}}, \quad (377)$$

where the ensemble is

$$\rho^{\text{GGE}} = \frac{e^{-\sum_k \lambda a_k^\dagger a_k}}{(1+n)^N} = \frac{e^{-\sum_j \lambda a_j^\dagger a_j}}{(1+n)^N} = \prod_{j=1}^N \frac{e^{-\lambda a_j^\dagger a_j}}{1+n}. \quad (378)$$

This GGE is clearly different from a thermal state $\propto e^{-\beta \sum_k \omega_k a_k^\dagger a_k}$ because $\omega_k = 2J(1 - \cos k)$ is not a constant. We can conclude that, in the integrable limit $J \rightarrow \infty$ of the non-integrable Bose-Hubbard model, the non-Gaussian initial Mott state relaxes *locally* to a steady non-thermal GGE.

A similar problem was addressed in Ref. [186] by numerical simulations of small lattices up to 12 sites. Figure 37 shows probability distributions p_α in the diagonal ensemble $\bar{\rho}$ in Eq. (313). A quench from the Mott-insulator to the superfluid phase prepares a clearly non-thermal diagonal ensemble, see Fig. 37d, but a small quench within the superfluid phase prepares a diagonal ensemble that looks more like a canonical ensemble, see Figs. 37a,c.

A sudden quench in the opposite direction, i.e. from the superfluid to Mott-insulator phase, was studied by exact diagonalisation [187], the adaptive time-dependent density matrix renormalisation group [169], and Bogoliubov theory [121]. The model is trivially integrable at $J = 0$, where unitary evolution factorises into a product over lattice sites $\prod_j e^{-in_j(n_j-1)/2}$. Since the quartic interaction $n_j(n_j-1)/2$ is an integer for any Fock state, the evolution is periodic in time with a period of 2π . Any initial wave function revives periodically and there is no question of any relaxation for $t \rightarrow \infty$. However, a non-zero hopping rate $J > 0$ leads to relaxation of these periodic revivals or even overdamped relaxation, see Ref. [128], Section 2.19.3 and the 2D experimental results in Fig. 29. The numerical data collected in Ref. [187] suggest that there are two distinct regimes: when J is close to the Mott-superfluid transition, then for simple observables the final steady state is a thermal state with an effective temperature determined by energy pumped into the system by the sudden quench, but when J is perturbatively small, then the steady state is not thermal and it retains memory of the initial state. The last result is further supported by Fig. 37b from Ref. [186].

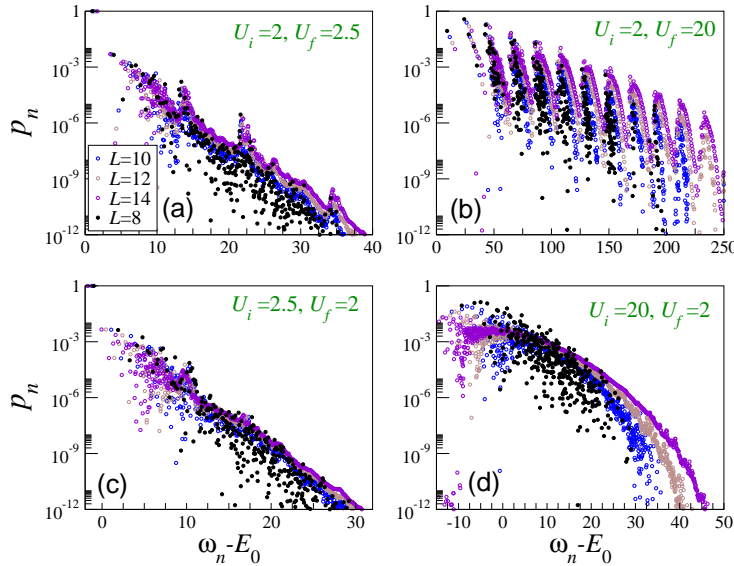


Figure 37. Here U_i and U_f are initial and final interaction strengths in the Bose-Hubbard Hamiltonian (229) in a sudden quench $U_i \rightarrow U_f$. The critical point between the Mott and superfluid phases is $U_c = 3.3$. The plots show probabilities p_n in a mixed time-averaged density matrix after a quench, $\bar{\rho} = \sum_n p_n |n\rangle\langle n|$, versus the excitation energy $\omega_n - E_0$ of an eigenstate $|n\rangle$. Panels a and c show roughly exponential dependence of p_n on energy, like in a canonical ensemble, while panels b and d indicate strong memory of the initial conditions. The results come from numerical calculations on a periodic lattice of 8, ..., 12 sites with a density of 1 particle per site. (Figure from Ref. [186])

The qualitatively different behaviour in the two regimes may be explained by a simple model in Ref. [121]. In this model, excitations of the Mott insulator state $|1, 1, 1, \dots\rangle$ are particles, created by p_s^\dagger and located at doubly occupied sites, and holes, created by h_s^\dagger and located at empty sites. When expanded to second order in the operators p, h the Bose-Hubbard Hamiltonian (229) becomes a quadratic Hamiltonian which can be diagonalised by a Bogoliubov transformation to a sum of non-interacting Bogoliubov quasiparticles, $H_2 = \sum_{k,\alpha} \omega_k \gamma_{k,\alpha}^\dagger \gamma_{k,\alpha}$. This quadratic model, which neglects any interactions between quasiparticles $\gamma_{k,\alpha}$, is accurate for small J . Thus the general argument in Section 3.4 predicts local relaxation to a non-thermal GGE with the integrals of motion $n_{k,\alpha} = \gamma_{k,\alpha}^\dagger \gamma_{k,\alpha}$.

In this model, thermalisation can occur due to quasiparticle interactions. For instance, quartic terms of the form $\gamma_q^\dagger \gamma_{k+q/2} \gamma_{-k+q/2} \gamma_0$ could make quasiparticle population equilibrate. Deep in the Mott regime, where the Mott gap $\simeq 1$ in the quasiparticle spectrum ω_k is large as compared to the quasiparticle bandwidth $\simeq J$, this process is not compatible with energy conservation, but it becomes increasingly effective as J approaches the gapless critical point and it may explain the thermalisation observed close to criticality. However, a limited accuracy of the leading quadratic model was discussed already in Ref. [121] and it is also not known how these qualitative observations depend on a finite system size.

3.9. GGE and a system solvable by Bethe Ansatz

Reference [188] considers a one-dimensional fermionic lattice Hamiltonian ¹

$$H = - \sum_s \left(c_{s+1}^\dagger c_s + \text{h.c.} \right) + V \sum_s n_s n_{s+1} \quad (379)$$

¹Transport was analysed in the system (379) in the first paper in Ref. [189].

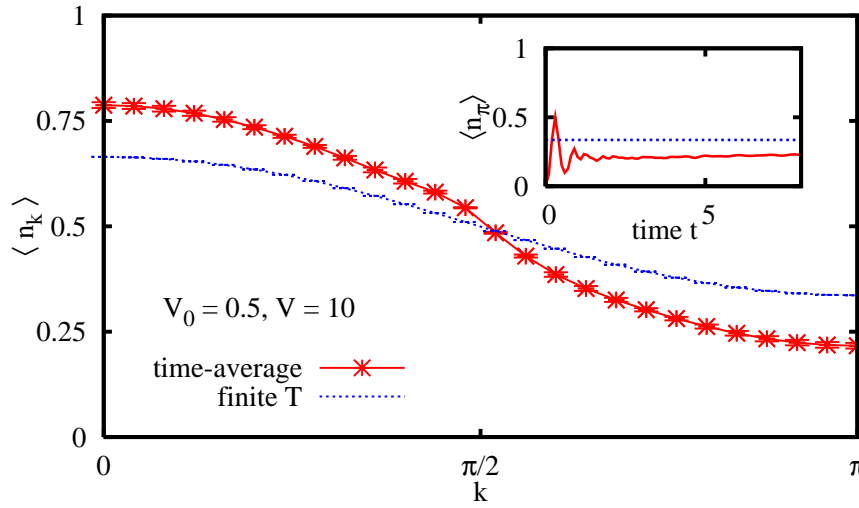


Figure 38. A time-averaged momentum distribution for the final $V = 10$, i.e., momentum distribution in the time-averaged diagonal ensemble $\bar{\rho}$, and thermal momentum distribution in a canonical ensemble. The inset shows a time dependence of $\langle n_k \rangle$ together with a (dotted) thermal average. (Figure from Ref. [188])

with nearest neighbour interaction V at half filling. This Hamiltonian is not quadratic and cannot be mapped to any quadratic Hamiltonian, but it is exactly solvable by Bethe ansatz. The model has a quantum critical point at $V_c = 2$ separating a Luttinger liquid (when $V < 2$) from a charge density wave insulator (when $V > 2$). Ref. [188] considers open chains up to 100 sites pushed out of equilibrium by sudden quenches from V_0 to V and evolved in time using the Lanczos time evolution method [190] and the adaptive DMRG [169]. The quantity of interest is momentum distribution after time t :

$$\langle n_k \rangle = \frac{1}{L} \sum_{m,n=1}^L e^{ik(m-n)} \text{Tr} \rho(t) c_m^\dagger c_n. \quad (380)$$

A general conclusion drawn from the numerical simulations in Ref. [188] is that the momentum distribution relaxes to a steady state, but the steady state is not a canonical ensemble, see Fig. 38.

Since the Hamiltonian (379) cannot be mapped to any quadratic Hamiltonian, Section 3.4 cannot tell us what might be the small set of integrals of motion I_α in the GGE (322). In principle, any quantum system has as many integrals of motion as the dimension of its Hilbert space given by the projectors $I_\alpha = |\alpha\rangle\langle\alpha|$ on the eigenstates $|\alpha\rangle$ of its Hamiltonian. However, GGE build out of these projectors is equal to the time-averaged diagonal ensemble

$$\bar{\rho} = \sum_{\alpha} p_{\alpha} |\alpha\rangle\langle\alpha| \quad (381)$$

which may be not a tractable statistical description of the state.

Another universal set of integrals of motion are integer powers of a finite Hamiltonian: $I_m = H^m$ with $m = 1, \dots, \dim(H)$. This set is as huge as the set of eigenstate projectors but, at least in the quench considered in Ref. (379), it can be accurately

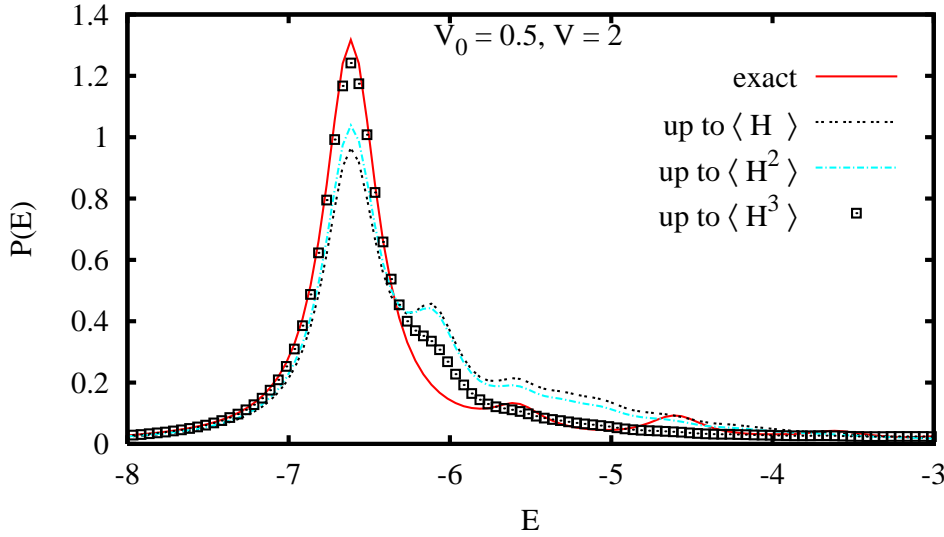


Figure 39. The exact energy distribution function $P(E)$ in the Hamiltonian after the quench (red) together with its approximations by the distribution in Eq. (383) for increasing $M = 1, 2, 3$. (Figure from Ref. [188])

truncated to a small number of M leading powers:

$$\rho^{\text{GGE}} = \mathcal{N} \exp \left(- \sum_{m=1}^M \lambda_m H^m \right) \quad (382)$$

with λ 's fixed by the conserved moments $\text{Tr} \rho^{\text{GGE}} H^m = \text{Tr} \rho(0) H^m$. The ensemble (382) can be rewritten as $\rho^{\text{GGE}} = \sum_{\alpha} p(E_{\alpha}) |\alpha\rangle\langle\alpha|$, where

$$p(E) = \mathcal{N} \exp \left(- \sum_{m=1}^M \lambda_m E^m \right). \quad (383)$$

This form reveals that the essence of the generalised GGE (382) simply is the assumption that p_{α} in Eq. (381) is a smooth localized function of the energy E_{α} , which can be accurately approximated by e.g. an exponent of a short polynomial in E_{α} . Good quality of this approximation for reasonably small M , with $M = 1$ being a canonical ensemble, is demonstrated in Fig. 39 which shows $p(E)$ multiplied by density of eigenstates $\rho(E)$, i.e., $P(E) = p(E)\rho(E)$.

3.10. Eigenstate thermalisation hypothesis (ETH)

Since a state after a sudden quench often has a narrow energy distribution in a final Hamiltonian, see e.g. Fig. 39, and the energy distribution $p(E)$ is conserved, it may be more accurate to describe a thermal state of an isolated quantum system by a microcanonical ensemble

$$p(E) = \mathcal{N} \begin{cases} 1, & \text{when } |E - \langle H \rangle| < \Delta E, \\ 0, & \text{otherwise,} \end{cases} \quad (384)$$

Here $\langle H \rangle$ is average energy after a quench and ΔE is a finite energy window. In this framework thermalisation of an observable O means that the exact time-averaged diagonal ensemble $\bar{\rho} = \sum_{\alpha} p_{\alpha} |\alpha\rangle\langle\alpha|$ and the microcanonical ensemble (384) give

the same expectation value of O :

$$\sum_{\alpha} p_{\alpha} \langle \alpha | O | \alpha \rangle = \mathcal{N} \sum_{|E_{\alpha} - \langle H \rangle| < \Delta E} \langle \alpha | O | \alpha \rangle, \quad (385)$$

where $|\alpha\rangle$ are eigenstates of the Hamiltonian.

One can imagine many different scenarios that might in principle imply the equality (385), but there is only one that does not depend on the initial state, except that p_{α} 's have to be localised around the average energy $\langle H \rangle$. The *eigenstate thermalisation hypothesis* suggested in Ref. [163] proposes that the expectation value $\langle \alpha | O | \alpha \rangle$ of a *few-body* observable O in an eigenstate $|\alpha\rangle$ with energy E_{α} of a large *many-body* Hamiltonian is the same for all eigenstates in the energy window $E_{\alpha} \pm \Delta E$.

ETH clearly implies the equality (385) independently of the details of p_{α} , provided that it is only localised around a given average energy. This is what is expected from thermalisation: the relaxed state should not depend on the initial state, except for its average energy.

The thermalisation mechanism implied by ETH is very simple: any eigenstate in the energy window gives the same expectation value of a few body observable O or, even stronger, any single eigenstate in the window provides the same average as the microcanonical ensemble. This mechanism is very different from the ergodicity required of a classical system. In a non-integrable isolated quantum system, each eigenstate of the Hamiltonian implicitly contains a thermal state. The coherence between the eigenstates initially hides it, but then time evolution reveals it after dephasing.

At present, there are no general theoretical arguments supporting ETH, but there are some results for restricted classes of Hamiltonians: Deutsch in Ref. [163] showed that ETH holds for an integrable Hamiltonian perturbed by a matrix from a random Gaussian ensemble, nuclear shell calculations have shown that individual wave functions reproduce thermodynamic predictions [191], some quantum systems whose classical versions are chaotic satisfy ETH in the semiclassical limit [192]. More generally, ETH follows from the Berry conjecture [86, 163] believed to hold in such systems [193].

In order to see if thermalisation occurs in a generic isolated quantum system and, in particular, if it occurs due to ETH, Ref. [194] considers a non-integrable system of 5 hard core bosons on a finite lattice of 21 sites in Fig. 40a described by the Hamiltonian

$$H = -J \sum_{\langle i,j \rangle} (b_i^{\dagger} b_j + \text{h.c.}) + U \sum_{\langle i,j \rangle} n_i n_j \quad (386)$$

with the nearest neighbour repulsion strength $U = 0.1J$. The bosons are initially confined to the bottom-right part of the lattice in the ground state of a confined Hamiltonian. At $t = 0$ they are allowed to tunnel to the initially empty top-left part. This set-up is a quantum analogue of an inflated balloon pierced inside a vacuum chamber to see that the released air will soon uniformly fill the chamber and velocity distribution of air molecules will relax to the Maxwell velocity distribution. Reference [194] considers momentum distribution. For instance, Fig. 40b shows relaxation of the distribution at $k_x = 0$ to the microcanonical ensemble. Fig. 40c shows that the momentum distribution in the dephased diagonal ensemble is clearly different from the initial momentum distribution, indistinguishable from the microcanonical momentum distribution, but significantly different from

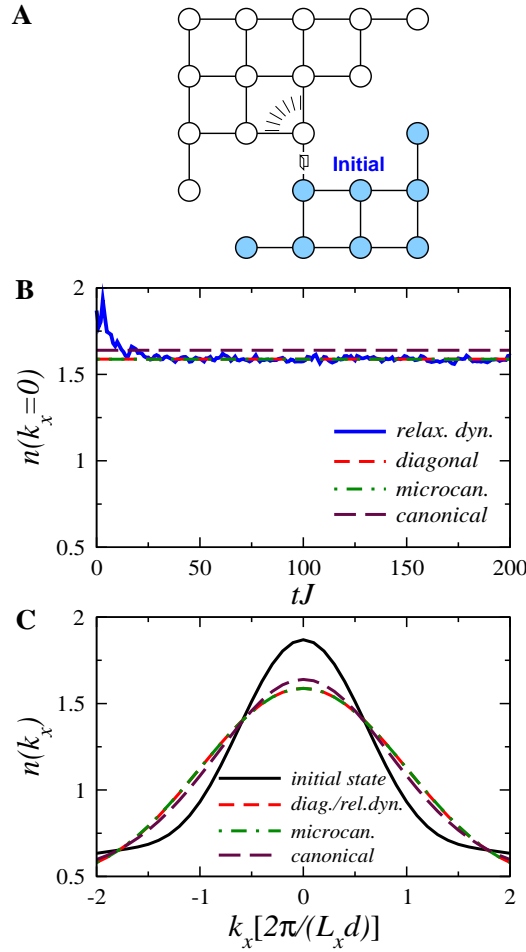


Figure 40. Panel A shows the lattice in the Hamiltonian (386). The bosons are initially prepared in the ground state of the sub-lattice in the bottom-right corner and then, at $t = 0$, released through the marked link. Panel B shows how the momentum distribution $n(k_x = 0)$ relaxes to the value in the diagonal ensemble which is the same as predicted by the microcanonical ensemble. Here $n(k_x, k_y) = L^{-2} \sum_{i,j} e^{-i\vec{k}(\vec{r}_i - \vec{r}_j)}/L$ with lattice size $L = 5$ and $n(k_x) = \sum_{k_y} n(k_x, k_y)$. Panel C, compares the initial momentum distribution $n(k_x)$ with the steady state diagonal ensemble which is indistinguishable from the microcanonical distribution but significantly different from the canonical one. (Figure from Ref. [194])

the canonical one.

Figure 41 compares results for the *non-integrable* system of 5 hard-core bosons on the lattice in Fig. 40a, which was considered so far, and a similar *integrable* system of 5 hard-core bosons in a one-dimensional chain of 21 sites. The bosons were initially prepared in the ground state of the 8-sites at one of the chain's ends, and then released by opening the link connecting the end to the rest of the chain. Results collected in Fig. 41 show that while ETH holds in the non-integrable system, it does not hold in the integrable one.

Similar results were also obtained in Ref. [195] for interaction quenches in a finite one-dimensional chain with hard-core bosons whose integrability can be gradually broken by turning on the next-nearest-neighbour hopping and repulsion. When it is not integrable the system thermalises and ETH holds, but as the next-nearest-neighbour terms are turned off and the system tends to the integrable limit both the thermalisation and ETH break down. The transition between the two regimes seems to be a smooth crossover, but it is not clear how much this conclusion depends on the finite system size.

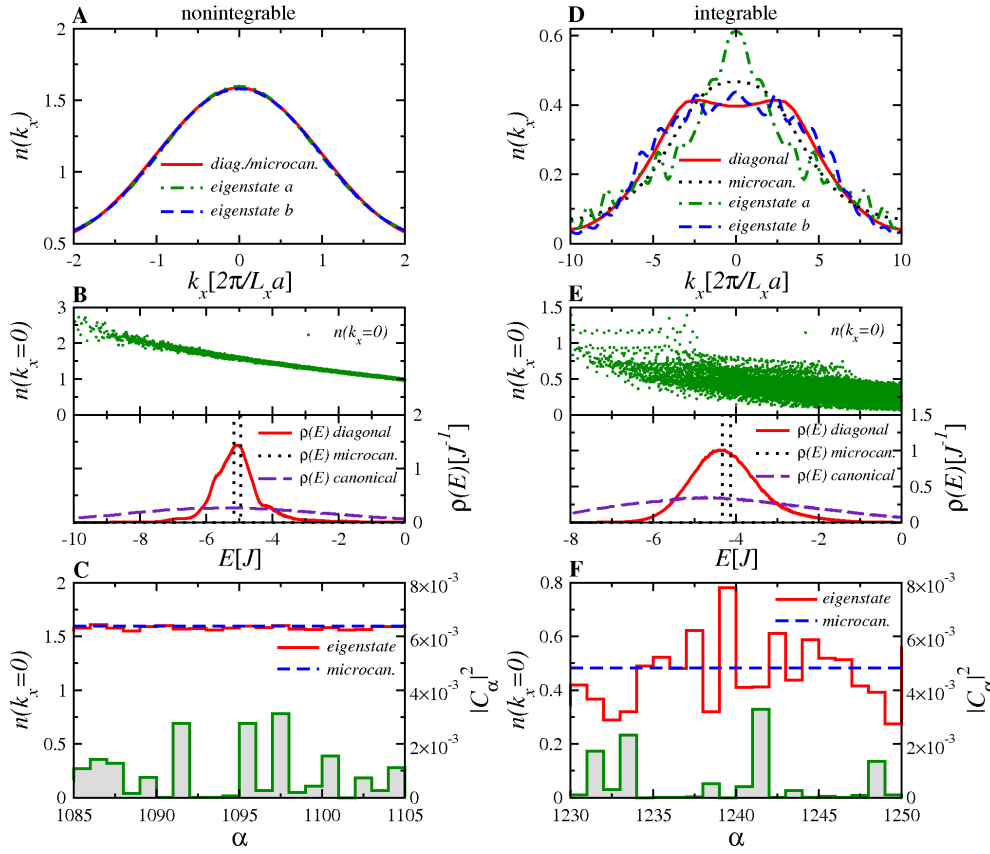


Figure 41. Left panels (A,B,C) correspond to the non-integrable system, and the right panels (D,E,F) to the integrable one. Panels A and D compare momentum distribution $n(k_x)$ with the microcanonical distribution, and with distributions in two typical eigenstates close to the average energy. The four distributions collapse in the non-integrable case (ETH holds), but they differ significantly in the integrable case (ETH does not hold). The top parts of panels B and E show expectation values of $n(k_x = 0)$ in eigenstates at different energies. The non-integrable case (B) looks like a smooth curve, but the integrable case (E) shows large fluctuations which do not resemble a smooth curve. The lower parts of panels B and E show that energy distributions are very similar in both non-integrable and integrable case. Finally, the upper parts of panels C and F show a focus on expectation values of $n(k_x = 0)$ in the eigenstates $|\alpha\rangle$ close to the mean energy, and the lower parts of panels C and F show probabilities p_α in these eigenstates. (Figure from Ref. [194])

3.11. Dynamics of relaxation to a steady state

So far we have discussed mainly the nature of the asymptotic steady state. Finally, it is time for the dynamics of relaxation to this state. In this Section we briefly review two References [196, 197] where the relaxation process was studied in some detail.

In the first of them [196] they study a one-dimensional fermionic Hubbard model

$$H = \sum_{ij\sigma} V_{ij} c_{i\sigma}^\dagger c_{j\sigma} + U \sum_i \left(n_{i\uparrow} - \frac{1}{2} \right) \left(n_{i\downarrow} - \frac{1}{2} \right). \quad (387)$$

Here the hopping matrix V_{ij} corresponds to a semi-elliptic density of states $\rho(\epsilon) = \sqrt{4 - \epsilon^2}/(2\pi)$. The system is initially in the ground state of the non-interacting Hamiltonian, $U = 0$ for $t < 0$, and then at $t = 0$ the Coulomb repulsion is switched to a finite U . The relaxation following this sudden quench was studied in Ref. [196] within the time-dependent dynamical mean-field theory. Evolution of two observables, the double occupancy $d(t) = \text{Tr} \rho(t) n_{i\uparrow} n_{i\downarrow}$ and the Fermi surface discontinuity $\Delta n(t)$, is shown in Fig. 42. For both $U \gg 1$ and $U \ll 1$, the two

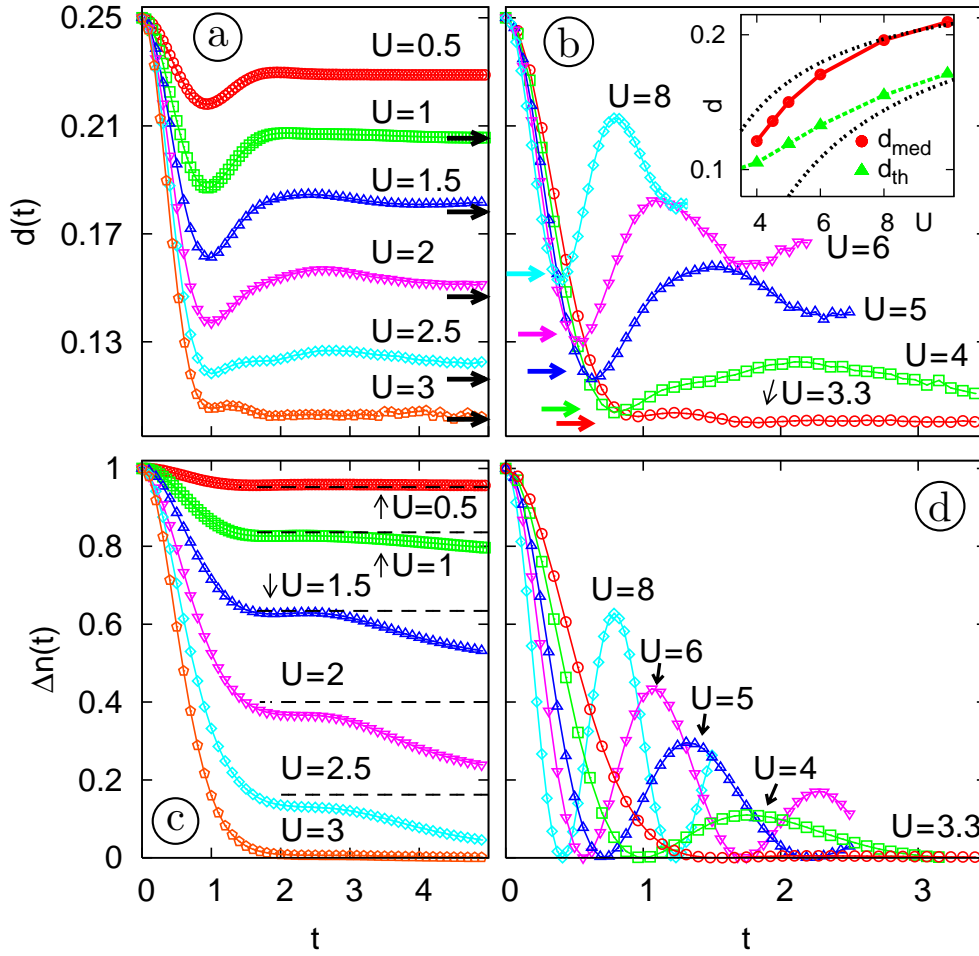


Figure 42. Double occupancy $d(t)$ and Fermi surface discontinuity $\Delta n(t)$ after quenches to $U \leq 3$ (left panels) and $U \geq 3.5$ (right panels). The horizontal dashed lines in panel c indicate the quasi-stationary value predicted in Ref. [143], and the horizontal arrows in panel a mark corresponding thermal values. (Figure from Ref. [196])

quantities pass through a plateau where, as predicted in Ref. [143], the system prethermalises in a quasi-steady state, before it finally relaxes to a thermal state. The size of the plateau depends on U . More detailed analysis shows that it is minimal at $U \approx 3.2$ marking a dynamical phase transition between the weak and strong coupling regimes where the thermalisation is postponed until after the prethermalization on intermediate time-scales. As remarked in Ref. [196], it is not clear whether and how this phenomenon is related to the existence of an equilibrium thermodynamic phase transition at $U_c = 4.76$, but the relaxation is the fastest at the crossover between the strong and weak coupling regimes.

A similar problem was considered in Ref. [197] in the antiferromagnetic XXZ model (solvable by Bethe ansatz) and the antiferromagnetic XZ model (integrable by mapping to a quadratic Hamiltonian),

$$H_{XXZ} = \sum_s (\sigma_s^x \sigma_{s+1}^x + \sigma_s^y \sigma_{s+1}^y + \Delta \sigma_s^z \sigma_{s+1}^z) , \quad (388)$$

$$H_{XZ} = \sum_s (2\sigma_s^x \sigma_{s+1}^x + \Delta \sigma_s^z \sigma_{s+1}^z) , \quad (389)$$

They studied unitary time evolution of the antiferromagnetic order starting from

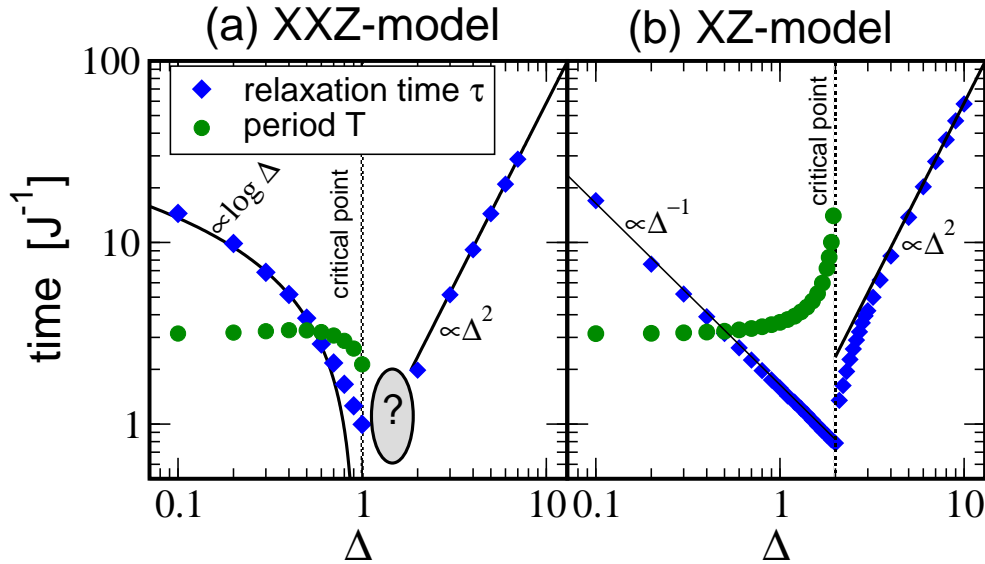


Figure 43. Relaxation time and oscillation period as functions of anisotropy Δ in the XXZ and XZ models. In both models the relaxation time is the shortest at the critical point. (Figure from Ref. [197])

the highly non-equilibrium Neel state. The order vanishes exponentially with relaxation being oscillatory or non-oscillatory, depending on the anisotropy parameter Δ . As demonstrated by the data collected in Fig. 43, the relaxation is the fastest near the quantum critical point contrary to the usual notion of critical slowing down. This effect can be explained by the gapped excitation spectrum away from the critical point. The relaxation is dominated by scattering between high-energy excitations introduced to the system through the highly excited initial state. The gap restricts the phase space available for scattering making relaxation slower. This leads to increasing relaxation time with increasing gap and minimal relaxation time near the critical point where the gap is zero.

In conclusion, in all models reviewed in this Section relaxation is the fastest either at a critical point or close to it. This is where either vanishing or small energy gap does not inhibit relaxation.

3.12. Summary

In this part we focused on the nature of the apparent stationary states long time after a sudden quench with a special emphasis on quadratic models. Dynamics of relaxation to the steady state was only touched in Section 3.11. This is a non-trivial problem, especially for a large sudden quench, where not only low energy states are excited, but also high energy ones which are not described by any universal low energy effective theory. This problem should in general be less serious after a linear quench where, despite some similarity to a sudden quench in the adiabatic-impulse-adiabatic approximation, only low energy modes are excited up to a cut-off set by the KZ length $\hat{\xi}$, and this length itself can be accurately obtained from a universal low energy theory. However, sudden quenches are interesting in their own right. After the pioneering theoretical work in the 1970's [198], they became recently the subject of dedicated experiments on oscillations and dephasing of the superfluid state after a sudden quench deep into the Mott insulator phase [2, 199].

There are integrable models where the time evolution can be solved exactly, like the XY chain [83, 178, 198], 1D hard-core bosons [174, 183], or the $\frac{1}{r}$ Hubbard chain [175], all of which are diagonalizable by the Jordan-Wigner transformation,

but this type of integrability may result in very specific relaxation dynamics [200]. In models integrable by the Bethe ansatz it was not possible to extract dynamics in general, but with the notable exceptions of the Richardson and Lieb-Liniger models [201]. In view of these difficulties, it is necessary to develop approximate and/or numerical methods such as solutions of the dynamics of field theoretical models at the renormalisation group fixed points [167, 177, 202], semiclassical theories [203], exact diagonalisation [186, 194, 204], time-dependent dynamical renormalisation group (tDMRG) in one dimension [78, 169, 187, 188, 204, 205], dynamical mean field theory in infinite dimensions [142, 196, 206], and other approximate methods [128]. Recently, new numerical schemes were proposed [207] which go beyond the standard tDMRG by focusing from the beginning on the dynamics of the interesting local observable rather than a quantum state as a whole. Some of the more universal results in the above papers concerning the final relaxed steady states were reviewed in this part, but the less universal dynamics of relaxation has been only touched.

As explained in the introductory Section 3.1, it makes sense to define a mixed steady state ρ_∞ even for an isolated quantum system in a pure state, provided that the statistical description is used only for observables O that are sufficiently local or coarse-grained. This observation encourages one to apply the usual concepts of thermodynamics to pure quantum states. The discussion in Section 3.1 revealed the central role played by the diagonal part $\bar{\rho} = \sum_\alpha p_\alpha |\alpha\rangle\langle\alpha|$ of the density matrix in the eigenbasis $|\alpha\rangle$ of the time-independent Hamiltonian H after the quench. Reference [208] goes further and argues that also for a time-dependent Hamiltonian $H(t)$ it is only the diagonal part $\bar{\rho}(t)$ of the density matrix $\rho(t) = |\psi(t)\rangle\langle\psi(t)|$ in the instantaneous eigenbasis of $H(t)$ that is relevant for thermodynamics, because any realistic measurement of a thermodynamic observable O actually measures its time average $\bar{O} = \text{Tr}\bar{\rho}O$. The time average dephases to zero any contribution from the off-diagonal elements of the density matrix $\rho(t)$, and for sufficiently coarse-grained observables the dephasing may be fast enough to justify using the time-dependent diagonal ensemble $\bar{\rho}(t)$ as a statistical description of the actual underlying pure state $|\psi(t)\rangle$. This observation motivates definition of the diagonal entropy

$$S_d = - \sum_\alpha p_\alpha \log_2 p_\alpha , \quad (390)$$

which is in general non-zero, in contrast to the vanishing von Neumann entropy $S = -\text{Tr}\rho(t) \log_2 \rho(t)$ of the underlying pure state. The diagonal entropy does not change in adiabatic processes when transitions between instantaneous energy levels are negligible and the diagonal probabilities p_α do not change. In Ref. [208] it is shown that when the system is initially in thermal equilibrium at temperature T , then S_d can only increase or stay the same, in accordance with the second law of thermodynamics. This and other properties [208] make the diagonal entropy a plausible candidate for the entropy of an isolated quantum system.

Another Ref. [209] derives microscopic expression for the heat generated in an arbitrary process as the energy generated due to transitions between different instantaneous energy levels. When the initial density matrix is diagonal in the Hamiltonian eigenbasis, then the expression for heat contains only squares of the absolute values of the evolution operator which can be interpreted as transition probabilities between instantaneous energy levels. It can be shown [209] that when the initial density matrix is passive, i.e. its diagonal elements p_α decrease with increasing eigenenergy, then the heat is non-negative.

A closely related issue is considered in Ref. [210], where a probability distribution $P(W)$ is derived for a work W done in an instantaneous quench starting at the

critical point of a quantum critical system. For instance, in the quantum Ising chain, a small sudden quench from the critical transverse magnetic field $g = 1$ to a nearby $g = 1 + \delta g$ does a work W with the Gamma distribution

$$P(W) \propto W^{(\delta g/2\pi)^2 - 1} e^{-W} . \quad (391)$$

This distribution exhibits an interesting edge singularity with the exponent $(\delta g/2\pi)^2$ depending on the size δg of the quench. Certainly, a lot of interesting research could be done along these lines and those of Ref. [209] especially in the context of the Jarzynski theorem [211].

Another Reference [212] considers spin susceptibility in a sudden quench of the transverse field g in the quantum Ising chain. After the field is instantaneously switched from an initial g_i to a final g_f the transverse magnetisation relaxes locally to a stationary value $m(g_i, g_f) = \text{Tr} \bar{\rho} \sigma_j^z$. One can define susceptibility to the initial field as $\chi_i = \partial m / \partial g_i$. Exact calculations in Ref. [212] show, among other things, that close to the criticality, when $g_i \approx 1$, the quench susceptibility has a logarithmic divergence

$$\chi(g_i, g_f) \approx -\frac{1}{\pi} \ln |g_i - 1| + F(g_f) , \quad (392)$$

where $F(g_f)$ is independent of g_i . Notice that the divergent susceptibility probes not only the ground state, which is known to undergo drastic changes at a quantum critical point, but also the excited states.

These are but a few examples which did not quite fit into the main story of Section 3, but which demonstrate that the subject is far from closed and we can expect exciting new developments in the near future.

4. Open problems

The main open problems appear to be:

- Once the non-adiabaticity of quantum critical systems has been well established, we must at last face the problem how to prevent the unwanted excitation in the adiabatic quantum state preparation. The non-linear quench or the inhomogeneous transition in Sections 2.5 and 2.8 respectively are the first proposals in this direction, but we certainly still need more ideas and more work to overcome this problem.
- Due to the quasiparticle horizon effect, the entropy of entanglement in the excited state grows linearly with time and makes simulations with classical computers a formidable task. On the other hand, the excited high energy eigenstates render low energy effective theories inaccurate. Thus an accurate solution of the relaxation dynamics in a large non-integrable system remains a challenge.

These and other open problems may require another review in the near future.

Acknowledgements

I would like to acknowledge stimulating interactions with Lukasz Cincio, Fernando Cucchietti, Bogdan Damski, Krzysztof Sacha, Jakub Meisner, Marek Rams, Anatoli Polkovnikov, Haitao Quan, Marek Tylutki, Jakub Zakrzewski, Michael Zwolak, and Wojciech Zurek. This work was supported by Polish Government scientific funds

(2009-2012) as a research project N202 124736 and by the Marie Curie ATK project COCOS (contract MTKD-CT-2004-517186).

References

- [1] M. Lewenstein, A. Sanpera, V. Ahufinger, B. Damski, A. Sen(De), and U. Sen, *Adv. in Phys.* **56** 243 (2007); A.M. Rey, V. Gritsev, I. Bloch, E. Demler, and M.D. Lukin, *Rev. Lett* **99**, 140601 (2007).
- [2] M. Greiner *et al.*, *Nature* **415**, 39 (2002); *Nature* **419**, 51 (2002).
- [3] T. Kinoshita, T. Wenger, and D.S. Weiss, *Science* **305**, 1125 (2004).
- [4] T. Kinoshita, T. Wenger, and D. S. Weiss, *Nature* **440**, 900 (2006).
- [5] B. Paredes *et al.*, *Nature* **429**, **277** (2004).
- [6] S. Trotzky *et al.*, *Science*, **319**, 295 (2008).
- [7] K. Henderson, C. Ryu, C. MacCormick, and M. G. Boshier, *New J. Phys.* **11** (2009) 043030.
- [8] E. Haller, R. Hart, M. J. Mark, J. G. Danzl, L. Reichsöllner, M. Gustavsson, M. Dalmonte, G. Pupillo, H.-Ch. Nägerl, arXiv:1004.3168.
- [9] A. Friedenauer, H. Schmitz, J. T. Glueckert, D. Porras, and T. Schaetz, *Nature Physics* **4**, 757 (2008); arXiv:0802.4072.
- [10] I. Bloch, J. Dalibard, and W. Zwerger, *Rev. Mod. Phys.* **80**, 885 (2008); L.-M. Duan, E. Demler, and M.D. Lukin, *Phys. Rev. Lett.* **91**, 090402 (2003); A. Micheli, G.K. Brennen, and P. Zoller, *Nature Physics* **2**, 341 (2006).
- [11] J. Zhang, F. M. Cucchiatti, C. M. Chandrashekar, M. Laforest, C. A. Ryan, M. Ditty, A. Hubbard, J. K. Gamble, R. Laflamme *Phys. Rev. A* **79**, 012305 (2009).
- [12] A. B. Finnila, M. A. Gomez, C. Sebenik, C. Stenson, and J. D. Doll, *Chem. Phys. Lett.* **219**, 343 (1994); T. Kadowaki and H. Nishimori, *Phys. Rev. E* **58**, 5355 (1998); J. Brooke, D. Bitko, T. F. Rosenbaum, and G. Aeppli, *Science* **284**, 779 (1999); G. E. Santoro, R. Martonak, E. Tosatti, and R. Car, *Science* **295**, 2427 (2002); A. Das and B. K. Chakrabarti, *Quantum Annealing and Related Optimization Methods*, Lecture Notes in Physics, Springer Verlag, 2005; G. E. Santoro and E. Tosatti, *J. Phys. A.: Math. Gen.* **39**, R393 (2006); M. Sarjala, V. Petäjä, and M. Alava, *J. Stat. Mech.* (2006) P01008.
- [13] C. Orzel, A. K. Tuchman, M. L. Fenselau, M. Yasuda, and M. A. Kasevich, *Science* **291**, 2386 (2001); A. K. Tuchman, C. Orzel, A. Polkovnikov, and M. A. Kasevich, *Phys. Rev. A* **74**, 051601 (2006); W. Li, A. K. Tuchman, H.-C. Chien, M. A. Kasevich, *Phys. Rev. Lett.* **98**, 040402 (2007).
- [14] E. Farhi *et al.*, *Science* **292**, 472 (2001); R. Schützhold and G. Schaller, *Phys. Rev. A* **74**, 060304 (2006).
- [15] S. Sachdev, *Quantum Phase Transitions* (Cambridge University Press, Cambridge UK, 2001).
- [16] R. Feynman, *Found. Phys.* **16**, 507 (1986).
- [17] L.D. Landau and E.M. Lifshitz, *Quantum Mechanics*, Pergamon, 1958; C. Zener, *Proc. R. Soc. A* **137**, 696 (1932).
- [18] P. Jordan and E. Wigner, *Z. Phys* **47**, 631 (1928).
- [19] M. Greiner, I. Bloch, O. Mandel, T. W. Haensch, T. Esslinger, *Phys. Rev. Lett.* **87**, 160405 (2001).
- [20] T. W. B. Kibble, *J. Phys. A* **9**, 1387 (1976); *Phys. Rep.* **67**, 183 (1980); *Physics Today*, 2007; 60 (9).
- [21] W. H. Zurek, *Nature* **317**, 505 (1985); *Acta Physica Polonica B* **24**, 1301 (1993); *Phys. Rep.* **276**, 177 (1996).
- [22] P. C. Hendry *et al.*, *Nature* **368**, 315 (1994).
- [23] M. E. Dodd *et al.*, *Phys. Rev. Lett.* **81**, 3703 (1998).
- [24] N. Antunes and R. Rivers, *Phys. Rev. D* **73**, 125003 (2006).
- [25] A.J. Bray, *Adv. Phys.* **43**, 357 (1994).
- [26] V.M.H. Ruutu *et al.*, *Nature* **382**, 334 (1996); C. Bäurle *et al.*, *ibid.* **382**, 332 (1996).
- [27] R. Monaco *et al.*, *Phys. Rev. Lett.* **89**, 080603 (2002); *Phys. Rev. B* **67**, 104506 (2003); *Phys. Rev. Lett.* **96**, 180604 (2006); *Phys. Rev. B* **80**, 180501 (2009).
- [28] P. Laguna and W.H. Zurek, *Phys. Rev. Lett.* **78**, 2519 (1997); *Phys. Rev. D* **58**, 5021 (1998); A. Yates and W.H. Zurek, *Phys. Rev. Lett.* **80**, 5477 (1998); G.J. Stephens *et al.*, *Phys. Rev. D* **59**, 045009 (1999); N.D. Antunes *et al.*, *Phys. Rev. Lett.* **82**, 2824 (1999); J. Dziarmaga, *Phys. Rev. Lett.* **81**, 5485 (1998); E. Moro and G. Lythe, *Phys. Rev. E* **59**, R1303 (1999); J. Dziarmaga, P. Laguna and W. H. Zurek, *ibid.* **82**, 4749 (1999); M.B. Hindmarsh and A. Rajantie, *ibid.* **85**, 4660 (2000); G. J. Stephens, L. M. A. Bettencourt, and W. H. Zurek, *ibid.* **88**, 137004 (2002).
- [29] I.L. Chuang *et al.*, *Science* **251**, 1336 (1991); M.I. Bowick *et al.*, *ibid.* **263**, 943 (1994).
- [30] R. Carmi and E. Polturak, *Phys. Rev. Lett.* **84**, 4966 (2000); A. Maniv, E. Polturak, and G. Koren, *ibid.* **91**, 197001 (2003); D. Golubchik, E. Polturak, and G. Koren, *Phys. Rev. Lett.* **104**, 247002 (2010).
- [31] S. Ducci, P.L. Ramazza, W. Gonzalez-Viñas, F.T. Arecchi, *Phys. Rev. Lett.* **83**, 5210 (1999); S. Casado, W. Gonzalez-Viñas, H. Mancini, S. Boccaletti, *Phys. Rev. E* **63**, 057301 (2001); S. Casado *et al.*, *Eur. Phys. J.* **146**, 87 (2007).
- [32] C. N. Weiler, T. W. Neely, D. R. Scherer, A. S. Bradley, M. J. Davis, and B. P. Anderson, *Nature* **455**, 948 (2008); J.R. Anglin and W.H. Zurek, *Phys. Rev. Lett.* **83**, 1707 (1999).
- [33] J. Dziarmaga, A. Smerzi, W. H. Zurek, and A. R. Bishop, *Phys. Rev. Lett.* **88**, 167001 (2002).
- [34] J. Dziarmaga, J. Meisner, and W.H. Zurek, *Phys. Rev. Lett.* **101**, 115701 (2008).
- [35] S. Deng, G. Ortiz, and L. Viola, *Eur. Phys. Lett.* **84**, 67008 (2008).
- [36] W.H. Zurek, U. Dornier and P. Zoller, *Phys. Rev. Lett.* **95**, 105701 (2005).
- [37] J. Dziarmaga, *Phys.Rev.Lett.* **95**, 245701 (2005).

- [38] L. Cincio, J. Dziarmaga, M. M. Rams, and W. H. Zurek, Phys. Rev. A **75**, 052321 (2007).
- [39] C. de Grandi, V. Gritsev, and A. Polkovnikov, Phys. Rev. B **81**, 012303 (2010); Phys. Rev. B **81**, 224301 (2010).
- [40] D. Sen, K. Sengupta, and S. Mondal, Phys. Rev. Lett. **101**, 016806 (2008); Phys. Rev. B **79**, 045128 (2009).
- [41] R. Barankov and A. Polkovnikov, Phys. Rev. Lett. **101**, 076801 (2008).
- [42] C. De Grandi, R.A. Barankov, and A. Polkovnikov, Phys. Rev. Lett. **101**, 230402 (2008).
- [43] G.G. Batrouni, V. Rousseau, R.T. Scalettar, M. Rigol, A. Muramatsu, P.J.H. Denteneer, and M. Troyer, Phys. Rev. Lett. **89**, 117203 (2002); G.G. Batrouni, H. R. Krishnamurthy, K. W. Mahmud, V.G. Rousseau, and R.T. Scalettar, Phys. Rev. A **78**, 023627 (2008); S.M. Pittman, G.G. Batrouni, R.T. Scalettar, arXiv:0808.2809.
- [44] W.H. Zurek and U. Dornier, Phil. Trans. R. Soc. A **366**, 2953 (2008).
- [45] J. Dziarmaga and M. M. Rams, New J. Phys. **12**, 055007 (2010).
- [46] B. Damski and W.H. Zurek, New J. Phys. **11**, 063014 (2009).
- [47] T. Platini, D. Karevski, L. Turban, J. Phys. A: Math. Theor. **40**, 1467 (2007); M. Collura, D. Karevski and L. Turban, J. Stat. Mech. P08007 (2009).
- [48] J. Dziarmaga and M. M. Rams, arXiv:1005.3763, A. Niederberger, M. M. Rams, J. Dziarmaga, F. M. Cucchietti, J. Wehr, and M. Lewenstein, arXiv:1004.1975.
- [49] T. W. E. Kibble and G. E. Volovik, JETP Letters **65**, 96 (1997); J. Dziarmaga, P. Laguna, and W. H. Zurek, Phys. Rev. Lett. **82**, 4749 (1999); N. B. Kopnin and E. V. Thuneberg, *ibid.* **83**, 116 (1999).
- [50] W.H.Zurek, Phys. Rev. Lett. **102**, 105702(2009); A. del Campo, G. De Chiara, G. Morigi, M. B. Plenio, and A. Retzker, arXiv:1002.2524.
- [51] G. Schaller, Phys. Rev. A **78**, 032328 (2008).
- [52] T. Platini, D. Karevski, L. Turban, J. Phys. A: Math. Theor. **40**, 1467 (2007); M. Collura and D. Karevski, Phys. Rev. Lett. **104**, 200601 (2010).
- [53] B. Damski, Phys. Rev. Lett. **95**, 035701 (2005).
- [54] B. Damski and W.H. Zurek, Phys. Rev. A **73**, 063405 (2006).
- [55] E. Timmermans, P. Tommasini, M. Hussein, and A. Kerman, Phys. Rep. **315**, 199 (1999).
- [56] N.V. Vitanov and B.M. Garraway, Phys. Rev. A **53**, 4288 (1996); N.V. Vitanov, Phys. Rev. A **59**, 988 (1999).
- [57] E.T. Whittaker and G.N. Watson, *A Course of Modern Analysis*, Cambridge University Press, Cambridge, UK, 1958.
- [58] R. W. Cherg and L. S. Levitov, Phys. Rev. A **73**, 043614 (2006).
- [59] V. Mukherjee, U. Divakaran, A. Dutta, and D. Sen, Phys. Rev. B **76**, 174303 (2007).
- [60] U. Divakaran, V. Mukherjee, A. Dutta, and D. Sen, J. Stat. Mech. P02007 (2009).
- [61] S. Deng, G. Ortiz, and L. Viola, Phys. Rev. B **80**, 241109 (2009).
- [62] U. Divakaran, A. Dutta, and D. Sen, Phys. Rev. B **78**, 144301 (2008); D. Chowdhury, U. Divakaran, and A. Dutta, Phys. Rev. E **81**, 012101 (2010).
- [63] K. Sengupta, D. Sen, and S. Mondal, Phys. Rev. Lett. **100**, 077204 (2008); S. Mondal, D. Sen, and K. Sengupta, Phys. Rev. B **78**, 045101 (2008); U. Divakaran and A. Dutta, Phys. Rev. B **79**, 224408 (2009).
- [64] A. Kitaev, Ann. Phys. (N.Y.) **321**, 2 (2006).
- [65] U. Divakaran, V. Mukherjee, A. Dutta, and D. Sen, arXiv:0908.4004, published in "Quantum Quenching, Annealing and Computation", Eds. A. Das, A. Chandra and B. K. Chakrabarti, Lect. Notes in Phys., Springer, Heidelberg (2009).
- [66] V. Mukherjee, A. Dutta, and D. Sen, Phys. Rev. B **77**, 214427 (2008); V. Mukherjee and A. Dutta, J. Stat. Mech. (2009) P05005; U. Divakaran and A. Dutta, Phys. Rev. B **79**, 224408 (2009); U. Divakaran, A. Dutta, and D. Sen, Phys. Rev. B **81**, 054306 (2010).
- [67] A. Dutta, R.R.P. Singh, and U. Divakaran, Eur. Phys. Lett. **89**, 67001 (2010).
- [68] B. Dora and R. Moessner, Phys. Rev. B **81**, 165431 (2010).
- [69] D. Chowdhury, U. Divakaran, and A. Dutta, Phys. Rev. E **81**, 012101 (2010).
- [70] A. Polkovnikov, Phys. Rev. B **72**, R161201 (2005); C. De Grandi and A. Polkovnikov, arXiv:0910.2236, contribution to "Quantum Quenching, Annealing and Computation", Eds. A. Das, A. Chandra and B. K. Chakrabarti, Lect. Notes in Phys., Springer, Heidelberg (2009, to be published).
- [71] E. Lieb *et al.*, Ann. Phys. (N.Y.) **16**, 406 (1961); S. Katsura, Phys. Rev. **127**, 1508 (1962).
- [72] G. Vidal, J.I. Latorre, E. Rico and A. Kitaev, Phys. Rev. Lett. **90**, 227902 (2003).
- [73] N. Laflorencie, Phys. Rev. B **72**, R140408 (2005).
- [74] G. Refael and J. E. Moore, Phys. Rev. Lett. **93**, 260602 (2004); R. Santachiara, J. Stat. Mech. L06002 (2006).
- [75] A. R. Its, B.-Q. Jin and V.E. Korepin, J. Phys. A: Math. Gen. **38**, 2975 (2005).
- [76] P. Calabrese and J. Cardy, J. Stat. Mech. 0406, P002 (2004); *ibid.* 0504, P010 (2005).
- [77] P. Calabrese and J. Cardy, Phys. Rev. Lett. **96**, 136801 (2006).
- [78] G. De Chiara, S. Montangero, P. Calabrese and R. Fazio, J. Stat. Mech. P03001 (2006).
- [79] B.-Q. Jin and V. E. Korepin, J. Stat. Phys. **116**, 79 (2004).
- [80] C. Holzhey, F. Larsen and F. Wilczek, Nucl. Phys. B **424**, 443 (1994).
- [81] F. Pollmann, S. Mukerjee, A.G. Green, and J.E. Moore, Phys. Rev. E **81**, 020101 (2010).
- [82] P. J. Forrester and N. E. Frankel, J. Math. Phys. **45**, 2003 (2004); M. E. Fisher and R. E. Hartwig, Adv. Chem. Phys. **15**, 333 (1968); E. L. Basor and C. A. Tracy, Phys. A **177**, 167 (1991); F. Franchini and A. G. Abanov, J. Phys. A: Math. Gen. **38**, 5069 (2005); correction in J. Phys. A: Math. Gen. **39**, 14533 (2006).
- [83] K.Sengupta, S. Powell, and S. Sachdev, Phys. Rev. A **69**, 053616 (2004).
- [84] G. Vidal, Phys. Rev. Lett. **91**, 147902 (2003); Phys. Rev. Lett. **93**, 040502 (2004).
- [85] L. Cincio, J. Dziarmaga, J. Meisner, and M.M. Rams, Phys. Rev. B **79**, 094421 (2009).

- [86] M.V. Berry, *J. Phys. A* **10**, 2083 (1977).
- [87] A.C.M. Carollo and J.K. Pachos, *Phys. Rev. Lett.* **95**, 157203 (2005); S.L. Zhu, *Phys. Rev. Lett.* **96**, 077206 (2006); A. Hamma, quant-ph/0602091; S. Oh, *Phys. Lett. A* **373**, 644 (2009).
- [88] B. Basu, *Phys. Lett. A* **374**, 1205 (2010).
- [89] S. Deng, L. Viola, and G. Ortiz, arXiv:0802.3941.
- [90] K. Sengupta and D. Sen, *Phys. Rev. A* **80**, 032304 (2009).
- [91] D.I. Tsomokos, A. Hamma, W. Zhang, S. Haas, R. Fazio, *Phys. Rev. A* **80**, 060302(R) (2009).
- [92] R. Shankar and G. Murthy, *Phys. Rev. B* **36**, 536 (1986); B.M. McCoy and T.T. Wu, *Phys. Rev.* **176**, 631 (1968); *ibid* **188**, 982 (1969); R.B. Griffiths, *Phys. Rev. Lett.* **23**, 17 (1969); B.M. McCoy, *Phys. Rev. Lett.* **23**, 383 (1969); *Phys. Rev.* **188**, 1014 (1969).
- [93] D.S. Fisher, *Phys. Rev. B* **51**, 6411 (1995).
- [94] J. Dziarmaga, *Phys. Rev. B* **74**, 064416 (2006);
- [95] T. Caneva, R. Fazio, G. E. Santoro, *Phys. Rev. B* **76**, 144427 (2007).
- [96] J. Zakrzewski and D. Delande, arXiv:0902.1117.
- [97] C.L. Kane, *Science* **314**, 1692 (2006).
- [98] Y. Hatsugai, *Phys. Rev. Lett.* **71**, 3697 (1993).
- [99] I. Affleck, T. Kennedy, E.H. Lieb, and H. Tasaki, *Phys. Rev. Lett.* **59**, 799 (1987).
- [100] X. Wen, *Advances in Physics* **44**, 405 (1995).
- [101] M. Koenig *et al.*, *Science* **318**, 766 (2007); D. Hsieh *et al.*, *Nature* **452**, 970 (2008), *Science* **323**, 919 (2009).
- [102] V.P. Gusynin and S.G. Sharapov, *Phys. Rev. Lett.* **95**, 146801 (2005); N. Goldman *et al.*, *Phys. Rev. Lett.* **103**, 035301 (2009).
- [103] C.L. Kane and E.J. Mele, *Phys. Rev. Lett.* **95**, 146802 (2005); *Phys. Rev. Lett.* **95**, 226801 (2005); B.A. Bernevig, T.L. Hughes, and S.-C. Zhang, *Science* **314**, 1757 (2006); L.Fu, C.L. Kane, and E.J. Mele, *Phys. Rev. Lett.* **98**, 106803 (2007); J.E. Moore and L. Balents, *Phys. Rev. B* **75**, 121306 (2007).
- [104] A.P. Schnyder, S.Ryu, A. Furusaki, and A.W.W. Ludwig, *Phys. Rev. B* **78**, 195125 (2008); Y. Kitaev, arXiv:0901.2686, Proceedings of the L.D.Landau Memorial Conference "Advances in Theoretical Physics", June 22-26, 2008, Chernogolovka, Moscow region, Russia.
- [105] Y. Kitaev, *Phys. Usp.* **44**, 131 (2001).
- [106] A.Y. Kitaev, *Ann. Phys.* **303**, 2 (2003); C. Nayak, S.H. Simon, A. Stern, M. Freedman, and S. Das Sarma, *Rev. Mod. Phys.* **80**, 1083 (2008).
- [107] N. Read and D. Green, *Phys. Rev. B* **61**, 10267 (2000).
- [108] L. Fu and C.L. Kane, *Phys. Rev. Lett.* **100**, 096407 (2008); *Phys. Rev. Lett.* **102**, 216403 (2009).
- [109] S. Tewari, C. Zhang, S. Das Sarma, C. Nayak, and D.-H. Lee, *Phys. Rev. Lett.* **100**, 027001 (2008); P.A. Lee, arXiv:0907.2681 (2009); Y. Tanaka, T. Yokoyama, and N. Nagaosa, arXiv:0907.2088; K.T. Law, P.A. Lee, and T.K. Ng, *Phys. Rev. Lett.* **103**, 237001 (2009).
- [110] A. Bermudez, L. Amico, and M.A. Delgado, *New J. Phys.* **12**, 055014 (2010).
- [111] A. Bermudez, D. Patane, L. Amico, and M.A. Delgado, *Phys. Rev. Lett.* **102**, 135702 (2009).
- [112] M. Creutz, *Phys. Rev. Lett.* **83**, 2636 (1999).
- [113] T. Caneva, R. Fazio, and G.E. Santoro, *Phys. Rev. B* **78**, 104426 (2008)
- [114] H.J. Lipkin, N. Meshkov, and A.J. Glick, *Nucl. Phys.* **62**, 188 (1965).
- [115] R. Botet and R. Jullien, *Phys. Rev. B* **28**, 3855 (1983); F. Pan and J. Draayer, *Phys. Lett.* **451**, 1 (1999); J. Links, H. Zhou, R. McKenzie, and M. Gould, *J. Phys. A* **36**, 63 (2003); O. Castanos, R. Lopez-Pena, J. Hirsch, and E. Lopez-Moreno, *Phys. Rev. B* **74**, 104118 (2006); R. Unanyan and M. Fleischhauer, *Phys. Rev. Lett.* **90**, 133601 (2003); S. Dusuel and J. Vidal, *Phys. Rev. Lett.* **93**, 237204 (2004); F. Leyvraz and W. Hess, *Phys. Rev. Lett.* **95**, 050402 (2005); S. Dusuel and J. Vidal, *Phys. Rev. B* **71**, 224420 (2005); G. Ortiz, R. Somma, J. Dukelsky, and S. Rombouts, *Nucl. Phys.* **707**, 421 (2005); G. Chen and J. Liang, *New J. Phys.* **8**, 297 (2006); W. Heiss, *J. Phys. A* **39**, 10081 (2006); P. Ribeiro, J. Vidal, and R. Mosseri, *Phys. Rev. Lett.* **99**, 050402 (2007); *Phys. Rev. E* **78**, 021106 (2008); G. Rosensteel, D. Rowe, and S. Ho, *J. Phys. A* **41**, 025208 (2008).
- [116] A. Das, K. Sengupta, D. Sen, and B.K. Chakrabarti, *Phys. Rev. B* **74** (2006) 144423.
- [117] L. Amico, A. Osterloh, and F. Cataliotti, *Phys. Rev. Lett.* **95**, 063201 (2005).
- [118] N. Goldenfeld, *Lectures on phase transitions and renormalisation group*, Perseus Books, Reading, Massachusetts, USA (1992); S.L. Sondhi, S.M. Girvin, J.P. Carini, and D. Shahar, *Rev. Mod. Phys.* **69**, 315 (1997).
- [119] T.D. Kühner, S.R. White, and H. Monien, *Phys. Rev. B* **61**, 12474 (2000); B. Damski and J. Zakrzewski, *Phys. Rev. A* **74**, 043609 (2006).
- [120] M.P.A. Fisher, P.B. Weichman, G. Grinstein, and D.S. Fisher, *Phys. Rev. B* **40**, 546 (1989).
- [121] E. Altman and A. Auerbach, *Phys. Rev. Lett.* **89**, 250404 (2002).
- [122] F. Pellegrini, S. Montangero, G.E. Santoro, and R. Fazio, *Phys. Rev. B* **77**, 140404 (2008); E. Canovi, D. Rossini, R. Fazio, G.E. Santoro, *J. Stat. Mech.* (2009) P03038.
- [123] F. Cucchietti, B. Damski, J. Dziarmaga and W. H. Zurek, *Phys. Rev. A* **75**, 023603 (2007).
- [124] D. R. Scherer, C. N. Weiler, T. W. Neely, and B. P. Anderson, *Phys. Rev. Lett.* **98**, 110402 (2007); R. Carretero-Gonzalez, B.P. Anderson, P.G. Kevrekidis, D.J. Frantzeskakis, and C.N. Weiler, *Phys. Rev. A* **77**, 033625 (2008).
- [125] D.F. Walls and G.J. Milburn, *Quantum Optics*, Springer-Verlag, Berlin 1994; M.J. Steel *et al.*, *Phys. Rev. A* **58**, 4824 (1998); A. Sinatra *et al.*, *PRL* **87**, 210404 (2001); *J. Phys. B* **35**, 3599 (2002); K. Goral *et al.*, *Opt. Express* **8**, 92 (2001); M. J. Davis and S. A. Morgan, *PRA* **68**, 053615 (2003); M. J. Davis *et al.* *J. Phys. B* **37**, 2725 (2004); *J. Phys. A* **38**, 10259 (2005); M. Brewczyk *et al.*, *J. Phys. B* **40**, R1 (2007); A. S. Bradley *et al.*, *PRA* **77**, 033616 (2008); P.B. Blakie, A. S. Bradley, M.J. Davis, R.J. Ballagh, and C.W. Gardiner, *Adv. Phys.*, **57**, 363 (2008); A. Polkovnikov, arXiv:0905.3384.
- [126] J. Dziarmaga, A. Smerzi, W. H. Zurek, and A. R. Bishop, arXiv:cond-mat/0403607, published in proceedings of NATO ASI *Patterns of Symmetry Breaking*, H. Arodz, J. Dziarmaga, and W.H.

- Zurek (Eds.), Kluwer Academic Publishers (2002).
- [127] R. Schützhold, M. Uhlmann, Y. Xu, and U.R. Fischer, *Phys. Rev. Lett.* **97**, 200601 (2006); U.R. Fischer, R. Schützhold, and M. Uhlmann, *Phys. Rev. A* **77**, 043615 (2008); R. Schützhold, *J. Low Temp. Phys.* **153**, 228 (2008).
- [128] U.R. Fischer and R. Schützhold, *Phys. Rev. A* **78**, 061603 (2008).
- [129] E.H. Lieb and W. Liniger, *Phys. Rev.* **130**, 1605 (1963).
- [130] F.D.M. Haldane, *Phys. Rev. Lett.* **47**, 1840 (1981).
- [131] M.A. Cazalilla, *J. Phys. B* **37**, 1 (2004).
- [132] M. Girardeau, *J. Math. Phys.* **1**, 516 (1960); C.N. Yang and Y.P. Yang, *J. Math. Phys.* **10**, 1115 (1969); L. Tonks, *Phys. Rev.* **50**, 955 (1936).
- [133] S. Coleman, *Phys. Rev. D* **11**, 2088 (1975).
- [134] A. Zamolodchikov, *Int. J. Mod. Phys. A* **10**, 1125 (1995).
- [135] L.E. Sadler, J.M. Higbie, S.R. Leslie, M. Vengalattore, and D.M. Stamper-Kurn, *Nature* **443**, 312 (2006).
- [136] A. Lamacraft, *Phys. Rev. Lett.* **98**, 160404 (2007).
- [137] M. Uhlmann, R. Schützhold, U. R. Fischer, *Phys. Rev. Lett.* **99**, 120407 (2007); *Phys. Rev. D* **81**, 025017 (2010); arXiv:1005.2649.
- [138] B. Damski and W. H. Zurek, *Phys. Rev. Lett.* **99**, 130402 (2007);
- [139] K. Murata, H. Saito, and M. Ueda, *Phys. Rev. A* **75**, 013607 (2007).
- [140] A. Polkovnikov and V. Gritsev, *Nature Physics* **4**, 477, 2008.
- [141] M. Eckstein and M. Kollar, *New J. Phys.* **12**, 055012 (2010).
- [142] J.K. Freedricks, V.M. Turkovski, and V. Zlatić, *Phys. Rev. Lett.* **97**, 266408 (2006); A. Hackl and S. Kehrein, *J. Phys. C* **21**, 015601 (2009).
- [143] M. Möckel and S. Kehrein, *Phys. Rev. Lett.* **100**, 175702 (2008); *Ann. Phys.* **324**, 2146 (2009).
- [144] O. Zobay and B.M. Garraway, *Phys. Rev. A* **61**, 033603 (2000); J. Liu *et al.*, *ibid* **66**, 023404 (2002).
- [145] A. Ishkhanyan *et al.*, *Phys. Rev. A* **73**, 043612 (2004).
- [146] I. Tikhonenkov *et al.*, *Phys. Rev. A* **73**, 043605 (2006).
- [147] A. Altland, V. Gurarie, T. Kriechenbauer, and A. Polkovnikov, *Phys. Rev. A* **79**, 042703 (2009).
- [148] H. Pu *et al.*, *Phys. Rev. Lett.* **98**, 050406 (2007); A.P. Itin and S. Watanabe, *ibid.* **99**, 223903 (2007); *Phys. Rev. E* **76**, 026218 (2007).
- [149] A.P. Itin *et al.*, *Physica D* **232**, 108 (2007).
- [150] A.P. Itin and P. Törma, arXiv:0901.4778; *Phys. Rev. A* **79**, 055602 (2009).
- [151] R.H. Dicke, *Phys. Rev.* **93**, 99 (1954).
- [152] C. Lee, *Phys. Rev. Lett.* **102**, 070401 (2009); T. Venumadhav, M. Haque, and R. Moessner, *Phys. Rev. B* **81**, 054305 (2010).
- [153] A.R. Its and A.A. Kapaev, *Izv. Akad. Nauk SSSS, Ser. Mat.* **51**, 878 (1987); D.L. Vainshtein *et al.*, *Plasma Phys. Rep.* **25**, 299 (1999).
- [154] S.-J. Gu, *Phys. Rev. E* **79**, 061125 (2009).
- [155] S.J. Gu and H.Q. Lin, arXiv:0807.3491.
- [156] L.C. Venuti and P. Zanardi, *Phys. Rev. Lett.* **99**, 095701 (2007).
- [157] A. Fubini, G. Falci, and A. Osterloh, *New J. Phys.* **9**, 134 (2007).
- [158] S. Mostame, G. Schaller, and R. Schützhold, *Phys. Rev. A* **76**, 030304 (2007).
- [159] M.H.S. Amin, C.J.S. Truncik, and D.V. Averin, *Phys. Rev. A* **80**, 022303 (2009).
- [160] D. Patane, A. Silva, L. Amico, R. Fazio, and G.E. Santoro, *Phys. Rev. Lett.* **101**, 175701 (2008); *Phys. Rev. B* **80**, 024302 (2009).
- [161] D. Patane, A. Silva, F. Sols, and L. Amico, *Phys. Rev. Lett.* **102**, 245701 (2009).
- [162] B. Damski, H. Quan, and W.H. Zurek, arXiv:0911.5729.
- [163] J.M. Deutsch, *Phys. Rev. A* **43**, 2046 (1991); M. Srednicki, *Phys. Rev. E* **50**, 888 (1994).
- [164] E. Fermi, J. Pasta, and S. Ulam, Los Alamos Report pp. LA-1940 (1955); Focus Issue: The “Fermi-Pasta-Ulam” Problem - The First 50 Years, *Chaos* **15**, 015101 (2005); B.V. Chirikov, *J. Nucl. Energy C* **1**, 253 (1960); F.M. Izrailev, A.I. Khisamutdinov, and B.V. Chirikov, Los Alamos Report pp. LA-4440-TR (1970).
- [165] X. Zotos, *J. Low T. Phys.*, **126**, 1185 (2002).
- [166] D. M. Gangardt and A. Kamenev, *Phys. Rev. Lett.* **104**, 190402 (2010).
- [167] P. Calabrese and J. Cardy, *J. Stat. Mech.* P04010 (2005); *Phys. Rev. Lett.* **96**, 136801 (2006); *J. Stat. Mech.* P06008 (2007); *J. Stat. Mech.* (2007) P10004.
- [168] J.L. Cardy, *Nucl. Phys. B* **240**, 514 (1984);
- [169] S.R. White and A.E. Feiguin, *Phys. Rev. Lett.* **93**, 076401 (2004); A.J. Daley, C. Kollath, U. Schölzow, and G. Vidal, *J. Stat. Mech.* P04005 (2004); D. Gobert *et al.*, *Phys. Rev. E* **71**, 036102 (2005).
- [170] G. De Chiara, S. Montangero, P. Calabrese, and R. Fazio, *J. Stat. Mech.* 0603 (2006) P001.
- [171] L. Amico, A. Osterloh, F. Plastina, R. Fazio, and G.M. Palma, *Phys. Rev. A* **69**, 022304 (2004); C. Kollath, U. Schollwoeck, J. von Delft, and W. Zwerger, *Phys. Rev. A* **71**, 053606 (2005); C. Kollath, U. Schollwoeck, and W. Zwerger, *Phys. Rev. Lett.* **95**, 176401 (2005); T.S. Cubitt and J.I. Cirac, quant-ph/0701053; M. Polini and G. Vignale, *Phys. Rev. Lett.* **98**, 266403 (2007); T. Antal, Z. Racz, A. Rakos, and G.M. Schutz, *Phys. Rev. E* **59**, 4912 (1999); D. Karevski, *Eur. Phys. J B* **27**, 147 (2001); Y. Ogata, *Phys. Rev. E* **66**, 066123 (2002); W.H. Aschbacher and C.-A. Pillet, *J. Stat. Phys.* **112**, 1153 (2003); T. Platini and D. Karevski, *Eur. Phys. J B* **48**, 225 (2005); W.H. Aschbacher and J.-M. Barbaroux, *Lett. Math. Phys.* **77**, 11 (2006); T. Platini and D. Karevski, *J. Phys. A* **40**, 1711 (2007); W.H. Aschbacher, *Lett. Math. Phys.* **79**, 1 (2007).
- [172] L. Mathey and A. Polkovnikov, *Phys. Rev. A* **81**, 033605 (2010).
- [173] E. H. Lieb and D. W. Robinson, *Comm. Math. Phys.* **28**, 251 (1972).
- [174] M. Rigol, A. Muramatsu, and M. Olshanii, *Phys. Rev. A* **74**, 053616 (2006); M. Rigol, V. Dunjko, V. Yurovsky, and M. Olshanii, *Phys. Rev. Lett.* **98**, 050405 (2007).
- [175] M. Kollar and M. Eckstein, *Phys. Rev. A* **78**, 013626 (2008).

- [176] T. Barthel and U. Schollwöck, Phys. Rev. Lett. **100**, 100601 (2008).
- [177] M.A. Cazalilla, Phys. Rev. Lett. **97**, 156403 (2006); Phys. Rev. A, **80**, 063619 (2009).
- [178] F. Igloi and H. Rieger, Phys. Rev. Lett. **85**, 3233 (2000).
- [179] D. Rossini, A. Silva, G. Mussardo, and G.E. Santoro, Phys. Rev. Lett. **102**, 127204 (2009).
- [180] J.M. Luttinger, J. Math. Phys. **4**, 1154 (1963); E.H. Lieb and D.C. Mattis, *ibid.* **6**, 304 (1965); A. Luther and I. Peschel, Phys. Rev. B **9**, 2911 (1974)
- [181] F.D.M. Haldane, Phys. Rev. Lett. **45**, 1358 (1980); J. Phys. C **14**, 2585 (1981); Phys. Rev. Lett. **47**, 1840 (1981); T. Giamarchi, *Quantum Physics in One Dimension*, Oxford University Press, Oxford 2004; A.O. Gogolin, A.A. Nersisyan, and A.M. Tsvelik, *Bosonization and Strongly Interacting Systems*, Cambridge University Press, Cambridge 1998.
- [182] M. Girardeau, J. Math. Phys. **1**, 516 (1960); A. Lenard, *ibid.* **5**, 930 (1964); H.G. Vaidya and C.A. Tracy, Phys. Rev. Lett. **42**, 3 (1979).
- [183] D.M. Gangardt and M. Pustilnik, Phys. Rev. A. **77**, 041604 (2008).
- [184] A. Minguzzi and D. M. Gangardt, Phys. Rev. Lett **94**, 240404 (2005).
- [185] M. Cramer, C.M. Dawson, J. Eisert, and T.J. Osborne, Phys. Rev. Lett. **100**, 030602 (2008); M. Cramer, A. Fleisch, I.P. McCulloch, U. Schollwöck, and J. Eisert, Phys. Rev. Lett. **101**, 063001 (2008).
- [186] G. Roux, Phys. Rev. A **79**, 021608 (2009).
- [187] C. Kollath, A.M. Läuchli, and E. Altman, Phys. Rev. Lett. **98**, 180601 (2007).
- [188] S.R. Manmana, S. Wessel, R.M. Noack, and A. Muramatsu, Phys. Rev. Lett. **98**, 210405 (2007); Phys. Rev. B **79**, 155104 (2009).
- [189] S. Mukerjee, V. Oganesyan, and D. A. Huse, Phys. Rev. B **73**, 035113 (2006); V. Oganesyan and D. A. Huse, Phys. Rev. B **75**, 155111 (2007); V. Oganesyan, A. Pal, and D. A. Huse, Phys. Rev. B **80**, 115104 (2009);
- [190] P. Schmitteckert, Phys. Rev. B **70**, 121302 (2004); S.R. Manmana, A. Muramatsu, and R.M. Noack, AIP Conf. Proc. **789**, 269 (2005); M. Hochbruck and C. Lubich, BIT **39**, 620 (1999); R.M. Noack and S.R. Manmana, AIP Conf. Proc. **789**, 93 (2005); N. Laflorencie and D. Poilblanc, Lect. Notes Phys. **645**, 227 (2004).
- [191] M. Horoi, V. Zelevinsky, and B.A. Brown, Phys. Rev. Lett. **74**, 5194 (1995).
- [192] A.I. Shnirelman, Usp. Mat. Nauk. **29**, 181 (1974); A. Voros, *Stochastic Behavior in Classical and Quantum Hamiltonian Systems*, Springer Verlag, Berlin, 1979; Y.C. de Verdiere, Comm. Math. Phys. **102**, 497 (1985); S. Zelditch, Duke Math J. **55**, 919 (1987).
- [193] E.J. Heller and B.R. Landry, J. Phys. A **40**, 9259 (2007).
- [194] M. Rigol, V. Dunjko, and M. Olshanii, Nature **452**, 854 (2008).
- [195] M. Rigol, Phys. Rev. Lett. **103**, 100403 (2009).
- [196] M. Eckstein, M. Kollar, and P. Werner, Phys. Rev. Lett. **103**, 056403 (2009); Phys. Rev. B **81**, 115131 (2010).
- [197] P. Barmettler, M. Punk, V. Gritsev, E. Demler, and E. Altman, Phys. Rev. Lett. **102**, 130603 (2009); arXiv:0911.1972.
- [198] P. Mazur, Physica **43**, 533 (1969); P. Pfeuty, Ann. of Phys. **57**, 79 (1970); E. Barouch, B. McCoy, and M. Dresden, Phys. Rev. A **2**, 1075 (1970); E. Barouch, B. McCoy, Phys. Rev. A **3**, 786 (1971); Phys. Rev. A **3**, 2137 (1971).
- [199] S. Hofferberth *et al.*, Nature **449**, 324 (2007).
- [200] G. Brioli, C. Kollath, and A.M. Läuchli, arXiv:0907.3731.
- [201] N. Kitanine, J.M. Maillet, N.A. Slavnov, and V. Terras, Nucl.Phys. B **729**, 558 (2005); J.-S. Caux and P. Calabrese, Phys.Rev. A **74**, 031605 (2006); J.-S. Caux, P. Calabrese, and N.A. Slavnov, J. Stat. Mech. (2007) P01008; A. Faribault, P. Calabrese, and J.-S. Caux, J. Stat. Mech. (2007) P01008. V. Gritsev, T. Rostunov, and E. Demler, J. Stat. Mech. (2010) P05012.
- [202] J. Berges, S. Borsnyi, and C. Wetterich, Phys. Rev. Lett. **93**, 14202 (2004); E. Bettelheim, A.G. Abanov, and P. Wiegman, Phys. Rev. Lett. **97**, 246402 (2006); A.A. Burkov, M.D. Lukin, and E. Demler, Phys. Rev. Lett. **98**, 200404 (2007); V. Gritsev, E. Demler, M. Lukin, and A. Polkovnikov, Phys. Rev. Lett. **99**, 200404 (2007); A. Iucci and M. Cazalilla, Phys. Rev. A **80**, 063619 (2009); J. Sabio and S. Kehrein, New J. Phys. **12**, 055008 (2010).
- [203] A. Polkovnikov, S. Sachdev, and S.M. Girvin, Phys. Rev. A **66**, 053607 (2002); A. Polkovnikov, Phys. Rev. A **68**, 033609 (2003); A. Polkovnikov, arXiv:0905.3384.
- [204] A.M. Läuchli and C. Kollath, J. Stat. Mech. P05018 (2008).
- [205] D. Gobert, C. Kollath, U. Schollwöck, and G. Schütz, Phys. Rev. E **71**, 036102 (2005); P. Barmettler *et al.*, Phys. Rev. A **78**, 012330 (2008); Phys. Rev. Lett. **102**, 130603 (2009); T. Barthel, C. Kasztelan, I.P. McCulloch, and U. Schollwöck, Phys. Rev. A **79**, 053627 (2009); A. Fleisch *et al.*, Phys. Rev. A **78**, 033608 (2008).
- [206] M. Eckstein and M. Kollar, Phys. Rev. Lett. **100**, 120404 (2008).
- [207] S.R. White and I. Affleck, Phys. Rev. B **77**, 134437 (2008); M.B. Hastings and L.S. Levitov, arXiv:0806.4283; T. Barthel, U. Schollwöck, and S.R. White, Phys. Rev. B **79**, 245101 (2009); M.B. Hastings, J. Math. Phys. **50**, 095207 (2009); M.C. Banuls, M.B. Hastings, F. Verstraete, and J.I. Cirac, Phys. Rev. Lett. **102**, 240603 (2009).
- [208] R. Barankov and A. Polkovnikov, arXiv:0806.2862.
- [209] A. Polkovnikov, Phys. Rev. Lett. **101**, 220402 (2008).
- [210] A. Silva, Phys. Rev. Lett. **101**, 120603 (2008).
- [211] C. Jarzynski, Phys Rev Lett **78**, 2690 (1997).
- [212] Ying Li, M.X. Huo, and Z. Song, Phys. Rev. B **80**, 054404 (2009).